Universität Stuttgart
Institut für Kernenergetik
und Energiesysteme

Experimental investigation on the heat transfer between condensing steam and supercritical CO_2 in compact heat exchangers

Marcel Strätz

Mai 2020 IKE 2-164

IKE

Universität Stuttgart
Institut für Kernenergetik
und Energiesysteme

Experimental investigation on the heat transfer between condensing steam and supercritical CO_2 in compact heat exchangers

von der Fakultät Energie-, Verfahrens- und Biotechnik der Universität Stuttgart zur Erlangung der Würde eines Doktor-Ingenieurs (Dr.-Ing.) genehmigte Abhandlung

vorgelegt von

M. Sc. Marcel Strätz

aus Augsfeld

Hauptberichter:	Prof. Dr.-Ing. Jörg Starflinger
Mitberichter:	Prof. Dr.-Ing. Dieter Brillert

Tag der Einreichung:	05.12.2019
Tag der mündlichen Prüfung:	18.05.2020

ISSN: 0173 - 6892

Mai 2020 IKE 2-164

Erklärung über die Eigenständigkeit

Ich versichere, dass ich die vorliegende Arbeit

„Experimental investigation on the heat transfer between condensing steam and supercritical CO_2 in compact heat exchangers“

selbstständig verfasst und keine anderen als die angegebenen Quellen und Hilfsmittel benutzt habe. Fremde Quellen und Gedanken sind als solche kenntlich gemacht.

Declaration of Authorship

I hereby certify that the dissertation

„Experimental investigation on the heat transfer between condensing steam and supercritical CO_2 in compact heat exchangers“

is my own work. Ideas from other sources are otherwise indicated clearly in the work.

Ort, Datum **Marcel Strätz**

Augsfeld, den 25.10.2020

Danksagung

Meine Forschungsarbeit auf dem Gebiet der Wärmeübertragung mit überkritischem CO_2 und kondensierendem Dampf in diffusionsgeschweißten Kompaktwärmeübertragern am Institut für Kernenergetik und Energiesysteme (IKE) der Universität Stuttgart wurde im Rahmen des EU-Projektes „sCO2-HeRo“ (Projekt-Nr. 662116) innerhalb des Forschungsprogramms „Horizon-2020“ durchgeführt. Für die finanzielle Förderung möchte ich mich bedanken. Eine anfängliche sowie abschließende Finanzierung meiner Arbeit erfolgte mit Hilfe eines Stipendiums des Forschungsinstituts für Kerntechnik und Energiewandlung e.V. Für diese unbürokratische Unterstützung sage ich herzlichen Dank.

Ein besonderer Dank gilt meinem Betreuer Herrn Prof. Dr.-Ing. Jörg Starflinger für die sehr gute wissenschaftliche Betreuung meiner Arbeit. Im Rahmen des Projektes fanden viele gemeinsame Dienstreisen wie z. B. nach Amerika, China, Niederlande, Österreich und Tschechien statt. Für Fragen stand er mir jederzeit zur Verfügung und während des Projektes unterstützte er mich mit wertvollen Hinweisen und Tipps. Mein herzlicher Dank geht auch an Herrn Prof. Dr.-Ing. Dieter Brillert für sein Engagement bei der Übernahme des Mitberichts.

Im Weiteren ist mein Abteilungsleiter Herr Dr.-Ing. Rainer Mertz zu nennen, welcher mir von Beginn an großes Vertrauen geschenkt und mich bei meiner Arbeit unterstützt hat. Besten Dank für die hilfreichen Kommentare bei Berichten und Veröffentlichungen. Es war eine sehr angenehme und freundschaftliche Zusammenarbeit.

Außerdem bedanke ich mich bei den Kolleginnen des Sekretariats und der Verwaltung für die vielfältige Unterstützung. Zu erwähnen wäre außerdem das Werkstatt-Team für die Fertigung meiner Versuchsplatten, da ohne diese keine experimentellen Untersuchungen hätten stattfinden können. Weiterhin bedanke ich mich bei allen Kollegen des IKE für das freundschaftliche Miteinander, den angenehmen wissenschaftlichen Diskussionen sowie den gemeinsamen Dienstreisen. Ein besonderer Dank gilt meinem geschätzten Zimmerkollegen Wolfgang Flaig für die nette Aufnahme in seinem Büro, die gute Zusammenarbeit sowie dem Entstehen einer großartigen Freundschaft.

Nicht zuletzt möchte ich mich bei meinen Eltern, Michael und Margit Strätz, für die fortlaufende Unterstützung meiner gesamten Ausbildung bedanken - ohne das Verständnis und die Hilfe eurerseits hätte ich diesen Weg nicht geschafft. Vielen Dank!

I Abstract

In the frame of the sCO2-HeRo project, a self-launching, self-propelling and self-sustaining decay heat removal system with supercritical CO_2 as working fluid is developed. This system can be attached to existing nuclear power plants and should reliably transfer the decay heat to an ultimate heat sink, in case of a combined station black-out and loss-of-the-ultimate-heat-sink accident scenario. Thereby the nuclear core is sufficiently cooled, which leads to safe conditions. To demonstrate the feasibility of such a system and to gain experimental experience, a small-scale sCO2-HeRo system is designed, built and installed into the pressurized water reactor glass model at GfS, Essen. The obtained experimental results are used to validate correlations and models for pressure drop and heat transfer, which are implemented in the German thermal-hydraulic code ATHLET. In consideration of the validated models and correlations, new ATHLET simulations of the sCO2-HeRo system attached to a NPP are performed and the results are analyzed.

After the motivation, the state of the art is summarized, including an outline of the simulation work with the ATHLET code, a summary of sCO_2 test facilities and a description of currently performed experimental heat transfer investigations in heat exchangers with sCO_2 as working fluid. The main objectives of the work are derived from there. The chapter "sCO2-HeRo" starts with a description of the pressurized water reactor glass model. Afterwards, the basic sCO2-HeRo system is explained before a detailed description of the sCO2-HeRo system for the PWR glass model and for the reactor application is presented. Afterwards, cycle calculations are performed for both systems to determine the design point parameters in consideration of boundary conditions, restrictions and assumptions with respect to maximum generator excess electricity. In the following chapter, the test facility for the investigations on the heat transfer capability between condensing steam and sCO_2 is described. It consists of the sCO_2 SCARLETT loop, a high-pressure steam cycle and a low-pressure steam cycle. The installed measurement devices, measurement uncertainties and calculated error propagations are explained as well. After a fundamental classification of heat exchangers, the 7 heat exchanger test configurations are summarized before the diffusion bonding technique, the used plate material, the mechanical design, the plate design and the manufacturing steps of the heat exchanger test plates are described. In the chapter "Results", the measurement points are described and an overview of the performed measurement configurations is given before a summary of all measurement results is presented. After that, experimental results of the sCO_2 pressure drop for unheated flows as well as for heated flows are depicted and explained, followed by the analysis of the experimental heat transfer results. The chapter "CHX for the PWR glass model" starts with a summary of the boundary

conditions and measurement results with regard to the design of the heat exchanger for the sCO2-HeRo system of the glass model. Subsequently, the plate design is presented and manufacturing steps of the heat exchanger are described by means of pictures. The chapter "ATHLET simulations" starts with an introduction before the development of performance maps, models and the validation of correlations based on experimental results as well as CFD simulation results are described. In the following, these models and performance maps are transferred to a sCO2-HeRo system that can be attached to a nuclear power plant. Finally, further cycle simulations are carried out and the simulation results are analyzed.

II Kurzfassung

Im Rahmen des sCO2-HeRo Projektes wird an der Entwicklung eines selbst-erhaltenden Nachwärmeabfuhrsystems mit überkritischem CO_2 als Arbeitsmedium geforscht. Dieses kann in bestehende Kraftwerksanlagen eingebaut werden und soll im Fall eines Stromausfalls sowie dem gleichzeitigen Verlust der Wärmesenke die anfallende Nachzerfallswärme zuverlässig an eine ultimative Wärmesenke transferieren. Hierdurch wird der nukleare Kern hinreichend gekühlt und befindet sich somit in einem sicheren Betriebszustand. Zur Demonstration der Machbarkeit wird eine skaliertes sCO2-HeRo System ausgelegt, gebaut und in das Druckwasserreaktor Glasmodell der GfS in Essen eingebaut. Im Weiteren werden mit Hilfe gewonnener experimenteller Ergebnisse implementierte Korrelationen und Modelle des Simulationscodes ATHLET validiert und gegebenenfalls angepasst. Anschließend wird das sCO2-HeRo System für die Reaktoranwendung mit Hilfe von ATHLET simuliert und die Ergebnisse ausgewertet.

Die vorliegende Arbeit beginnt mit der Motivation sowie dem aktuellen Stand der Technik. Hierbei wird u. a. ein Augenmerk auf die numerische Arbeit mit Hilfe des Simulationscodes ATHLET gelegt, bestehende sCO_2 Versuchsanlagen zusammengefasst und experimentelle Arbeiten im Bereich der Wärmeübertragung mit überkritischem CO_2 als Arbeitsmedium beschrieben. Anschließend werden die Ziele der Arbeit definiert. Im Kapitel „sCO2-HeRo“ wird zu Beginn das Druckwasserreaktor Glasmodell beschrieben. Anschließend wird der grundsätzliche Aufbau des sCO2-HeRo Systems erläutert bevor detailliert auf das sCO2-HeRo System für das Glasmodell sowie für die Reaktoranwendung eingegangen werden. Für beide sCO2-HeRo Systeme finden im Weiteren Kreislaufberechnungen statt und die Auslegungspunkte werden unter Berücksichtigung von Randbedingungen, Restriktionen und Annahmen in Bezug auf einer maximalen Überschussenergie am Generator festgelegt. Im nachfolgenden Kapitel wird zu Beginn der Versuchsstand zur experimentellen Untersuchung der Wärmeübertragungsleistung von kondensierendem Dampf auf sCO_2 beschrieben. Dieser setzt sich aus der sCO_2 SCARLETT Versuchsanlage, einem hoch-druck Dampfkreislauf sowie einem nieder-druck Dampfkreislauf zusammen. Im Weiteren werden installierte Messinstrumente, Messunsicherheiten sowie Fehlerfortpflanzungen erläutert. Nach einer grundsätzlichen Klassifizierung der Wärmeübertrager werden die 7 Wärmeübertragerkonfigurationen beschrieben, mit Hilfe deren die experimentellen Versuche durchgeführt werden. Außerdem wird auf das Diffusionsschweißen, das verwendete Plattenmaterial, die mechanische Auslegung sowie das Plattendesign und die Plattenfertigung eingegangen. Im Kapitel „Results“ werden die festgelegten Messpunkte beschrieben sowie ein Überblick über durchgeführte Messkonfigurationen gegeben,

bevor eine Zusammenfassung aller Messergebnisse folgt. Anschließend werden u. a. experimentelle Ergebnisse der sCO_2 Druckverluste für unbeheizte sowie beheizte Strömungen dargestellt. Die Auswertung, graphische Darstellung und Analyse der Wärmeübertragungsversuche schließen sich an. Das Kapitel „CHX for the PWR glass model“ beginnt mit einer Zusammenfassung aller Randbedingungen und Messergebnissen, im Hinblick auf die Auslegung des Wärmeübertragers für das sCO2-HeRo Systems des Glasmodells. Im Folgenden wird das Plattendesign vorgestellt und entscheidende Herstellungsschritte des Wärmeübertrages anhand von Bildern beschrieben. Im Kapitel „ATHLET simulations“ wird zu Beginn eine Einleitung gegeben bevor die Entwicklung von Kennlinien, Modellen und die Validierung von Korrelationen anhand gewonnener experimenteller Ergebnisse sowie CFD Simulationsergebnisse beschrieben wird. Diese Modelle sowie Kennlinien werden auf ein sCO2-HeRo System, welches in Kernkraftwerken installiert werden kann, übertragen bevor weitere Kreislaufsimulationen stattfinden und die Simulationsergebnisse beschrieben werden.

III Table of Contents

IV List of figures

V List of tables

VI Nomenclature

Latin Symbols

A	m²	Area
a	mm	Channel Height
b	mm	Channel Width
C	mm	Plate Width
d	mm	Diameter
e	-	Correction Factor
f	-	Reduction Factor
G	(kJ·m²)/kg	Heating Load
h	kJ/kg	Enthalpy
H	mm	Heat Exchanger Height
K	mm	Roughness
L	mm	Heat Exchanger Length
l	mm	Channel Length
$\dot{m}$	kg/s	Mass Flow Rate
n	rpm	Rotational Speed
N	-	Number of sCO2-HeRo Units
Nu	-	Nusselt Number
$\overline{Nu}$	-	Averaged Nusselt Number
P_{el}	W	Electrical Power
p	bar	Pressure
Δp	bar	Pressure Drop
Pr	-	Prandtl Number
Q	W	Heat Power

q	W/m	Heat Power Density
r	mm	Radius
R	-	Transfer Ratio
$R_{p0.2}$	N/mm²	Yield Strength
Re	-	Reynold Number
$\overline{Re}$	-	Averaged Reynolds Number
S	-	Safety Factor
s	kJ/(kg·K)	Entropy
t	mm	Wall Thickness
t_a	mm	Wall Thickness Outer Wall
t_h	mm	Wall Thickness Between H_2O and sCO_2 Channel
t_p	mm	Wall Thickness Pipe
t_w	mm	Wall Thickness Between Neighbored Channels
T	°C	Temperature
TO	°C	Temperature Surface sCO_2 Plate
TD	°C	Temperature Surface H_2O Plate
ΔT	°C	Temperature Difference
U	mm	Circumference
V	m³	Volume
v	m/s	Velocity
x_1	mm	Length 1
x_2	mm	Length 2
X	mm	Measurement Position

Greek Symbols

α	W/(m^2·K)	Heat Transfer Coefficient
c_p	J/(kg·K)	Isobaric Specific Heat Capacity
η	%	Efficiency
ρ	kg/m³	Density
μ	Pa·s	Dynamic Viscosity
λ	W/(m·K)	Heat Conductivity
6	N/mm²	Stress
σ	-	Uncertainty
ξ	-	Friction Coefficient
δ	°	Deflection Degree
π	-	Pressure Ratio

Parameters

d_h	mm	Hydraulic Diameter	$d_h = 4 \cdot \frac{A}{U}$
Nu	-	Nusselt Number	$Nu = \frac{\alpha \cdot d}{\lambda}$
Pr	-	Prandtl Number	$Pr = \frac{\mu \cdot c_p}{\lambda}$
Re	-	Reynold Number	$Re = \frac{\rho \cdot v \cdot d}{\mu}$

Subscripts and Superscripts

1	Inlet Compressor
2	Inlet Compact Heat Exchanger
3’	Inlet Slave Electrical Heater
3	Inlet Turbine
4	Inlet Ultimate Heat Sink
a	Axial
air	Air
av	Averaged
c	Critical
C	Compressor
CHX	Compact Heat Exchanger
$calc$	Calculated
$channel$	Channel
$CO2$	Carbon Dioxide
$Condi$	Conditioning Cooling
$Conde$	Condenser
d	Deflection
e	Expansion
el	Electricity
$Evap$	Evaporator
exp	Experiment
Gas	Gas Chiller
GM	Glass Model
$Heat$	Heating
$H2O$	Water
i	Inner

in	Input
is	Isentropic
$loss$	Losses
m	Model
max	Maximum
min	Minimum
n	Narrowing
NPP	Nuclear Power Plant
$plenum$	Plenum
$pipe$	Pipe
r	Radial
SHE	Slave Electrical Heater
$sCO2$	Supercritical Carbon Dioxide
t	Tangential
tr	Triple Point
T	Turbine
UHS	Ultimate Heat Sink
o	Outer
$offset$	Offset
out	Output
x	Position

Abbreviations

ASME	American Society of Mechanical Engineers
ATHLET	Analysis of Thermal-hydraulics of Leaks And Transients
BWR	Boiling Water Reactor
$C_2H_2F_4$	Tetrafluorethan
CAD	Computer Aided Design
CD	Core Degradation
CFD	Computational Fluid Dynamics
CHX	Compact Heat Exchanger
CMHE	Cast Metal Heat Exchanger
CO_2	Carbon Dioxide
CV	Control Volume
CVR	Centrum Výzkumu Řež
DIN	Deutsches Institut für Normung
DP	Design Point
EPR	European Pressurized Reactor
EU	European Union
GCSM	General Control Simulation Module
GfS	Gesellschaft für Simulatorschulung GmbH
H_2O	Water
He	Helium
HeRo	Heat Removal
HECU	Heat Transfer and Heat Conduction Module
HP	High Pressure
HPLC	High Performance Liquid Chromatography
HX	Heat Exchanger
IKE	Institute of Nuclear Technology and Energy Systems

INES	International Nuclear and Radiological Event Scale
KAERI	Korean Atomic Energy Research Institute
KAIST	Korea Advanced Institute of Science and Technology
LOCA	Loss of Coolant Accident
LP	Low Pressure
LUHS	Loss of Ultimate Heat Sink
LWR	Light Water Reactor
MIT	Massachusetts Institute of Technology
NEUKIN	Neutron Kinetics Module
NPP	Nuclear Power Plant
ODP	Out of Design Point
ODP II	Out of Design Point II
P&I	Piping and Instrumentation
PCHE	Printed Circuit Heat Exchanger
PHE	Plate Heat Exchanger
PI	Proportional Integral
PM	Performance Maps
POSTECH	Pohang University of Science and Technology
PWR	Pressurized Water Reactor
RBMK	Russian Graphite Moderated Water Cooled Boiling Water Reactor
RCIC	Reactor Core Isolation Cooling
SCARLETT	Supercritical Carbon Dioxide Loop at IKE Stuttgart
SBO	Station Black Out
SCIEL	Supercritical CO_2 Integral Experiment Loop
sCO_2	Supercritical Carbon Dioxide
S-CO2	Supercritical Carbon Dioxide Brayton Cycle Test Facility
SEH	Slave Electrical Heater

SNL	Sandia National Lab
SUSEN	Sustainable Energy
TCS	Turbo Compressor System
TFD	Thermo Fluid Dynamic Module
TIT	Tokyo Institute of Technology
TMI	Three Mile Island
TRL	Technology Readiness Level
UDE	University of Duisburg-Essen
UHS	Ultimate Heat Sink
USTUTT	University of Stuttgart

1 Introduction

1.1 Motivation

The demand of primary energy all over the world rise from 260 EJ in the year 1973 to 580 EJ in 2016, which is an increase of about 125 %. The energy is provided by oil (31 %), coal (29 %), gas (21 %), renewable energy (14 %) and nuclear energy (5 %) [1]. Compared to the world average, the composition of primary energy in Germany is quite similar and consists of oil (35 %), coal (22 %), gas (24 %), renewable energy (13 %) and nuclear energy (6 %) [2]. To achieve about 6 % of the primary energy with nuclear power, there are about 450 nuclear reactors in operation and 58 under construction worldwide. Countries with more than 20 operating reactors are currently China (37), France (58), India (22), Japan (43), Korea (25), Russia (35) and the USA (99) [3]. Neighboring on Germany, there are also countries like France, the Netherlands, Belgium, Switzerland and the Czech Republic, which are operating nuclear power plants (NPP). In Germany there are currently 7 nuclear reactors in operation, which can be classified into the boiling water reactor (BWR) and pressurized water reactor (PWR). The BWR Gundremmingen and the PWR's Isar 2, Brokdorf, Philippsuburg 2, Grohnde, Emsland and Neckarwestheim 2 will be switched off consecutively by 2022 due to the nuclear phase-out decision in Germany from 2011 [4].

Despite the phase-out in Germany, nuclear energy continues to play an important role globally because of various advantages compared to other energy sources. For instance, nuclear energy is irreplaceable when it comes to complying with the COP21 Paris Agreement of decarbonizing the electrical system and achieving the aim of keeping global warming below 1.5 °C. This technology has one of the lowest total energy costs and ensures the supply of energy in combination with highly fluctuating renewable energies because of its high availability and regardless of weather conditions. The access to uranium sources, the low sensitivity to price variations and the small quantities of uranium required must be also considered and lead to reduced dependency on fossil fuels [5]. Due to its high energy density, the land use is lower than for renewable energies like solar or wind power, which is a benefit for biodiversity and for the protection of natural habitats. In addition, the high energy density makes it possible to store fuel assemblies on-site for a number of years of operation, which leads to means greater independence from supply chains.

Besides the advantages of nuclear power plants, also negative aspects like accidents and their impact on human beings and nature must be taken into account. The INES scale (International Nuclear and Radiological Event Scale) is developed for classifying such events. Events with low priority and no impact on safety are classified as 0 and incident anomalies as 1. Incidents are classified as 2 and serious incidents as 3. The step towards an accident with local consequences is reached at 4 and with wider consequences at 5. A serious accident is classified as 6 and a major accident as 7. Between 1991 and 2012, only events classified as 0 (2908 / 97.4 %), 1 (75 / 2.5 %) and 2 (3 / 0.1 %) occurred in Germany [6]. The three well-known accidents in conventional nuclear power plants, with significant impact on humans and nature, occur in the reactors of Three Mile Island, Chernobyl and Fukushima-Daiichi. The accident of Three Mile Island (TMI) happens on 28 March 1979 in Harrisburg (USA) as a combination of the loss of coolant inventory in the reactor and misinterpretations by the operators. During the accident small amounts of radioactive gases are released into the environment, contaminated water is pumped into the river and the core is molten down up to 50 %. This accident is the most serious one in the USA and it is classified to INES by 5. The accident in Chernobyl (Ukraine) on 26 April 1986 is the worst NPP accident worldwide and is classified as 7. During a test procedure of the emergency power supply in the Russian graphite moderated water cooled boiling water reactor (RBMK) the operators commit serious mistakes, leading to an explosion and furthermore to a graphite fire, which releases most of the radiation into the atmosphere. Compared to German reactor types, the RBMK has several disadvantages like no existing containment and a huge amount of combustible graphite. Safety systems are not always redundantly available and the loss of coolant can lead to a positive void power increase. The accident in the Japanese nuclear power plant Fukushima-Daiichi on 11 March 2011 is initiated by an earthquake, causing several flood waves. The first wave destroys the external power supply as well as the seawater pump of the cooling system and the second one put the emergency diesel generators out of order. In the following the scrammed reactor core is not cooled sufficiently, the water inventory is gradually evaporated, the core is partially uncovered and hydrogen is generated due to the evolving zirconium oxidation. The hydrogen explosion destroys parts of the reactor building and radioactive inventory is released uncontrolled into the environment. The accident in Fukushima is classified similar to Chernobyl as 7 according to INES. However, the amount of released radioactive inventory with 5 % - 10 % of Chernobyl is much lower and the negative impacts on humans and nature are less significant.

The accidents of Three Mile Island, Chernobyl and Fukushima-Daiichi show that the increase of safety in existing NPP and the design of advanced new reactor types has to be one main objective for scientists and power plant operators. New reactor concepts are designed to withstand extremely unlikely serious accident scenarios by equipping them with advanced passive and self-sustaining safety systems. The European Pressurized Reactor (EPR), for instance, is a new generation III reactor that will be able to withstand accident scenarios with core degradation due to the installation of a core catcher. To date, one EPR is under construction in Olkiluoto (Finland), one in Flamanville (France) and two in Taishan (China). Besides new reactor concepts, scientists and power plant operators are working together to improve the safety of still operating NPPs by designing and investigating retrofittable safety systems like core catchers, thermo-siphons and self-sustaining decay heat removal systems. According to [7], [8] a core catcher is designed as passive or active safety system with various inlet conditions of the coolant, like top or bottom flooding. This system can be used in the late phase of a sever accident scenario, in which the core is gradually degraded, the melt penetrates the pressure vessel and the core catcher is the last possibility of melt retention within the containment. The thermo-siphon technology is applied according to Grass [9] as a passive heat removal system for cooling wet storage pools in an NPP in case of a station-blackout scenario. The heat of the wet storage pool is transferred, driven by natural convection and without any external power, from the evaporation zone of the thermo-siphon to the condensing zone, which is located at the ambient air. This system is considered as a retrofittable, self-launching and self-propelling back-up heat removal system for wet storage pools. In case of a combined station black-out (SBO) and loss-of-ultimate-heat-sink (LUHS) accident scenario in a NPP, the reactor is scrammed and the main coolant pumps as well as the turbine are switched off. The decay must be transferred reliably to an ultimate heat sink to ensure that the core is cooled sufficiently. If this is not guaranteed, core degradations, failures of the reactor pressure vessel and the release of radioactive material can occur. To prevent such a Fukushima-like event, scientists are working on a self-launching, self-propelling and self-sustaining decay heat removal system with supercritical CO_2 (sCO_2) as working fluid. This system is a Brayton cycle, consisting of a compressor, a compact heat exchanger, a turbine, a gas cooler and a generator. In the design point of this system, it is assumed that the turbine provides more power than used for the compression, leading to a self-sustaining system, which fulfills the aim of transferring the decay heat from the reactor core to an ultimate heat sink.

Venker et al. [10 - 15] carry out a feasibility study of such a sCO_2 decay heat removal system, attached to a generic BWR. The simulation results show that the grace time for interaction can be increased to more than 72 hrs in consideration of the assumptions and implemented component models. Based on those results, six partners from three European countries are working together in the European project “sCO2-HeRo” (supercritical CO2 Heat Removal System) for the design and assessment of such a cycle. Within the project a two-scale approach is applied. In the first step on the small-scale a demonstrator unit is designed and installed into the PWR glass model at Gesellschaft für Simulatorschulung GmbH (GfS), Essen. This is the step towards Technology Readiness Level 3 (TRL 3), meaning the step from theory to a demonstrator unit. Therefore, models and correlations for pressure drop, heat transfer, etc. are validated by using single-effect experiments. These results are used also for the design of the components of the demonstrator unit. After manufacturing, the performance of each component is tested before the entire system is installed. After installation, further investigations are performed to receive more data and to gain experiences of the sCO2-HeRo cycle behaviour, especially during start-up, steady state and transient conditions. In the second step, the validation and test results are transferred to component models or performance maps on power plant size. These are implemented into the thermal-hydraulic system code ATHLET (Analysis of THermal-hydraulics of LEaks and Transients) [16] and further simulations of the sCO2-HeRo system, attached to a nuclear power plant, are carried out.

Within the project IKE (Institute of Nuclear Technology and Energy Systems), the University of Stuttgart, Germany is responsible for the cycle calculations as well as for the design and manufacturing of the compact heat exchanger of the demonstrator unit, connecting the steam side of the PWR glass model with the sCO2-HeRo system. The experimental investigations on the heat transfer between condensing steam and sCO_2 in the heat exchanger test plates take place in the laboratory of IKE by using the sCO_2 SCARLETT (Supercritical CARbon dioxide Loop at IKEStuTTgart) test loop and the low-pressure or high-pressure steam cycle. The investigations for the demonstrator unit are performed by using the low-pressure steam cycle, which provides steam similar to the PWR glass model conditions (0.3 bar and 70 °C). For NPP application, heat transfer investigations are carried out by using the SCARLETT loop and the high-pressure steam cycle (70 bar and 286 °C). The received experimental data are used firstly for the design of the compact heat exchanger for the glass model and secondly for validation purposes, code improvement and advanced sCO2-HeRo cycle simulations for NPP applications by using the ATHLET code.

1.2 State of the art

Simulation work with ATHLET

The German thermal-hydraulic code ATHLET is used for the simulation of the thermal behavior and for power plant transients, e.g. an SBO & LUHS accident scenario, as well as for several LOCA (loss-of-coolant accident) accidents with different diameters of the break in light water reactors. In the advanced ATHLET code version (ATHLET-CD), there is also the possibility to simulate severe accident scenarios with core degradations. The code is capable of simulating mechanical fuel behavior, core melting, fuel rod cladding and relocation of material combined with debris bed formation. Moreover, different coolants and working fluids like heavy water and carbon dioxide are implemented.

Venker [10] conducts a feasibility study, in which she determines the minimum necessary decay heat which must be removed from the reactor core in case of a SBO & LUHS accident scenario to ensure a long-term coolability. The results show that, for a boiling water reactor with a thermal power of 3840 MW, a heat removal of 60 MW is sufficient to prevent the depressurization of the primary circuit through permanently opened safety and relief valves, leading to enough coolant inventory in the primary circuit. Furthermore, four decay heat removal systems in parallel (4 x 15 MW) are used because there is the possibility of switching off the systems consecutively and following the decay heat curve, which leads to increased operational time. In the following, the design point parameters of the decay heat removal systems are determined with respect to maximum generator excess electricity and the main components are roughly dimensioned. Afterwards, Venker defines four test cases and evaluates the impact of the decay heat removal on the core cooling. In the first case, the grace time of the retrofitted BWR is extended by around 30 minutes. The heat removal systems stops after the depressurization of the reactor pressure vessel, initiated by the reactor protection system due to low coolant inventory in the core. In the second test case, the partial depressurization is considered as deactivated, which leads to minor losses of the coolant inventory and thus to increased operation time of the decay heat removal systems. After 17 hours, the heat removal exceeds the produced decay heat, which results in a depressurization of the reactor pressure vessel and thus to decreased steam temperatures. Decreasing steam temperatures cause declining sCO_2 inlet temperatures at the turbine, and this has a negative effect on the cycle efficiency until the systems are stopped. The third test case is similar to the second one, just with an additional control system for consecutively switching off the decay heat removal

systems. At the start of the accident scenario four systems are in operation and transferring the decay heat from the reactor core to the ultimate heat sink, the ambient air. After about 1.5 hours, the removed heat exceeds the decay heat, leading to a decrease of the pressure and saturated steam temperature in the pressure vessel. After reaching a defined threshold pressure, the first system is switched off and the pressure recovers due to an imbalance of the heat removal, here too low. In the following, the same procedure occurs again and the second system is switched off. This control strategy finally leads to a balance of decay heat generation in the core and heat removal by the decay heat removal system. This balance stabilizes the pressure and temperature in the reactor pressure vessel, and both decrease slowly with decreasing decay heat. This procedure leads to a grace time of about 72 hours. In case four the decay heat removal systems is combined with a reactor core isolation cooling system (RCIC). If a SBO & LUHS accident scenario occurs, steam from the reactor pressure vessel is released via a turbine into the condensation chamber, located in the containment of the NPP. The steam-driven turbo-pump of the RCIC system injects water from the condensation chamber back into the reactor pressure vessel, independent from external power and coolant. However, this system is just designed for increasing the time to recover active safety systems because it is only able to transfer heat from the reactor core into the condensation chamber, but not to remove the heat out of the containment. Moreover, the RCIC system is one of the remaining safety systems available in the Fukushima accident 2011 [17]. The ATHLET simulation results of the latter case show that the combination of the decay heat removal systems with the RCIC system is very beneficial because the necessary amount of removed heat capacity can be reduced significantly. This is achieved by the condensation chamber, which acts as a supplementary heat sink right at the beginning of the accident scenario, where the peak in the decay heat occurs.

Finally, Venker summarizes that the simulation results are derived in consideration of implemented component models, e.g. for the turbine, compressor and heat exchangers and recommends that further experimental data should be provided for validation and improvement of component models in the code. For instance, the pressure drop in the turbine, compressor, heat exchangers and pipes should be investigated more in depth and compared to simulation results. Furthermore, the behavior of the turbine and compressor should be analyzed to receive data under design point and out of design point conditions. The thermal behavior of the compact heat exchanger has to be understood better, to be able to draw definite conclusions about the heat transfer capability and the pressure drop inside the component. Therefore, further experimental investigations should be performed.

sCO_2 test facilities

The focus on sCO_2 and their test facilities gains worldwide attention in recent years because this technology shows the potential of high thermal cycle efficiencies at relatively low temperatures and the advantage of designing compact components, which results in lower costs, less thermal inertias and the possibility of retrofitting systems. Moreover, these systems can be applied to various heat sources like nuclear, coal and gas as well as to renewable energy sources like solar power, geothermal power and waste heat of high temperature fuel cells [18]. Plenty of test facilities are in operation and under construction for the experimental investigation of such sCO_2 cycles and their components. A summary of existing sCO_2 test facilities is provided for instance by Vojacek et al. [19]. He classifies the loops according to: 1. sCO_2 facilities for high temperature investigations to heated surfaces near the pseudo-critical point, 2. Experimental sCO_2 facilities for high temperature investigations in coolers, 3. Experimental sCO_2 facilities for high temperature investigations in printed circuit heat exchangers and 4. Design comparison of sCO_2 integral test loops. Furthermore, the year of construction as well as the achievable cycle parameters like temperatures, pressures, mass flow rates and heat power density are given. In the work of Gampe et al. [20] various sCO_2 test facilities are depicted as a function of the thermal design power and the upper process temperature. Some operating sCO_2 test loops are summarized in Table 1-1.

Table 1-1: sCO2 test loops

Location	Name	$\dot{m}_{sCO2}$[kg/s]	p_{sCO2}[bar]	T_{sCO2}[°C]
Institute of Nuclear Technology and Energy Systems – IKE (Germany) [21]	SCARLETT	0.1	140	150
Korean Atomic Energy Research Institute - KAERI (Korea) [18]	SCIEL	4.8	200	500
Knolls Atomic Power Lab - (US) [22]	S-CO_2	5.0	140	280
Research Centre Rez - (CZE) [23]	SUSEN	0.4	300	550
Sandia National Lab - (US) [24]	S-CO_2	3.5	140	540

The sCO_2 SCARLETT loop is a multipurpose test facility designed and built at the Institute of Nuclear Technology and Energy Systems (IKE) in Stuttgart, Germany in 2015. Various test sections such as pipes, heat exchangers, turbines e.g. can be installed and the measurement data are used for fundamental research, validation purposes and applied science. For instance, the investigation on the heat transfer between condensing steam and sCO_2 in diffusion bonded heat exchangers and the occurring pressure drop is currently one scientific topic. Besides that, pressure drop and heat transfer investigations in directly electrically heated or water-cooled pipe configurations are performed as well. The piston compressor provides a maximum sCO_2 mass flow rate of about 0.1 kg/s, the pressure is limited to 140 bar and the temperature to 150 °C due to material restrictions. Korean scientists from KAERI (Korean Atomic Energy Research Institute), KAIST (Korea Advanced Institute of Science and Technology) and POSTECH (Pohang University of Science and Technology) designed and set up at KAERI a Supercritical CO_2 Integral Experiment Loop, called SCIEL [25]. The main objectives of SCIEL are to gain sCO_2 cycle experiences under steady state and transient operation, to establish a convenient control system and to develop strategies for start-up, normal operation and shutdown scenarios. Physical phenomena in components like the turbine, compressor and heat exchangers should be studied as well. The maximum sCO_2 mass flow rate of the recompression cycle is determined at 4.8 kg/s, the pressure at 200 bar and the temperature at the inlet of the high pressure turbine at 500 °C. The inlet and outlet temperature difference at the printed circuit heat exchangers is limited to 200 °C in order to manage the thermal stresses. In cooperation with Bechtel Marine Propulsion Corporation, an integrated supercritical carbon dioxide Brayton cycle test facility, called S-CO_2, is designed and built at the Knolls Atomic Power Lab in Schenectady, USA. The first start-up of the two-shaft recuperated system with a variable speed turbine driven compressor and a constant speed turbine driven generator is initiated in 2012 [22]. The main goals are to demonstrate operational, control and performance characteristics of the two-shaft sCO_2 cycle over a wide range of conditions. Moreover, the experimental data are used for further improvements of cycle components, material selection, code validation and for up-scaling approaches. The variable speed turbine driven compressor can provide a maximum sCO_2 mass flow rate of 5.0 kg/s at a pressure of 140 bar. The temperature at the inlet of the power turbine is limited to 280 °C. The sCO_2 test loop at the Research Centre Rez (CVR) is constructed as a flexible, modifiable and multipurpose test facility, in which performance tests of key components of sCO_2 Brayton cycles such as compressors, turbines and heat exchangers can be carried out. Moreover, it is intended to perform material investigations of seals, lubrications and valves. The loop is designed and built within the Sustainable Energy project,

called SUSEN, and first operational experiences are gained in 2017. The variable speed driven piston pump provides a maximum sCO_2 mass flow rate of 0.4 kg/s at a maximum pressure of 300 bar. The electrical heaters with a total power of 110 kW can increase the sCO_2 temperature at the inlet of the test section to 550 °C [19]. In 2018, Barber Nichols and the Sandia National Lab (SNL) designed and built a small-scale supercritical CO_2 ($S\text{-}CO_2$) compression test loop to investigate the technology issues associated with sCO_2 cycles and their components. One key issue is the experimental research of the compressor performance in combination with the control strategy of the system near the critical point where significant changes of fluid properties occur. Besides that, various supporting technology issues like bearing types, bearing cooling, choice of convenient seals, thrust load behavior and rotor windage losses of compressors are investigated in depth. During the first investigations, a turbo-compressor system reaches a speed of 65000 rpm, a pressure ratio of 1.65 and a maximum mass flow rate of about 4.0 kg/s. According to SNL, the received experimental data agree well with model predictions and they have a positive implication for the further success of the sCO_2 cycle technology [24]. The main compressor in the $S\text{-}CO_2$ test loop is a 50 kW motor-driven radial compressor which provides a sCO_2 mass flow rate of 3.5 kg/s in the design point at 75000 rpm. The pressure is limited to 140 bar and the electrical heating power is sufficient to provide sCO_2 temperatures of about 540 °C. Currently a sCO_2 Brayton cycle test facility with an installed thermal power of more than 10 MW is under construction at the Southwest Research Institute, San Antonio, Texas. The main focus will be the experimental investigation of electricity production technologies, their components and limiting conditions.

Experimental work on sCO_2 heat exchangers

The following provides a summary of research activities of heat exchangers for sCO_2 power cycle applications, as this is one main topic of this work. According to Carlson et al. [26], heat exchangers for sCO_2 power cycles face significant mechanical and thermal loads. Depending on the cycle design, sCO_2 temperatures between 75 °C and 800 °C and pressures from 75 bar to 400 bar can occur. Additionally, space limitations in containments etc. must be taken into account. Only a few heat exchanger types are suitable for these boundary conditions. The first one is a printed circuit heat exchanger (PCHE), which is widely used in sCO_2 test facilities. The flow passages of PCHE's are normally chemically etched into the plates before they are stacked together. Afterwards the heat exchanger block is diffusion bonded and headers as well as pipe connections are attached. A new type, the cast metal heat exchanger (CMHE), is under development at Sandia National Laboratories. The idea is derived from the concept on the

interconnectivity of the flow channels, which are used for advanced PCHE surfaces like the S-shape and airfoil fins. In the future, the CMHE type may offer similar performances like PCHE's at lower manufacturing costs and allowing more flexibility in material selection and channel geometries [26]. In the work of Nikitin et al. [27] experimental pressure drop and heat transfer investigations are performed by using a PCHE, designed and manufactured by Heatric. 12 plates with a total of 144 channels, a channel diameter of 1.9 mm and an active channel length of 1000 mm are used on the low-pressure side of the heat exchanger and 6 plates with 66 channels, a channel diameter of 1.8 mm and an active channel length of 1100 mm on the high-pressure side. During the investigations, the sCO_2 inlet temperature on the high-pressure side (65 bar - 105 bar) is adjusted from 90 °C to 108 °C and on the low-pressure side (22 bar - 32 bar) between 280 °C and 300 °C. The sCO_2 mass flow rate is similar for both sides and it is varied between 11 g/s and 22 g/s. At the Tokyo Institute of Technology (TIT), Tokyo, Japan, Ngo et al. [28] design a PCHE with advanced S-shaped fins. This heat exchanger is to replace a hot water supplier in which water is heated from 7 °C to 90 °C by using sCO_2 with a temperature of 118 °C and a pressure of 115 bar. The comparison of the two 4.6 kW heat exchangers shows that on the one hand, the compactness of the new PCHE is 3.3 times higher and on the other hand, the sCO_2 and H_2O pressure drops are lower compared to the old one. The thermal-hydraulic performance is additionally confirmed in a simplified test loop at TIT. Moreover, the thermal-hydraulic performance of PCHE's with Z-shaped fines is analyzed by Ma et al. [29], [30] and for arc-shaped fins by Lee et al. [31], [32]. In the work of Song et al. [33] experimental investigations are conducted on the heat transfer capability between sCO_2 and water in PCHE's with zigzag flow channels. Tsuzuki et al. [34] investigates a PCHE with S-shapes. The numerical results show that the PCHE with S-shaped fins has similar heat transfer performances and decreased pressure drop results compared to zigzag-shaped PCHE's. In the work of Chu et al. [35] a PCHE with straight fins, semi-circular flow channels, four hot and five cold plates is manufactured and diffusion bonded. The plates have a height of 2.2 mm, the wall thickness between two neighboring channels is 1.2 mm and the semi-circular flow channels have a radius of 1.4 mm. The overall plate length is determined at 150 mm and the width at 100 mm. After successfully passing a pressure test of up to 150 bar, the PCHE is installed in the test section and experiments are carried out. On the one hand, hot and cold water heat transfer experiments are performed, in which the mass flow rate on both sides of the PCHE is varied between 42 g/s to 306 g/s. Furthermore, heat transfer investigations with hot sCO_2 and cold water are conducted. The sCO_2 inlet mass flow rate is varied from 42 g/s to 181 g/s, the pressure from 80 bar to 110 bar and the sCO_2 inlet temperature between 37 °C

and 102 °C in order to receive measurement data under different conditions. The results show, for instance, that the heat balance between the absorbed heat of water and the released heat of sCO_2 can be re-calculated with a deviation of less than 7 %. Moreover, the Dittus-Boelter equation can be obtained on the water side of the PCHE after a correction with experimental data. Hence, the Nusselt number as well as the friction factor of water in the PCHE should be corrected with experimental results. The data analysis also shows that the achievable heat transfer from sCO_2 to water is 1.2 - 1.5 times higher than from water to water, which means that the heat transfer ability of sCO_2 is better. The CO_2 pressure dependency on the heat transfer performance is furthermore investigated.

1.3 Objectives of the work

The objectives of this work originate from the sCO2-HeRo project, in which an innovative, self-launching, self-propelling and self-sustaining decay heat removal system with supercritical CO_2 as working fluid is designed. This system should be able to transfer reliably and without the requirement of external power the decay heat from the nuclear core to an ultimate heat sink, which leads to an increase of the safety of currently operating light-water rectors in case of a combined station black-out and loss-of-ultimate-heat-sink accident scenario. A small-scale demonstrator unit is designed and attached to the PWR glass model at GfS, Essen to show the feasibility of such a system and receive experimental knowledge.

One main objective is to determine the design point parameters of the sCO2-HeRo demonstrator unit and for the sCO2-HeRo system of a nuclear power plant. Therefore, cycle calculations are performed and the design point parameters for both systems are determined with respect to maximum generator excess electricity, given boundary conditions and restrictions like minimum necessary mass flow rates and maximum achievable temperatures. To support the installation of the sCO2-HeRo demonstrator unit, a piping and instrumentation diagram is developed. It includes the main components of the sCO2-HeRo system like the compressor, the heat exchangers, the turbine, the slave electrical heater and the generator as well as valves and components for the start-up procedure like pressure vessels and the leakage pump.

The second main objective is the experimental investigation on the heat transfer capability between condensing steam and sCO_2 in diffusion bonded compact heat exchangers. The diffusion bonding technology has never been applied before to heat exchangers (HX) of such a

decay heat removal system and offers excellent opportunities to reduce the system dimensions. Furthermore, no experimental data of the pressure drop and the heat transfer performance of such heat exchangers are available for nuclear power plant conditions, especially for design point and out of design point parameters that can occur for decreasing decay power curves. Because of that, the influence of the channel dimension, the channel shape, the plenum geometry and the kind of heat input into the sCO_2 on the pressure drop and heat transfer capability is experimentally investigated within this work. Heat exchangers with rectangular 2x1 mm and 3x1 mm channels, with straight H_2O and straight sCO_2 channels as well as straight H_2O and Z-shaped sCO_2 channels, with 15 channels per plate and 1 plate on each side as well as heat exchangers with 5 channels per plate and 3/2/1 plates on each side are designed and manufactured for this purpose. The sCO_2 SCARLETT test loop and new constructed steam cycles are used for the experimental investigations. The low-pressure steam cycle generates steam similar to the steam conditions of the PWR glass model (0.3 bar, 70 °C) and the high-pressure steam cycle provides steam with a pressure of 70 bar and a temperature of 286 °C, similar to the steam conditions in a nuclear power plant. The experiments are carried out according to the determined measurement points and the obtained data are analyzed. These data are used on the one hand for the determination of the compact heat exchanger for the sCO2-HeRo demonstrator unit and on the other hand for validation of correlations and models, which are implemented into the German thermo-hydraulic code ATHLET.

Based on the results of Venker, the third main objective is to perform new sCO2-HeRo cycle simulations for the nuclear power plant application by using the ATHLET 3.1 code with advanced models, developed performance maps and validated correlations. For this purpose, performance maps of the turbo-compressor system of the small-scale sCO2-HeRo demonstrator unit are developed in consideration of received CFD data. Next, these are transferred to nuclear power plant scale using the affinity laws and afterwards they are implemented into the ATHLET code. The heat transfer capability and the control strategy of the ultimate heat sink is simulated with a developed heat transfer model. The occurring sCO_2 pressure drop and the heat transfer capability in the compact heat exchanger for the nuclear power plant application are simulated using developed models. For this purpose, the received experimental results of the single-effect experiments are used for the validation of correlations and models. In the following, these models are applied for the determined heat exchanger for the nuclear power plant application. Finally, further sCO2-HeRo cycle simulations are performed and the results are analyzed.

2 sCO_2 heat removal system

The EU-Project sCO2-HeRo applies a two-scale approach. Showing the feasibility of the sCO2-HeRo system in a first step on a small-scale, a demonstrator unit is designed, the components are manufactured and installed at the PWR glass model at GfS. The results of the single-effect experiments of each component and the results of the sCO2-HeRo demonstrator unit are used for the validation of models, correlations and performance maps. In the second step, the validated models and test results are transferred to component models and performance maps on power plant size. These advanced models and performance maps are implemented into the thermo-hydraulic code ATHLET and further simulations of the sCO2-HeRo system, attached to a NPP, are carried out.

2.1 The PWR glass model

At the start a description is given of the PWR glass model in which the sCO2-HeRo demonstrator unit is installed. It is a demonstration facility of a two loop PWR in the scale 1:10 made of glass. During training and education lectures it is also used as a visualization device for the thermal-hydraulic behaviour in the core, in steam generators and the piping. Additionally, complex thermal-hydraulic phenomena in the system are demonstrated during normal operation and for any kind of accident scenario. The main components like reactor pressure vessel, steam generators, pipes of the primary and secondary circuit, measurement devices, flanges and valves are depicted in Figure 2-1.

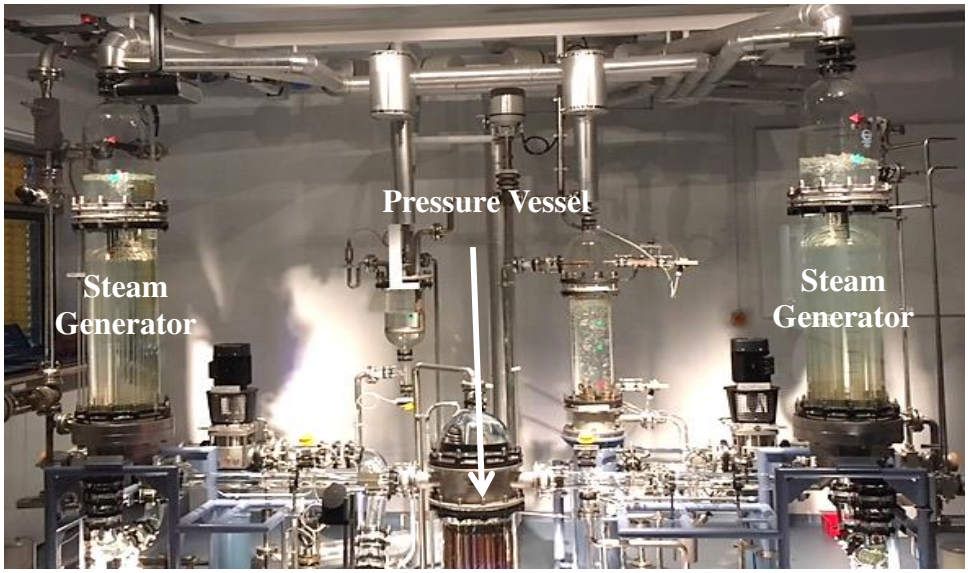

Figure 2-1: PWR glass model at GfS, Essen [65]

During normal operation, the water in the reactor pressure vessel is electrically heated with a maximum heating power of 60 kW. The hot coolant leaves the pressure vessel at the top and flows into one of the two steam generators (Figure 2-1). In the steam generator, the heat is transferred from the primary circuit to the secondary circuit with the consequence of cooling down the coolant of the primary circuit and evaporating the water of the secondary circuit. The water of the primary circuit is pumped back into the reactor pressure vessel by main coolant pumps. The steam in the secondary circuit enters an additional condenser at the ceiling where, it is condensed before it re-enters the steam generator. The pressure in the glass model is limited to about 2 bar due to internal pressure and temperature restrictions.

Since also SBO & LUHS accident scenarios can be simulated in the glass model, it is predestined for retrofitting a sCO2-HeRo demonstrator unit and showing the feasibility of such a system. The boundary conditions of the steam in the glass model during a simulated accident scenario are determined by experimental investigations [36]. The received experimental results in Table 2-1 show that the simulated decay heat power does not exceed 12 kW and that the steam temperature in the secondary circuit of the glass model is a function of the removed decay heat. This means that the steam temperature decreases if the removed decay heat is increased. In addition, the steam temperature corresponds to the steam pressure at saturation conditions in the secondary circuit, which leads for instance to a steam temperature of about 94 °C at 0.80 bar (0.0 kW), to 80 °C at 0.50 bar (3.2 kW) and 61 °C at 0.20 bar (12 kW). The steam mass flow rates in the secondary circuit can be calculated for each removed decay heat power by means of evaporation enthalpy.

Table 2-1: Experimental results at the glass model

Removed Decay Heat [kW]	Steam Temperature [°C]	Steam Pressure [bar]
0.0	93.5	0.80
0.9	90.0	0.70
1.4	88.0	0.65
2.4	83.4	0.54
3.2	79.7	0.47
4.5	74.9	0.38
5.6	71.4	0.33
6.9	67.4	0.28
9.6	63.2	0.23
12.0	60.7	0.21

Numerical investigations of the sCO2-HeRo system show furthermore, that an achievable simulated decay heat power of 12 kW and a saturated steam temperature of 61 °C are not sufficient for running several small-scale sCO2-HeRo units in parallel. According to Hacks et al. [37] a turbine inlet temperature of 200 °C and a sCO_2 mass flow rate of 0.65 kg/s are necessary for designing and manufacturing the most compact turbo-compressor-system for such application. Consequently, one sCO2-HeRo unit is determined for the PWR glass model. This system is connected to one of the two steam generators, the left one in Figure 2-1. This one is chosen due to its location near the window, with regard to the installation of the UHS outside the building. The second steam generator is separated from the cycle in case of a simulated SBO & LUHS accident scenario.

2.2 sCO2-HeRo system

In case of a combined SBO & LUHS accident scenario in a NPP, plant accident measures strongly depend on the availability of external power. If this is not guaranteed, the reactor core can be violated if no other cooling measures will be successful. Such accident scenarios lead to the development of a self-launching, self-propelling and self-sustaining decay heat removal system, called sCO2-HeRo. The system is independent from external energy but fulfills the safety function of transferring the decay heat from the reactor core to an ultimate heat sink, e.g. the ambient air. A scheme of the sCO2-HeRo system is shown in Figure 2-2. The main components are a turbo-compressor-system (TCS), a compact heat exchanger (CHX) and an air-cooled heat exchanger, called ultimate heat sink (UHS). The TCS consists of a turbine, a compressor and a generator, which are mounted at one shaft. During normal operation, the working fluid enters the compressor (1), where it is compressed and simultaneously compression-heated before it flows into the compact heat exchanger (2). In the CHX, the heat is transferred from the primary to the secondary side, leading to steam condensation and heating-up of the working fluid (Q_{in}). In the following, the working fluid enters the turbine (3) and is expanded. Before re-entering the compressor, it flows through the ultimate heat sink (4), in which it is cooled down (Q_{out}) to compressor inlet conditions. Since the turbine produces more power than is used for the compression work, excess electricity (P_{el}) can be generated in the generator for the air-fans of the UHS and for any kind of auxiliary devices in the NPP.

In fact, the sCO2-HeRo system (Figure 2-2) is a simple Brayton cycle without any recompression and recuperation because the main objective is to build a robust and self-sustaining system, which transfers the decay heat reliably from the reactor core to an ultimate heat sink. On the one hand, sCO_2 is chosen as working fluid due to his fluid properties (Appendix A), which allows designing compact components. This is especially important for the CHX, connecting the steam generator of the NPP with the sCO2-HeRo cycle, because of space limitations in containments. On the other hand, achievable cycle efficiencies as well as moderate temperatures and pressures of CO_2 near the critical point are promising for closed clockwise thermodynamic power cycles [39], [71], [73]. The Massachusetts Institute of Technology (MIT) conducts in 2004 a study, in which the feasibility of CO_2 as working fluid is investigated [38]. The results show cycle efficiencies of up to 45 % for heat source temperatures of 600 °C. Taken into account the results of MIT, Sandia National Laboratory [39] build-up a test facility for the investigation of sCO_2 as working fluid for high-temperature nuclear power plant applications. Due to his advantageous cycle efficiencies, CO_2 as an alternative working fluid for conventional steam power generation cycles is examined for instance by Angelino [66], [67], [68] and Feher [69]. Both investigate supercritical, subcritical and gaseous CO_2 power cycles. One major advantage of sCO_2 cycles for power generation, compared to partly supercritical or overheated cycles, is the relatively low compression work caused by the high density of the working fluid near the critical point [74]. A decreased compression work in combination with a constant expansion work leads to increased generator excess electricity. Compared to the steam Rankine cycle the sCO_2 Brayton cycle is additionally less complex and more compact, leading to lower investment and maintenance costs [72], [73]. Besides that, also low-temperature applications with CO_2 are of interest. For instance, Venker [15] investigates a decay heat removal system for a NPP with heat source temperatures of 280 °C.

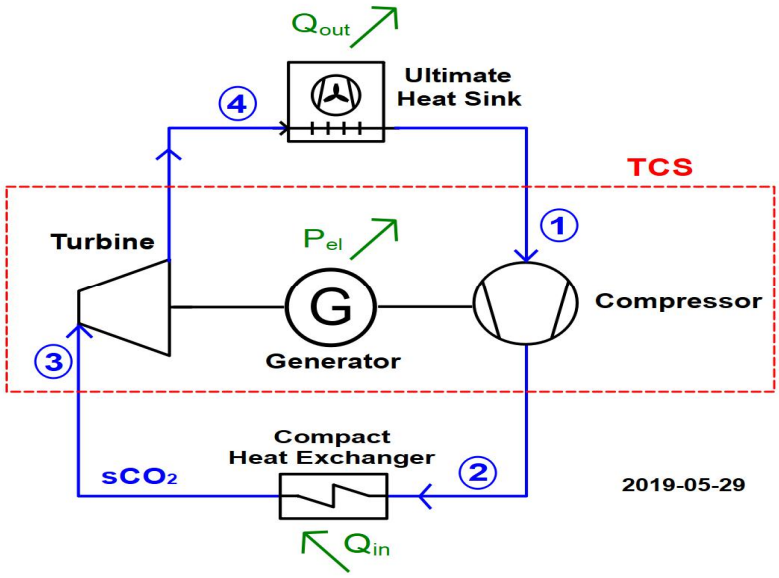

Figure 2-2: Scheme of sCO2-HeRo system

The sCO2-HeRo system for the PWR glass model

A schematic drawing of the small-scale sCO2-HeRo demonstrator unit, attached to the steam generator of the PWR glass model is shown in Figure 2-3. At the start of a simulated SBO & LUHS accident scenario, solenoid valve I is closed and solenoid valve II is opened automatically, establishing a natural circulation-driven cooling loop in the primary loop, marked in red (Figure 2-3). Driven by natural convection, the steam flows upwards into the compact heat exchanger (IV) located above the steam generator, where the heat is transferred to the sCO_2 and thereby the steam is condensed. The condensate flows downwards, driven by gravity, and re-enters the steam generator of the glass model through the feedwater line. The latent heat of the steam heats up the sCO_2 on the secondary side of the CHX (2→3'), located in the building. Afterwards, it flows into a slave electrical heater (SEH), which is only used for the PWR glass model application because of the given boundary conditions like a pressure of less than 2 bar, a steam temperature of less than 94 °C and a simulated decay heat power of less than 12 kW. In the SHE (IV') the sCO_2 temperature at the inlet of the turbine (III) can be conditioned to a defined temperature. Moreover, it can be also used for out of design point experiments by adjusting the electrical heating power, which leads to different sCO_2 temperatures at the inlet of the turbine. Besides that, experiments even without the glass model can be carried out using the SHE. This enables the most flexible operation of the sCO2-HeRo cycle. After heating up the sCO_2 in the CHX and the SEH (3'→3), it enters the turbine (III),

where it is expanded (3→4) and then cools down to a defined temperature (4→1) in an air-cooled gas cooler (V) called ultimate heat sink and located at the outdoor area. Air-fans at the UHS are intended to improve the heat transfer capability between the gas-cooler and the ultimate heat sink, the ambient air. After cooling down the sCO_2 it flows back into the compressor where it is compressed (1→2) before it re-enters the CHX. If the turbine (III) produces more power than it is used in the compressor (I), the system will be self-sustaining and the generated excess electricity at the generator (II) can be used e.g. for the power supply of the electrical driven air-fans of the UHS and for any kind of auxiliary devices in the NPP.

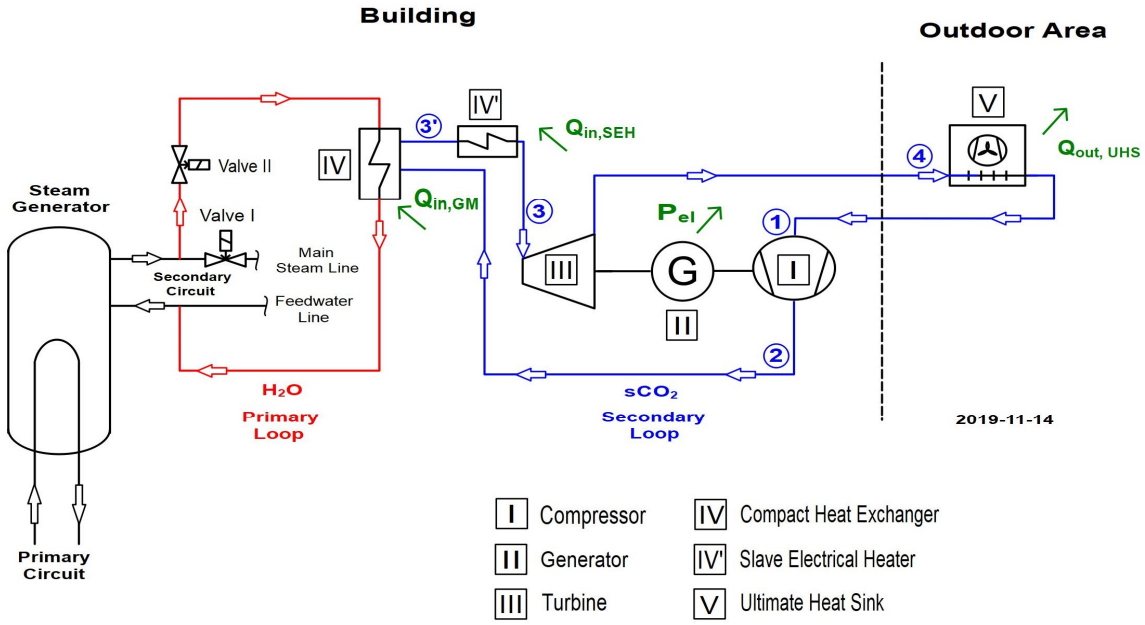

Figure 2-3: Scheme of the sCO2-HeRo system for PWR glass model

To support the construction of the sCO2-HeRo demonstrator unit, a detailed piping and instrumentation (P&I) diagram is developed (Appendix B). It includes all components of the main sCO2-HeRo system, components for start-up procedures, measurement devices and measurement positions. Different kind of valves, e.g. needle valves, spring actuated valves and check valves, are installed in the cycle for safety reasons, for start-up procedures and for control purposes. Moreover, there are measurement points located upstream and downstream of each component, which are necessary to monitor the cycle behavior during operation and to obtain experimental data. These data can be used, for instance, to validate turbine and compressor efficiencies as well as pressure drop and heat transfer correlation for the working fluid sCO_2.

For the control strategy of the cycle, it is also advantageous to have plenty of measurement positions and measurement devices that provide a whole range of measurement data as input parameters for the control system. This high density of measurement devices also provides the possibility to compare the results with each other and to gain information about the quality of measurement device calibration. Moreover, a unique nomenclature similar to that of the glass model is introduced. Each component and measurement device is clearly defined by the nomenclature, which consists of two blocks with letters and numbers, separated by one blank. The nomenclature as well as a detailed description is given in [36]. For reasons of clarity the entire sCO2-HeRo set-up is divided into 8 sections according to Appendix B.

Figure 2-4 shows a scheme of section 1 and section 2. Section 1 presents the main sCO2-HeRo cycle, which is marked with blue and red pipes. The red high-pressure side includes the compressor, the compact heat exchanger, the slave electrical heater and the turbine. The low-pressure side is marked with blue pipes and includes the turbine, the ultimate heat sink and the compressor. Temperature (T), pressure (p), mass flow rate (F) and density (ρ) measurement devices as well as different kinds of valves are installed to obtain measurement data and for control purposes. The blue dashed line marked with number 2 (Figure 2-4) depicts the generator unit of the turbo-compressor-system, which is monitored by a FAG-Smart-Check for measuring the frequency and a frequency converter. The frequency converter controls the mechanical load (M), the revolution speed (n), the excess electricity (P) and the temperature (T) at the generator, according to Hacks et al. [40]. The electricity supply for the frequency converter and for the FAG-Smart-Check is controlled with voltage (U) and electrical current (I) measurement devices. To reduce friction losses in the generator and to prevent any kind of damage in the bearings of the TCS due to high pressure, there is the possibility to have a defined sCO_2 leakage flow in the housing of the TCS [37]; [40], marked with grey pipes. The leakage flow and the corresponding pressure in the housing can be adjusted by the revolution speed of the leakage pump and the installed valves. For monitoring the bearing temperatures and the vibration of the shaft four temperature (T) und two vibration measurement devices (f) are installed.

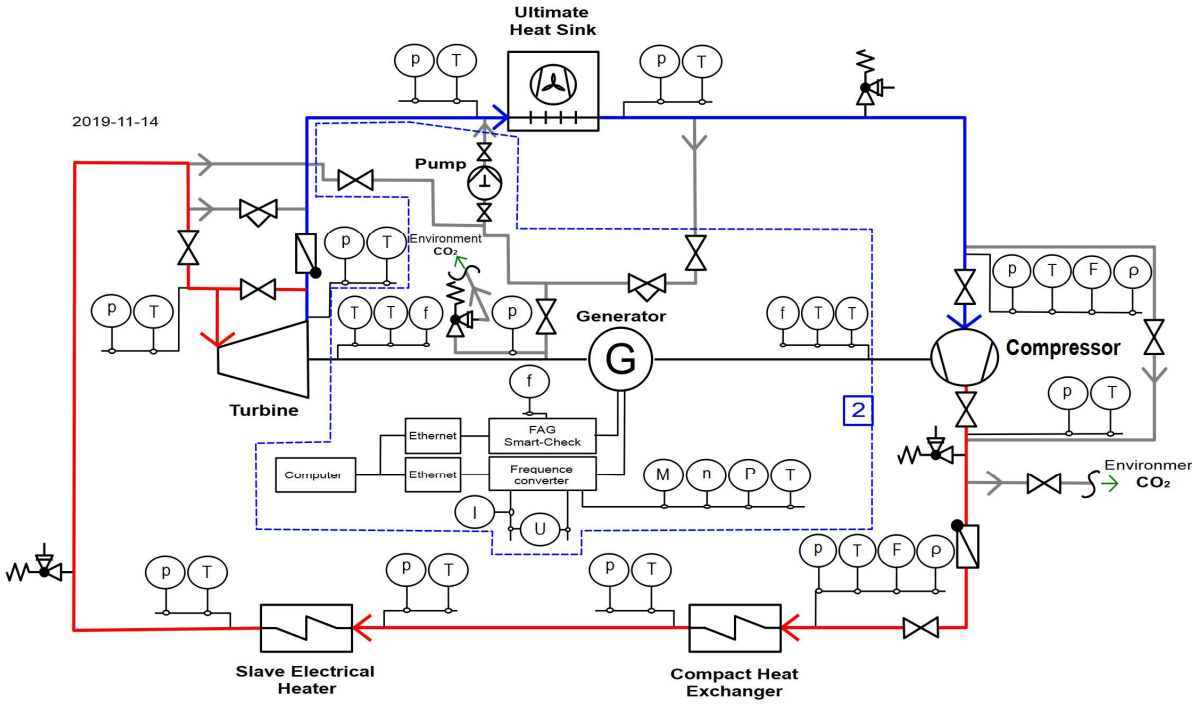

Figure 2-4: Scheme of section 1 and 2 of the sCO2-HeRo cycle

The turquoise dashed line on the left in Figure 2-5 shows section 3, the slave electrical heater, designed and manufactured by ELMESS [41]. The heat input from the SEH into the sCO_2 is controlled and monitored with the measured voltage (U) and current (I) values. Three temperature measurements (T) at the SEH are used for limiting the electrical heating power because of internal temperature restrictions. The heat input into the sCO_2 can be realized in two ways. The first one is by adjusting a constant electrical heat power with fixed voltage and electrical current values and the second one is by means of controlling them via a master-slave controller. In the master-slave configuration the electrical heating power is adjusted according to the heat input from the compact heat exchanger, which means that an increased heat input at the CHX leads to an increased electrical heating power of the SEH. The air side of the ultimate heat sink is shown on the right in Figure 2-5, marked with a yellow dashed line and numbered with 4. The air temperature (T) is measured on both sides of the UHS and the pressure (p) as well as the mass flow rate (F) are measured at the inlet. Since the heat removal to the UHS is supported by electrical driven fans, voltage (U) and current values (I) can be adjusted and monitored. An increasing revolution speed of the fans leads to increasing heat transfer capabilities in the UHS.

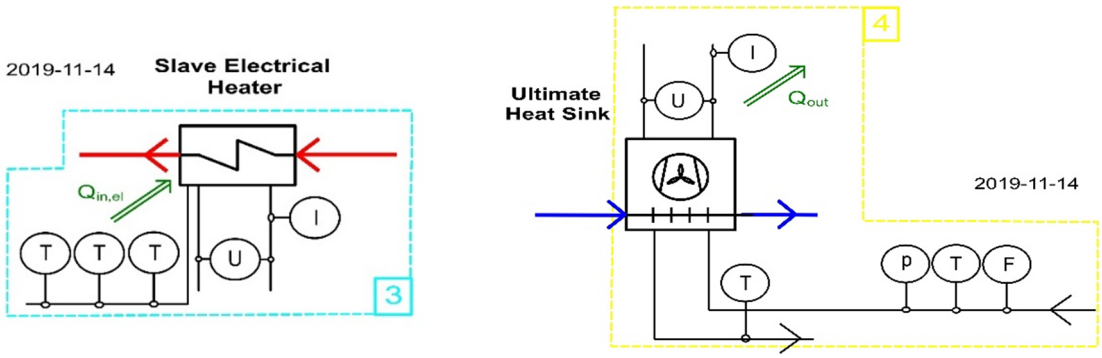

Figure 2-5: Scheme of section 3 and 4 of the sCO2-HeRo cycle

On the left in Figure 2-6, section 5 shows the steam side of the CHX, marked with a purple dashed line. Measurement devices for measuring the pressure (p) and temperature (T) are installed at the inlet and outlet of the CHX. The steam mass flow rate (F) is monitored at the inlet of the CHX. The two needle valves at the inlet and outlet of the CHX on the steam side are used for connecting or disconnecting the CHX from the PWR glass model. One start-up and pressure control possibility of the sCO2-HeRo demonstrator unit is shown in section 6, marked with a green dashed line (on the right in Figure 2-6) [40], [75], [76]. The sCO_2 conditions in the lower chambers of the piston pressure vessels I and II are measured with pressure gauges (p) and thermocouples (T). It is assumed that in case of an initiated start-up procedure the needle valve at the bottom of pressure vessel I will be opened and due to the adjusted pressure difference between the main cycle and the pressure vessel the fluid is forced to flow into the sCO_2-HeRo cycle. It is heated in the CHX and in the slave electrical heater before entering the turbine, where it forces the turbine to start rotating. After the expansion in the turbine, it flows through the UHS before it is subdivided into two parts. One part of the sCO_2 mass flow rate enters the lower chamber of pressure vessel II and the other part bypasses the compressor and re-enters the CHX. After reaching break-even point, the pistons in pressure vessel I and II come up to defined levels and the TCS is self-sustaining. The amount of sCO_2 mass flow rate as well as the pressure on the high pressure and low pressure side of the cycle can be controlled and adjusted by varying the nitrogen pressure in the upper chambers of pressure vessel I and II. To avoid any kind of mechanical overloads in both vessels, spring load safety valves are mounted at the top of the nitrogen chambers.

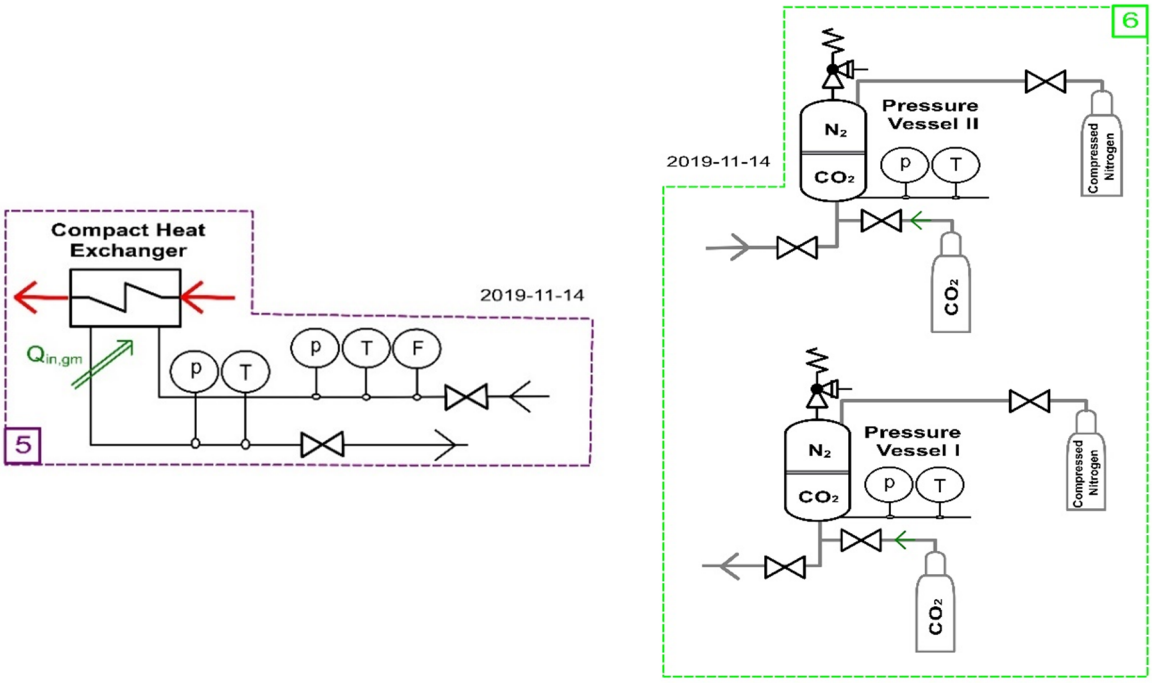

Figure 2-6: Scheme of section 5 and 6 of the sCO2-HeRo cycle

Before starting operation, the sCO_2-HeRo cycle has to be evacuated and filled with CO_2. The evacuation is performed by the vacuum-pump unit, marked with a black dashed line, numbered with 8 and shown on the right in Figure 2-7. For this, the needle valve has to be opened at the beginning of the evacuation process and closed afterwards. After evacuating the cycle, it is filled with CO_2 by using the blue marked filling-unit of section 7, which is shown on the left in Figure 2-7. To reduce the chance of freezing, in the first step gaseous CO_2 is filled into the cycle followed by filling with liquid CO_2 until the calculated amount of CO_2 is reached [40]. Currently the crossed-out needle valve and the CO_2-Pump are not installed.

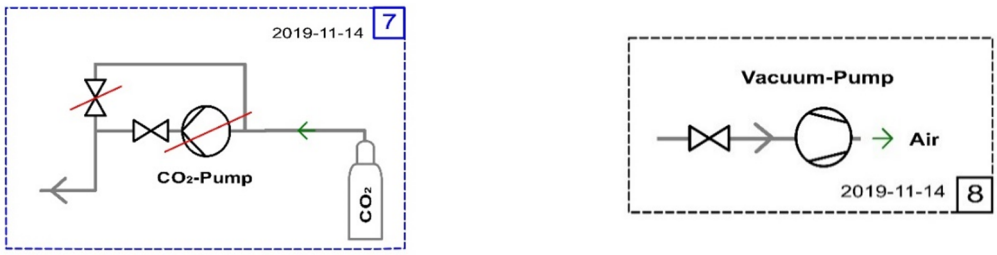

Figure 2-7: Scheme of section 7 and 8 of the sCO2-HeRo cycle

Table 2-2: Components of the sCO2-HeRo system

Component	Manufacturer / Vendor
Compact Heat Exchanger	University of Stuttgart
Compressor	University of Duisburg-Essen
FAG-Smart-Check	Schaeffler Technologies AG & Co. KG
Frequency Converter	Vogelsang Elektromotoren GmbH
Generator	E+A Elektrotechnik und Aggregatebau mbH
Mass Flow Meters	Endress & Hauser Messtechnik GmbH & Co. KG
Pressure Gauges	ES Electronic Sensor GmbH
Pressure Vessel I	Roth Hydraulics GmbH
Pressure Vessel II	Roth Hydraulics GmbH
Pump	Speck-Triplex-Pumpen GmbH & Co. KG
Slave Electrical Heater	Elmess Thermosystemtechnik
Stainless Steel Pipes	Swagelok
Thermal Resistance Thermometers	ES Electronic Sensor GmbH
Turbine	University of Duisburg-Essen
Ultimate Heat Sink	Güntner AG & Co. KG
Vacuum-Pump	Available at the glass model
Valves	Swagelok
Vibration Sensors	Kistler Instrumente GmbH

The components of the sCO2-HeRo demonstrator unit are either manufactured or purchased. The TCS with integrated generator is designed, manufactured and experimentally investigated at the University of Duisburg-Essen (UDE), for instance. The compact heat exchanger is designed, manufactured and testes at the University of Stuttgart (USTUTT). The gas-coolers of the ultimate heat sink are purchased and investigated at the Research Centre Rez, Prague. The slave electrical heater, the pressure vessels for the start-up procedure, the stainless steel pipes as well as the spring-actuated overflow valves, check valves, safety-shut-down valves and pressure-control valves are purchased. Also the piezo-resistive pressure transmitters, resistance thermometers, volt- and ampere meters, mass flow meters, frequency converters, FAG Smart-Checks, electric cables, installation materials, isolating materials, pumps, CO_2, nitrogen, etc. are purchased from different suppliers. After the delivery of all components the system is built in consideration of the P&I diagram (Appendix B) and commissioning tests are performed. The most important components are summarized in Table 2-2 in alphabetical order.

The sCO2-HeRo system for the nuclear power plant

A scheme of the sCO2-HeRo system, attached to the steam generator of a nuclear pressure water reactor, is shown in Figure 2-8. During normal operation in a PWR, the heat power from the nuclear core is transferred to the steam generator from the primary circuit to the secondary circuit. The transferred heat power generates steam in the secondary circuit, which flows through the main steam line to the turbine, in which it is expanded and condensed before it re-enters the steam generator via the feedwater line. In case of a combined SBO & LUHS accident scenario, the reactor is automatically scrammed and the main coolant pumps as well as the turbine are switched off. To prevent any kind of core damage due to uncontrolled heating processes, the decay heat must be transferred reliably from the reactor core to the ultimate-heat-sink. The amount of the decay heat right after shutdown of the reactor is approximately 6 % of the nominal thermal power and decreases exponentially as a function of the time [10]. Comparing the schemes of the sCO2-HeRo demonstrator unit (Figure 2-3) and the sCO2-HeRo system for the NPP (Figure 2-8), it can be seen that both systems are quite similar. Only the SEH is no longer used in the nuclear power plant application because the amount of decay heat, the steam pressure and the corresponding steam temperature are sufficient for designing a self-sustaining decay heat removal system.

Similar to the glass model procedure, at the initiating accident scenario the solenoid valve I is closed and solenoid valve II is opened automatically, establishing a natural circulation driven cooling loop in the primary loop, marked in red (Figure 2-8). Driven by natural convection, the steam flows upwards into a CHX (IV), where the heat is transferred to the sCO_2 and the steam is condensed. The condensate flows downwards and re-enters the steam generator through the feedwater line. The latent heat of the steam heats up the sCO_2 on the secondary side of the CHX (2→3), located in the containment. After heating up the sCO_2 it enters the turbine (III) in the reactor building, where it is expanded (3→4), followed by cooling down (4→1) in an air-cooled gas cooler (V) called ultimate heat sink and located at the outdoor area, to a defined temperature. Air-fans at the UHS are intended to improve the heat transfer capability between the gas-cooler and the UHS, the ambient air. After cooling down the sCO_2 it flows back into the compressor, where it is compressed (1→2) before it re-enters the CHX. If the turbine (III) produces more power than is used in the compressor (I), the system will be self-sustaining and the excess electricity at the generator (II) can be used e.g. for the power supply of the electrical driven air-fans of the UHS and for any kind of auxiliary devices in the nuclear power plant.

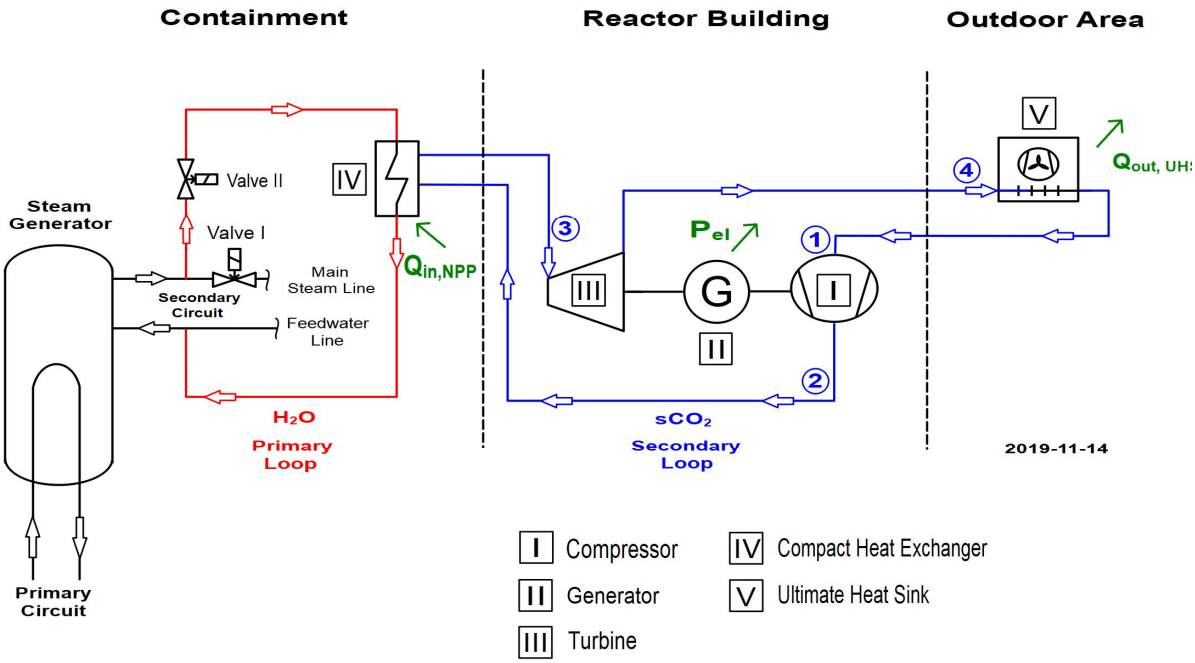

Figure 2-8: Scheme of the sCO2-HeRo system for NPP

2.3 sCO2-HeRo cycle calculations

After a detailed description of the sCO2-HeRo set-up for the PWR glass model and for the NPP, the cycle parameters of both sCO2-HeRo systems are determined in this chapter. For this purpose, cycle calculations are carried out and the design point parameters are determined with respect to maximum generator excess electricity.

sCO2-HeRo cycle calculations for the PWR glass model

Boundary conditions

The boundary conditions on the steam and sCO_2 side are summarized in Table 2-3. The achievable simulated decay heat power in the PWR glass model is determined by experiments, according to chapter 2.1. The results show firstly that the higher the heat removal from the condenser, the lower is the pressure in the steam generator and secondly that the simulated decay heat power does not exceed 12 kW, which is not suitable for operating more than one sCO2-HeRo loop at the glass model. In consideration of the experimental data, in which a higher transferred heat power decreases the driving temperature difference across the CHX and a lower power remove leads to a very small simulated decay heat power, as a compromise the design point for the simulated decay heat power is determined at 6 kW. This leads to a saturated

steam temperature of about 70 °C and a pressure of about 0.3 bar in the steam generator. In addition, starting from that point, there is also the possibility to perform off-design point experiments with varying simulated decay heat powers.

The boundary conditions on the sCO_2 side must be also considered. For instance, the pressure and temperature at the inlet of the compressor are the values close to the critical point in the entire sCO2-HeRo cycle. During operation it must be guaranteed that the inlet conditions are always above the critical point, which leads to a minimum pressure of about 74 bar and a minimum temperature of 31 °C. To reduce the complexity and to increase the robustness of the system, a single stage compressor with a pressure ratio of about 1.5 is chosen [37], [70]. It can compress the sCO_2 from the low-pressure side to a pressure of about 120 bar on the high-pressure side. To prevent any kind of manufacturing problems of the TCS due to very small components like the impellers, the minimum necessary sCO_2 mass flow rate is set to 0.65 kg/s. The electrical heating power of the SEH is determined, with respect to the accessible electrical installation power, at 200 kW. This is sufficient for heating up the sCO_2 mass flow rate to a turbine inlet temperature of 200 °C, which is similar to NPP conditions. The turbine efficiency of 75 % and the compressor efficiency of 65 % are conservative assumptions for such a small machine from the colleagues from University of Duisburg-Essen (UDE) and they are assumed to be constant for the entire range of cycle calculations.

Table 2-3: Boundary conditions - cycle calculations glass model

Variable	Value	Unit	Description
$Q_{in,GM}$	6	kW	Decay Heat Power Per Unit - Glass Model
p_{H2O}	0.3	bar	Pressure - Steam
T_{H2O}	70	°C	Temperature - Steam
$Q_{in,SEH}$	200	kW	Heating Power - SEH
$p_{CO2,min}$	74	bar	Pressure - Minimum sCO_2
$p_{CO2,max}$	120	bar	Pressure - Maximum sCO_2
$T_{CO2,min}$	31	°C	Temperature - Minimum sCO_2
$\dot{m}_{CO2,min}$	0.65	kg/s	Mass Flow Rate - Minimum sCO_2
$\eta_{C,is}$	0.65	%	Isentropic Efficiency - Compressor
$\eta_{T,is}$	0.75	%	Isentropic Efficiency - Turbine
N	1	-	Number of sCO2-HeRo Demonstrator Units

Cycle calculations

A scheme of the sCO2-HeRo demonstrator unit, attached to the PWR glass model, is shown on the left and the corresponding temperature-entropy (T-S) diagram on the right in Figure 2-9. The main components are numbered with I, II, III, IV, IV', V and the thermodynamic state in front and behind of each component with 1, 2, 3, 3' and 4.

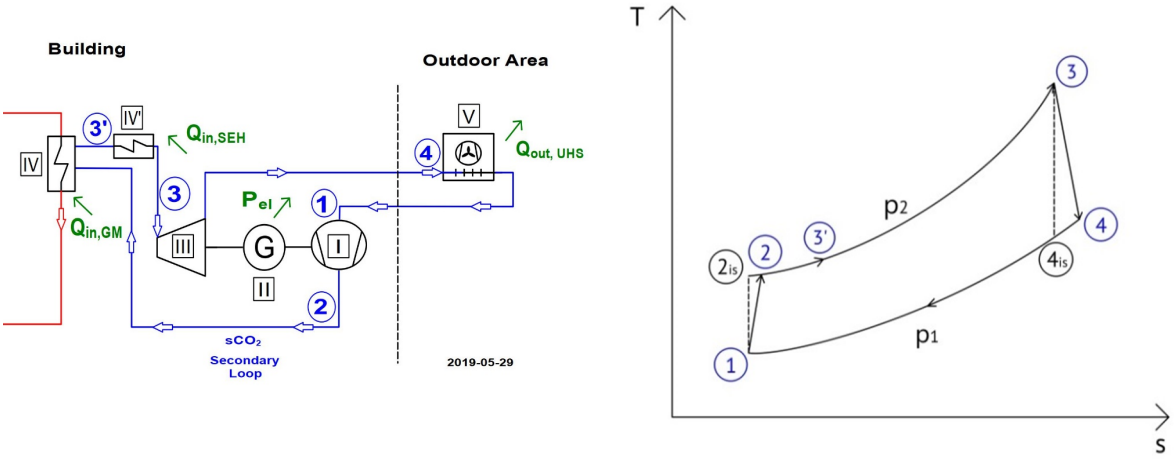

Figure 2-9: Scheme of the sCO2-HeRo system for GM and T-S diagram

For the cycle calculations it is necessary to specify the compressor inlet pressure p_1, the compressor inlet temperature T_1, the isentropic compressor efficiency $\eta_{C,is}$ and the isentropic turbine efficiency $\eta_{T,is}$. Required thermo-physical fluid properties are obtained from the database NIST Refprop [43].

The calculation starts at point 1 in the T-S diagram (Figure 2-9), where the thermodynamic state is already defined by the selected pressure p_1 and temperature T_1. The enthalpy h_1 (Eq. (2-1)) and entropy s_1 (Eq. (2-2)) at the inlet of the compressor (I) are functions of the pressure p_1 and temperature T_1. Both are calculated with NIST Refprop.

$$h_1 = f(p_1, T_1) \tag{2-1}$$

$$s_1 = f(p_1, T_1) \tag{2-2}$$

The enthalpy h_2 and temperature T_2 at the outlet of the compressor (I) are calculated by Eq. (2-3) and Eq. (2-4). The used isentropic enthalpy h_{2is} is calculated with Refprop as a function of the determined pressure p_2 on the high pressure side and the entropy s_{2is} by Eq. (2-5). It is assumed that the entropy s_{2is} is equal to s_1 (Eq. (2-6)).

$$h_2 = \frac{h_{2is} - h_1}{\eta_{C,is}} + h_1 \tag{2-3}$$

$$T_2 = f(p_2, h_2) \tag{2-4}$$

$$h_{2is} = f(p_2, s_{2is}) \tag{2-5}$$

$$s_{2is} = s_1 \tag{2-6}$$

The enthalpy h_3 at the inlet of the turbine (III) is calculated according to Eq. (2-7) as a function of the turbine inlet pressure p_3 and the determined turbine inlet temperature T_3. It is assumed that no pressure drop occurs in the CHX (IV) and in the SHE (IV'), hence p_3 is equal to p_2 (Eq. (2-8)). Furthermore, the sCO_2 heat input occurs in two steps, firstly from the CHX into the sCO_2 ($h_2 \rightarrow h_{3'}$) and secondly from the SEH into the sCO_2 ($h_{3'} \rightarrow h_3$). The entropy s_3 at the inlet of the turbine is a function of the pressure p_3 and the temperature T_3 according to Eq. (2-9).

$$h_3 = f(p_3, T_3) \tag{2-7}$$

$$p_3 = p_2 \tag{2-8}$$

$$s_3 = f(p_3, T_3) \tag{2-9}$$

The enthalpy h_4 and temperature T_4 at the outlet of the turbine are calculated by Eq. (2-10) and Eq. (2-11). The used isentropic enthalpy h_{4is} is calculated by Eq. (2-12) as a function of the pressure p_4 and the entropy s_{4is}. It is assumed that the pressure p_4 is equal to the compressor inlet pressure p_1 (Eq. (2-13)), which means that no pressure drop occurs in the UHS (V) and that the entropy s_{4is} is equal to the entropy s_3 (Eq. (2-14)).

$$h_4 = h_3 - (h_3 - h_{4is}) \cdot \eta_{T,is} \tag{2-10}$$

$$T_4 = f(p_4, h_4) \tag{2-11}$$

$$h_{4is} = f(p_4, s_{4is}) \tag{2-12}$$

$$p_4 = p_1 \tag{2-13}$$

$$s_{4is} = s_3 \tag{2-14}$$

According to an energy balance, the excess power of the cycle is the difference between turbine and compressor work multiplied by the mass flow rate $\dot{m}$. Assuming a generator efficiency of 100 %, the excess electricity P_{el} can be calculated by Eq. (2-15).

$$P_{el} = \dot{m} \cdot ((h_3 - h_4) - (h_2 - h_1)) \tag{2-15}$$

Within the cycle calculations, a parameter study is conducted with varying cycle parameters like the turbine inlet pressure p_3, the turbine inlet temperature T_3, the mass flow rate $\dot{m}$, the temperature at the inlet of the compressor T_1 and the pressure at the inlet of the compressor p_1. Moreover, the number of TCS for parallel use depends on the required operational time of the sCO2-HeRo system, the existing amount of decay heat power and the determined sCO_2 mass flow rate. Several turbo-machine sets in parallel give the opportunity to shut down one after another while the decay heat is decreasing. In consideration of the given boundary conditions at the glass model, like a decay heat power of 6 kW and a sCO_2 mass flow rate of 0.65 kg/s, the calculations are performed only for one sCO2-HeRo unit.

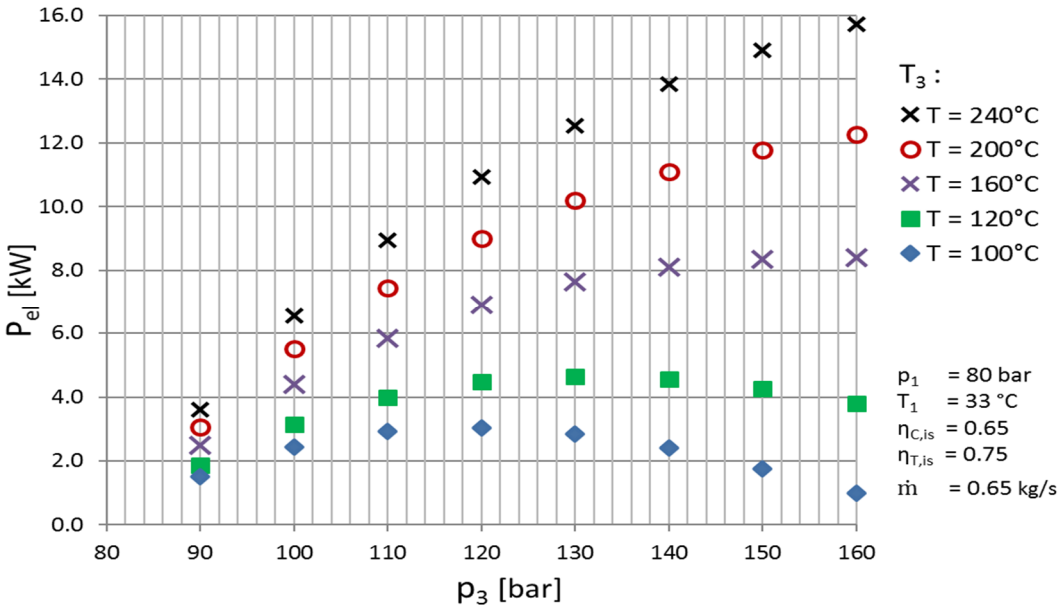

Figure 2-10: Cycle calculation results - Glass model

As an example, cycle calculation results of the generator excess electricity P_{el} are shown in Figure 2-10 as a function of the turbine inlet pressure p_3 and turbine inlet temperature T_3. A constant compressor inlet pressure p_1, compressor inlet temperature T_1, sCO_2 mass flow rate $\dot{m}$, turbine efficiency $\eta_{T,is}$ and compressor efficiency $\eta_{C,is}$ are assumed for these calculations. In addition, it is assumed that there are no pressure losses and heat losses. The results of the excess power P_{el} show similar tendencies for varying turbine inlet temperatures T_3 and turbine inlet pressures p_3. In general, it can be seen that firstly for a constant turbine inlet temperature T_3 the generator excess electricity P_{el} increases until a maximum is reached and afterwards it decreases again with increasing pressures p_3, secondly that the maximum generator excess electricity P_{el} is shifted towards higher pressures p_3 for increasing turbine inlet temperatures T_3, and thirdly that the generator excess electricity P_{el} increases for increasing turbine inlet temperatures T_3 and a constant turbine inlet pressure p_3. For instance, for a turbine inlet temperature of 100 °C, the generator excess electricity increases from about 1.5 kW at 90 bar to 3 kW at 120 bar before it decreases again to 1 kW at 160 bar. This can be explained by the higher increase in the compression work compared with the increase in turbine work, leading to decreasing generator excess electricity P_{el} for pressures higher than 120 bar. Moreover, a turbine inlet pressure of 120 bar and a turbine inlet temperature of 100 °C leads to a excess electricity of 3 kW and 200 °C leads to 9 kW. This can be explained by nearly constant compressor work and increasing turbine work, due to higher turbine inlet temperatures.

In consideration of the boundary conditions (Table 2-3) and the cycle calculation results, the design point parameters of the sCO2-HeRo demonstrator are determined (Table 2-4). The compressor inlet pressure p_1 and inlet temperature T_1 are set to 78.3 bar and 33 °C, with respect to their location near the critical point (74 bar / 31 °C). The installed electrical heating power of the SEH with 200 kW and the comparability with NPP conditions leads to a turbine inlet temperature T_3 of 200 °C. For heating up the sCO_2 mass flow rate $\dot{m}$ of 0.65 kg/s from about 49 °C at the outlet of the CHX, to 200 °C at the inlet of the turbine, an electrical heating power of about 196 kW is used. With respect to the achievable compression ratio of the single-stage compressor, the turbine inlet pressure p_3 is set to 117.45 bar. The compressor efficiency $\eta_{C,is}$ and the turbine efficiency $\eta_{T,is}$ of 0.65 and 0.75 are conservative assumptions for such small engines. A cooling power of about 187 kW is necessary to cool down the sCO_2 mass flow rate in the UHS. In the design point, the generator provides an excess electricity P_{el} of about 9 kW.

Table 2-4: sCO2-HeRo cycle parameters for the PWR glass model

Variable	Value	Unit	Description
p_1	78.3	bar	Pressure - Inlet Compressor
T_1	33.0	°C	Temperature - Inlet Compressor
$\eta_{C,is}$	65	%	Isentropic Efficiency - Compressor
p_3	117.45	bar	Pressure - Inlet Turbine
T_3	200.0	°C	Temperature - Inlet Turbine
$\eta_{T,is}$	75	%	Isentropic Efficiency - Turbine
$\dot{m}$	0.65	kg/s	Mass Flow Rate - sCO_2
$Q_{in,SEH}$	195.56	kW	Heat Input - SEH
$Q_{out,UHS}$	186.83	kW	Heat Output - UHS
P_{el}	8.7	kW	Excess Electricity - Generator
$Q_{in,GM}$	6	kW	Heat Input - Glass Model

sCO2-HeRo cycle calculations for a NPP

Boundary conditions

The boundary conditions for the sCO2-HeRo cycle calculations are summarized in Table 2-5. The simulation results of Venker [10] for a BWR with a thermal power of 3860 MW show for instance that 60 MW decay heat must be removed by the sCO2-HeRo cycle in order to achieve a long-term coolability of the nuclear core and to prevent any kind of depressurization. Any surplus decay heat occurring right after shut-down is stored additionally inside the condensation chamber. Moreover, saturated steam conditions with a steam pressure of 70 bar and a corresponding steam temperature of 286 °C are assumed. Furthermore, a minimum temperature difference of 5 °C is defined for both heat exchangers to ensure an efficient heat transfer. The temperature of the ambient air is conservatively set to 37 °C.

Table 2-5: Boundary conditions - cycle calculations NPP

Variable	Value	Unit	Description
$Q_{in,NPP}$	15	MW	Decay Heat Power Per Unit - NPP
p_{H2O}	70	bar	Pressure - Steam
T_{H2O}	286	°C	Temperature - Steam
$p_{CO2,min}$	75	bar	Pressure - Minimum sCO_2
$p_{CO2,max}$	200	bar	Pressure - Maximum sCO_2
$T_{CO2,min}$	42	°C	Temperature - Minimum sCO_2
$T_{CO2,max}$	281	°C	Temperature - Maximum sCO_2
$\eta_{C,is}$	0.75	%	Isentropic Efficiency - Compressor
$\eta_{T,is}$	0.85	%	Isentropic Efficiency - Turbine
N	4	-	Number of sCO2-HeRo Units

These boundary conditions lead to a minimum sCO_2 temperature of 42 °C at the outlet of the UHS and a maximum sCO_2 temperature of 281 °C at the inlet of the turbine. The minimum sCO_2 pressure at the inlet of the compressor is set to 75 bar, with respect to its location near to the critical point. Furthermore, an isentropic turbine efficiency $\eta_{T,is}$ of 0.85, an isentropic compressor efficiency $\eta_{T,is}$ of 0.75 and a compression ratio of 3 are assumed. Venker also recommends that the amount of removed decay heat should be adjusted according to the existing decay heat in order to ensure a high temperature difference between the ambient air

and the primary steam, which results in increased operational time of the sCO2-HeRo system. This is realized by using four equal 15 MW sCO2-HeRo units in parallel, instead of one 60 MW unit, which can be individually controlled and switched off consecutively. In addition, four sCO2-HeRo units can be build as physically separated units inside an NPP, which is an advantage in case of accident scenarios like fire and mechanical impacts.

Cycle calculations

A scheme of a 15 MW sCO2-HeRo unit is shown on the left in Figure 2-11 and the T-S diagram on the right. The main components are numbered with I, II, III, IV, V and the thermodynamic state in front of and behind each component with 1, 2, 3 and 4. Comparing the schemes of the demonstrator (Figure 2-9) and the system for a NPP (Figure 2-11) it can be seen that both are quite similar. Only the SEH (IV') is no longer used in the NPP, because the amount of decay heat and the steam temperature are high enough for the self-sustaining of the sCO2-HeRo.

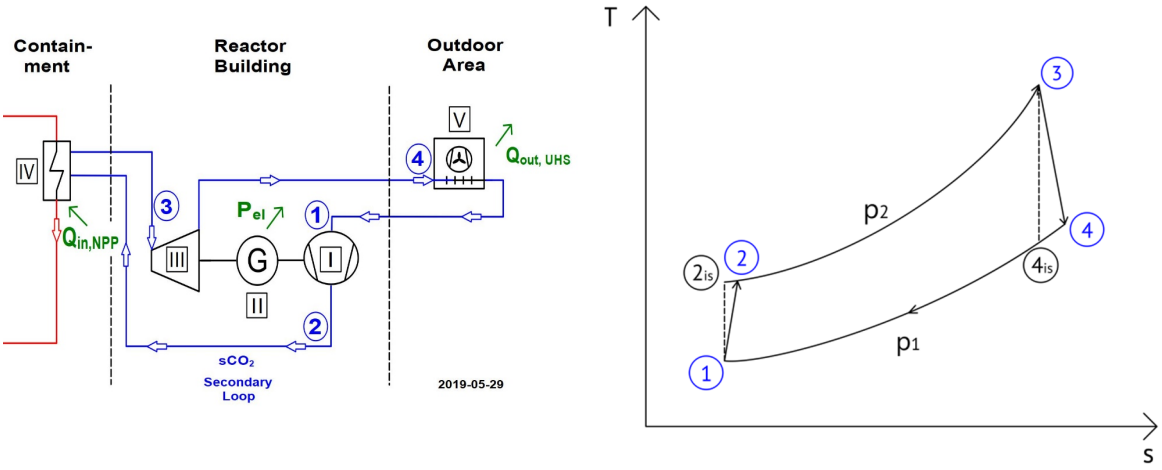

Figure 2-11: Scheme of the sCO2-HeRo system for NPP and T-S diagram

The cycle calculations are carried out similar to those of the sCO2-HeRo demonstrator unit, just without the SEH. It must be mentioned that a constant sCO_2 mass flow rate $\dot{m}$ of 0.65 kg/s and constant turbine inlet temperatures T_3 are assumed for the sCO2-HeRo demonstrator, leading to different electrical heating powers $Q_{in,SEH}$ of the SEH. In the sCO2-HeRo system for a NPP, a constant transferred decay heat power $Q_{in,NPP}$ of 15 MW and constant turbine inlet temperatures T_3 are assumed, leading to varying sCO_2 mass flow rates $\dot{m}$. At the start, the

compressor inlet pressure p_1, the compressor inlet temperature T_1, the isentropic compressor efficiency $\eta_{C,is}$, the isentropic turbine efficiency $\eta_{T,is}$ the condensing power of the steam $Q_{in,NPP}$ and the turbine inlet temperature T_3 are determined. Furthermore, no pressure losses and heat losses are assumed. Thermo-physical fluid properties are obtained from the database NIST Refprop [43]. The cycle calculations are performed according to Eq. (2-1) - (2-14) in consideration of varying compressor inlet pressures p_1 from 75 bar to 199 bar, turbine inlet pressures p_3 from 76 bar to 200 bar and turbine inlet temperatures T_3 of 280 °C, 250 °C, 200 °C and 150 °C. The compressor inlet temperature T_1, the isentropic compressor efficiency $\eta_{C,is}$, the isentropic turbine efficiency $\eta_{T,is}$ and the transferred condensing power of the steam $Q_{in,NPP}$ are assumed to be constant for the calculations. The necessary sCO_2 mass flow rate $\dot{m}$ is calculated with the help of the steam condensing power $Q_{in,NPP}$ and the used turbine inlet temperature T_3. The excess electricity at the generator P_{el} is calculated for each configuration according to Eq. (2-15).

A few results of cycle calculation of the generator excess electricity P_{el} are shown in Figure 2-12 as a function of the sCO_2 turbine inlet pressure p_3 and the turbine inlet temperature T_3. The compressor inlet pressure p_1, the compressor inlet temperature T_1, the turbine efficiency $\eta_{T,is}$, the compressor efficiency $\eta_{C,is}$ and the transferred condensing power of the steam $Q_{in,NPP}$ are assumed to be constant and given on the bottom right.

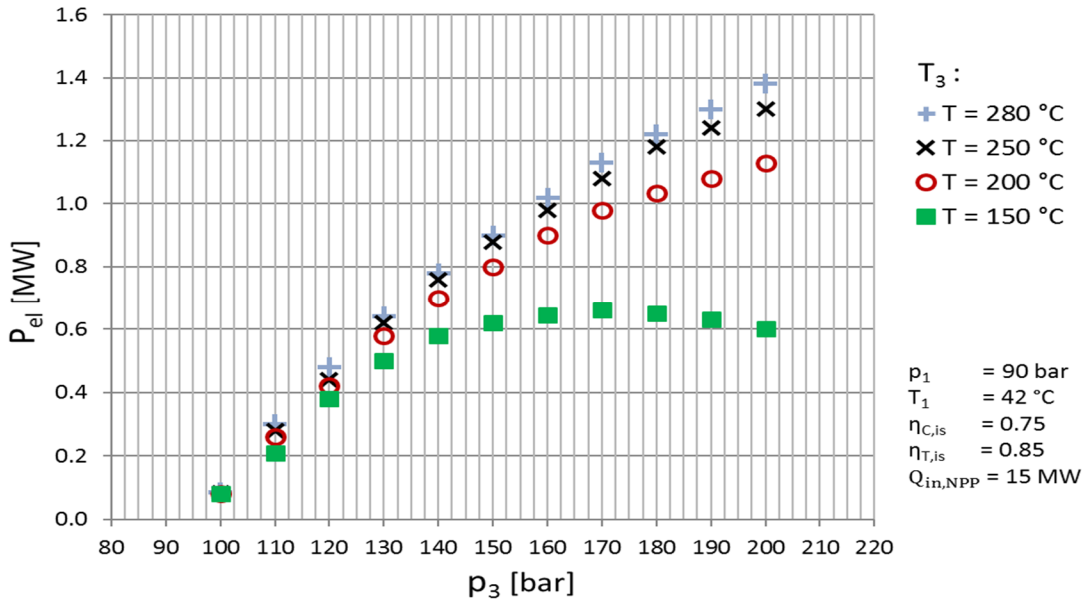

Figure 2-12: Cycle calculation results - NPP

The results in Figure 2-12 show that, for a constant turbine inlet temperature T_3, the generator excess electricity P_{el} increases until a maximum is reached and decreases again with increasing pressures p_3. Moreover, the maximum generator excess electricity P_{el} is shifted towards higher pressures p_3 for increasing turbine inlet temperatures T_3 and the generator excess electricity P_{el} increases for increasing turbine inlet temperatures T_3 and constant turbine inlet pressures p_3. The results for a turbine inlet temperature of 150 °C show that a turbine inlet pressure of 120 bar leads to a generator excess electricity of 0.38 MW, 170 bar leads to 0.68 MW and 200 bar leads to 0.60 MW. Furthermore, a constant turbine inlet pressure of 180 bar and a turbine inlet temperature of 150 °C leads to a generator excess electricity of 0.64 MW, 200 °C to 1.02 MW, 250 °C to 1.18 MW and 280 °C to a generator excess electricity of 1.22 MW.

For the determination of the optimum pressure ratio of the sCO2-HeRo system, with respect to maximum excess electricity and the given boundary conditions, the calculated results of the excess electricity are presented in Figure 2-13 by specific colors. The excess electricity is calculated by using the generator excess electricity minus the necessary electricity of the air fans, determined by Venker [10] at 0.165 MW for a 15 MW sCO2-HeRo unit. Areas colored in blue present pressure ratios where maximum excess electricity is achieved for all investigated turbine inlet temperatures and areas colored in yellow show pressure ratios where excess electricity is reached. Areas colored in green show pressure ratios where negative excess electricity occurs if the turbine inlet temperature does not exceed 150 °C and areas colored in red present pressure ratios where negative excess electricity occurs at turbine inlet temperatures which are less than 280 °C. The depicted results show that maximum excess electricity is achieved for the blue colored pressure ratios of 90/160 bar, 90/170 bar, 90/180 bar, 90/190 bar, 90/200 bar, 100/180 bar, 100/190 bar¸ 100/200 bar and 110/200 bar. Negative excess electricity occurs for green colored pressure ratios of 80/170 bar, 80/180 bar, 80/190 bar, 80/200 bar, 120/130 bar, 170/190 bar and 180/200 bar if the turbine inlet temperature does not exceed 150 °C. The red colored pressure ratios of 130/140 bar, 140/150 bar, 150/160 bar, 160/170 bar, 170/180 bar, 180/190 bar and 190/2000 bar show pressure ratios, where negative excess electricity occurs, if the turbine inlet temperature is less than 280 °C. For the design of the 15 MW sCO2-HeRo unit, it is recommended to use pressure ratios colored in blue, because these are most promising for a robust and self-sustaining system. Pressure ratios colored in red, green and yellow should be avoided, because they would lead to low or negative excess electricity. The results also show that maximum excess electricity is achieved for a compressor inlet pressure of 90 bar, except for a turbine inlet temperature of 150 °C.

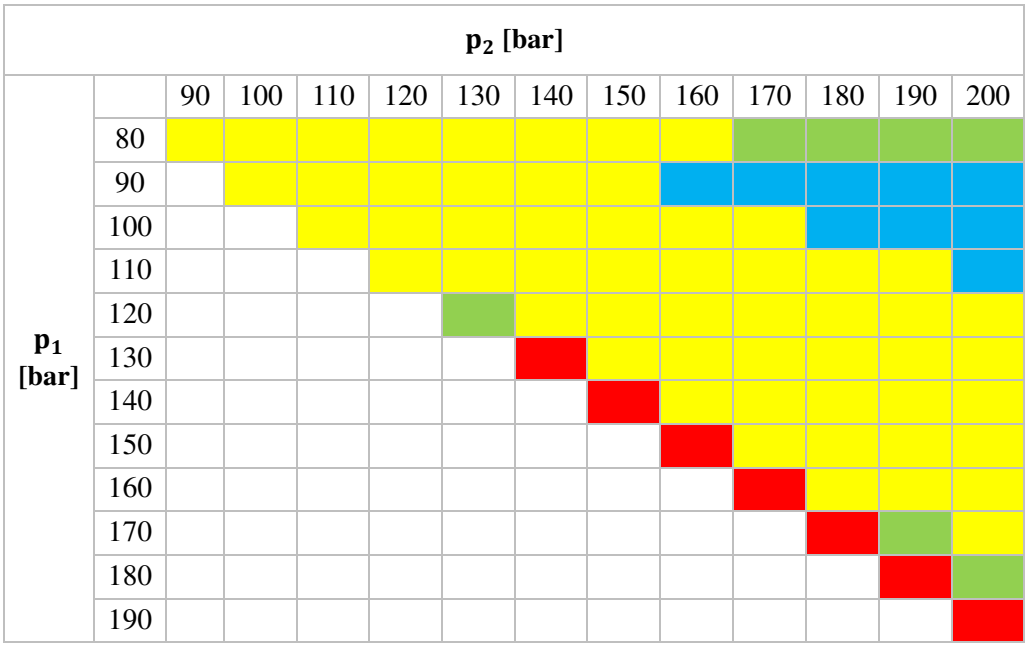

Figure 2-13: Cycle calculation results - NPP II

Because of that, the compressor inlet pressure p_1 is determined at 90 bar and the compressor inlet temperature T_1 is set to 42 °C, with respect to an ambient air temperature of 37 °C and a minimum temperature difference of 5 °C in the UHS. Furthermore, the results verify that a compressor inlet pressure of 90 bar and increasing turbine inlet pressures p_3 results in increasing excess electricity. Various issues like pressure restrictions, material costs, thermal inertias, heat transfer behaviors, achievable pressure ratios and the cycle behavior outside the design point must be taken into account for the determination of the turbine inlet pressure p_3. In consideration of the results, the pressure at the inlet of the turbine is set to 180 bar, which leads to an excess electricity of 1.21 MW for a turbine inlet temperature T_3 of 280 °C. Finally, the sCO_2 mass flow rate $\dot{m}$ of 47.7 kg/s, the generator excess electricity P_{el} of 1.38 MW and the transferred heat power in the UHS $Q_{out,UHS}$ of 13.62 MW are calculated for the design point. The sCO2-HeRo cycle parameters for a nuclear power plant are summarized in Table 2-6.

Table 2-6: sCO2-HeRo cycle parameters for a NPP

Variable	Value	Unit	Description
p_1	90	bar	Pressure - Inlet Compressor
T_1	42	°C	Temperature - Inlet Compressor
$\eta_{C,is}$	75	%	Isentropic Efficiency - Compressor
p_3	180	bar	Pressure - Inlet Turbine
T_3	280	°C	Temperature - Inlet Turbine
$\eta_{T,is}$	85	%	Isentropic Efficiency - Turbine
$\dot{m}$	47.7	kg/s	Mass Flow Rate - sCO_2
$Q_{out,UHS}$	13.6	MW	Heat Output - UHS
P_{el}	1.38	MW	Excess Electricity - Generator
$Q_{in,NPP}$	15	MW	Heat Input - NPP

3 Test facility and HX test plates

3.1 Test facility

Three test facilities are used for the experimental investigation on the heat transfer between condensing steam and supercritical CO_2 in compact heat exchangers. The first one is the SCARLETT loop, which provides sCO_2 under defined conditions, the second one is a newly constructed low-pressure steam cycle, which generates steam similar to the steam conditions at the glass model, and the third one is a newly constructed high-pressure steam cycle, which provides steam similar to the steam conditions in a nuclear power plant.

3.1.1 sCO_2 SCARLETT loop

The SCARLETT loop is designed and built at the Institute of Nuclear Technology and Energy Systems, Stuttgart. It is a multi-purpose test facility that provides supercritical CO_2 under defined conditions for different kind of experiments like heat transfer investigations and research in material science. A simplified piping and instrumentation diagram of the loop is depicted in Figure 3-1 and described below.

Before starting operation, the SCARLETT loop (Figure 3-1) is evacuated with a vacuum pump of the filling unit (0). For this purpose, the valves V1 and V2 are opened and the vacuum pump is switched on until a pressure of less than 0.05 bar is reached. Afterwards, valve V1 is closed and valves V2 and V3 are opened before gaseous CO_2 is filled into the loop until a pressure of about 7 bar is reached. In the following, the storage vessel (1) is filled with liquid CO_2 by a gas bottle until the necessary amount of CO_2 is reached before all valves are closed again. After finishing the evacuation and filling procedure, the SCARLETT loop is ready for operation. During normal operation liquid CO_2 flows from the storage vessel (1) through the electrical heated evaporator (2) and is slightly overheated. After leaving the droplet separator (3), where remaining liquid CO_2 is separated from the flow, it enters the compressor (4). In the piston compressor the CO_2 is compressed up to a certain pressure and simultaneously heated-up. Before entering the test section, marked in green, there is the possibility of conditioning (5) the sCO_2. This means that a defined temperature can be adjusted by means of cooling or heating the sCO_2. In the test section different kind of experiments can be performed, for instance investigation on the heat transfer capability in CHXs, electrically heated plates and material science. The installed measurement devices, e.g. pressure gauges, resistance thermometers

(Pt-100) and mass flow meters, at the inlet (5) and outlet (5') of the test section measure relevant parameters of the experiments. After leaving the test section, the sCO_2 is cooled down in the gas chiller (6) at the outdoor area and afterwards it is expanded in the expansion valve (7). Before entering the storage vessel, it is cooled down again in a condenser (8).

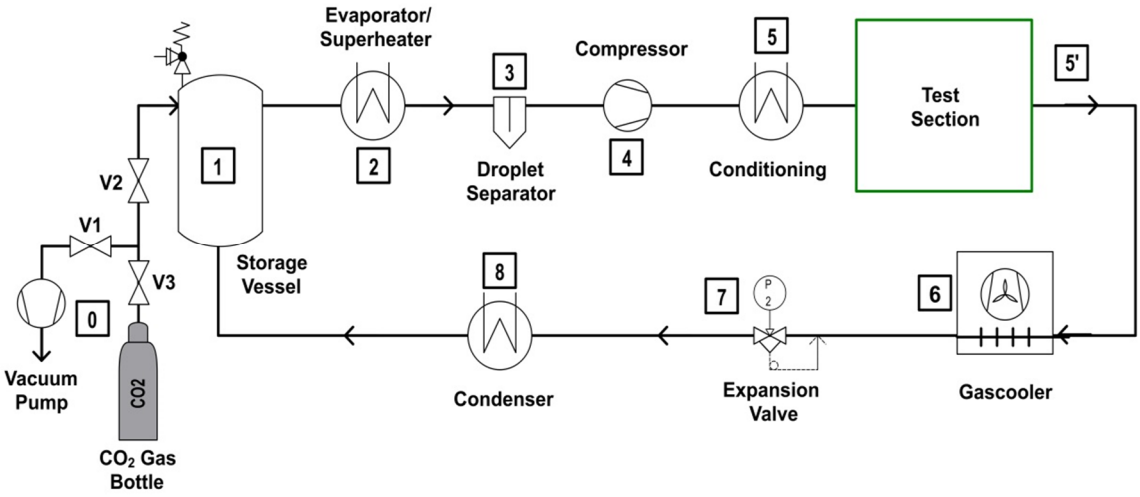

Figure 3-1: P&I diagram of the SCARLETT loop

Table 3-1 summarizes the boundary conditions of the SCARLETT loop. The sCO_2 mass flow rate $\dot{m}$ can be adjusted from about 10 g/s to 110 g/s by setting the rotational speed of the piston compressor. In addition, the achievable mass flow rate depends on the performance map of the compressor, which leads to a lower mass flow rate at higher pressure ratios and vice versa. The temperature T at the inlet of the test section can be varied between 0 °C to 150 °C by means of cooling or heating, while the pressure p can be adjusted from 75 bar to 120 bar. For evaporating and overheating the CO_2 mass flow rate before it enters the compressor, there is an electrical heating power $Q_{in,Evap}$ of 36 kW installed. After the compressor the sCO_2 can be conditioned before entering the test section by cooling with a power of 48 kW ($Q_{out,Condi}$) or heating with 16 kW ($Q_{in,Heat}$). The installed gas chillers can transfer about 32 kW ($Q_{out,Gas}$) of waste heat from the loop to the ambient air. After the expansion in the expansion valve, the CO_2 can be cooled down again in the condenser with a condensing power $Q_{out,Conde}$ of 13 kW before it re-enters the storage vessel. The storage vessel has a volume V of 0.07 m³.

Table 3-1: SCARLETT parameters

Variable	Value	Unit	Description
$\dot{m}$	10 - 110	g/s	sCO2 Mass Flow Rate
T	0 - 150	°C	Temperature - Inlet Test Section
p	75 - 120	bar	Pressure - Inlet Test Section
$Q_{in,Evap}$	36	kW	Power - Evaporator
$Q_{out,Condi}$	48	kW	Power - Conditioning Cooling
$Q_{in,Heat}$	16	kW	Power - Conditioning Heating
$Q_{out,Gas}$	32	kW	Power - Gas Chiller
$Q_{out,Conde}$	13	kW	Power - Condenser
V	0.07	m³	Volume - Pressure Vessel

3.1.2 Steam cycle

High-pressure steam cycle

The high-pressure steam cycle is constructed to provide steam with a pressure of 70 bar and a temperature of 286 °C, similar to the steam conditions in a NPP. It is used in the current work for the experimental investigation of the heat transfer capability between condensing steam and sCO_2 in heat exchangers. The P&I diagram of the high-pressure steam cycle (red pipes), the installed two-plate CHX and the sCO_2 side (green pipes) is depicted in Figure 3-2. Before starting operation, a vessel (1) is filled with deionized water. The water is pumped from the vessel (1) by a high-performance liquid chromatography pump (3) (HPLC) through a filter (2) into an electrical heated evaporator (4). Inside the water is evaporated and slightly overheated before the steam enters a test section (5). Different kind of components like two-plate CHX's and shell-and-tube heat exchangers can be installed in the test section. The pressure in the cycle can be adjusted by the mechanical primary pressure control valve (6). After the expansion in the pressure control valve, the condensate flows into a second vessel (7) and is pumped back into vessel (1). For monitoring the cycle behavior during operation, measurement devices like resistance thermometers (T), pressure gauges (p) and a mass flow meter ($\dot{m}$) are installed. The measurement position and the nomenclature of each measurement device are also shown. A detailed description of the used measurement devices, their measurement range and the measurement uncertainties are given in the following chapter.

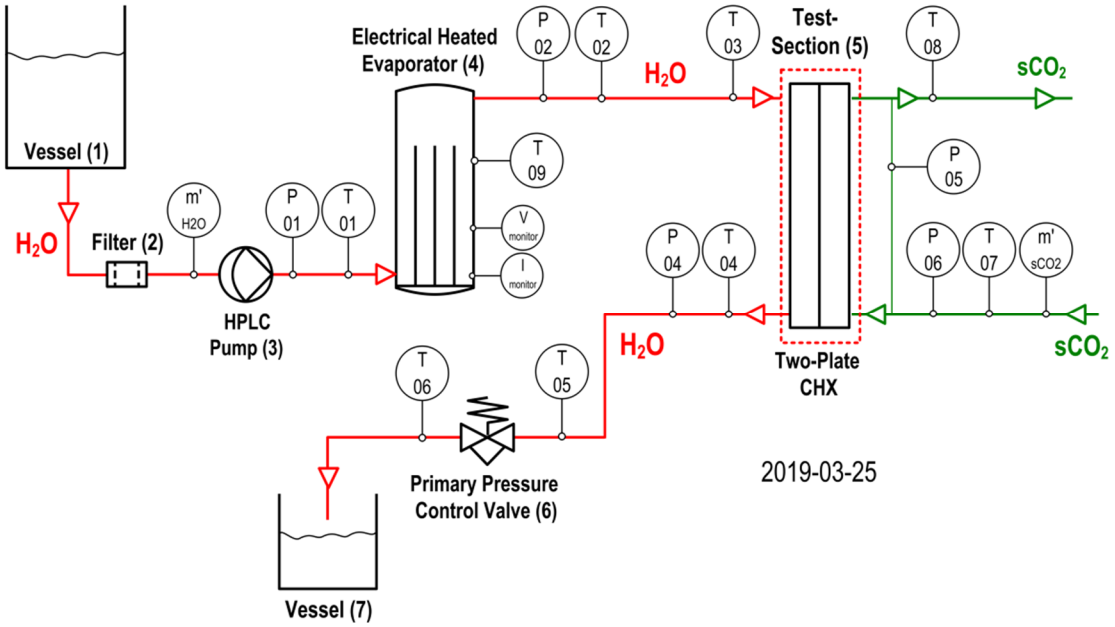

Figure 3-2: P&I diagram of the high-pressure steam cycle with two-plate CHX

The boundary conditions of the high-pressure steam cycle and a summary of the main components are given in Table 3-2 and Table 3-3. The water volume flow rate $\dot{m}_{H2O}$ can be adjusted by the HPLC pump (3) from 0.05 l/h to 2.5 l/h and the electrical heating power $Q_{in,Evap}$ of the evaporator (4) with 1.6 kW is sufficient for evaporating and overheating the adjusted water volume flow rates. The pressure p at the inlet of the test section can be adjusted by the mechanical primary pressure control valve (6) from 1 bar to 105 bar and the corresponding steam temperature T rises from 100 °C to 315 °C. The water storage vessels (1) and (7) have a volume V of about 2 liters each and they are manufactured by IKE. A fuel filter (2) from Festo is installed in front of the HPLC pump to ensure that only pure water flows through the pump. The HPLC pump (3) and the electrical heated evaporator (4) are purchased from the company TTI-GmbH-CHEMPION. The primary pressure control valve (6) of the series 26-1700 is purchased from TESCOM EUROPE GmbH. The ½" and ¼" stainless steel pipes, valves and pipe connectors from Swagelok are selected with respect to existing pressures and temperatures. Rock wool and high-temperature Armaflex are used as insulation materials.

Table 3-2: High-pressure steam cycle parameters

Variable	Value	Unit	Description
$\dot{m}_{H2O}$	0.05 - 2.5	l/h	H_2O Volume Flow Rate
T	100 - 315	°C	Temperature - Inlet Test Section
p	1 - 105	bar	Pressure - Inlet Test Section
$Q_{in,Evap}$	1.6	kW	Power - Evaporator
V	2	L	Volume - Vessel

Table 3-3: High-pressure steam cycle components

Number	Component	Type	Manufacturer / Seller
1	Vessel	-	IKE
2	Filter	Fuel filter - 8 mm	Festo
3	HPLC Pump	OEM - HPLC - Pump	TTI-GmbH-CHEMPION
4	Electrical heated evaporator	XX-1-6161-30	TTI-GmbH-CHEMPION
5	Test section	-	-
6	Primary pressure control valve	Series 26-1700	TESCOM EUROPE GmbH
7	Vessel	-	IKE

Low-pressure steam cycle

The low-pressure steam cycle is constructed to provide steam with a pressure from 0.1 bar to 1.0 bar and a corresponding steam temperature between 50 °C and 100 °C, which is similar to the steam conditions in the PWR glass model. It is used for the experimental investigation on the heat transfer between condensing steam and sCO_2 in the compact heat exchangers. Figure 3-3 shows a P&I diagram of the low-pressure steam cycle (red pipes), the two-plate CHX test section, the sCO_2 side, the installed measurement devices and their location. Before starting operation of the test facility, the low-pressure steam cycle is evacuated by the vacuum-pump (7) and the water storage vessel (1) is filled with distilled water. During operation, the water is pumped from the vessel (1) via the filter (2) through the membrane pump (3) into the electrical heated evaporator (4). Inside, the water is evaporated and slightly overheated before it enters the two-plate CHX, installed at the test section (5). In the CHX, the heat is transferred from the steam side to the sCO_2 side and thereby the steam is condensed

before it flows downwards driven by gravity and leaves the two-plate CHX at the bottom. Due to different test configurations, it can happen that the steam is not completely condensed at the outlet of the test section. Therefore, an additional condenser is installed to ensure that only condensate re-enters the water storage vessel (1). The sCO_2 enters the test section from the bottom right, flows upwards in the CHX, is heated and leaves the test section at the top right. For monitoring the cycle, measurement devices like mass flow rate meter ($\dot{m}$), temperature measurement devices (T), pressure gauges (p) as well as Voltage and Ampere meters are installed. The measurement position and the nomenclature of each measurement device are depicted in Figure 3-3. Important measurement points are the temperatures, mass flow rates and pressures at the inlet and outlet of the CHX on both sides and the electrical heating power of the evaporator, calculated with the Voltage- and Ampere measurement data. A detailed description of the used measurement devices, their measurement ranges and their measurement uncertainties are given in the following chapter.

The boundary conditions of the low-pressure steam cycle are shown in Table 3-4 and the components are summarized in Table 3-5. The water volume flow rate $\dot{m}_{H2O}$ can be adjusted by the membrane pump (3) from 0.05 l/h to 2.5 l/h and the electrical heating power $Q_{in,Evap}$ of the evaporator (4) with 1.6 kW is sufficient for evaporating and overheating the adjusted water volume flow rates. The pressure p at the inlet of the test section can be adjusted from 0.1 bar to 1.0 bar and the corresponding steam temperature T rises from about 50 °C to 100 °C. The water storage vessel (1) has a volume V of about 2 liters and is manufactured by IKE. A fuel filter (2) from Festo is installed in front of the membrane pump to ensure that only pure water flows through the pump. The membrane pump (3) and the electrical heated evaporator (4) are purchased from TTI-GmbH-CHEMPION. The condenser (6) is designed as double-pipe heat exchanger and manufactured by IKE. The vacuum pump (7) is purchased from Pfeiffer and the ½" and ¼" stainless steel pipes, valves and pipe connectors are bought from the manufacturer Swagelok. High-temperature Armaflex is used as insulation material.

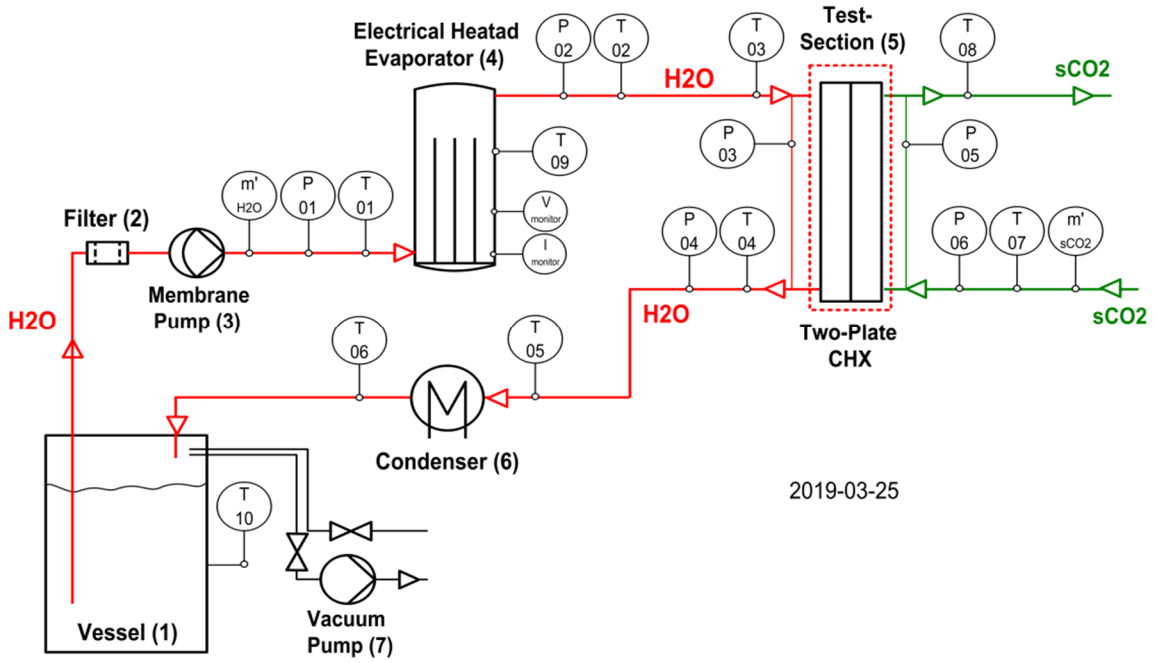

Figure 3-3: P&I diagram of the low-pressure steam cycle with two-plate CHX

Table 3-4: Low-pressure steam cycle parameters

Variable	Value	Unit	Description
$\dot{m}_{H2O}$	0.05 - 2.5	l/h	H_2O Volume Flow Rate
T	50 - 100	°C	Temperature - Inlet Test Section
p	0.1 - 1.0	bar	Pressure - Inlet Test Section
$Q_{in,Evap}$	1.6	kW	Power - Evaporator
V	2	L	Volume - Vessel

Table 3-5: Low-pressure steam cycle components

Number	Component	Type	Manufacturer / Seller
1	Vessel	-	IKE
2	Filter	Fuel filter - 8 mm	Festo
3	Membrane pump		TTI-GmbH-CHEMPION
4	Electrical heated evaporator	XX-1-6161-30	TTI-GmbH-CHEMPION
5	Test section	-	-
6	Condenser	-	IKE
7	Vacuum pump	Uno 6	Pfeiffer

3.1.3 Measurement devices and uncertainties

This chapter includes a general description of the installed measurement devices and their measurement techniques. Afterwards, they measurement uncertainties are described followed by a discussion of the error propagation for calculated parameters.

Type of measurement

Temperature

Thermal resistance platinum thermometers (Pt-100) are used for temperature measurements. They are classified according to A and B, and the Pt-100 A type is used in both steam cycles. The Pt-100 has a nominal resistance of 100 Ω at 0 °C and a nearly linear change in the resistance as a function of the temperature. A mean temperature coefficient of 0.0039 $\frac{1}{°C}$ is assumed for 0 °C to 100 °C. The measurement uncertainty of the temperature σ is given by the equation $\pm(0.15\ °C + 0.002 \cdot \mathrm{T}\ [°C])$, which leads to an uncertainty of ± 0.35 °C at 100 °C, ± 0.55 °C at 200 °C and ± 0.75 °C at 300 °C. To improve the measurement accuracy and to compensate resistances in cables, a 4-wire measurement technique is selected. The Pt-100 technology is chosen because it can be applied for temperatures between - 200 °C and 850 °C, it has a high measurement accuracy, it is easily replaceable and it guarantees a high long-term stability.

Pressure

The pressure in both steam cycles is measured with piezoresistive pressure transmitters from Keller, Switzerland. The piezoresistive effect is based on the change in electrical resistance of the piezoresistive material as a function of the mechanical stress. The mechanical stress, or more in detail the change in the electrical resistance, is converted into a voltage signal, which can be used via 3-wire measurement technique in the measurement data acquisition. Piezoresistive pressure transmitters are constructed as absolute, relative and differential pressure transmitters. They can be applied for different kind of working fluids with pressures from 0.2 bar to 1000 bar and temperatures from - 40°C to 300 °C. In consideration of the existing pressures in the low-pressure steam cycle (0.1 bar - 1.0 bar) and high-pressure steam cycle (1 bar - 105 bar), the temperatures in the low-pressure steam cycle (20 °C - 100 °C) and high-pressure steam cycle (100 °C - 315 °C) as well as the occurring pressure drops in the two-plate CHX test section (0 bar - 3 bar), the pressure transmitters are selected with respect to each application. A detailed specification of each pressure transmitter and his measurement error is given in Table 3-6.

Mass and volume flow rate

The sCO_2 mass flow rate is measured with a Coriolis mass flow meter from Schwing Verfahrenstechnik GmbH, Germany. The chosen RHM-03 measurement transducer is designed for measuring sCO_2 mass flow rates from 0 g/s to 100 g/s with temperatures up to 120 °C and pressures up to 200 bar. The measurement system is constructed as a two-pipe configuration with a pipe diameter of 3 mm, arranged in parallel. The transmitter RHE-16 is chosen as analysis unit with a 4 mA - 20 mA analog output. In general, with Coriolis mass flow meters pressures up to 1000 bar, temperatures from - 196 °C to 350 °C and mass flow rates between 1 g/min and 1500 t/h can be measured for various liquid and gaseous working fluids. In addition, measurement ranges of more than 50:1, measurement uncertainties of less than $\pm$ 0.2 % and reproducibility's higher than $\pm$ 0.1 % can be achieved. The measurement technique is non-invasive, suitable for pulsating mass flow rates, insensitive to gas inclusions and based on the Coriolis effect, which is described briefly. Sensors are mounted at the inlet and outlet of the oscillating system of the Coriolis mass flow meter. If there is no mass flow, the signals are in phase; otherwise, a phase shift between the two signals occurs. This phase shift is proportional to the mass flow rate in the measurement device. The water volume flow rate is measured with the calorimetric volume flow meter DTH08 from the manufacturer PKP-Prozessmesstechnik. It can be applied for liquid working fluids, has a measurement range from 0.06 l/h to 120 l/h, withstands temperatures up to 70 °C and pressures up to 10 bar. For the investigations it is calibrated from 0 l/h to 5 l/h. It is a non-invasive measurement technology, insensitive to dirt and the measurement device provides 0 V - 10 V analog output signals for the measurement data acquisition. The measurement technique consists of two temperature sensors, one is heated. If no working fluid flows through the measurement device, a constant temperature at the heated sensor and a constant gradient between both sensors exist. If a media flows, the heated sensor is cooled down and the gradient of the cooling procedure is proportional to the volume flow rate. A measurement uncertainty of less than $\pm$ 5 % of the measured value can be assumed.

Measurement devices installed

The measurement devices installed at the low-pressure (LP) and high-pressure (HP) steam cycle are summarized in Table 3-6. After each variable name, the measurement range, a short description, the measurement uncertainty and the type of each measurement device are given. The uncertainties are derived from manufacturers instructions. The uncertainty of the temperature measurement, for instance, is given as a function of the measured temperature T according to $\pm(0.15\,°C + 0.002 \cdot \mathrm{T}\,[°\mathrm{C}])$ and the uncertainty of the pressure measurement depends on the measurement device as well as on the measurement range. The uncertainty of the water volume flow rate measurement is given by the manufacturer with $\pm$ 5 % of the measurement value, leading to higher absolute uncertainties for higher volume flow rates and the uncertainty of the sCO_2 mass flow rate is given with $\pm$ 0.8 g/s.

Table 3-6: Installed measurement devices at LP and HP steam cycle

Variable	Cycle	Value	Unit	Description	Errors	Device
$\dot{m}_{H2O}$	LP	0 - 5	l/h	H_2O volume flow rate	± 5 % of measurement	DTH08 - calorimetric volume flow meter
	HP	0 - 5	l/h	H_2O volume flow rate	± 5 % of measurement	DTH08 - calorimetric volume flow meter
$\dot{m}_{sCO2}$	LP	0 - 100	g/s	sCO_2 mass flow rate	± 0.8 g/s	RHM-03/RHE-16 - Coriolis mass flow meter
	HP	0 - 100	g/s	sCO_2 mass flow rate	± 0.8 g/s	RHM-03/RHE-16 - Coriolis mass flow meter
$T01$ - $T10$	LP	0 - 400	°C	Temperature	$\pm(0.15\,°C + 0.002 \cdot T)$	Pt-100 A - thermal resistance thermometer
	HP	0 - 400	°C	Temperature	$\pm(0.15\,°C + 0.002 \cdot T)$	Pt-100 A - thermal resistance thermometer
$p01$	LP	0 - 1.0	bar	Pressure - inlet H_2O evaporator	$\pm(1.0\,\% \cdot FS)$ (FS = 1 bar)	PAA-23SY - piezoresistive pressure transmitter
	HP	0 - 100	bar	Pressure - inlet H_2O Evaporator	$\pm(0.5\,\% \cdot FS)$ (FS = 100 bar)	PA-23SY - piezoresistive pressure transmitter
$p02$	LP	0 - 0.6	bar	Pressure - inlet H_2O CHX	$\pm(1.5\,\% \cdot FS)$ (FS = 1 bar)	PAA-23SY - piezoresistive pressure transmitter
	HP	0 - 100	bar	Pressure - inlet H_2O CHX	$\pm(0.5\,\% \cdot FS)$ (FS = 100 bar)	PA-35XHTC - piezoresistive pressure transmitter
$p03$	LP	0 - 3.0	bar	Differential pressure - H_2O CHX	$\pm(0.15\,\% \cdot FS)$ (FS = 3 bar)	PD-33X - diff. piezoresistive pressure transmitter
$p04$	LP	0 - 0.6	bar	Pressure - outlet H_2O CHX	$\pm(1.5\,\% \cdot FS)$ (FS = 1 bar)	PAA-23SY - piezoresistive pressure transmitter
	HP	0 - 100	bar	Pressure - outlet H_2O CHX	$\pm(0.5\,\% \cdot FS)$ (FS = 100 bar)	PA-35XHTC - piezoresistive pressure transmitter
$p05$	LP	0 - 5.0	bar	Differential pressure - sCO_2 CHX	$\pm(0.15\,\% \cdot FS)$ (FS = 10 bar)	PD-33X - diff. piezoresistive pressure transmitter
	HP	0 - 5.0	bar	Differential pressure - sCO_2 CHX	$\pm(0.15\,\% \cdot FS)$ (FS = 10 bar)	PD-33X - diff. piezoresistive pressure transmitter
$p06$	LP	0 - 140	bar	Pressure - inlet sCO_2 CHX	$\pm(0.5\,\% \cdot FS)$ (FS = 200 bar)	PAA-23SY - piezoresistive pressure transmitter
	HP	0 - 140	bar	Pressure - inlet sCO_2 CHX	$\pm(0.5\,\% \cdot FS)$ (FS = 200 bar)	PAA-23SY - piezoresistive pressure transmitter

Measurement uncertainties and error propagations

The measurement uncertainties of the measurement devices are summarized in Table 3-6. The error propagation for calculated parameters like enthalpies or heat inputs, with measurement data from the experiments, are described exemplarily for the sCO_2 side. If the deviations are independent from each other, the equation for the statistical error propagation according to Eq. (3-1) can be applied.

$$\sigma = \sqrt{\sigma_1^2 + \sigma_2^2 + \cdots} \tag{3-1}$$

σ_1 presents the measurement uncertainty of the first independent parameter and σ_2 the measurement uncertainty of the second independent parameter. It is assumed that all uncertainties to be not correlated.

The sCO_2 enthalpies at the inlet and outlet of the CHX are calculated with the NIST database Refprop [43] as a function of two independent parameters, the measured temperatures and pressures. Therefore, the sCO_2 inlet temperature $T07$, the outlet temperature $T08$, the inlet pressure $p06$ and the outlet pressure $p_{sCO2,out}$ are used. For values calculated with Refprop, the commonly used statistical error propagation equation (Eq. (3-1)) is adjusted. If normally distributed uncertainties in temperature and pressure lead to normally distributed uncertainties in enthalpy, error propagations can be performed by translating the differential quotient to a quotient of differences. The propagated sCO_2 enthalpy uncertainties for the inlet $\sigma_{h_{sCO2,in}}$ and outlet $\sigma_{h_{sCO2,out}}$ are calculated according to Eq. (3-2) and Eq. (3-3).

$$\begin{aligned}\sigma_{h_{sCO2,in}} = \frac{1}{2}\Big[&\Big(h_{sCO2,in}\big|_{T07/p06_{max}} - h_{sCO2,in}\big|_{T07/p06_{min}}\Big)^2 \\ &+ \Big(h_{sCO2,in}\big|_{p06/T07_{max}} - h_{sCO2,in}\big|_{p06/T07_{min}}\Big)^2\Big]^{\frac{1}{2}}\end{aligned} \tag{3-2}$$

$$\begin{aligned}\sigma_{h_{sCO2,out}} = \frac{1}{2}\Big[&\Big(h_{sCO2,out}\big|_{T08/p_{sCO2,out,max}} - h_{sCO2,out}\big|_{T08/p_{sCO2,out,min}}\Big)^2 \\ &+ \Big(h_{sCO2,out}\big|_{p_{sCO2,out}/T08_{max}} - h_{sCO2,out}\big|_{p_{sCO2,out}/T08_{min}}\Big)^2\Big]^{\frac{1}{2}}\end{aligned} \tag{3-3}$$

The calculation of the sCO_2 enthalpy uncertainty at the inlet of the CHX $\sigma_{h_{sCO2,in}}$ is based on four enthalpies. The first one is $h_{sCO2,in}\big|_{T07/p06_{max}}$, which is calculated with the measured sCO_2 inlet temperature $T07$ and the maximum possible inlet pressure $p06_{max} = p06 + (0.5\% \cdot 200bar)$. The second one is $h_{sCO2,in}\big|_{T07/p06_{min}}$, calculated with the measured sCO_2 inlet temperature $T07$ and the minimum possible inlet pressure $p06_{min} = p06 - (0.5\% \cdot 200bar)$. The third one is $h_{sCO2,in}\big|_{p06/T07_{max}}$, calculated with the measured sCO_2 inlet pressure $p06$ and the maximum possible inlet temperature $T07_{max} = T07 + (0.15\,°C + 0.002 \cdot \mathrm{T\,[°C]})$. The fourth one is $h_{sCO2,in}\big|_{p06/T07_{min}}$, calculated with the measured sCO_2 inlet pressure $p06$ and the minimum possible inlet temperature $T07_{min} = T07 - (0.15\,°C + 0.002 \cdot \mathrm{T\,[°C]})$. The propagated sCO_2 enthalpy uncertainty at the outlet of the CHX $\sigma_{h_{sCO2,out}}$ is calculated according to Eq. (3-3) similar to $\sigma_{h_{sCO2,in}}$, only with the sCO_2 outlet temperature $T08$ and outlet pressure $p_{sCO2,out}$.

The heat input into the sCO_2 is calculated with $Q_{sCO2,} = \dot{m}_{sCO2} \cdot (h_{sCO2,in} - h_{sCO2,out})$. It can be seen that Q_{sCO2} is a function of three independent parameters. According to the linearized Taylor-series and the propagation of uncertainty, the uncertainty for independent parameters can be calculated in general for a function of $y = y(x_{1,}x_{2,}x_{3,}\ldots)$ according to Eq. (3-4). The error propagation $\sigma_{Q_{sCO2}}$ is calculated by Eq. (3-5).

$$\sigma_y = \sqrt{(\frac{dy}{dx_1} \cdot \sigma_{x_1})^2 + (\frac{dy}{dx_2} \cdot \sigma_{x_2})^2 + (\frac{dy}{dx_3} \cdot \sigma_{x_3})^2 + \ \ldots} \tag{3-4}$$

$$\sigma_{Q_{sCO2}} = \left[(\frac{d}{d\dot{m}_{sCO2}} Q_{sCO2} \cdot \sigma_{\dot{m}_{sCO2}})^2 + (\frac{d}{dh_{sCO2,in}} Q_{sCO2} \cdot \sigma_{h_{sCO2,in}})^2 + (\frac{d}{dh_{sCO2,out}} Q_{sCO2} \cdot \sigma_{h_{sCO2,out}})^2\right]^{\frac{1}{2}} \tag{3-5}$$

After deriving Q_{sCO2} according to Eq. (3-5) it can be simplified to Eq. (3-6).

$$\sigma_{Q_{sCO2}} = \left[\left(\left(h_{sCO2,out} - h_{sCO2,in}\right) \cdot \sigma_{\dot{m}_{sCO2}}\right)^2 + \left(\dot{m}_{sCO2} \cdot \left(\sigma_{h_{sCO2,out}} - \sigma_{h_{sCO2,in}}\right)\right)^2\right]^{\frac{1}{2}} \tag{3-6}$$

The error propagation $\sigma_{Q_{sCO2}}$includes the calculated sCO_2 enthalpies at the inlet $h_{sCO2,in}$ and outlet $h_{sCO2,out}$ of the CHX, the measurement uncertainty of the sCO_2 mass flow rate $\sigma_{\dot{m}_{sCO2}}$, the measurement results of the sCO_2 mass flow rate $\dot{m}_{sCO2}$ and the calculated enthalpy uncertainties $\sigma_{h_{sCO2,Out}}$ and $\sigma_{h_{sCO2,in}}$. The error propagation is applied in the same way for the steam side of the CHX and for all calculated values.

3.2 Heat exchanger

3.2.1 Classification

A classification of heat exchangers according to a) transfer process, b) number of fluids, c) surface compactness, d) construction type, e) flow arrangement and f) heat transfer mechanism is given for instance in the book of Shah [44]. The transfer process (a) is furthermore divided into the indirect contact type, in which the fluids are separated and the heat transfer occurs through walls, and the direct contact type, in which the hot and cold fluid interact. The classification according to the number of fluids (b) is further divided into two-fluid systems, three-fluid systems and more than three-fluid systems. The two-fluid system is the most common one in technical applications and usually used for heating, cooling or heat recovery. Three-fluid systems are used for cryogenic and chemical processes and fluid systems with more than three fluids are special applications e.g. in the chemical industry. The classification according to the surface compactness (c) is divided into the gas-to-fluid and the liquid-to-liquid & phase-change heat exchangers. The first one is called compact, if the ratio of heat transfer area to volume is more than 700 m^2/m^3 or a hydraulic channel diameter of less than 6 mm is used. The second one is compact, if the ratio is more than 400 m^2/m^3 or the hydraulic diameter is less than 6 mm. Furthermore, heat exchangers can be classified into four

construction types (d): tubular, plate-type, extended surface and regenerative. The tubular type includes for instance the double-pipe and the well-known and commonly used shell-and-tube heat exchanger. The plate-type is subdivided into the plate heat exchanger, the spiral, the plate coil and printed circuit heat exchanger. The extended surface type is subdivided into the plate-fin and tube-fin exchangers. Regenerative heat exchangers, also called regenerators, are constructed as rotary, fixed-matrix or rotating hood systems. The flow arrangement (e) can be divided into the single-pass and multi-pass flow. The single-pass flow can be designed as counter-current-flow, co-current-flow, cross-flow, split-flow and divided-flow configuration. Multi-pass flows configurations are applied for extended-surface, shell-and-tube and plate heat exchangers. The heat transfer mechanism (f) is further divided into the single-phase convection on both sides, the single-phase convection on one side and a two-phase convection on the other side, two-phase convection on both sides and the combined convection.

Plate-type heat exchangers can be broken down into the plate, the spiral, the plate-coil and printed circuit heat exchangers. These four types are described more in detail, because the heat transfer between condensing steam and sCO_2 in plate-type heat exchangers is experimentally investigated in this work. A gasketed plate heat exchanger (PHE) is shown on the top left in Figure 3-4. It consists of rectangular plates that are clamped together with two cover plates, carrying bars and bolts. The corrugated surface pattern of the plate is usually manufactured by stamping or embossing. To ensure leak-tightness, different kind of gasketed materials are used, depending on the operation temperature and pressure. PHE are designed for temperatures below 150 °C and pressures up to 10 bar, and they are commonly used in the food or chemical industry. The main advantages of a gasketed PHE are that they can be easily disassembled for cleaning or inspection and the heat transfer area can be easily adjusted by adding or removing plates. If higher operation temperatures and pressures are required, the gasketed PHE can be replaced by welded or brazed plate heat exchangers, which are able to withstand temperatures up to 350 °C and pressures up to 40 bar. A spiral-plate heat exchanger is shown on the top right. It consists of two metal strips, which are wrapped helically to form a long pair of spiral channels for two fluids in a compact manner. The fluids usually flow through the heat exchanger in counter-current-flow and single-passage configuration. Spiral-plate heat exchangers are used for more viscous and fouling liquids. Compared to other heat exchangers the flow passages are easier to clean and no insulation is needed at the outer shell because the cold fluid flows there. For larger heat transfer units, the temperature is limited to 200 °C and the pressure to 25 bar. A plate-coil heat exchanger is shown on the bottom left. It consists of a plate with attached

channels. It can be used as heat sink or heat source, depending on the operational purpose and the given boundary conditions. The heat exchanger can be manufactured with different plate materials like carbon steel, stainless steel and titanium by means of die-stamping, spot-welding or roll-bonding. They withstand pressures up to 18 bar, are relatively cheap and the heat exchanger design can be changed easily. They are usually used in industrial applications like the cryogenics, the chemical industry and for solar power applications. A printed circuit heat exchanger (PCHE) is shown on the bottom right. Stainless steel, titanium or nickel alloys are used as plate material. The channels are chemically etched or milled into the plates, leading to rectangular or semi-circular channels with a depth from 0.1 mm to 2 mm. The channels can be designed as straight or wavy channels with varying angles, depending on process requirements. It must be considered that increasing channel angles lead to higher flow turbulences, which results in increased heat transfer capabilities, but also in increased pressure drops. The flow arrangement between the hot and cold side can be designed as co-current, counter-current and cross flow. In the co-current flow, both fluids enter the heat exchanger at one side, flow parallel in the same direction and leave the heat exchanger at the other side. In counter-current flow heat exchangers, both fluids flow parallel to each other but in opposite directions. According to [44], [45], [46] the counter-current flow configuration is thermodynamically superior to any other; it is the most efficient and the highest temperature changes in each fluid can be achieved for given boundary conditions like the fluid mass flow rates and the fluid inlet temperatures. In cross flow heat exchangers, the fluids flow in directions normal to each other. Thermodynamically, the effectiveness is between the co-current flow and counter-current flow. After designing and manufacturing the plates of the PCHE, they are stacked together before the diffusion bonding. The diffusion bonding is applied because it provides homogeneous material properties, which result in higher pressure resistances and higher heat conductivities. Finally, the fluid inlet and outlet connections are electronic beam welded onto the heat exchanger unit. PCHE's can achieve surface area densities of about 650 m^2/m^3 - 1300 m^2/m^3, leading to compact components. This is especially important if space limitations must be taken into account. Moreover, they are able to withstand pressures up to 500 bar and temperatures up to 800 °C. They are usually used for clean gases, liquids and phase-change fluids in the chemical industry, waste heat recovery, power and energy fields and power plant applications.

1) Plate heat exchanger

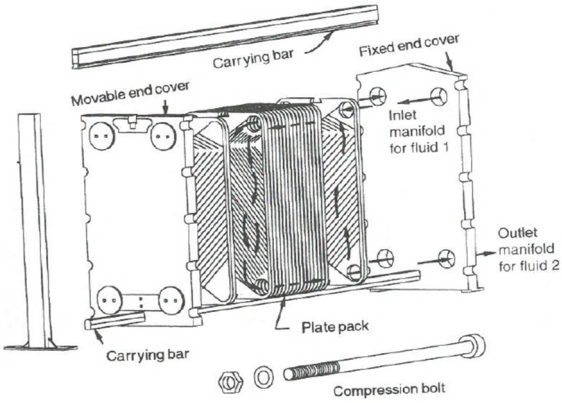

2) Spiral heat exchanger

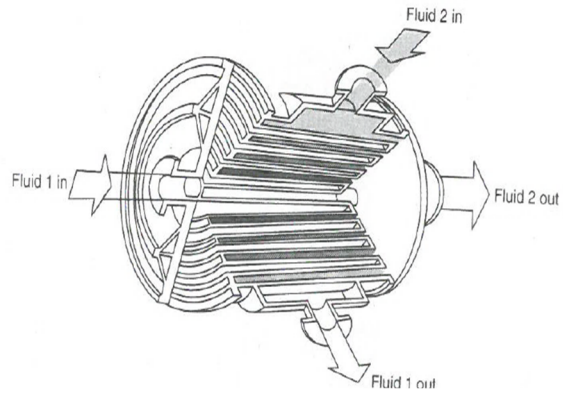

3) Plate coil heat exchanger

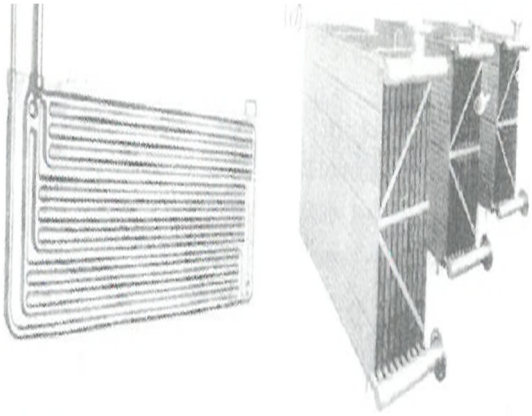

4) Printed circuit heat exchanger

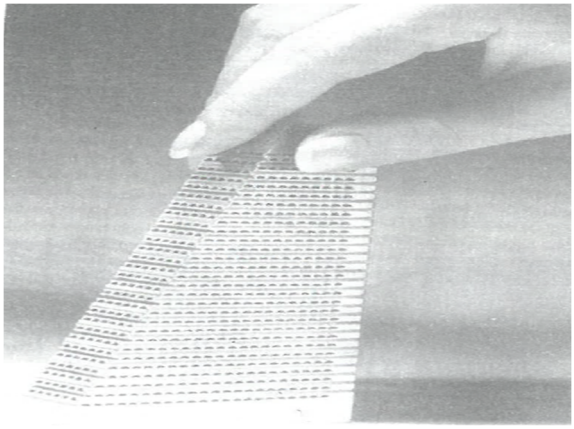

Figure 3-4: Plate-type heat exchangers [44]

3.2.2 CHX test plates

The experimental investigation on the heat transfer is performed with diffusion bonded heat exchangers, which are designed and manufactured in the frame of this work. This chapter describes the determination of the heat exchangers, the diffusion bonding processes, the selection of the plate material, the mechanical design as well as the determination of the plate design and the manufacturing of the heat exchangers.

Heat exchanger test configurations

The channel dimensions, number of channels per plate / number of plates, channel shapes and heat exchanger test configurations are summarized in Table 3-7. Furthermore, a unique nomenclature with alphabetic letters (A, B, C, D) is introduced for simplicity.

Table 3-7: Heat exchanger configurations and nomenclature

1. Channel Dimension		**2. Number of Channels p. p. / number of plates**				**3. Channel shape**	
3x1 mm	2x1 mm	15/1	5/1	5/2	5/3	I/I	I/Z
A	B	A	B	C	D	A	B
Heat exchanger test configurations							
1	AAA			5	BBB		
2	AAB			6	BCB		
3	BAA			7	BDB		
4	BAB						

A typical manufacturing process of the channels of a compact heat exchanger, in serial production, is the chemical etching due to small required channel dimensions and fast fabrication time. This method leads to semi-circular channel geometries, in which the channel width is a function of the channel depth. For instance, a channel depth of 0.6 mm leads to a minimum channel width of about 0.95 mm [47]. The boundary conditions of the chemical etching combined with the aim to build compact heat exchangers leads to channel diameters from about 1 mm to 5 mm. Shah [44] also suggests channel diameters between 0.5 mm and 8 mm for CHX's. To investigate the influence of the channel dimension on different phenomena, e.g. the heat transfer and the pressure drop, two channel configurations with equal rectangular channels dimensions on both sides (H_2O, sCO_2) are determined with respect to recommended diameters for CHX`s from the literature [44], [48]. According to Table 3-7, channels with a width of 3 mm and a height of 1 mm (A) as well as with a width of 2 mm and a height of 1 mm (B) are chosen. The rectangular channel dimension is selected with respect to an easier and more flexible manufacturing process by milling. The heat exchanger configurations AAA, AAB, BAA and BAB are designed as so-called "two-plate" heat exchangers with 15 channels per plate and one plate on each side (15/1). To investigate further the influence of the plenum geometry on phenomena like the pressure drop, heat exchangers

with 5 channels per plate (5/1) and a varying number of plates on each side are designed. Heat exchangers with 1 plate on the steam side and 1 plate on the sCO_2 side are called B (5/1), with 2 plates on each side with C (5/2) and with 3 plates on each side are called D (5/3). These heat exchangers can also be used for the investigation of the maximum heat transfer because of the possibility of gradually decreasing the heat transfer area. The influence of the channel shape on the pressure drop and heat transfer is investigated, too. For this, two-plate heat exchangers with straight channels on both sides (AAA, BAA) and two-plate heat exchangers with straight channels on the H_2O side and Z-shaped channels on the sCO_2 side (AAB, BAB) are designed and manufactured. The Z-shape of the sCO_2 channels is necessary to connect two of the four plenums with the H_2O side and two of the four plenums with the sCO_2 side, in consideration of a stacked CHX with more than one plate on each side. The Z-shape is used on the sCO_2 side because of forced convection, generated by the compressor of the sCO2-HeRo system. To clarify the introduced nomenclature, one example is given. A heat exchanger with rectangular 2x1 mm channels, 15 channels per plate, one plate on each side and straight channels on both the H_2O and sCO_2 side is called BAA.

Diffusion bonding

Diffusion bonding is a solid state welding technique, in which two components can be joined, based on the atomic diffusion of elements at the joining surface by the application of pressure and temperature [49], [50]. Similar or dissimilar material combinations of titanium alloys, zirconium alloys and nickel-based alloys can be joined without macroscopic deformation or relative motion of the parts. The bonding process can be divided into two parts. In the first step, a sufficient contact between the components must be achieved by applying pressure, which deforms the surface roughness and disrupts any kind of contamination. According to KE-Technology [51] pressures between 350 kg/cm² and 700 kg/cm² are used for the bonding process, depending on the materials and geometries. The second step includes the diffusion process itself and the grain growth at the bonding line in consideration of constant pressures and gradually increasing temperatures up to 1200 °C. This step leads to a metallic bonding without any visible contact surface line. The contact surfaces must be clean, smooth and free from oxides to guarantee a successful bonding. If the bonding is successful, the microstructure at the bonding region has nearly the same physical and mechanical properties as the base material. This leads to high heat conductivity as well as high pressure and temperature resistance at the bonding line, which are desirable for compact heat exchangers. At the

KE-Technology, the vacuum bonding technique is applied, which is usually used for materials like stainless steel and alloys. The working area of the diffusion bonding device is limited to a diameter of 325 mm and a height of 350 mm, which must be considered in the design of components. The pressure is adjusted by hydraulic pistons and the inductive heating process is carried out in a vacuum chamber.

Plate material

The austenitic stainless steel 1.4301 (X5CrNi18-10 / 304) with 5 % carbon, 18 % chrome and 10 % nickel is chosen as plate material for the heat exchangers. It has a corrosion resistance up to 925 °C, but a continuous use between 425 °C and 860 °C is not recommended if corrosion resistance in combination with water is required. Furthermore, it has average mechanical properties, a good forgeability, an excellent weldability and an averaged machinability [52]. The excellent weldability and the machinability are important reasons, why 1.4301 is chosen as plate material. It can be purchased as strips, tubes, pipes, and plates for different kinds of applications like the chemical industry and the mechanical engineering. At a temperature of 20 °C it has a density of 8000 kg/m³, a melting point of 1450 °C, a thermal conductivity of 16 W/(m·K), a specific heat capacity of 500 J/(kg·K), a minimum yield strength of 210 N/mm², a minimum tensile strength of 520 N/mm² and it is slightly magnetisable [53]. Moreover, the yield strength $R_{p0.2}$ is a function of the temperature, leading to 160 N/mm² at 100 °C, 140 N/mm² at 150 °C, 130 N/mm² at 200 °C, 120 N/mm² at 250 °C and 110 N/mm² at 300 °C. For successfully diffusion bonded components the yield strength is assumed to be more than 70 % of the yield strength of the base material [54], [55]. This reduction in the yield strength must be considered by employing a factor f in the mechanical design of diffusion bonded components to prevent any kind of material failure.

Mechanical design

There are currently no international standard or generally admitted calculation methods for the mechanical design of compact heat exchangers. Because of that, common methods for ordinary geometries like pipes, vessels e.g. have to be adjusted. DIN EN 13445-3, for instance, includes a calculation method in which the wall thickness of a rectangular pressure vessel with supporting structures can be determined. The heat exchanger manufacturer Heatric uses the

ASME-BPVC-VIII code for the design of PCHE's. The models of ASME code are similar to them of DIN EN but Heatric additionally implemented semi-circular channel geometries [54]. Another approach for the mechanical design of compact heat exchangers is to transform rectangular channel geometries into circular pipe geometries. This method is used then for the determination of the minimum wall thickness by ordinary calculation methods like the Kesselformel or the analytic calculation method for thick-walled pressure vessels.

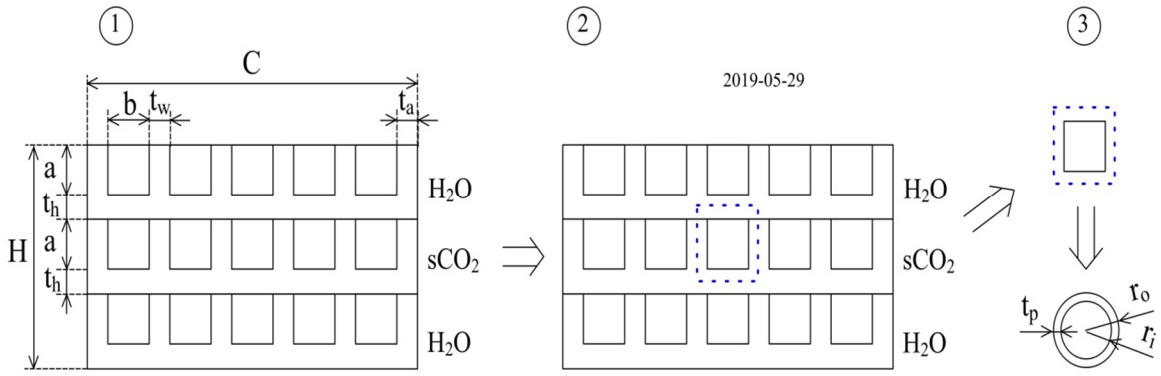

Figure 3-5: Schemes of CHX dimensioning

A sketch of the dimensioning steps from (1) to (3), for the determination of the minimum wall thicknesses of the CHX, is shown in Figure 3-5. The dimensioning starts on the left (1), in which a fictitious HX with a width C, a height H and a length L is shown. It consists of two H_2O plates and one sCO_2 plate, which are alternately stacked together. Each plate has 5 rectangular channels with a channel width b and a channel height a. The wall thickness between two neighboring channels at one plate is t_w, the wall thickness between one H_2O and one sCO_2 channel is t_h, and the outer wall thickness is t_a. For the compact heat exchangers, equal wall thicknesses of t_w and t_h are chosen. At point (2) a representative rectangular sCO_2 channel is marked with a dashed blue line, shown as a separate component on the top right at point (3). This channel is then transformed by the hydraulic diameter equation into a circular pipe geometry with an outer radius r_o, an inner radius r_i and a wall thickness t_p. The minimum wall thickness t_p of the pipe is determined by common equations for pressure vessels and pipe geometries. For the calculation, a sCO_2 pressure of 180 bar and a steam pressure of 1 bar are assumed. The sCO_2 pressure is derived from cycle calculation results of the sCO2-HeRo system for a NPP and the steam pressure is conservatively set to ambient pressure.

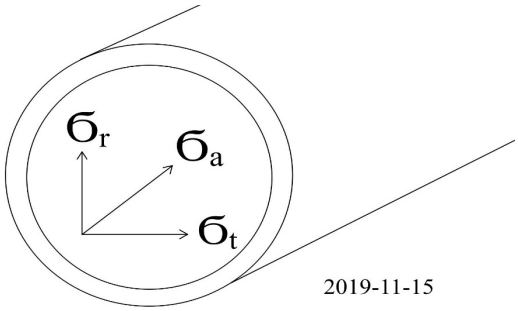

Figure 3-6: Schemes of pipe stresses

The tangential stress σ_t in a pipe (Figure 3-6) can be calculated in general according to Eq. (3-7) by using the internal pressure p_i, the radius at the inner wall $r_{i,t}$, the radius at the outer wall $r_{o,t}$ and the radius $r_{x,t}$ at position x [56], [57].

$$\sigma_t = p_i \cdot \frac{{r_{i,t}}^2}{{r_{o,t}}^2 - {r_{i,t}}^2} \cdot \left(\frac{{r_{o,t}}^2}{{r_{x,t}}^2} + 1\right) \tag{3-7}$$

Eq. (3-7) shows that σ_t is a function of the radius $r_{x,t}$ with a maximum stress at the inner wall radius $r_{i,t}$ and a minimum stress at the outer wall radius $r_{o,t}$. The maximum tangential stress $\sigma_{t,max}$ can be calculated by Eq. (3-9) after replacing $r_{x,t}$ by $r_{i,t}$ in Eq. (3-7).

$$\sigma_{t,max} = p_i \cdot \frac{{r_{i,t}}^2}{{r_{o,t}}^2 - {r_{i,t}}^2} \cdot \left(\frac{{r_{o,t}}^2}{{r_{i,t}}^2} + 1\right) \tag{3-8}$$

For a given pressure p_i and a maximum tangential stress $\sigma_{t,max}$ of the material, the necessary outer wall radius $r_{o,t}$, is calculated according to Eq. (3-9) after rewriting Eq. (3-8).

$$r_{o,t} = \sqrt{\frac{(p_i + \sigma_{t,max})}{\sigma_{t,max} - p_i} \cdot {r_{i,t}}^2} \tag{3-9}$$

The radial pipe stress 6_r (Figure 3-6) is calculated similar to the tangential stress by Eq. (3-10) as a function of the radius $r_{x,r}$. The internal pressure p_i, the radius at the inner wall $r_{i,r}$ and the radius at the outer wall $r_{o,r}$ are used for this.

$$6_r = - p_i \cdot \frac{{r_{i,r}}^2}{{r_{o,r}}^2 - {r_{i,r}}^2} \cdot (\frac{{r_{o,r}}^2}{{r_{x,r}}^2} - 1) \tag{3-10}$$

Eq. (3-10) shows that a minimum radial pipe stress 6_r occurs if $r_{x,r}$ is $r_{o,r}$ and a maximum radial stress occurs if $r_{x,r}$ is $r_{i,r}$. The maximum radial pipe stress $6_{r,max}$ is calculated by Eq. (3-11) after replacing $r_{x,r}$ by $r_{i,r}$ (Eq. (3-10)).

$$6_{r,max} = - p_i \cdot \frac{{r_{i,r}}^2}{{r_{o,r}}^2 - {r_{i,r}}^2} \cdot (\frac{{r_{o,r}}^2}{{r_{i,r}}^2} - 1) \tag{3-11}$$

The axial stress 6_a (Figure 3-6) in a pipe can be calculated according to Eq. (3-12) by using the internal pressure p_i, the outer pressure p_o, the radius at the inner wall $r_{i,a}$ and outer wall $r_{o,a}$.

$$6_a = \frac{p_i \cdot {r_{i,a}}^2 - p_o \cdot {r_{o,a}}^2}{{r_{o,a}}^2 - {r_{i,a}}^2} \tag{3-12}$$

The minimum outer wall radius $r_{o,a}$ can be calculated according to Eq. (3-13) after rewriting Eq. (3-12). Therefore, the internal pressure p_i, the outer pressure p_o, the radius at the inner wall $r_{i,a}$ and the allowed axial stress $6_{a,max}$ of the material are used.

$$r_{o,a} = \sqrt{\frac{(p_i + 6_{a,max})}{6_{a,max} + p_o} \cdot {r_{i,a}}^2} \tag{3-13}$$

The boundary conditions for the mechanical design, like pressures and temperatures, and the calculation results are summarized in Table 3-8. The maximum allowed material stress 6_{max} of stainless steel 1.4301 is calculated according to Eq. (3-14) to 29.6 N/mm². For this, a maximum steam temperature T_{H2O} of 300 °C is defined, leading to a yield strength $R_{p0.2,300°C}$

of 110 N/mm². Moreover, uncertainties of the diffusion bonding process are considered by using a reduction factor of 0.7 and a safety factor S of 2.6. The sCO_2 pressure p_{sCO2} at the inner pipe wall is set to 180 bar and the outer pressure p_{H2O} to 1 bar. The pipe inner radius r_i is calculated for the rectangular 2x1 mm channel geometry as 0.65 mm and for the 3x1 mm geometry as 0.75 mm. The minimum outer radius of the pipe r_o is determined for both channel geometries according to Eq. (3-9) and Eq. (3-13) for the tangential stress $r_{o,t}$ and for the axial stress $r_{o,a}$. Comparing the results of $r_{o,t}$ and $r_{o,a}$ they show that for the tangential stress thicker walls are necessary. The minimum wall thickness t_p of the pipe is determined (Eq. (3-15)) with the inner pipe radius r_i and the outer pipe radius $r_{o,t}$ for the 2x1 mm channel geometry to 0.67 mm and for the 3x1 mm channel geometry to 0.77 mm. The radial stress 6_r is calculated for both geometries according to Eq. (3-11) and compared to allowable material stresses.

$$6_{max} = R_{p0.2,300°C} \cdot 0.7 \cdot S \tag{3-14}$$

$$t_p = r_{o,t} - r_i \tag{3-15}$$

Table 3-8: Mechanical design parameters

Variable	Value	Unit	Description
6_{max}	29.6	N/mm²	Material Stress 1.4301 (300 °C / 70 % / 2.6)
S	2.6	-	Safety Factor
T_{H2O}	300	°C	Max. Temperature - H_2O
p_{sCO2}	180	bar	Max. Pressure - sCO_2
p_{H2O}	1	bar	Max. Pressure - H_2O
$r_{i,2x1}$	0.65	mm	Inner Radius Pipe - 2x1 Channel
$r_{i,3x1}$	0.75	mm	Inner Radius Pipe - 3x1 Channel
$r_{o,t,2x1}$	1.32	mm	Outer Radius Pipe - Tangential - 2x1 Channel
$r_{o,t,3x1}$	1.52	mm	Outer Radius Pipe - Tangential - 3x1 Channel
$r_{o,a,2x1}$	0.82	mm	Outer Radius Pipe - Axial - 2x1 Channel
$r_{o,a,3x1}$	0.95	mm	Outer Radius Pipe - Axial - 3x1 Channel
$t_{p,2x1}$	0.67	mm	Min. Wall Thickness Pipe - 2x1 Channel
$t_{p,3x1}$	0.77	mm	Min. wall thickness pipe - 3x1 Channel

Plate design and manufacturing

The heat exchanger plates are designed with the information of the plate material and the wall thickness. The minimum wall thickness t between two neighboring channels of one plate is set to 1.4 mm (2 x 0.67 mm) for the 2x1 mm channels and to 1.6 mm (2 x 0.77 mm) for the 3x1 mm channels. Equal wall thicknesses are planned between one H_2O and one sCO_2 channel. The effective channel length is determined at 150 mm with respect to a maximum working area of the diffusion bonding machine. According to Table 3-7, seven heat exchanger test configurations are manufactured with different channel dimensions, numbers of channels per plate / numbers of plates and channel shapes.

As an example, the technical drawings of the heat exchanger of case BAB (2x1 mm - 15/1 - IZ) are shown in Figure 3-7 without dimensioning, for simplification. The technical drawings of all seven investigated heat exchangers, including dimensioning, are attached in Appendix C. The first technical drawing in Figure 3-7 shows the cover plate with a plate thickness of 4 mm, a length of 247.6 mm and a width of 95.6 mm. The four drillings with a diameter of 12.7 mm are for the inlet and outlet of the H_2O into the plenums of the steam plate. The steam plate with 15 straight rectangular 2x1 mm channels and a plate thickness of 2.4 mm is shown in the second drawing. The length of the plenum with 49.6 mm is determined by the number of 15 channels and a wall thickness of 1.4 mm between the channels. The plenum width of 13 mm results from the diameter of the ½" pipe connections. The two 4 mm drillings are used only for adjusting the plates against each other during the diffusion bonding process. The third drawing shows the sCO_2 plate with a plate thickness of 5 mm, a length of 247.6 mm and a width of 95.6 mm. For the sCO_2 inlet and outlet into the plenums also four drillings are implemented. Two plenums of the heat exchanger connect the straight water channels. The other two plenums connect the sCO_2 channels. They are mounted at the side, thus the sCO_2 channels are Z-shaped, in consideration of a stacked CHX with more than one plate on each side. In counter-current flow configuration, the steam enters the two-plate CHX at the top and leaves it driven by gravity as condensate at the bottom. The sCO_2 enters the CHX at the bottom left and leaves it at the top right. The effective channel length for sCO_2 is determined at 150 mm, which is the straight length of the middle part of the channels.

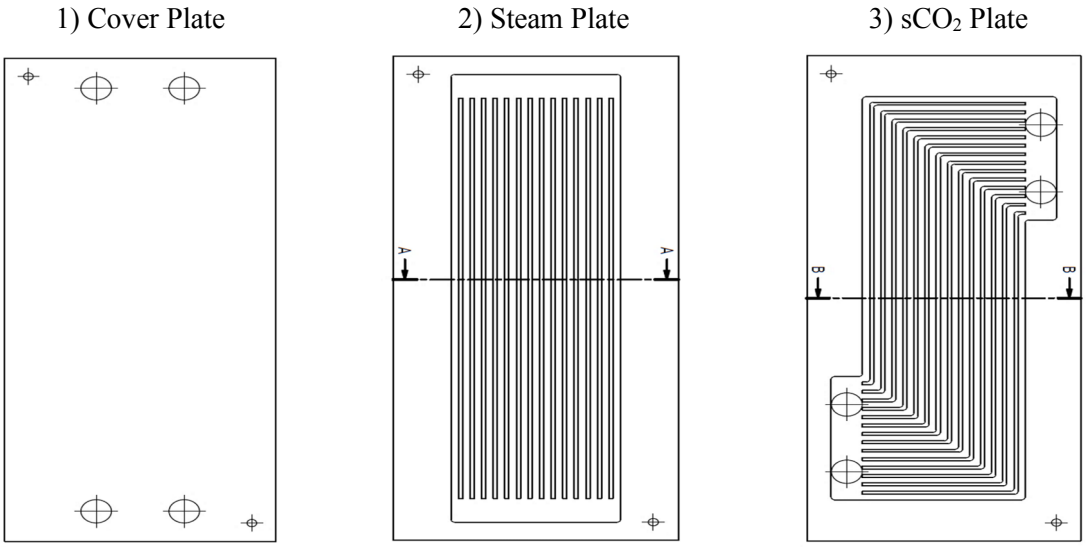

Figure 3-7: Plate design of case BAB

Pictures of the manufacturing steps of the heat exchanger BAB are shown in Figure 3-8 as an example. At the start, the cover, steam and sCO_2 plates are manufactured in the workshop by milling according to the technical drawings (Figure 3-7). The drillings at the outer area of the plates are only for adjusting the plates during the milling process and for diffusion bonding. Afterwards, they are cleaned and stacked together, as shown on the left in Figure 3-8. In the second step, the plates are diffusion bonded before the H_2O and sCO_2 pipe connections are electron beam welded onto the plates, which is shown in the center of Figure 3-8. After welding, a pressure and leakage test is carried out. The pressure test is depicted on the right in Figure 3-8. After successfully passing both tests, the heat exchanger is ready for installation and experimental investigations can be performed.

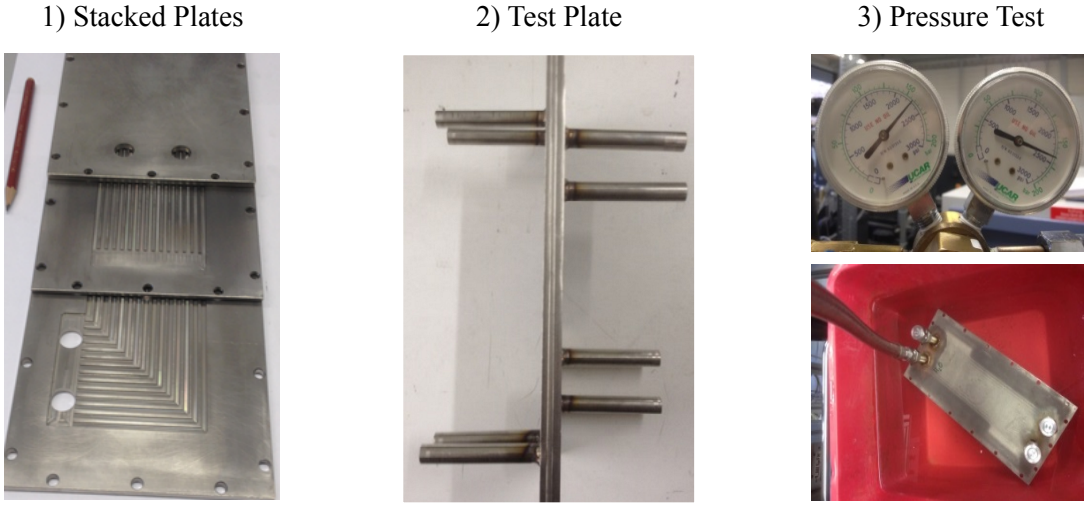

Figure 3-8: Manufacturing steps of case BAB

4 Results

4.1 Measurement points

The measurement points for the experimental investigations are summarized in Table 4-1. They are defined in consideration of boundary conditions, derived from investigations at the glass model as well as from internal restrictions at the SCARLETT loop and both steam cycles. To be able to compare the results of the low-pressure and high-pressure steam cycle, similar measurement campaigns are chosen. The low-pressure steam cycle experiments are carried out according to campaign 1 - 6 with a steam pressure of 0.3 bar, a steam temperature of 70 °C, varying steam volume flow rates, varying sCO_2 mass flow rates and sCO_2 inlet pressures of 95 bar, 100 bar and 110 bar. These results are used for the design of the compact heat exchanger for the sCO2-HeRo demonstrator unit, attached to the PWR glass model. The high-pressure steam cycle experiments are carried out according to campaigns 1 - 9. A steam pressure of 70 bar, a steam temperature of 286 °C, varying steam volume flow rates, varying sCO_2 mass flow rates and sCO_2 inlet pressures of 95 bar, 100 bar and 110 bar are used to obtain results of the heat transfer performance under "Design point" (DP), "Out of design point" (ODP) and "Out of design point II" (ODP II) conditions. These results are used for validation purpose and for the improvement of the German thermo-hydraulic code ATHLET.

In the DP experiments the sCO_2 mass flow rates $\dot{m}_{sCO2}$ (37 g/s - 68 g/s) and water volume flow rates $\dot{m}_{H2O}$ (0.53 l/h - 0.97 l/h) of the measurement campaign 1, 2 and 3 are scaled down in the same ratio according to the entire amount of sCO_2 mass flow rate of 650 g/s and water volume flow rate of 9.3 l/h, which are used in the design point of the sCO2-HeRo demonstrator unit at the glass model. The electrical heating power of the evaporator $Q_{in,Evap}$ is adjusted according to the water volume flow rates from 380 W to 680 W to ensure that the water inventory is completely evaporated. The minimum sCO_2 mass flow rate of 37 g/s and the maximum sCO_2 mass flow rate of 68 g/s are limited by the SCARLETT test facility. To investigate the heat transfer also ODP, measurement campaigns 4, 5 and 6 are performed. A constant sCO_2 mass flow rate $\dot{m}_{sCO2}$ of 37 g/s and gradually increasing water volume flow rates $\dot{m}_{H2O}$ from 0.53 l/h to 1.74 l/h are applied. The power of the electrically heated evaporator $Q_{in,Evap}$ is adjusted according to the water volume flow rates from 380 W to 1230 W. The water volume flow rate is limited to 2 l/h and the power of the electrical heated evaporator to 1300 W because of temperature restrictions. In the ODP II measurement campaigns 7, 8 and 9, investigations with

a constant water volume flow rate of 1.74 l/h and an electrical heating power of 1230 W are performed. The sCO_2 mass flow rate is gradually decreased from 37 g/s to about 6 g/s by adjusting a needle valve and bypassing a part of the sCO_2 mass flow rate. To investigate additionally the influence of the sCO_2 inlet pressure $p06$ on phenomena like the heat transfer and the pressure drop, sCO_2 inlet pressures of 110 bar, 100 bar and 95 bar with an inlet temperature of 40 °C are chosen. The maximum sCO_2 inlet pressure is limited by pressure restrictions at the SCARLETT loop, the minimum pressure is determined with respect to the location near to the critical point of sCO_2 and the temperature is limited by internal temperature restrictions at the conditioning unit.

Table 4-1: Measurement points

Campaign	$\boldsymbol{p06}$ **[bar]**	$\boldsymbol{T07}$ **[°C]**	**Status**
1	110	40	Design Point "DP"
2	100	40	
3	95	40	
4	110	40	Out of Design Point "ODP"
5	100	40	
6	95	40	
7	110	40	Out of Design Point II "ODP II"
8	100	40	
9	95	40	
$\dot{m}_{sCO2}$ **[g/s]**	$\dot{m}_{H2O}$ **[l/h]**	$Q_{in,Evap}$ **[W]**	**Status**
37	0.53	380	DP
46	0.65	460	DP
56	0.80	560	DP
68	0.97	680	DP
37	0.53	380	ODP
37	0.65	460	ODP
37	0.80	560	ODP
37	0.97	680	ODP
37	1.17	830	ODP
37	1.43	1010	ODP
37	1.74	1230	ODP
37 - 6	1.74	1230	ODP II

The nomenclature introduced in Table 3-7 is extended by two more alphabetic letters according to Table 4-2. The first letter describes the “Type of heat input” into the sCO_2. A heat input with condensing steam of the high-pressure (HP) steam cycle is named (A), a heat input with condensing steam of the low-pressure (LP) steam cycle is (B) and no heat input is (C). Moreover, the “Measurement point campaign” is identified for the “Design point” (DP) experiments with (A), for the “Out of design point” (ODP) experiments with (B) and for the “Out of design point II” (ODP II) experiments with (C). To clarify the introduced nomenclature, one example is given: BAB-AA presents the heat exchanger with rectangular 2x1 mm channels (B), 15 channels per plate and 1 plate on each side (A), straight H_2O channels and Z-shaped sCO_2 channels (B), the high-pressure steam cycle is used for the heat input (A) and the design point measurement campaign (A) is performed.

Table 4-2: Extension of nomenclature

4. Type of heat input			**5. Measurement point campaign**		
HP	LP	NO	DP	ODP	ODP II
A	B	C	A	B	C

An overview of the measurement configurations is shown in Table 4-3. It includes the channel geometries (3x1 mm / 2x1 mm), the channel/plate configurations (15/1 / 5/1 / 5/2 / 5/3), the channel shapes (II / IZ), the type of heat inputs (HP / LP / NO) and the measurement campaigns (DP / ODP / ODP II). The investigated ones are marked with “X”. It can be seen that all seven heat exchangers are used without a heat input from the steam cycle for the DP, ODP and ODP II measurement points. These results are used to obtain the pressure drops of unheated flows. The measurement time for unheated experiments is set to 10 minutes after reaching steady state configurations. The LP steam cycle experiments are performed to determine the compact heat exchanger for the sCO2-HeRo demonstrator unit at GfS. For this purpose, the 3x1 mm and 2x1 mm channel geometry, a channel/plate configuration of (15/1) as well as straight H_2O and Z-shaped sCO_2 channels (IZ) are investigated according to the DP and ODP measurement campaigns. The HP steam cycle experiments are used for all heat exchanger configurations, except the heat exchangers with a channel geometry of 2x1 mm and channel/plate configurations of (5/2) and (5/3). A measurement time of 15 minutes, after reaching steady state configurations is defined for heated experiments.

Table 4-3: Overview of performed measurement configurations

		3x1		2x1				
		15/1		15/1		5/1	5/2	5/3
		II	IZ	II	IZ	IZ	IZ	IZ
HP	DP	X	X	X	X	X	-	-
	ODP	X	X	X	X	X	-	-
	ODP II	X	X	X	X	X	-	-
LP	DP	-	X	-	X	-	-	-
	ODP	-	-	-	X	-	-	-
	ODP II	-	-	-	-	-	-	-
NO	DP	X	X	X	X	X	X	X
	ODP	X	X	X	X	X	X	X
	ODP II	X	X	X	X	X	X	X

4.2 Summary of measurement results

An example of measurement results is given in Table 4-4 for the LP steam cycle and the 3x1 mm / 15/1 / IZ heat exchanger configuration. It includes the water volume flow rate $\dot{m}_{H2O}$, the H_2O pressure $p02$ at the inlet of the CHX, the H_2O pressure $p04$ at the outlet of the CHX, the H_2O temperature $T03$ at the inlet of the CHX, the H_2O temperature $T04$ at the outlet of the CHX , the calculated electrical heating power of the evaporator $Q_{in,Evap}$, the sCO_2 mass flow rate $\dot{m}_{sCO2}$, the sCO_2 pressure drop $\Delta p05$ in the CHX, the sCO_2 inlet pressure $p06$ into the CHX as well as the sCO_2 inlet temperature $T07$ and outlet temperatures $T08$ at the CHX. The number in brackets in the first column in Table 4-4 identifies the measurement campaign according to Table 4-1. All measurement results are summarized in Appendix D.

Table 4-4: Experimental results

Low-pressure steam cycle / sCO_2 SCARLETT loop											
3x1 mm / 15/1 / IZ											
	$\dot{m}_{H2O}$	$p02$	$p04$	$T03$	$T04$	$Q_{in,Evap}$		$\dot{m}_{sCO2}$	$\Delta p05$	$p06$	$T07$	$T08$
	[l/h]	[bar]	[bar]	[°C]	[°C]	[W]		[g/s]	[bar]	[bar]	[°C]	[°C]
DP (1)	0.54	0.317	0.300	69.99	37.72	385		36.94	0.675	109.282	39.21	41.23
	0.61	0.321	0.299	70.23	37.83	455		45.98	0.975	108.824	39.38	41.11
	0.74	0.329	0.300	70.75	37.48	550		55.92	1.425	108.343	39.13	40.78
	0.97	0.354	0.311	72.34	38.28	678		67.35	2.053	107.516	39.12	40.63
DP (2)	0.55	0.323	0.305	70.42	36.68	389		36.45	0.672	99.255	39.34	40.59
	0.64	0.332	0.309	71.02	37.21	462		45.28	1.023	98.803	39.24	40.34
	0.79	0.360	0.330	72.87	37.51	549		56.15	1.548	98.148	39.02	39.93
	0.95	0.359	0.317	72.68	36.82	685		67.40	2.226	97.177	38.63	39.35
DP (3)	0.53	0.336	0.320	71.33	37.58	374		36.90	0.728	94.214	38.99	39.80
	0.67	0.346	0.325	71.99	37.77	452		45.66	1.106	93.746	39.10	39.69
	0.79	0.358	0.329	72.72	37.40	544		52.30	1.493	93.021	39.15	39.66
	0.98	0.352	0.307	72.21	37.55	685		67.81	2.459	92.134	38.83	38.74

4.3 Pressure drop results

In the following, representative measurement results of the sCO_2 pressure drop of unheated and heated sCO_2 flows are analyzed. These results are used for the design specification of the compact heat exchanger.

4.3.1 Pressure drop results of unheated sCO_2 flows

Experimental results of the sCO_2 pressure drop $\Delta p05$ in the heat exchangers of Case BAA and AAA are shown in Figure 4-1 as a function of the sCO_2 mass flow rate $\dot{m}_{sCO2}$ and the sCO_2 inlet pressure. The heat exchanger BAA has a rectangular 2x1 mm channel dimension, a channel length of 150 mm, straight H_2O and straight sCO_2 channels, 15 channels per plate and 1 plate on each side. The HX of Case AAA is similar to BAA, except for the channel dimension of 3x1 mm. The measurements are performed without a sCO_2 heat input and a sCO_2 inlet temperature of about 39 °C.

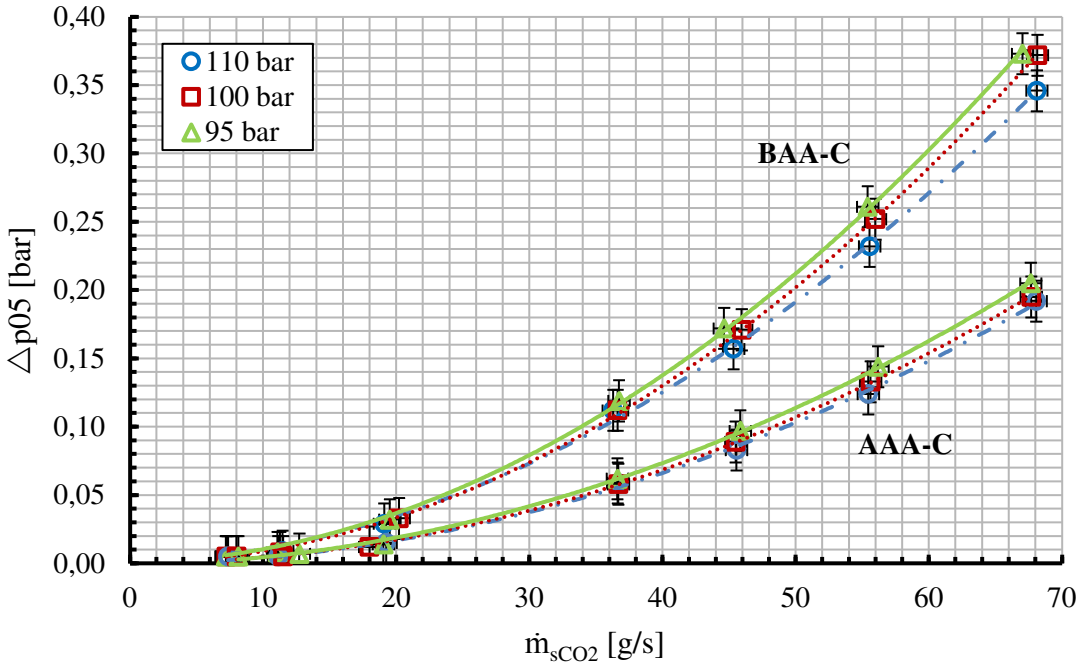

Figure 4-1: Results of Δp05 as function of $\dot{m}_{sCO2}$ of Case BAA-C & AAA-C

The upper three graphs in Figure 4-1 show the experimental results of the sCO_2 pressure drop $\Delta p05$ as a function of the mass flow rate $\dot{m}_{sCO2}$ and the sCO_2 inlet pressure $p06$ for the unheated DP and ODP II investigations of Case BAA-C and the lower three graphs of AAA-C. The ODP II investigations are carried out with mass flow rates between 7 g/s and 20 g/s and the DP investigation from about 37 g/s to 68 g/s. The results show that an increasing sCO_2 mass flow rate and a constant sCO_2 inlet pressure leads to a parabolic increase of the sCO_2 pressure drop. Furthermore they show that an increasing sCO_2 inlet pressure leads to decreasing pressure drops $\Delta p05$ for constant sCO_2 mass flow rates $\dot{m}_{sCO2}$. This can be explained by the fluid density, where an increased sCO_2 inlet pressure leads to an increased fluid density and thus to a decreased pressure drop due to lower fluid velocities in the channels of the HX. For the 2x1 mm channel dimension, a sCO_2 mass flow rate of about 68 g/s and an sCO_2 inlet pressure of about 110 bar leads to a pressure drop of 0.346 bar, 100 bar to 0.372 bar, and an inlet pressure of 95 bar leads to a pressure drop of 0.373 bar. A comparison of the results of the sCO_2 pressure drop of Case BAA (2x1 mm) and Case AAA (3x1 mm) shows that a decreasing flow area and a constant sCO_2 mass flow rate leads to increasing pressure drop results at constant sCO_2 inlet pressures. This can be explained by increased flow velocities in the channels. For example, a sCO_2 inlet pressure of 110 bar and a mass flow rate of 68 g/s leads to a pressure drop of

0.346 bar for the 2x1 mm channels and to 0.192 bar for the 3x1 mm channels. Furthermore, an increase of the channel dimension from 2x1 mm to 3x1 mm leads to a reduction of the sCO_2 pressure drop of more than 45 %, for all shown measurement results and mass flow rates.

In the following, the sCO_2 pressure drop is re-calculated for unheated sCO_2 flows by means of correlations for the heat exchangers of Case BAA and AAA and compared to experimental results. The results are depicted in Figure 4-1. The pressure drop $\Delta p05$ can be calculated for single-phase flows in general according to Eq. (4-1) [58]. The correction factor e, the friction coefficient ξ, the density of the fluid ρ and the velocity of the fluid v are used for this.

$$\Delta p05 = e \cdot \xi \cdot \frac{\rho \cdot v^2}{2} \tag{4-1}$$

The correction factor e determines the type of flow. For a common channel flow, e is a function of the channel length l and channel diameter d (Eq. (4-2)); for cross-section area changes or flow deflections, e is set to 1 (Eq. (4-3)).

$$e = f\left(\frac{l}{d}\right) \tag{4-2}$$

$$e = 1 \tag{4-3}$$

The pressure drop in the channel $\Delta p_{channel}$ can be calculated in general after inserting Eq. (4-2) into Eq. (4-1) and rewriting it according to Eq. (4-4).

$$\Delta p_{channel} = \xi_{channel} \cdot \frac{l}{d} \cdot \frac{\rho \cdot v^2}{2} \tag{4-4}$$

There are two common approaches for determining the friction coefficient of the channel $\xi_{channel}$ (Eq. (4-4)). The first one is by using a Moody diagram, where $\xi_{channel}$ is shown as a function of the Reynolds number Re and the ratio of pipe roughness K to pipe diameter d [59]. Besides that, the friction coefficient $\xi_{channel}$ can be calculated with correlations [58] for laminar and turbulent flow regimes. Laminar flow regimes occur at $Re < 2320$, turbulent flow

regimes occur at $Re > 8000$ and the transition zone is between $2320 < Re < 8000$. For laminar flow regimes in smooth channels, the friction coefficient $\xi_{channel}$ can be determined according to Eq. (4-5). For turbulent flow regimes, various correlations can be applied, depending on the Reynolds number. The correlation of Blasius (Eq. (4-6)) can be chosen for $3000 < Re < 10^5$, the correlation of Konakov (Eq. (4-7)) for $10^4 < Re < 10^6$ and the correlation of Filonenko (Eq. (4-8)) for $10^5 < Re < 5 \cdot 10^7$. The results of the correlation of Filonenko have a deviation of less than 0.5 % compared with the results of Eq. (4-9), which is derived from the implicit correlation of Prandtl and Karman according to Eq. (4-9) and is valid for $Re > 10^6$.

$$\xi_{channel} = \frac{64}{Re} \tag{4-5}$$

$$\xi_{channel} = \frac{0.3164}{\sqrt[4]{Re}} \tag{4-6}$$

$$\xi_{channel} = (1.8 \cdot lg(Re) - 1.5)^{-2} \tag{4-7}$$

$$\frac{1}{\sqrt{\xi_{channel}}} = 1.819 \cdot lg(Re) - 1.64 \tag{4-8}$$

$$\frac{1}{\sqrt{\xi_{channel}}} = -0.8 + 2 \cdot lg\left(Re \cdot \sqrt{\xi_{channel}}\right) \tag{4-9}$$

The pressure drop due to cross section area changes and flow deflections Δp_{loss} can be calculated according to Eq. (4-10) after inserting Eq. (4-3) into Eq. (4-1) and rewriting it.

$$\Delta p_{loss} = \xi_{loss} \cdot \frac{\rho \cdot v^2}{2} \tag{4-10}$$

For cross section area changes (like in the plenum of a CHX) there are two possibilities: contraction and expansion. A channel flow with a sudden contraction of the cross section area is shown on the top left in Figure 4-2. According to [58] $\xi_{loss,n}$ can be determined as a function of the ratio of inlet cross section area A_1 and outlet cross section area A_2 as well as the Reynolds number Re_2 downstream. The depicted diagram on the bottom left (Figure 4-2) shows that for

turbulent flow regimes with $Re > 10^4$, the friction coefficient $\xi_{loss,n}$ has a linear tendency with decreasing values for increasing ratios of the cross section area changes and vice versa. $\xi_{loss,n}$ can be determined with a linear function according to Eq. (4-11). A pipe flow with a sudden cross section area expansion is shown on the top right in Figure 4-2. The friction loss coefficient $\xi_{loss,e}$ can be calculated according to Eq. (4-12).

$$\xi_{loss,n} = 0.5 - 0.4 \cdot \frac{A_2}{A_1} \tag{4-11}$$

$$\xi_{loss,e} = \left(1 - \frac{A_1}{A_2}\right)^2 \tag{4-12}$$

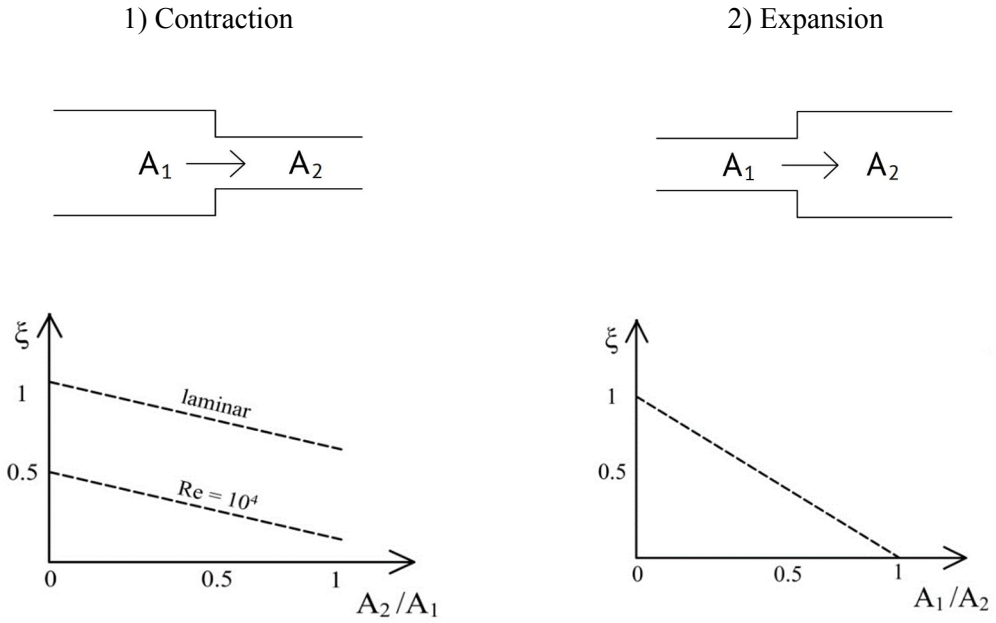

Figure 4-2: Cross section area changes

The friction loss coefficient $\xi_{loss,d}$ of flow deflections in elbows can be determined by means of diagrams. There $\xi_{loss,d}$ is shown as a function of the deflection degree δ and the roughness of the channel K [58]. For a rough channel and a deflection of 90°, the friction loss coefficient $\xi_{loss,d}$ can be determined according to Eq. (4-13) to 1.25.

$$\xi_{loss,d} = 1.25 \tag{4-13}$$

The overall sCO_2 pressure drop $\Delta p05$ in the HX's can be re-calculated in general according to Eq. (4-14). It consists of two parts: the pressure losses due to friction in channels $\Delta p_{channel}$ and pressure losses due to flow deflections and cross section area changes Δp_{loss}.

$$\Delta p05 = \sum_{k=1}^{i} \Delta p_{channel,k} + \sum_{j=1}^{n} \Delta p_{loss,j} \tag{4-14}$$

Considering friction losses as well as flow deflections and cross section area changes in the HX of Case BAA and AAA, the pressure drop $\Delta p05$ can be re-calculated according to Eq. (4-15).

$$\begin{aligned}\Delta p05 = {} & \Delta p_{pipe,in} + \Delta p_{loss,d,plenum,in} + \Delta p_{loss,n,plenum,in} + \Delta p_{plenum,in} \\ & + \Delta p_{loss,n,channel,in} + \Delta p_{channel} + \Delta p_{loss,e,channel,out} \\ & + \Delta p_{plenum,out} + \Delta p_{loss,e,plenum,out} + \Delta p_{loss,d,plenum,out} \\ & + \Delta p_{pipe,out}\end{aligned} \tag{4-15}$$

The pressure drop due to friction in the inlet pipe of the heat exchanger into the plenum is considered by $\Delta p_{pipe,in}$, the flow deflection in the plenum by $\Delta p_{loss,d,plenum,in}$, the change of the cross section area from the inlet pipe into the plenum by $\Delta p_{loss,n,plenum,in}$, the friction in the plenum by $\Delta p_{plenum,in}$, the cross section area change from the plenum into the channel by $\Delta p_{loss,n,channel,in}$, the friction in the channel by $\Delta p_{channel}$, the cross section area change from the channel into the plenum $\Delta p_{loss,e,channel,out}$, the friction in the plenum by $\Delta p_{plenum,out}$, the cross section are change from the plenum into the pipe by $\Delta p_{loss,e,plenum,out}$, the flow deflection in the plenum by $\Delta p_{loss,d,plenum,out}$ and the pressure drop due to friction in the outlet pipe of the heat exchanger by $\Delta p_{pipe,out}$.

The friction loss coefficients are determined for channel flows according to Eq. (4-6) - (4-8) and for deflections as well as cross section area changes according to Eq. (4-11) - (4-13).

Experimental and calculated sCO_2 pressure drop results are shown in Figure 4-3 as a function of the sCO_2 mass flow rate for the heat exchangers of Case BAA (2x1 mm) and AAA (3x1 mm). Both heat exchangers have straight H_2O and sCO_2 channels (II), 15 channels per plate and 1 plate on each side (15/1) and a straight channel length of 150 mm. The experiments are

performed without a heat input into the sCO_2, a sCO_2 inlet pressure of 110 bar, an inlet temperature of 39 °C and sCO_2 mass flow rates between 8 g/s and 68 g/s. The calculated sCO_2 pressure drop is determined according to Eq. (4-15) by using the correlation of Konakov (Eq. (4-7)) for the calculation of the friction coefficient $\xi_{channel}$. Furthermore, a homogeneous sCO_2 mass flow distribution in the channels and no heat losses are assumed.

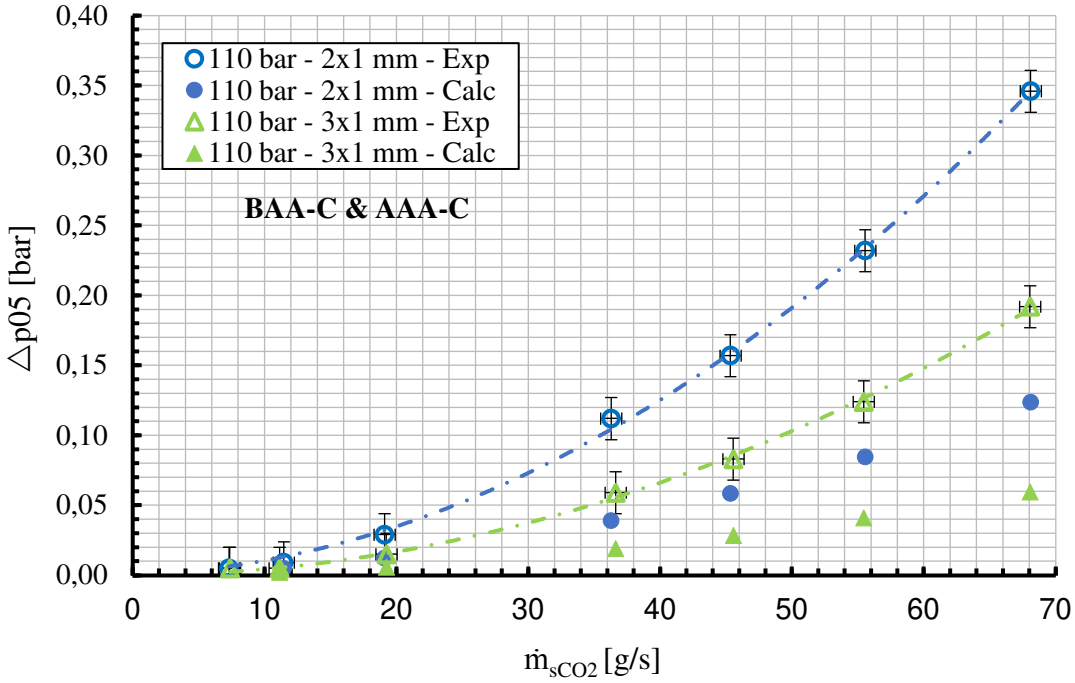

Figure 4-3: Exp. VS. cal. results of Δp05 as function of $\dot{m}_{sCO2}$ of Case BAA-C & AAA-C

The graphs in Figure 4-3 show similar parabolic tendencies with increasing sCO_2 pressure drops $\Delta p05$ for increasing sCO_2 mass flow rates $\dot{m}_{sCO2}$ and vice versa. A comparison of the results shows that the calculated results are always lower than the experimental ones. For instance, for the 2x1 mm channel dimension a sCO_2 mass flow rate of about 36 g/s leads to an experimental sCO_2 pressure drop of 0.112 bar and to an calculated pressure drop of 0.039 bar, 56 g/s leads to 0.232 bar and 0.084 bar, and 68 g/s leads to 0.346 bar and 0.124 bar. For both channel dimensions (2x1 mm and 3x1 mm) and all investigated mass flow rates, the calculated sCO_2 pressure drop is always 2 to 3 times lower than the experimental one. Similar deviations between calculated and experimental results can be seen in the work of Flaig [60]. According to him, the inappropriate plenum geometry and the unsuitable sCO_2 inflow conditions into the plenum are most responsible for that.

The influence of the channel shape on the sCO_2 pressure drop $\Delta p05$ is shown in Figure 4-4 as a function of the sCO_2 mass flow rate $\dot{m}_{sCO2}$ and the sCO_2 inlet pressure $p06$. The upper three graphs show pressure drop results of the heat exchanger of Case BAA with a rectangular channel dimension of 2x1 mm and straight H_2O and Z-shaped sCO_2 channels (IZ). The lower three graphs show sCO_2 pressure drop results of Case BAB with 2x1 mm channels and straight H_2O and sCO_2 channels (II). Both heat exchangers have an effective straight channel length of 150 mm, 15 channels per plate and 1 plate on each side. All measurements are performed without a heat input into the sCO_2 and a sCO_2 inlet temperature of about 39 °C.

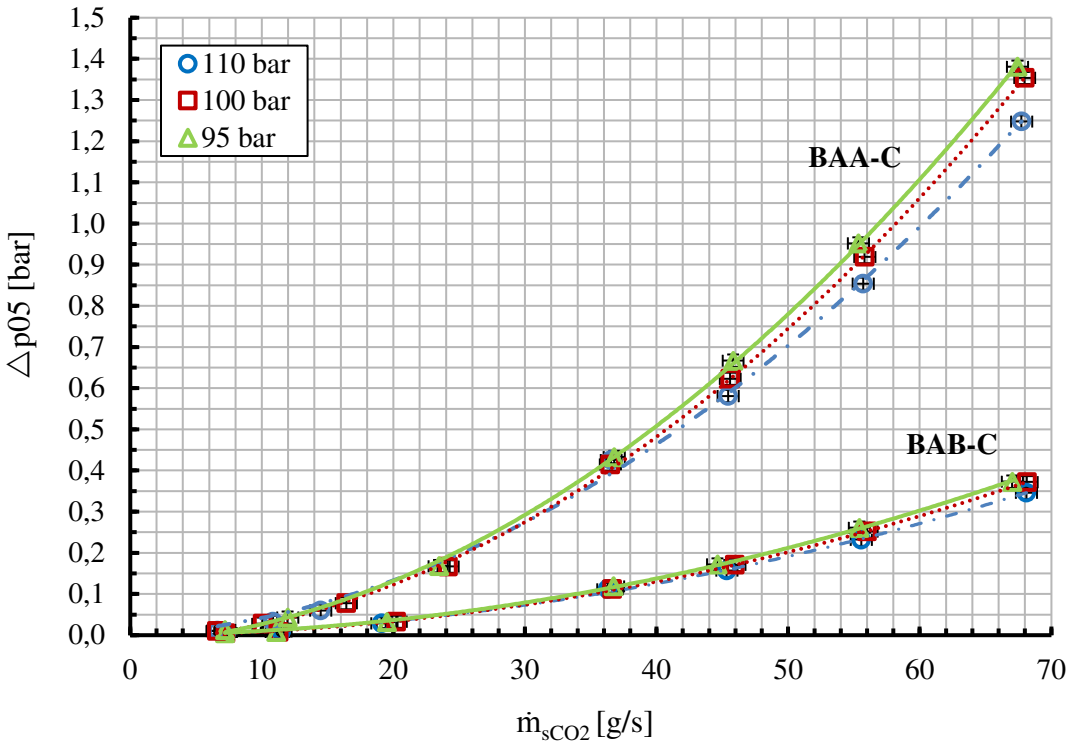

Figure 4-4: Results of Δp05 as function of $\dot{m}_{sCO2}$ of Case-BAA-C & BAB-C

For all measurements, the results depicted in Figure 4-4 show a parabolic tendency of the sCO_2 pressure drop $\Delta p05$ as a function of the sCO_2 mass flow rate $\dot{m}_{sCO2}$ and the sCO_2 inlet pressure $p06$. An increasing mass flow rate leads to increased pressure drops. Furthermore, the experimental results of the pressure drop of Case BAB (2x1 mm - IZ) are shifted towards higher $\Delta p05$ values for similar inlet conditions, compared to Case BAA (2x1 mm - II). Especially for increasing sCO_2 mass flow rates the deviation between Case BAB and BAA is increasing. For instance, a sCO_2 inlet pressure of 110 bar and a mass flow rate of about 37 g/s

leads to a sCO_2 pressure drop of 0.112 bar for the 2x1 mm - II configuration, and to 0.426 bar for the 2x1 mm - IZ configuration. A sCO_2 mass flow rate of 68 g/s leads to 0.346 bar (II) and 1.248 bar (IZ), which is about 4 times higher. In addition, the straight 2x1 mm channel shape reduces the sCO_2 pressure drop for the depicted measurement results by more than 70 % compared with the Z-shaped channels. These deviations can be explained by the channel shape, the channel length and manufacturing issues. The channel shape of Case BAB with straight H_2O and Z-shaped sCO_2 channels is designed for a heat exchanger with more than one plate on each side. The Z-shape is necessary to connect two of the four plenums with the H_2O side and two of the four plenums with the sCO_2 side. In the Z-shaped plate there are two sharp-edged corners, in which the sCO_2 flow is deflected twice and the sCO_2 pressure drop is increased. Furthermore, the flow length in the Z-shaped channels is design-specific more than 150 mm, which leads to increased pressure drop values. Manufacturing issues like the accuracy, diffusion bonding and the arrangement of the pipe connections onto the heat exchangers must be taken also into account, because they influence the sCO_2 pressure drop in the HX's.

The influence of the plenum geometry on the sCO_2 pressure drop is further investigated by using the heat exchangers of Case BAB and BDB. The heat exchanger BAB has rectangular 2x1 mm channels, 15 channels per plate and one plate on each side, straight H_2O and Z-shaped sCO_2 channels and an effective straight channel length of 150 mm. As 15 channels are arranged in parallel at one plate, the inlet plenum has a width of about 50 mm, a height of 1 mm and a length of 13 mm. This plenum geometry is inappropriate for homogeneous inflow and flow distributions, especially if the inlet pipe is arranged vertically and the sCO_2 flow has to be deflected 90 degrees within 1 mm height. Because of that, the heat exchanger of Case BDB is designed and manufactured. Compared to Case BAB, BDB has equal channel dimensions, channel shapes and channel length, but the 15 channels are arranged on 3 plates, with 5 channels each. Such design leads to a more cubic plenum, in which the sCO_2 mass flow rate can be distributed more homogeneously and the flow is less deflected. The results depicted in Figure 4-5 show experimental results of the sCO_2 pressure drop $\Delta p05$ as a function of the sCO_2 mass flow rate $\dot{m}_{sCO2}$ of Case BAB and BDB. The sCO_2 inlet pressure $p06$ is adjusted from 110 bar to 95 bar, the unheated sCO_2 mass flow rate $\dot{m}_{sCO2}$ is gradually increased from about 7 g/s to 68 g/s and the sCO_2 enters the heat exchangers with a temperature of about 39 °C.

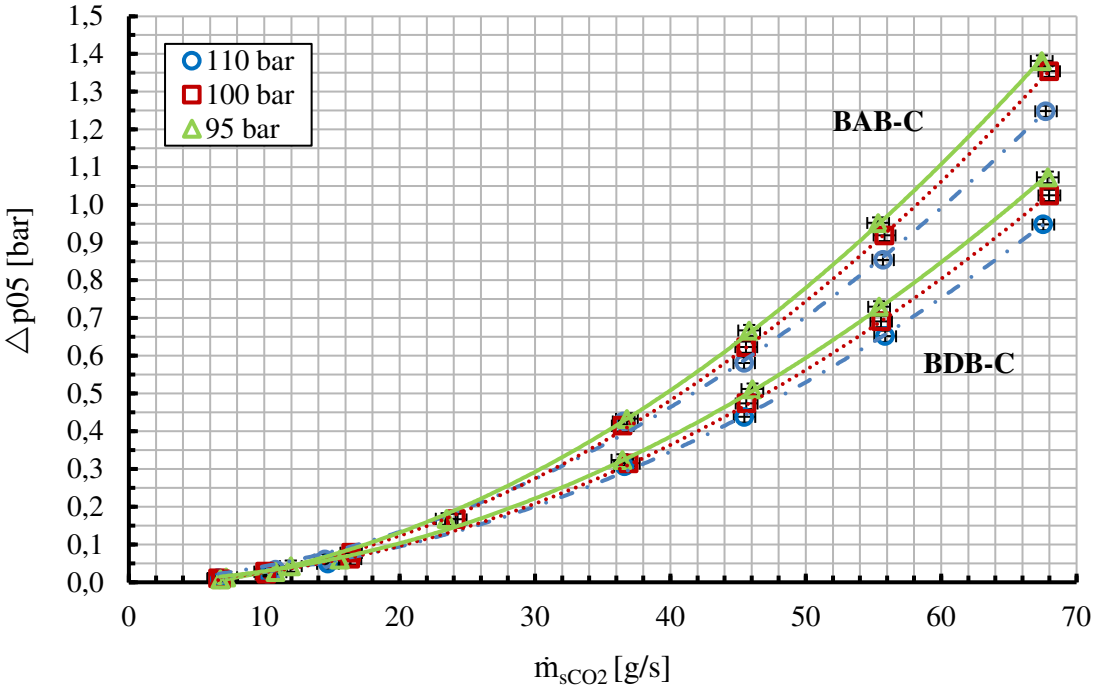

Figure 4-5: Results of Δp05 as function of $\dot{m}_{sCO2}$ of Case BAB-C & BDB-C

The upper three graphs in Figure 4-5 show sCO_2 pressure drop results of Case BAB-C with 15 channels per plate and one plate on each side. The lower three graphs show results of Case BDB with 5 channels per plate and 3 plates on each side of the HX. In general, for both HX a parabolic tendency of the sCO_2 pressure drop as a function of the sCO_2 mass flow rate can be seen, with increasing $\Delta p05$ values for increasing mass flow rates. Furthermore, an increasing sCO_2 inlet pressure $p06$ and a constant mass flow rate leads to lower pressure drop values. The shift towards lower pressure drop values for the 5/3 channel configuration verifies that a more cubic plenum geometry is beneficial for lower pressure drops. The pressure drop decreases by more than 20 % for all shown measurement results compared with the 15/1 channel configuration. This can be seen for instance at the 110 bar graphs, in which a sCO_2 mass flow rate of about 68 g/s leads to a pressure drop of 0.948 bar (5/3) and to 1.248 bar (15/1). The decrease of the sCO_2 pressure drop in more cubic plenum geometries is beneficial for the sCO2-HeRo system and can be explained for instance by more homogeneous inflow conditions and reduced flow deflections in the HX's.

Finally, results of the sCO_2 pressure drop $\Delta p05$ of unheated sCO_2 flows are shown in Figure 4-6 as a function of the averaged sCO_2 Reynolds number $\overline{Re}_{sCO2}$ of Case BAB-C and BDB-C. $\overline{Re}_{sCO2}$ is calculated according to Eq. (4-16) as averaged value of the Reynolds number at the inlet $Re_{sCO2,in}$ (Eq. (4-17)) and outlet $Re_{sCO2,out}$ (Eq. (4-18)) of the HX. Both heat exchangers have rectangular 2x1 mm channels, an effective straight channel length of 150 mm, straight H_2O and Z-shaped sCO_2 channels. BAB has 15 channels at 1 plate and one plate on each side (15/1) and BDB has 5 channels at 1 plate and 3 plates on each side (5/3).

$$\overline{Re}_{sCO2} = 0.5 \cdot \left(Re_{sCO2,in} + Re_{sCO2,out}\right) \tag{4-16}$$

$$Re_{sCO2,in} = f(\dot{m}_{sCO2}, p06, T07) \tag{4-17}$$

$$Re_{sCO2,out} = f\left(\dot{m}_{sCO2}, p_{sCO2,out}, T08\right) \tag{4-18}$$

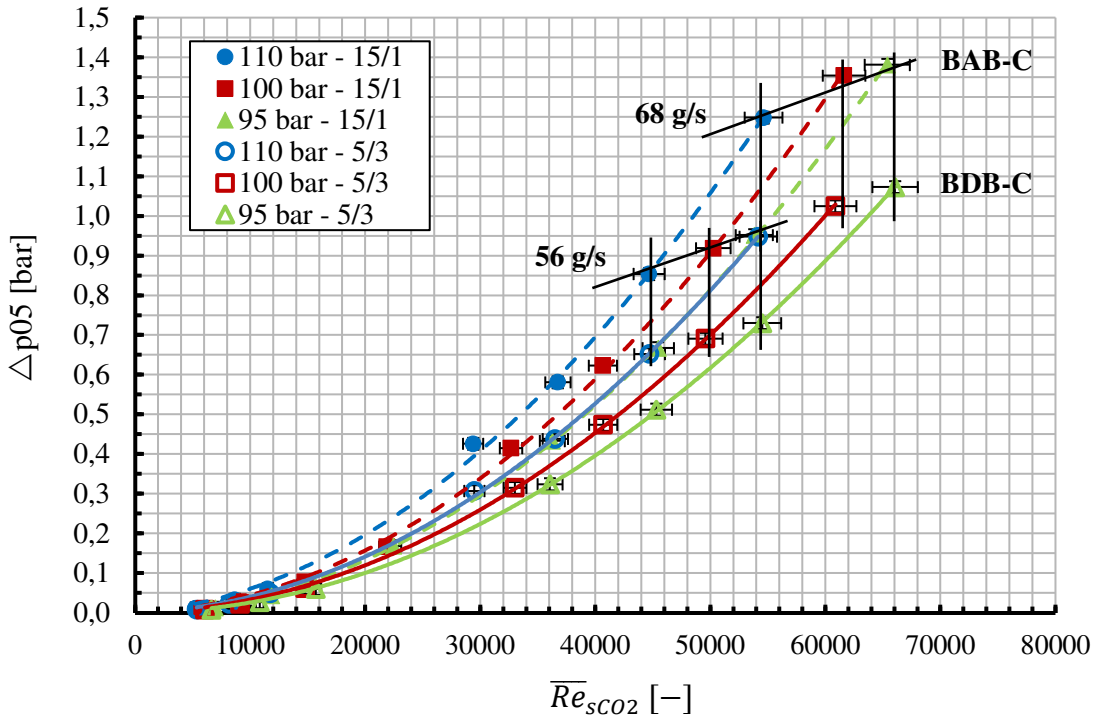

Figure 4-6: Results of Δp05 as function of $\overline{Re}_{sCO2}$ of Case BAB-C & BDB-C

The results depicted in Figure 4-6 show parabolic tendencies of the sCO_2 pressure drop $\Delta p05$ as a function of $\overline{Re}_{sCO2}$ with increasing pressure drops for increasing Reynolds numbers. A constant Reynolds number and a constant sCO_2 inlet pressure leads to higher sCO_2 pressure drops for the 15/1 plate configuration (dashed lines), compared to the 5/3 configuration (lines). This corresponds to the results shown in Figure 4-5 and can be explained by the inappropriate plenum geometry. Furthermore, an increasing sCO_2 inlet pressure and a constant sCO_2 mass flow rate leads to a decreasing Reynolds number on the one hand and on the other hand to a decreasing pressure drop. This is depicted for instance for sCO_2 mass flow rates of 68 g/s and 56 g/s in Figure 4-6 and can be explained by the pressure dependency of the sCO_2 density. A mass flow rate of 68 g/s leads to a Reynolds number of about 55000 for 110 bar (15/1), 62000 for 100 bar (15/1) and to 65000 for 95 bar (15/1). The sCO_2 pressure drop decreases from about 1.381 bar at 95 bar (15/1) to 1.248 bar at 110 bar (15/1) and from 1.073 bar at 95 bar (5/3) to 0.948 bar at 110 bar (5/3).

4.3.2 Pressure drop results of heated sCO_2 flows

As the sCO_2 pressure drop $\Delta p05$ depends on the heat input into the sCO_2 and on the sCO_2 mass flux, it is shown in Figure 4-7 as a function of the heating load G. It is defined according to Eq. (4-19) as ratio of the sCO_2 heat input Q_{sCO2} and the sCO_2 mass flux j_{sCO2}. The sCO_2 heat input is determined according to Eq. (4-20) with the sCO_2 mass flow rate $\dot{m}_{sCO2}$ and the sCO_2 enthalpies at the inlet $h_{sCO2,in}$ and outlet $h_{sCO2,out}$ of the HX. The enthalpies are calculated according to Eq. (4-21) and Eq. (4-22) by using the NIST database Refprop in consideration of the measured temperatures and pressures. The sCO_2 mass flux j_{sCO2} is defined according to Eq. (4-23) as ratio of the measured sCO_2 mass flow rate $\dot{m}_{sCO2}$ and the cross section area A. The heat input into the sCO_2 is provided by condensing steam of the HP steam cycle, which generates saturated steam with a pressure of about 70 bar, a steam temperature of about 286 °C and adjustable water volume flow rates from about 0.53 l/h to 1.74 l/h. According to the measurement points, the heating power of the electrical heated evaporator is adjusted from about 460 W to 1230 W. The heat exchanger of Case BAB has rectangular 2x1 mm channels, an effective straight channel length of 150 mm, straight H_2O and Z-shaped sCO_2 channels, 15 channels per plate and 1 plate on each side (15/1). For the experimental investigations sCO_2 inlet pressures of 95 bar, 100 bar and 110 bar, gradually increasing sCO_2 mass flow rates from about 5 g/s to 68 g/s and sCO_2 heat inputs from about 460 W to 1230 W are used.

$$G = \frac{Q_{sCO2}}{j_{sCO2}} \tag{4-19}$$

$$Q_{sCO2} = \dot{m}_{sCO2} \cdot \left(h_{sCO2,out} - h_{sCO2,in}\right) \tag{4-20}$$

$$h_{sCO2,in} = f(p06, T07) \tag{4-21}$$

$$h_{sCO2,out} = f\left(p_{sCO2,out}, T08\right) \tag{4-22}$$

$$j_{sCO2} = \frac{\dot{m}_{sCO2}}{A} \tag{4-23}$$

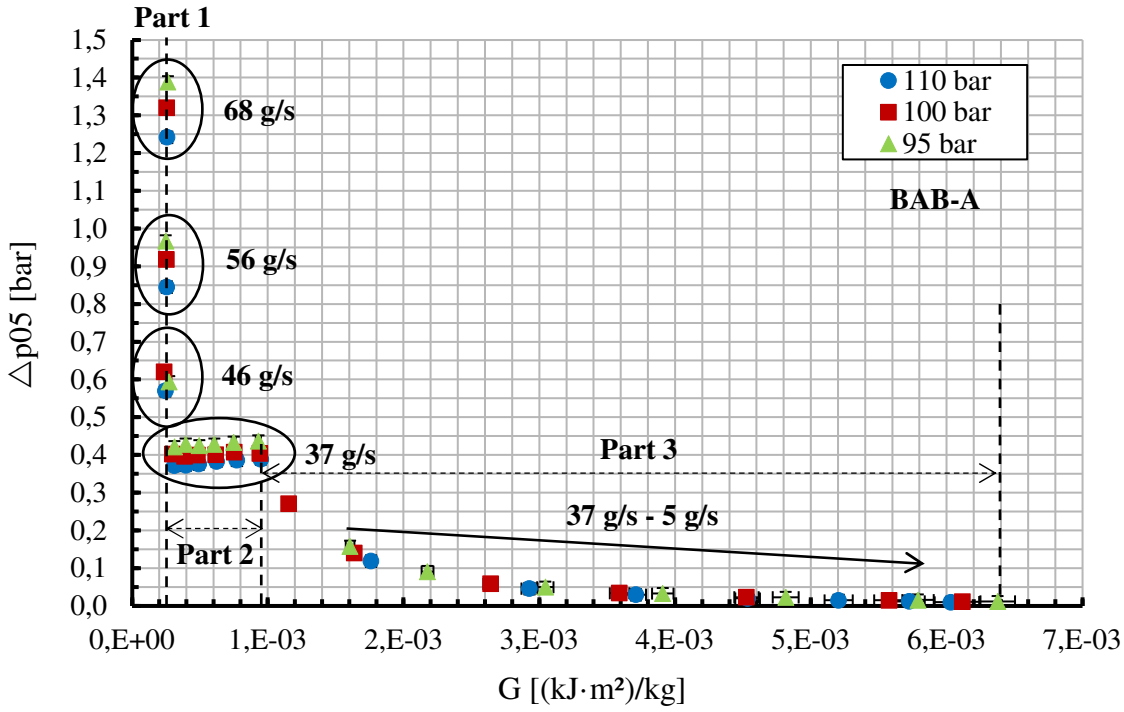

Figure 4-7: Results of Δp05 as function of G of Case BAB-A

The results depicted in Figure 4-7 can be generally classified into three parts: Part 1 is shown on the left with a heating load of 0.00025 (kJ·m²)/kg. These are the results of the DP campaigns, in which sCO_2 mass flow rates from 68 g/s to 37 g/s, sCO_2 inlet pressures of 95 bar, 100 bar and 110 bar and electrical heating powers between 380 W and 680 W are chosen. Each of them shows an increasing pressure drop for decreasing sCO_2 inlet pressures, in consideration of a constant sCO_2 mass flow rate and heat input. Furthermore, a decreasing sCO_2 mass flow rate

leads to decreasing $\Delta p05$ values for constant sCO_2 inlet pressures and sCO_2 heat inputs. The results of the ODP measurement campaigns, with heating loads from 0.00031 (kJ·m²)/kg to 0.00095 (kJ·m²)/kg, are shown in the center of Part 2. These experiments are performed with a sCO_2 mass flow rate of 37 g/s, varying sCO_2 inlet pressures and gradually increasing sCO_2 heat inputs from 380 W to 1230 W. For all sCO_2 inlet pressures, a nearly linear profile with increasing pressure drop values for increasing sCO_2 heat inputs can be obtained. This can be explained by the decreasing fluid density of sCO_2 for increasing temperatures, leading to higher flow velocities and thus to higher pressure drops in the heat exchanger. The results of the ODP II measurement campaigns are shown on the right at Part 3. They are performed with heating loads from 0.0012 (kJ·m²)/kg to 0.0064 (kJ·m²)/kg, which are achieved by adjusting the sCO_2 mass flow rate from about 30 g/s to 5 g/s and by setting an electrical heating power of about 1230 W. These results show a parabolic decrease of the sCO_2 pressure drop for decreasing heating loads from about 0.0012 (kJ·m²)/kg to 0.0030 (kJ·m²)/kg, which corresponds to mass flow rates from 29.5 g/s to 9.4 g/s, and a linear decrease from about 0.0030 (kJ·m²)/kg to 0.0064 (kJ·m²)/kg. The results verify a strong influence of the sCO_2 mass flow rate on the sCO_2 pressure drop as well as an influence of the heat input on the pressure drop. Both phenomena can be explained by changes of the flow velocity and the fluid density.

The kind of heat input into the sCO_2 and the influence on the pressure drop is also investigated. Figure 4-8 shows results of the sCO_2 pressure drop $\Delta p05$ as a function of the averaged Reynolds number $\overline{Re}_{sCO2}$ for heat inputs with condensing steam of the low-pressure (LP) steam cycle, the high-pressure (HP) steam cycle and for unheated (No) sCO_2 flows. The LP steam cycle provides saturated steam with a pressure of about 0.3 bar and a temperature of about 70 °C. The HP steam cycle generates steam with a pressure of about 70 bar and a temperature of about 286 °C. The heating power of the electrical heated evaporator is limited for both steam cycles to about 1230 W. The results are obtained from experiments with a sCO_2 inlet pressure of 95 bar, varying sCO_2 mass flow rates and sCO_2 heat inputs. The heat exchanger of Case BAB is used. It has rectangular 2x1 mm channels, an effective straight channel length of 150 mm, straight H_2O and Z-shaped sCO_2 channels, 15 channels per plate and one plate on each side (15/1).

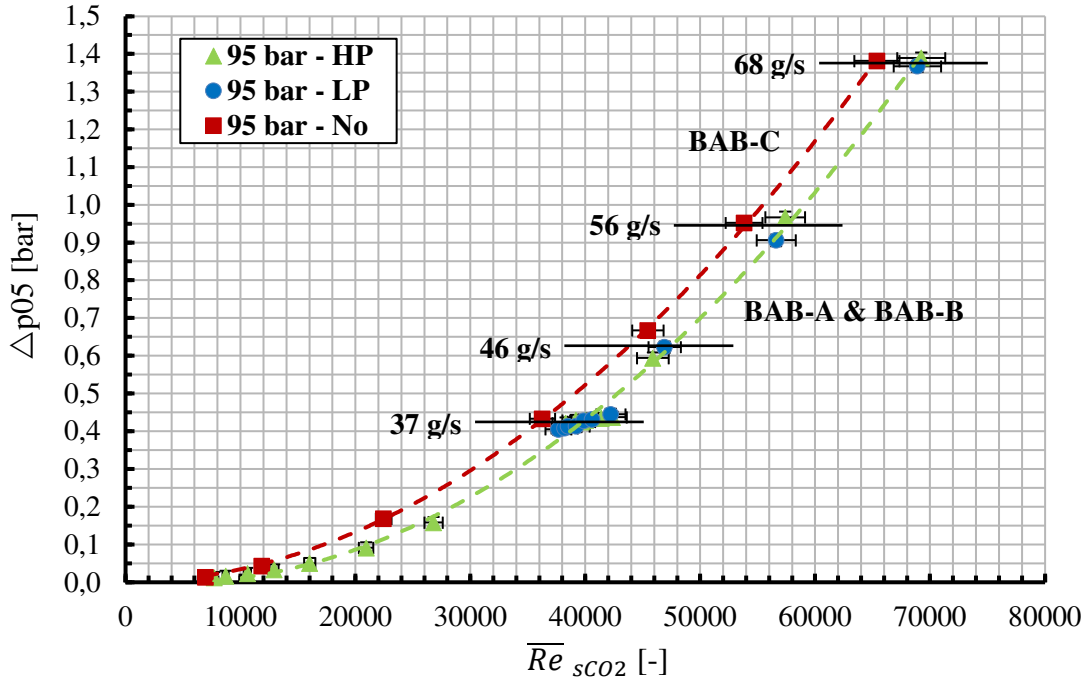

Figure 4-8: Results of Δp05 as function of $\overline{Re}_{sCO2}$ of Case BAB-A & BAB-B & BAB-C

The results in Figure 4-8 show that a heat input via the high-pressure (HP) steam cycle, a sCO_2 inlet pressure of 95 bar and consecutively increasing sCO_2 mass flow rates lead to a parabolic tendency of the sCO_2 pressure drop $\Delta p05$ as a function of $\overline{Re}_{sCO2}$. For instance, an averaged Reynolds number of about 16000 leads to a pressure drop of 0.050 bar, 26800 to 0.158 bar, 42300 to 0.494 bar 57400 to 0.967 bar and 69200 to 1.389 bar. Comparing the results of the HP steam cycle (triangle) and low-pressure (LP) steam cycle (circle) it can be seen that both graphs have similar tendencies with deviations of less than 2 %. This verifies that the pressure drop is not influenced by the kind of heat input. Only the amount of heat input and the sCO_2 inlet conditions into the heat exchanger, like the inlet pressure, inlet temperature and mass flow rate influence the sCO_2 pressure drop. The results show further that for unheated flows (squares) and constant sCO_2 mass flow rates the Reynolds numbers are shifted towards lower values. This can be explained by increasing fluid densities, resulting in decreasing flow velocities and thus to decreasing $\overline{Re}_{sCO2}$ values.

The pressure drop and the heat transfer capability are important for the design of heat exchangers. As an example, results of the sCO_2 pressure drop $\Delta p05$ of Case BAB are shown in Figure 4-9 as a function of the averaged Nusselt number $\overline{Nu}_{sCO2}$. The averaged Nusselt number is defined according to Eq. (4-24) as averaged value of the Nusselt numbers at the inlet $Nu_{sCO2,in}$ (Eq. (4-25)) and outlet $Nu_{sCO2,in}$ (Eq. (4-26)). Both are calculated by using the Gnielinski correlation (Eq. (4-27)) for turbulent flow regimes as a function of Re and Pr.

$$\overline{Nu}_{sCO2} = 0.5 \cdot \left(Nu_{sCO2,in} + Nu_{sCO2,out}\right) \tag{4-24}$$

$$Nu_{sCO2,in} = f\left(Re_{sCO2,in}, Pr_{sCO2,in}\right) \tag{4-25}$$

$$Nu_{sCO2,out} = f\left(Re_{sCO2,out}, Pr_{sCO2,out}\right) \tag{4-26}$$

$$Nu = \frac{\frac{\xi}{8} \cdot Re \cdot Pr}{1 + 12.7\sqrt{\frac{\xi}{8}} \cdot \left(Pr^{2/3} - 1\right)} \tag{4-27}$$

$$\xi = \left(1.8 \cdot \lg(Re) - 1.5\right)^{-2} \tag{4-28}$$

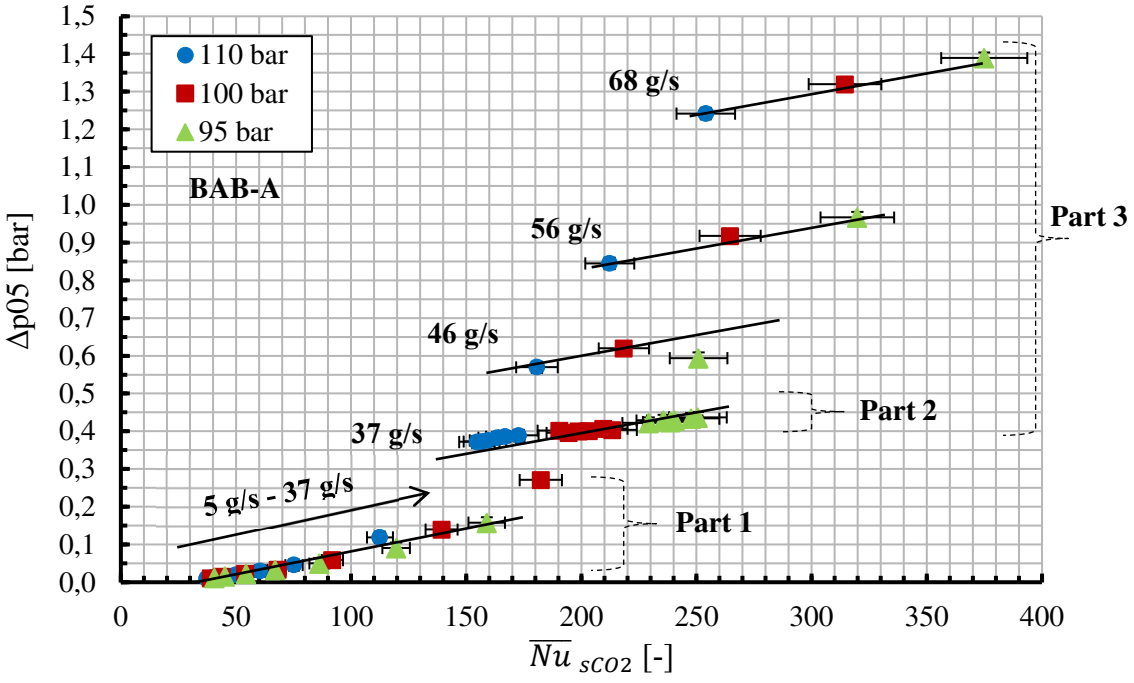

Figure 4-9: Results of Δp05 as function of $\overline{Nu}_{sCO2}$ of Case BAB-A

The results in Figure 4-9 show similar tendencies of the sCO_2 pressure drop $\Delta p05$ as a function of $\overline{Nu}_{sCO2}$ for different sCO_2 inlet pressures and mass flow rates. For instance, an increasing sCO_2 inlet pressure leads to decreasing pressure drops and Nusselt numbers for constant sCO_2 mass flow rates. The results can be classified into three parts. Part 1 shows results of the ODPII investigations with a heat input of about 1230 W and mass flow rates from about 5 g/s to 37 g/s, Part 2 depicts results of the ODP investigations with a sCO_2 mass flow rate of 37 g/s and heat inputs from about 380 W to 1230 W and Part 3 shows results of the DP investigations with mass flow rates from 37 g/s to 68 g/s and heat inputs from 380 W to 680 W. The results confirm that a sCO_2 inlet pressure of 95 bar leads to maximum $\overline{Nu}_{sCO2}$ values, which is beneficial for the heat transfer. Furthermore, an inlet pressure of 95 bar leads to maximum sCO_2 pressure drops for constant sCO_2 mass flow rates, which is inappropriate for heat exchangers which should be used in the sCO2-HeRo system because these pressure drops must be compensated by the TCS and thus results into lower excess electricity. In addition, a constant sCO_2 mass flow rate and an increasing sCO_2 inlet pressure leads to a lower sCO_2 pressure drop and a decreasing Nusselt number. The increase of the sCO_2 inlet pressure from 95 bar to 100 bar leads to a decrease of the Nusselt number of about 25 % and a decrease of the pressure drop of about 5 %.

4.4 Heat transfer results

Results of the calculated sCO_2 heat input Q_{sCO2} are shown in Figure 4-10 as a function of the calculated steam condensing power Q_{H2O} for the heat transfer investigations at the heat exchanger of Case BAB. It has rectangular 2x1 mm channels, an effective channel length of 150 mm, straight H_2O and Z-shaped sCO_2 channels (IZ), 15 channels per plate and 1 plate on each side (15/1). The sCO_2 heat input is provided by condensing steam of the HP steam cycle with a pressure of about 70 bar and a temperature of about 286 °C. The water volume flow rates and the corresponding heating power of the electrical heated evaporator are adjusted according to the measurement points (Table 4-1). The sCO_2 heat input Q_{sCO2} is calculated according to Eq. (4-20) by means of the measured sCO_2 mass flow rate $\dot{m}_{sCO2}$ and the sCO_2 enthalpy difference between the inlet $h_{sCO2,in}$ (Eq. (4-21)) and outlet $h_{sCO2,out}$ (Eq. (4-22)). The condensing power of the steam Q_{H2O} is calculated according to Eq. (4-29) by using the measured water volume flow rate $\dot{m}_{H2O}$ and the enthalpy difference between the inlet $h_{H2O,in}$ (Eq. (4-30)) and outlet $h_{H2O,out}$ (Eq. (4-31)). The enthalpies are calculated with NIST Refprop [43] as a function of the measured fluid temperatures and pressures.

$$Q_{H2O} = \dot{m}_{H2O} \cdot \left(h_{H2O,in} - h_{H2O,out}\right) \tag{4-29}$$

$$h_{H2O,in} = f(p02, T03) \tag{4-30}$$

$$h_{H2O,in} = f(p04, T04) \tag{4-31}$$

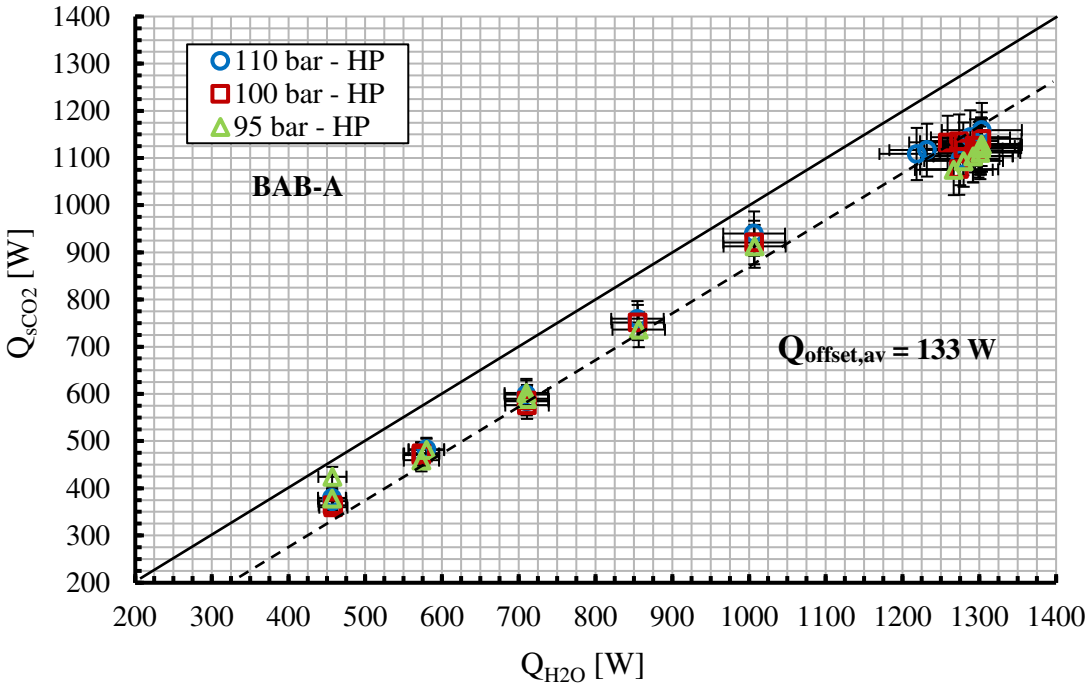

Figure 4-10: Results of Q_{sCO2} as function of Q_{H2O} of Case BAB-A

The depicted results in Figure 4-10 show similar linear tendencies for varying sCO_2 inlet pressures and a schematic offset between the calculated condensing power of the steam Q_{H2O} and the calculated sCO_2 heat input Q_{sCO2}. For instance, a sCO_2 inlet pressure of 110 bar and a calculated condensing power of the steam of 457 W leads to a calculated sCO_2 heat input of 372 W, 854 W leads to 759 W, 1006 W leads to 940 W and 1218 W leads to 1109 W. Such offset can be explained by thermal losses due to high operation temperatures of about 290 °C and an inappropriate ratio of heat emitting to heat transfer area. The offset at each measurement point Q_{offset} can be determined by the energy balance according to Eq. (4-32).

$$Q_{offset} = Q_{H2O} - Q_{sCO2} \tag{4-32}$$

$$Q_{offset,av} = \frac{1}{N}\sum_{k=i}^{N} Q_{offset_k} \tag{4-33}$$

$$R = \frac{Q_{sCO2}}{\mathrm{Q}_{H2O} - Q_{offset,av}} \tag{4-34}$$

The averaged offset $Q_{offset,av}$ is calculated according to Eq. (4-33) to 133 W and shown by the black dashed line in Figure 4-10. Neglecting thermal losses, the calculated heat transfer ratio R (Eq. (4-34)) is more than 90 % for all 48 measurement points, except 5. The theoretical heat transfer ratio R of 100 % is visualized by the black line. The results of the steam temperature measurement $T04$ at the outlet of the heat exchanger verify additionally that the maximum achievable amount of steam in the test section is completely condensed and subcooled even for all ODP measurement points. This means that the heat exchanger installed at the test section is over-dimensioned and would be able to transfer more heat power from the steam side to the sCO_2 side than could be investigated.

The influence of the steam inlet conditions on the heat transfer is also investigated. Condensing steam of the low-pressure (LP) steam cycle and high-pressure (HP) steam cycle are used for this purpose. Figure 4-11 shows experimental results of the calculated sCO_2 heat input Q_{sCO2} as a function of the calculated steam condensing power Q_{H2O} for a sCO_2 inlet pressure of 110 bar and varying steam inlet conditions. These results are obtained from experimental investigations of the heat exchanger of Case BAB, which has rectangular 2x1 mm channels, an effective channel length of 150 mm, straight H_2O and Z-shaped sCO_2 channels (IZ), 15 channels per plate and 1 plate on each side (15/1).

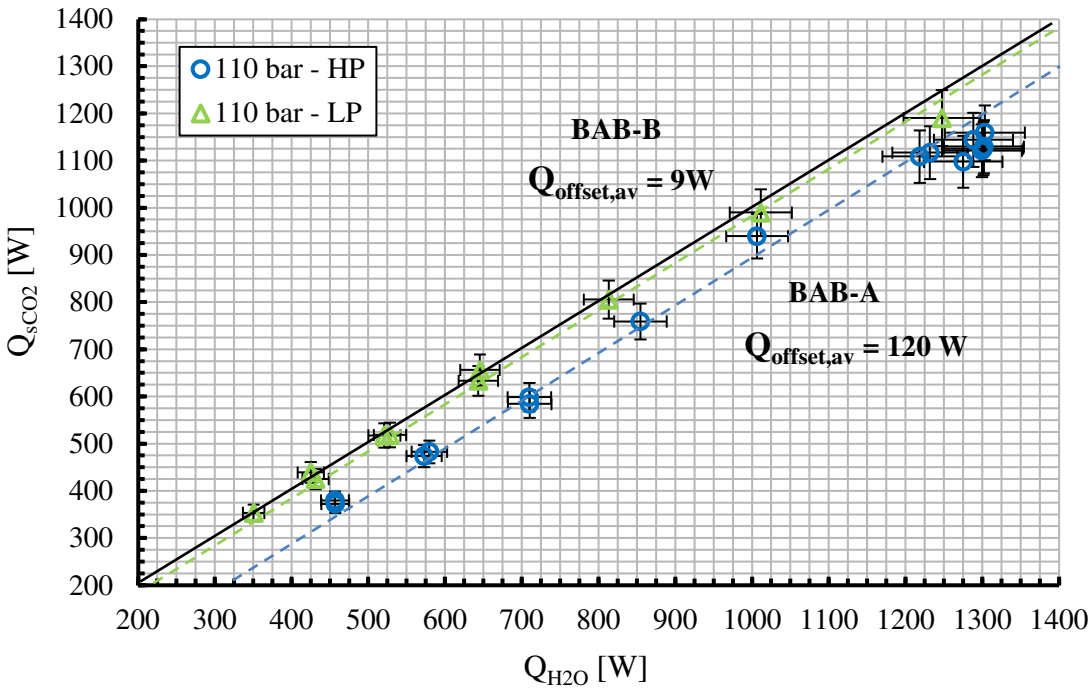

Figure 4-11: Results of Q_{sCO2} as function of Q_{H2O} of Case BAB-A & BAB-B

The depicted graphs in Figure 4-11 show linear tendencies with increasing sCO_2 heat inputs Q_{sCO2} for increasing condensing powers of the steam Q_{H2O}. For instance, the results of the LP steam cycle (triangle) experiments show that a sCO_2 inlet pressure of 110 bar and a steam condensing power of 431 W leads to a sCO_2 heat input of 425 W, 643 W to 633 W, 813 W to 806 W and 1247 W to 1190 W. The averaged offset of the LP steam cycle experiments is calculated (Eq. (4-33)) to 9 W and visualized by the upper dashed line. The solid line presents a theoretical heat transfer ratio R of 100 %, if no heat losses occur. A comparison of the results of the LP steam cycle (triangle) and HP steam cycle (circle) experiments shows that the heat transfer ratio R is lower for the HP steam cycle experiments. This can be explained by increasing thermal losses due to higher steam temperatures of about 290 °C, compared to steam temperatures of about 70 °C. The averaged offset of the results of the HP steam cycle measurements is calculated according to Eq. (4-33) to 133 W and visualized by the lower dashed line.

To investigate the influence of the channel dimension (2x1 mm & 3x1 mm) and the channel shape (IZ & II) on the heat transfer, experiments according to Case AAB-A, BAB-A and BAA-A are performed. The heat exchanger of Case AAB has rectangular 3x1 mm channels, 15 channels per plate and 1 plate on each side (15/1), an effective channel length of 150 mm, straight H_2O and Z-shaped sCO_2 channels (IZ). The heat exchanger BAB is similar to AAB, except the channel dimension of 2x1 mm. BAA is similar to BAB, except the straight sCO_2 channels (II). The sCO_2 heat input is provided by condensing steam with a pressure of about 70 bar and a steam temperature of 286 °C, generated in the high-pressure steam cycle. The results depicted in Figure 4-12 are obtained from experiments with a sCO_2 inlet pressure of 110 bar and mass flow rates according to the determined measurement points (Table 4-1).

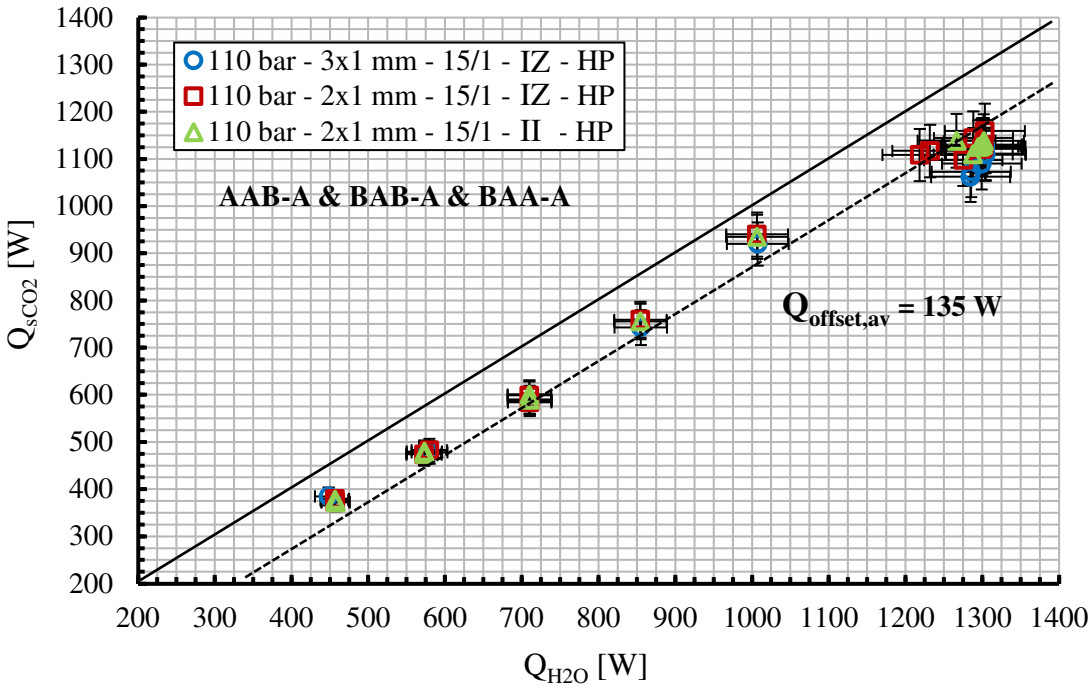

Figure 4-12: Results of Q_{sCO2} as function of Q_{H2O} of Case AAB-A & BAB-A & BAA-A

The electrical heating power of the steam evaporator with 1600 W is limited to 1300 W due to internal temperature restrictions of the heating cartridge. In the SCARLETT loop, a minimum sCO_2 mass flow rate of 37 g/s can be provided, and this can be additionally reduced to about 5 g/s at the inlet of the test section by means of a needle valve and bypassing a part of the flow. Because of that, there is only one possibility to investigate the transferrable heat in the HX's, the decrease of the heat transfer area. For this purpose, the heat exchanger of Case BBB

is designed and manufactured. It has rectangular 2x1 mm channels, 5 channels per plate and 1 plate on each side (5/1), straight H_2O and Z-shaped sCO_2 channels (IZ) and an effective straight channel length of 150 mm. Within the experiments, the sCO_2 mass flow rates, the water volume flow rates and the electrical heating power of the steam evaporator are adjusted according to the measurement points (Table 4-1). Figure 4-13 shows results of the calculated sCO_2 heat input Q_{sCO2} as a function of the calculated condensing power of the steam Q_{H2O} of Case BAB-A and BBB-A. The sCO_2 heat input is provided by condensing steam with a pressure of 70 bar and a temperature of 286 °C, generated in the high-pressure steam cycle.

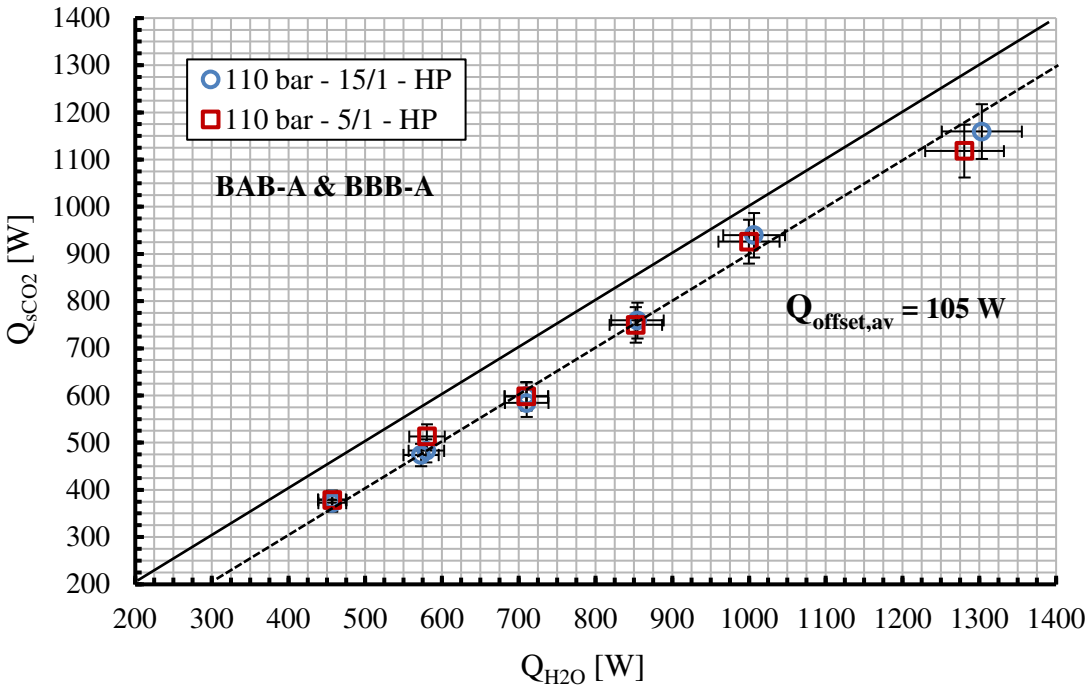

Figure 4-13: Results of Q_{sCO2} as function of Q_{H2O} of Case BAB-A & BBB-A

The depicted graphs in Figure 4-13 show results of the ODP measurement campaigns of Case BAB and BBB with a sCO_2 mass flow rate of 37 g/s, gradually increasing steam condensing power from 460 W to 1250 W and a sCO_2 inlet pressure of 110 bar. For both heat exchangers, an increasing condensing power of the steam Q_{H2O} leads to a linear increase of the sCO_2 heat input Q_{sCO2}. Furthermore, there is an averaged offset of about 105 W, which is shown by the black dashed line. The results further verify that the heat exchanger of Case BBB with 5 channels at each side (5/1) and an effective straight channel length of 150 mm is sufficient to transfer a heat power of about 1250 W from the steam side to the sCO_2 side. Further

experiments of Case BBB with gradually decreasing sCO_2 mass flow rates from about 37 g/s to 2 g/s show that a sCO_2 mass flow rate of about 2 g/s is also sufficient to transfer a heat power of about 1250 W from the steam side to the sCO_2 side. The sCO_2 enters the heat exchanger with a pressure of 110 bar, a mass flow rate of 1.93 g/s and a temperature of 38.48 °C and leaves the heat exchanger with a temperature of 203.11 °C. The steam enters the HX with a pressure of 70 bar, a volume flow rate of 1.74 l/h and a temperature of 284.44 °C and leaves the heat exchanger subcooled with 148.64 °C.

After presenting experimental results of the calculated sCO_2 heat input Q_{sCO2} as a function of the calculated condensing power of the steam Q_{H2O} (Figure 4-10 - Figure 4-13), results of the calculated sCO_2 temperature increase ΔT_{sCO2} are shown as a function of Q_{sCO2}. The temperature increase ΔT_{sCO2} is calculated according to Eq. (4-35) by means of the measured sCO_2 temperatures at the inlet $T07$ and at the outlet $T08$ of the HX. The sCO_2 heat input is calculated according to Eq. (4-20) in consideration of the sCO_2 mass flow rate and the enthalpy difference between the inlet and outlet.

$$\Delta T_{sCO2} = T08 - T07 \tag{4-35}$$

Figure 4-14 shows results of ΔT_{sCO2} as a function of Q_{sCO2} of Case-BAB-A. These experiments are carried out with sCO_2 heat inputs from 380 W to 1200 W, provided by condensing steam of the high-pressure steam cycle. A sCO_2 mass flow rate of 37 g/s and sCO_2 inlet pressures of 110 bar, 100 bar and 95 bar are used.

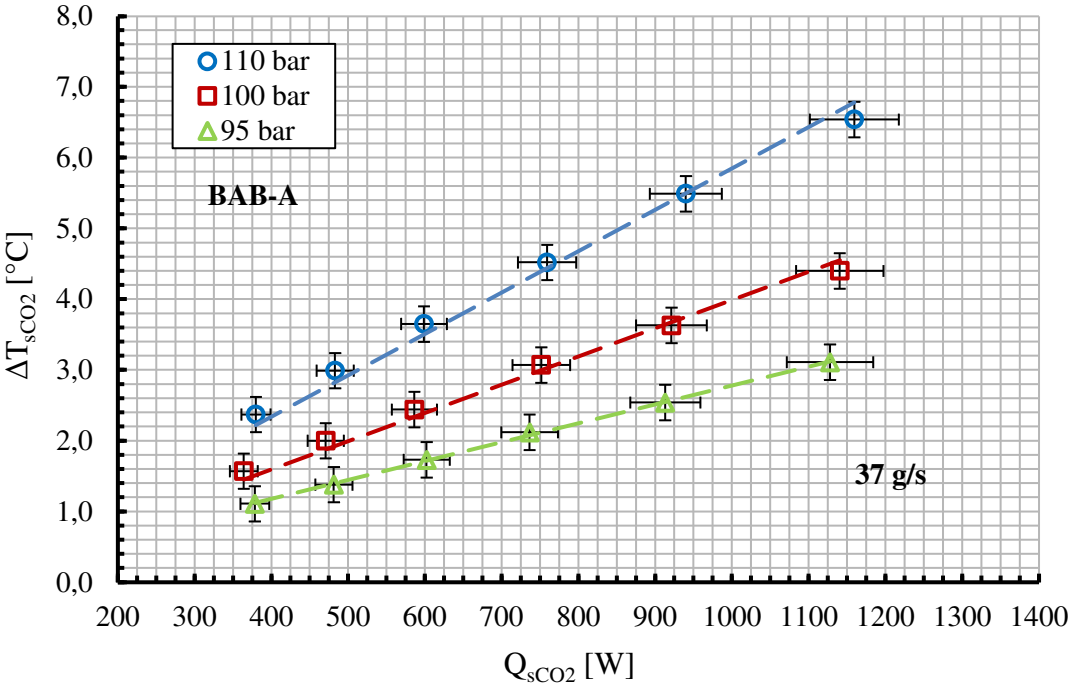

Figure 4-14: Results of Q_{sCO2} as function of ΔT_{sCO2} of Case BAB-A

The graphs in Figure 4-14 show linear tendencies for varying sCO_2 inlet pressures with different gradients and an increasing sCO_2 temperature increase for higher sCO_2 heat inputs. The results of the 95 bar measurement campaign (triangle) show, for instance, that a sCO_2 heat input of 378 W leads to a sCO_2 temperature increase of 1.1 °C, 602 W leads to 1.7 °C, 913 W leads to 2.5 °C and 1128 W leads to 3.1 °C. Moreover, a decreasing sCO_2 inlet pressure leads to decreasing sCO_2 temperature increases because of higher specific heat capacities near the critical point. A sCO_2 heat input of about 1150 W, combined with a mass flow rate of 37 g/s and a sCO_2 inlet temperature of about 39.5 °C, leads to a sCO_2 temperature increase ΔT_{sCO2} of 6.5 °C for 110 bar, to 4.4 °C for 100 bar, and to 3.1 °C for 95 bar. The specific heat capacity c_p can be determined for each measurement point according to Eq. (4-36) by using the sCO_2 heat input Q_{sCO2}, the mass flow rate $\dot{m}_{sCO2}$ and the temperature increase ΔT_{sCO2}. For an inlet pressure of 110 bar, the specific heat capacity c_p is between 4.4 kJ/(kg·K) and 4.8 kJ/(kg·K), for 100 bar between 6.3 kJ/(kg·K) and 7.1 kJ/(kg·K) and for the 95 bar campaign between 9.4 kJ/(kg·K) and 10.0 kJ/(kg·K).

$$c_p = \frac{Q_{sCO2}}{\dot{m}_{sCO2} \cdot \Delta T_{sCO2}} \tag{4-36}$$

The influence of the channel dimension (2x1 mm / 3x1 mm) and channel shape (II / IZ) on the sCO_2 temperature increase ΔT_{sCO2} is further investigated. Figure 4-15 shows results of ΔT_{sCO2} as a function of the sCO_2 heat input Q_{sCO2} of Case BAB-A & BAA-A & AAB-A & AAA-A. The heat exchanger of Case BAB has rectangular 2x1 mm channels, 15 channels per plate and 1 plate on each side (15/1), straight H_2O and Z-shaped sCO_2 channels (IZ) and an effective straight channel length of 150 mm. The heat exchanger BAA is similar to BAB, except for the straight sCO_2 channels (II). AAB is similar to BAB, except for the 3x1 mm channels and AAA is similar to AAB, except for the straight sCO_2 channels. The results are obtained from experiments with condensing steam of HP steam cycle (A), a sCO_2 mass flow rate of 37 g/s, a sCO_2 inlet pressure of 110 bar and varying sCO_2 heat inputs from 380 W to 1200 W.

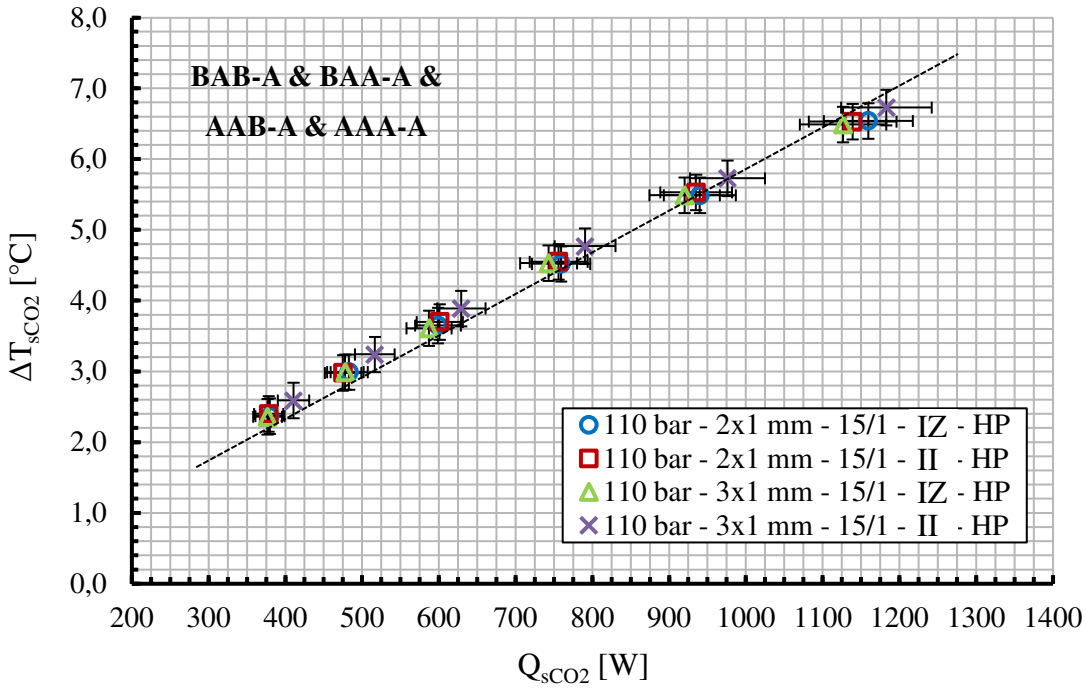

Figure 4-15: Results of Q_{sCO2} as function of ΔT_{sCO2} of Case BAB/BAA/AAB-A/AAA

The graphs in Figure 4-15 show similar linear tendencies with increasing sCO_2 temperature increases ΔT_{sCO2} for increasing sCO_2 heat inputs Q_{sCO2}, visualized by the black dashed line. For instance, a sCO_2 heat input of 380 W leads to a sCO_2 temperature increase of 2.37 °C, 759 W to 4.52 °C and 1159 W to 6.54 °C for the "110 bar - 15/1 - IZ - 2x1 - HP" configuration. Moreover, for a constant sCO_2 heat input the deviation between the temperature increases ΔT_{sCO2} is less than 4 %. This means that neither the channel dimension nor the channel shape

has an influence on the sCO_2 temperature increase for the current experiment - only the amount of heat input Q_{sCO2} and the sCO_2 inlet conditions at the heat exchanger are responsible for the sCO_2 temperature increase ΔT_{sCO2}.

To monitor the surface temperature distribution during the experiments, nine resistance thermometers (Pt-100) are mounted symmetrically on both sides of the heat exchangers of Case BAB and BBB. Figure 4-16 shows on the left a CAD (Computer Aided Design) drawing of the heat exchanger of Case BAB with the measurement positions on the sCO_2 plate and on the right a picture of the HX in the test section with installed Pt-100 measurement devices.

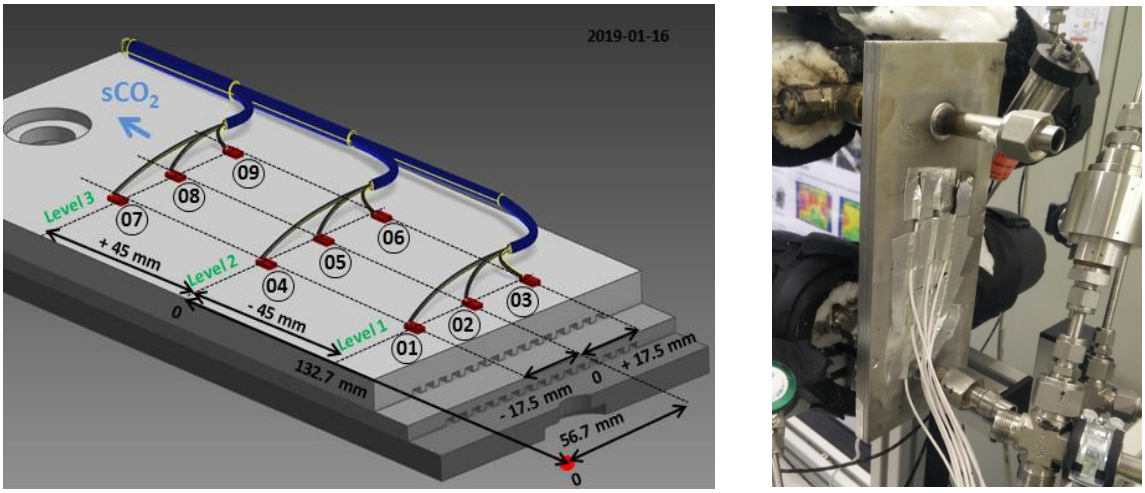

Figure 4-16: CAD drawing and picture of HX with installed Pt-100 of Case BAB

The resistance thermometers are mounted symmetrically in three levels on the surface of the sCO_2 plate of Case BAB, as shown in the CAD drawing (Figure 4-16). The coordinate origin is located at the bottom left, marked with a red dot. Level 2 is located 132.7 mm above the coordinate origin in the center line of the plate. Level 1 is located 45 mm below level 2 and level 3 is located 45 mm above level 2. Pt-100 02, 05 and 08 are mounted in the center line of the plate, 56.7 mm to the right of the coordinate origin. Pt-100 01, 04 and 07 are located 17.5 mm to the left of the center line and Pt-100 03, 06 and 09 17.5 mm to the right. The measurement positions of the Pt-100 on the H_2O plate are arranged similar but mirror-inverted.

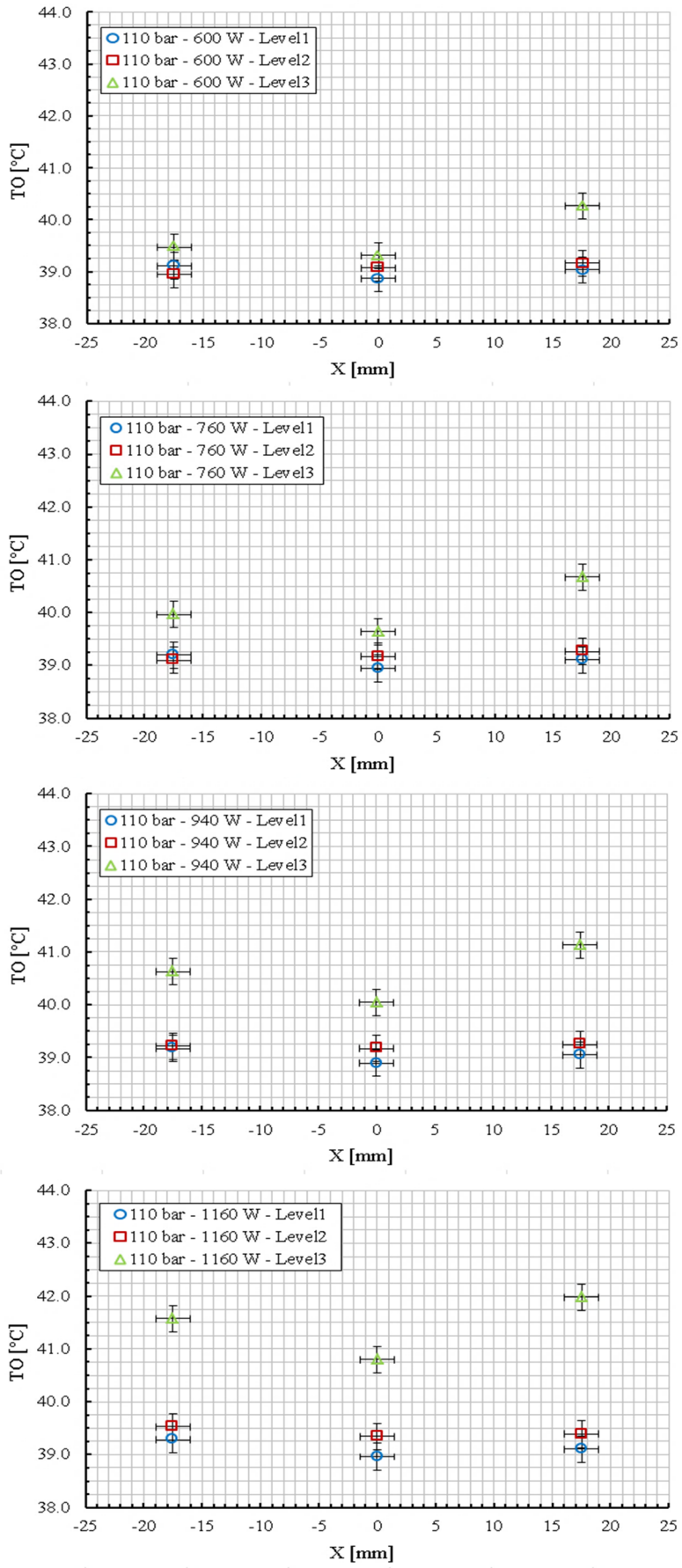

Figure 4-17: Results of TO as function of position X of Case BAB-A

Experimental results of the sCO_2 surface temperatures TO of Case BAB-A are depicted in Figure 4-17 as a function of the Pt-100 measurement position X and the sCO_2 heat input Q_{sCO2}. The heat exchanger of Case BAB has rectangular 2x1 mm channels, an effective straight channel length of 150 mm, straight H_2O and Z-shaped sCO_2 channels (IZ), 15 channels per plate and 1 plate on each side (15/1). The heat input is provided by condensing steam of the high-pressure steam cycle with a pressure of about 70 bar and a temperature of 286 °C. The water volume flow rates and the corresponding heating powers of the electrical evaporator are adjusted accordingly to the ODP measurement campaigns, and the sCO_2 mass flow rate is set to 37 g/s. The sCO_2 heat input is calculated according to Eq. (4-20) by means of the measured mass flow rate and the enthalpy difference between the inlet and outlet. The enthalpies are calculated with Refprop [43] in consideration of the measured temperatures and pressures.

The first graphs (Figure 4-17) are obtained from measurements with a sCO_2 heat input of 600 W, the second ones with 760 W, the third ones with 940 W and the graphs at the bottom with 1160 W. A sCO_2 inlet temperature of about 39.5 °C, a mass flow rate of 37 g/s and an inlet pressure of 110 bar are chosen. The results show generally a symmetrical temperature profile with lower surface temperatures in the center line of the HX and higher surface temperatures at the outer area. Furthermore, a higher sCO_2 heat input Q_{sCO2} leads to increasing surface temperatures, especially at the top of the heat exchanger (level 3). This can be explained by the counter-current flow configuration, in which the steam enters the HX at the top, transfers the heat to the sCO_2 side, is condensed and flows downwards driven by gravity. The sCO_2 enters the heat exchanger at the bottom, flows upwards and leaves the heat exchanger at the top. An increasing sCO_2 heat input corresponds to an increasing steam condensing power and thus to an increasing steam volume flow rate. Higher steam volume flow rates require an increasing heat transfer area and this leads to a forced steam flow downwards the HX in the direction of level 2 and level 1. The results of the surface temperatures TO are described for a sCO_2 heat input of 1160 W, as shown on the bottom (Figure 4-17), as example. The temperature profile at level 3 shows that the surface temperatures TO_07 with 41.6 °C and TO_09 with 42.0 °C are higher than TO_08 with 40.8 °C. The increasing temperatures from level 1 to level 3 are taken from position $X = 0$ mm. The sCO_2 enters the HX at the bottom with a temperature of about 39.5 °C and flows upwards into the channels. Level 1 is located 87.7 mm above the end of the sCO_2 plate and the measured surface temperature TO_02 is 39.0 °C. Flowing upward, the sCO_2 is heated due to the heat transfer of condensing steam. This leads to a surface temperature TO_05 of 39.3 °C on level 2 and TO_08 of 40.8 °C on level 3. In addition, the

surface temperatures are in relation to the results of the sCO_2 temperature increases ΔT_{sCO2} (Figure 4-15). There, a sCO_2 mass flow rate of 37 g/s, an inlet pressure of 110 bar, an inlet temperature of about 39.5 °C and a heat input of 1160 W leads to a temperature increase of about ΔT_{sCO2} of 6.5 °C - which corresponds to the measured surface temperature TO_09 on level 3 with 42.0 °C. The measured surface temperatures are always lower than the sCO_2 fluid temperatures at the outlet of the HX because of thermal losses and the location of the measurement position of level 3, which is about 30 mm below the sCO_2 outlet.

For comparison of the H_2O and sCO_2 surface temperatures, results of the surface temperatures $TD\ (TD\_01 - TD\_09)$ on the H_2O side of the heat exchanger of Case BAB are analyzed further. Again, there are symmetrical profiles with lower surface temperatures in the center line and higher surface temperatures at the outer area. Further, an increasing sCO_2 heat input Q_{sCO2} leads to increasing surface temperatures and the increase of the surface temperatures at level 3 is higher than at level 1. Furthermore, the surface temperatures on the H_2O side are always higher than on the sCO_2 side, which is necessary to ensure a heat transfer from the steam side to the sCO_2 side. In consideration of a steam inlet temperature of 286 °C and H_2O surface temperatures on level 3 of about 50 °C, it could be assumed firstly that the steam is condensed within the first 30 mm and secondly that the heat exchanger of Case BAB would be able to transfer much more heat power.

Because of limitations in the steam provision of about 1300 W and the aim to investigate the maximum achievable heat transfer, the heat exchanger of Case BBB is designed. It is similar to the heat exchanger of Case BAB, except the number of channels. It has 5 channels at one plate and 1 plate on each side (5/1), which is a third of the heat transfer area of Case BAB. In the following, results of the surface temperatures on the H_2O side TD and sCO_2 side TO of Case BBB are described. These results are obtained from experiments with a sCO_2 inlet pressure of 110 bar, a sCO_2 heat input of 1160 W and a mass flow rate of 1.93 g/s.

The results show that the surface temperatures TD on the H_2O plate on level 3 and on level 2 are close to the steam inlet temperature of about 286 °C, which confirms that at these measurement positions, steam still exists in the HX. Going downstream, the surface temperatures on level 1 with about 210 °C are significantly lower than on level 2 and level 3.

This indicates that the steam is condensed completely between level 2 and level 1. The results of the temperature measurement $T04$ at the outlet of the HX on the H_2O side shows additionally that the steam is condensed and sub-cooled for all measurement points (Appendix D). The temperature measurements TO on the surface of the sCO_2 plate show similar profiles with lower surface temperatures, compared to the surface temperatures on the H_2O side. The results verify that a heat exchanger with 5 rectangular 2x1 mm channels and an effective straight channel length of 150 mm is able to transfer a heat power of about 1160 W from the condensing steam side to the sCO_2 side, for a sCO_2 inlet pressure of 110 bar, a sCO_2 mass flow rate of 1.93 g/s, a steam inlet pressure of 70 bar and a corresponding steam inlet temperature of 286 °C.

In consideration of the received experimental data, in the following the compact heat exchanger for the sCO2-HeRo demonstrator unit, which will be installed at the pressurized water reactor glass model at GfS, is constructed.

5 CHX for the PWR glass model

5.1 Boundary conditions and measurement results

The inlet conditions at the compact heat exchanger for the PWR reactor glass model are summarized in Table 5-1. The sCO_2 inlet pressure, the inlet temperature and the mass flow rate are defined in consideration of the cycle calculation results according to chapter 2.3. These parameters are chosen with respect to maximum generator excess electricity and other criteria like the achievable compression ratio of a single stage compressor and the necessary sCO_2 mass flow rate of the TCS. The inlet conditions on the steam side of the CHX are obtained from experimental investigations at the glass model according to [36]. The results show that a transferred simulated decay heat power of 6 kW leads to a steam pressure of 0.32 bar and a steam temperature of 70.27 °C.

Table 5-1: Boundary conditions of the glass model CHX

Side	Variable	Value	Unit	Description
sCO_2	p_{sCO2}	117.45	bar	Pressure - Inlet CHX
	T_{sCO2}	46.84	°C	Temperature - Inlet CHX
	$\dot{m}_{sCO2}$	650	g/s	sCO_2 Mass Flow Rate
H_2O	p_{H2O}	0.32	bar	Pressure - Inlet CHX
	T_{H2O}	70.27	°C	Temperature - Inlet CHX
	$\dot{m}_{H2O}$	2.60	g/s	H_2O Mass Flow Rate
-	Q_{H2O}	6.00	kW	Transferred Heat Power

A sCO_2 mass flow rate of 650 g/s is about six times higher than the achievable sCO_2 mass flow rate in the SCARLETT loop of about 110 g/s. Because of that, scaled down HX's according to Table 3-7 are experimentally investigated. In the DP measurement points (Table 4-1) the sCO_2 mass flow rates as well as water volume flow rates are scaled down in the same ratio according to the overall amount of sCO_2 (650 g/s) and water (2.60 g/s / 9 l/h), which will be used in the glass model. Further ODP and ODPII experiments are performed and the influence of the channel dimensions and channel shape on phenomena like the pressure drop or the transferred heat power is investigated.

To determine the channel dimension and number of channels, the experimental results from chapter 4 are considered. These show for instance, that the heat is reliably transferred from the steam side to the sCO_2 side for all measurements. In consideration of space limitations and the aim to build a compact heat exchanger, the entire number of plate pairs could be determined conservatively at 9 ((650 g/s)/(68 g/s) = 8.8). This would lead to a transferred heat power of about 640 W per plate, which is achievable. Another important parameter is the sCO_2 pressure drop, because it must be compensated by the TCS. A lower sCO_2 pressure drop would be desirable because it leads to lower compression work and thus to increased excess electricity at the generator. The experimental results of Case BAB-B show, for instance, that a sCO_2 inlet pressure of 110 bar and a sCO_2 heat input of 353 W leads to a sCO_2 pressure drop of 0.372 bar for a sCO_2 mass flow rate of 36.8 g/s, 425 W to 0.547 bar for 45.7 g/s, 519 W to 0.794 bar for 54.8 g/s, and 633 W leads to a pressure drop of 1.190 bar for a mass flow rate of 67.8 g/s. The choice of the rectangular 2x1 mm channel dimension and an entire number of 14 plate pairs with 15 channels per plate is a compromise of compactness and acceptable sCO_2 pressure drop. 14 pairs of plates lead to a sCO_2 mass flow rate of about 46 g/s per plate and to a sCO_2 pressure drop of about 0.547 bar. The results further show that the HX of Case BAB is able to transfer more condensing power of the steam than is used in the defined design point.

5.2 CHX channel and plate design

The technical drawings of the plates of the CHX for the glass model are shown in Figure 5-1. The entire plate length and width is chosen with respect to the working area of the diffusion bonding machine. The wall thickness between neighboring channels, the plate thickness and the outer wall thickness are determined according to chapter 3.2.2.

1) Cover plate

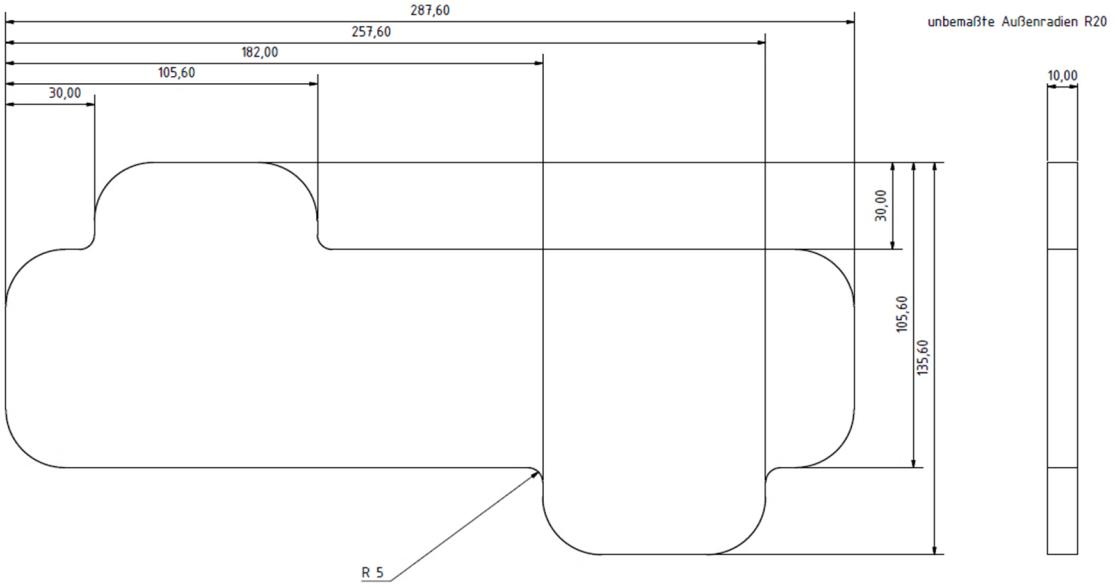

2) sCO_2 plate

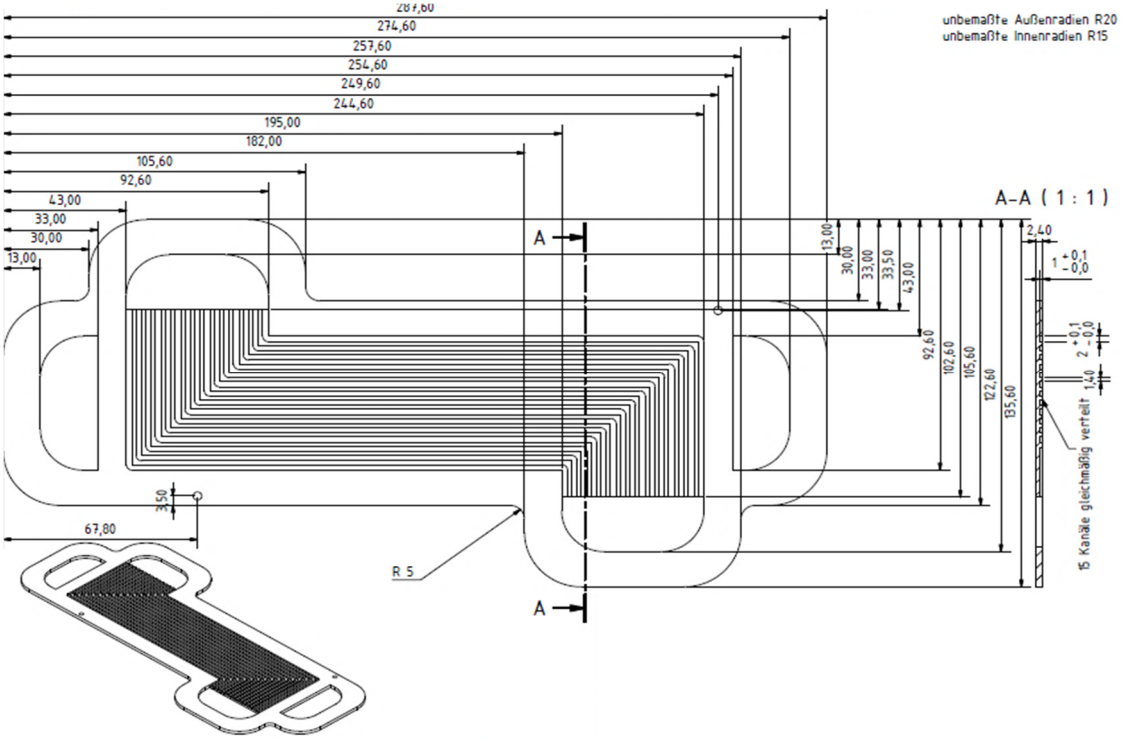

3) H_2O plate

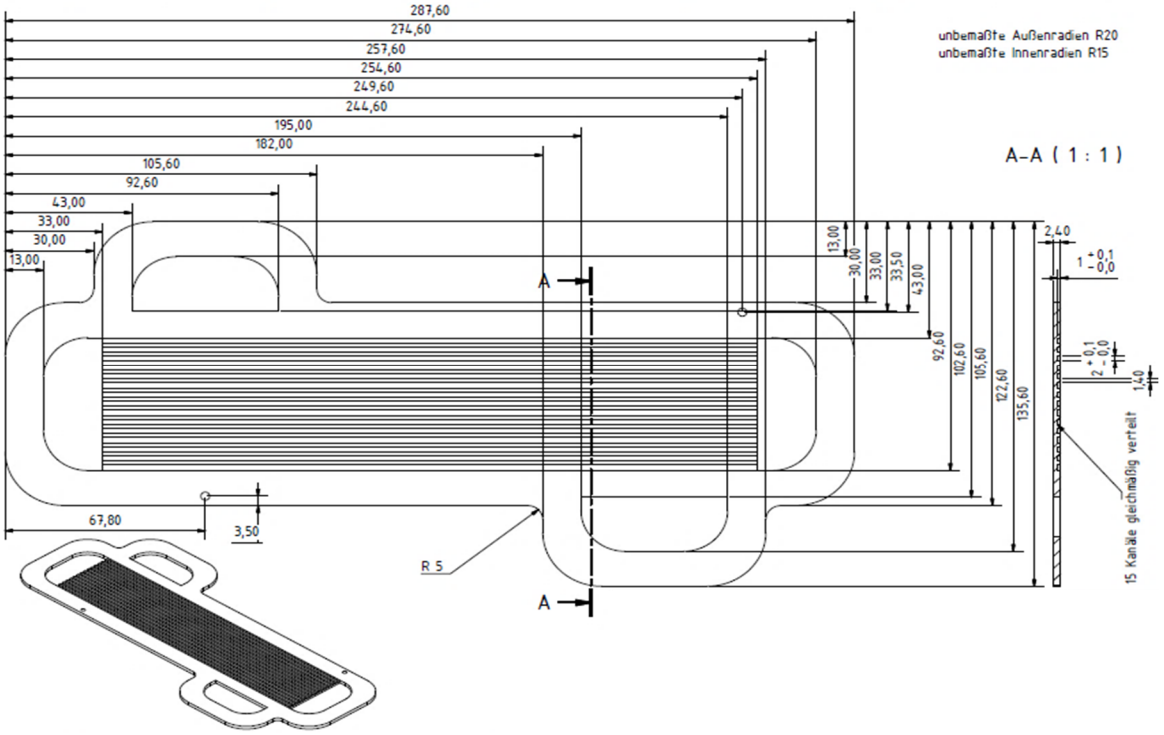

4) sCO_2 cover plate

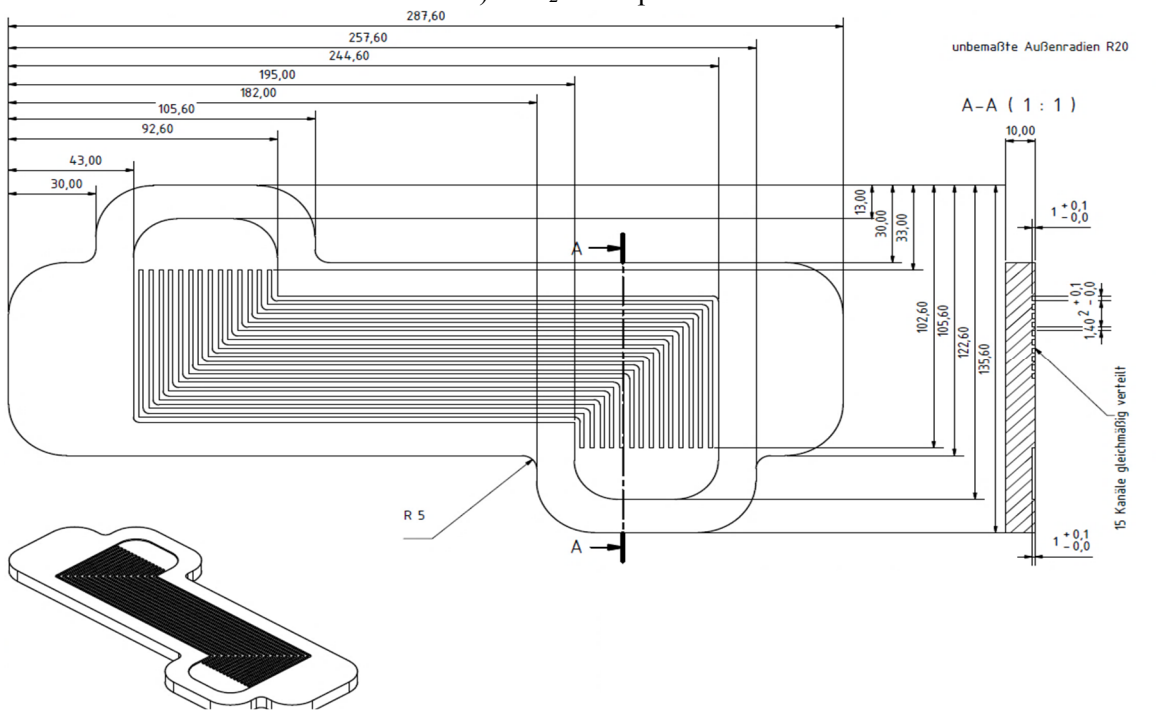

Figure 5-1: Glass model CHX plates

The upper technical drawing in Figure 5-1 shows the cover plate with a total length of 287.6 mm, a width of 135.6 mm and a plate thickness of 10 mm. The second drawing shows a sCO_2 plate with 15 rectangular Z-shaped channels with a channel dimension of 2x1 mm. The plate has a length of 287.6 mm, a width of 135.6 mm and a thickness of 2.4 mm. Two plenums are available for the inlet and outlet of the sCO_2 into the channels of the stacked plates. Compared to other CHX designs, it must be mentioned that in this approach, the plenums are already integrated into the plates, which is beneficial because no further welding processes are required for the plenums. The Z-shape of the sCO_2 channels is important to connect two of the four plenums with the sCO_2 side and the other two with the steam side. Due to counter-current flow, the steam enters the HX at the top, transfers the heat to the sCO_2 side, is condensed and leaves it as condensate at the bottom. The sCO_2 enters the HX at the bottom and leaves it heated at the top. The effective straight sCO_2 channel length is 150 mm, which is the straight length of the middle part of the Z-shaped channels. The third technical drawing shows a steam plate with 15 rectangular straight channels with a channel dimension of 2x1 mm, an entire plate length of 287.6 mm, a width of 135.6 mm and a thickness of 2.4 mm. There are also two plenums integrated on the steam side, one for the steam inlet and one for the outlet. The drawing at the bottom in Figure 5-1 shows the sCO_2 cover plate with 15 integrated channels and a plate thickness of 10 mm. The channel dimension, channel shape, plate length and plate width are similar to the plates above.

5.3 Manufacturing steps of CHX

To demonstrate the manufacturing process of the CHX, a few pictures of the plates and the manufacturing steps are shown in Figure 5-2. The first picture shows a H_2O plate with 15 straight rectangular 2x1 mm channels and four integrated plenums. Two of them are used for the inlet and outlet of the H_2O into the channels of the CHX. The second picture shows a sCO_2 plate with 15 rectangular 2x1 mm Z-shaped channels and two integrated plenums for the sCO_2 flow. After manufacturing and cleaning the plates in the workshop, they are alternately stacked together as depicted in picture 3. The two drillings at the outer area are only used for adjusting and centering the plates during the manufacturing process and for diffusion bonding. Picture 4 shows one plenum in more detail, so that the plates and the inlets into the channels can be seen. After stacking the plates, they are pulled together by clamps and additional metal strips are welded onto the CHX to prevent any kind of slippage during the welding (picture 5).

Picture 6 shows the CHX after the diffusion bonding. The homogenous deformation of the metal strips verifies that the deformation process of the diffusion bonding is evenly distributed. After welding, the CHX is checked with a leakage and a pressure test. Picture 7 shows the leakage test, in which the CHX is evacuated and all welds are successfully tested with helium. In case of a leakage, the device is able to detect the helium inside the CHX and signals it. After the leakage test, a pressure test is performed. For this, the CHX, placed in a water vessel, is connected to a gas bottle and the pressure is gradually increased to about 160 bar, seen in picture 8. After a three-day test procedure with no pressure losses, the test is successfully finished. Finally, the sCO_2 pipe and H_2O flange connections are electron beam welded onto the CHX before it is ready for the installation into the PWR glass model (picture 9). To ensure the quality of the entire CHX, with pipe and flange connections, a second pressure test is performed at the MPA University of Stuttgart. Picture 10 shows the CHX attached to the steam generator of the PWR glass model.

1) H_2O plate

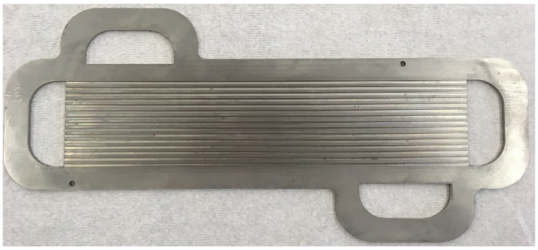

2) sCO_2 plate

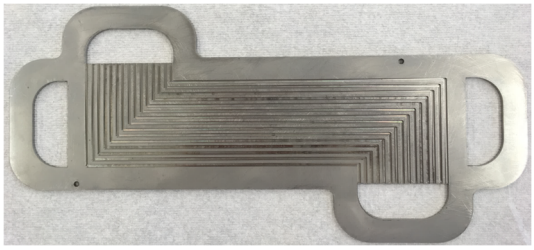

3) Stacked plates

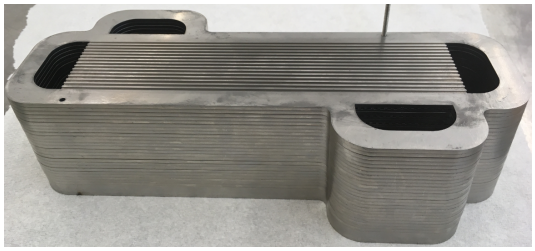

4) View into the plenum

5) Preparation for diffusion bonding

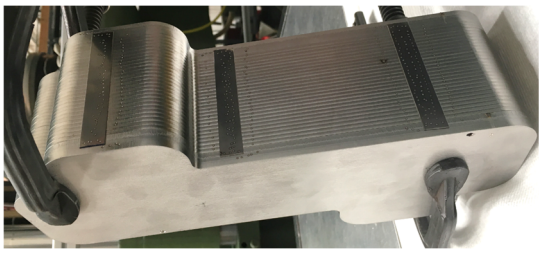

6) After diffusion bonding

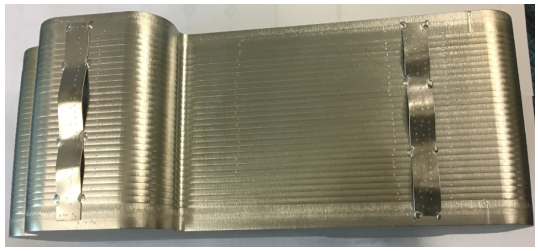

7) Leakage test

8) Pressure test

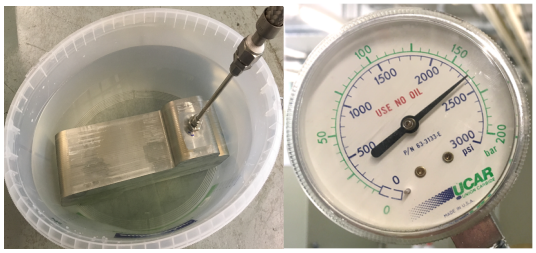

9) CHX for the glass model

10) Installed at the glass model

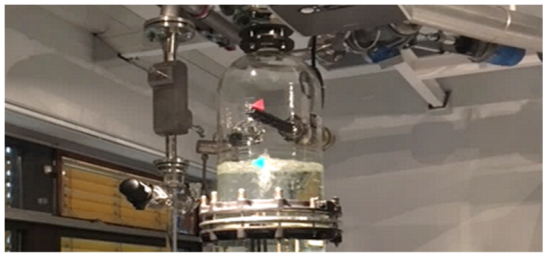

Figure 5-2: Manufacturing steps of CHX

6 ATHLET simulations

6.1 Introduction

In the sCO2-HeRo project a decay heat removal system with sCO_2 as working fluid is designed, manufactured and installed at the PWR glass model at GfS, Essen, Germany. The received experimental results, e.g. of the turbine, the compressor and the heat exchangers, are used to determine the design of the sCO2-HeRo components on the one hand and for the validation and enhancement of the German thermo-hydraulic code ATHLET on the other. In the first step, ATHLET is used to simulate the thermodynamic behavior of the sCO2-HeRo system by means of component models based on developed performance maps and correlations. A code validation can be achieved by comparing experimental results with simulation results. In the second step the implemented component models and performance maps are scaled up to nuclear power plant size and simulations will be carried out for nuclear light water-reactors (LWR) with a sCO2-HeRo system attached.

The German thermal-hydraulic code ATHLET can be used for the simulation of power plant transients like SBO & LUHS scenarios and for different kinds of leaks and breaks in light water reactors. The ATHLET version ATHLET-CD also includes the possibility to simulate accident scenarios with core degradation (CD). The code simulates mechanical fuel behavior, core melting, fuel rod cladding and relocation of material in combination with debris bed formation. Moreover, the applicability of different coolants and working fluids like heavy water, helium, sodium and carbon dioxide are implemented. The code structure is highly modular with several basic modules for the calculation of different phenomena. Important modules are the Thermo-Fluid-Dynamic-Module (TFD), the Heat-Transfer-And-Heat-Conduction-Module (HECU), the Neutron-Kinetics-Module (NEUKIN) and the General-Control-Simulation-Module (GCSM). With the basic modules, a thermal-hydraulic system, e.g. the steam cycle of a Boiling-Water-Reactor or the sCO2-HeRo system, can be simulated by connecting and defining different elements like pipes, branches and special objects such as turbines, pumps and heat exchangers. The heat conduction and heat transfer simulation in structures, fuel rods, electrical heaters and heat exchangers are performed by the HECU module.

Venker et al. [10] - [15] perform sCO2-HeRo cycle simulations with ATHLET for a BWR and the results show that the grace time between an initiating SBO & LUHS accident scenario and the start of any kind of cooling action can be increased up to 72 hrs (grace period). The results are obtained from ATHLET in consideration of the implemented component models, e.g. for the turbine, compressor and heat exchangers. For code improvement and validation, further ATHLET simulations of the sCO2-HeRo demonstrator unit will be conducted and the experimental results will be compared with simulation results. This improvement will be achieved in two steps. In the first step, the ATHLET code from Venker is used to simulate the sCO2-HeRo glass model setup followed by simulations with an enhanced ATHLET code with modified performance maps and, if necessary, adjusted correlations for the implemented models. To develop these performance maps, the turbine, the compressor, the compact heat exchanger and the sink heat exchanger are manufactured and tested, e.g. in the sCO_2 SCARLETT test facility at the University of Stuttgart or the SUSEN sCO2-facility at CVR, Rez. The performance maps are provided and implemented by means of experimental results or results from CFD simulations. New simulations are performed and the results are compared to the experimental one.

6.2 Development of performance maps and used correlations

6.2.1 Compressor

The performance maps (PM) of the pressure ratio of the compressor π_C and the compressor efficiency η_C are developed in consideration of the CFD simulation results, validated by measurements, delivered by University of Duisburg-Essen [61]. The results are depicted on the left and the developed performance maps on the right in Figure 6-1.

Simulation results - Compressor

Pressure ratio of compressor π_C [-] as function of sCO_2 outlet mass flow rate $\dot{m}_{out,C}$ [kg/s]

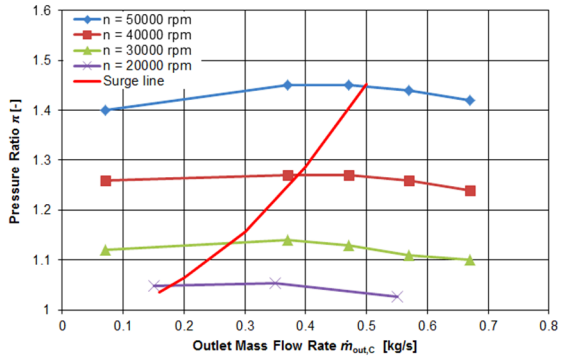

Compressor efficiency η_C [%] as function of sCO_2 outlet mass flow rate $\dot{m}_{out,C}$ [kg/s]

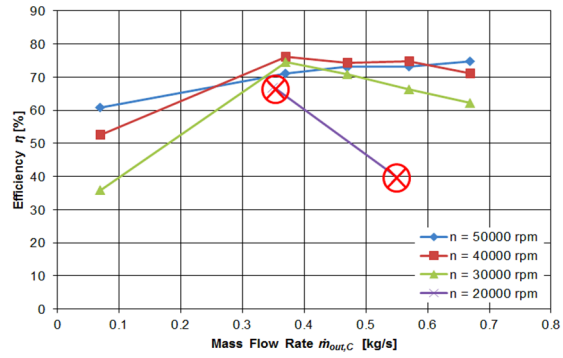

Developed performance maps - Compressor

Performance map of pressure ratio of compressor π_C [-] as function of sCO_2 outlet mass flow rate $\dot{m}_{out,C}$ [kg/s] and rotational speed n_C [1/min]

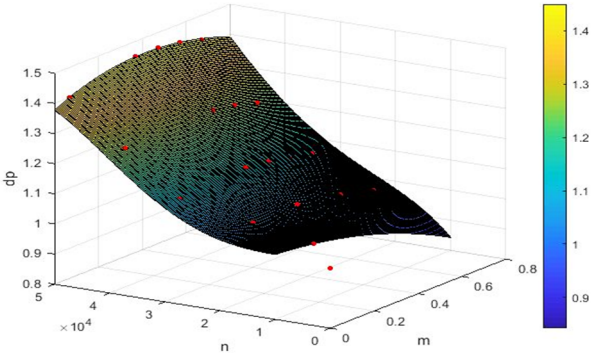

Performance map of compressor efficiency η_C [%] as function of sCO_2 outlet mass flow rate $\dot{m}_{out,C}$ [kg/s] and rotational speed n_C [1/min]

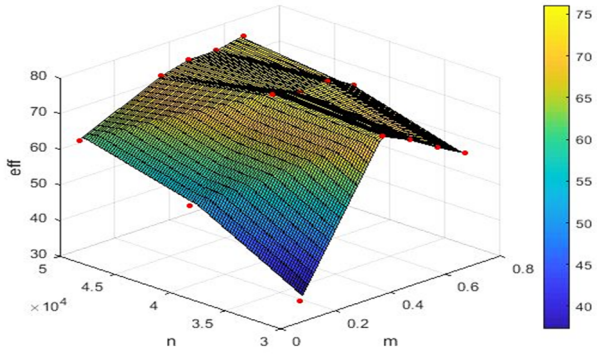

Figure 6-1: Simulation results and developed performance maps for the compressor

The simulation results of the pressure ratio π_C as a function of the sCO_2 outlet mass flow rate $\dot{m}_{out,C}$ and the rotational speed n_C of the compressor are summarized on the top left in Figure 6-1. Constant inlet conditions at the compressor of 78.3 bar and 33 °C are assumed for the simulations. Additionally, the surge line of the compressor is shown as a red line. The developed 3D performance map of the pressure ratio π_C as a function of $\dot{m}_{out,C}$ and n_C is depicted at the top right in Figure 6-1. For the development, three additional interpolation points are determined to be able to extrapolate the mass flow rate and rotational speed for further simulations. The first additional interpolation point is set at a mass flow rate of 0 kg/s and a rotational speed of 0 rpm, which leads to a pressure ratio of 1. As only three data points are available for the rotational speed of 20000 rpm, another performance point is obtained via linear extrapolation technique to a pressure ratio of 1, which leads to a mass flow rate of 0.7 kg/s. The third additional interpolation point is defined by using a parabolic function according to $m(n) = an^2+bn+c$. The parameters a, b and c are chosen with respect to existing interpolation points to a = 1.75E-9, b = 0 and c = 0, which leads to a function according to $m(n) = 1.75E\text{-}9n^2$. This parabolic function is afterwards used for the calculation of the sCO_2 mass flow rate of 0.174 kg/s for a pressure ratio of 1 and a rotational speed of 10000 rpm. Taking into account the 18 data points and the interpolation points, the polynomial surface fit function for the compressor ratio π_C with degrees x : 3 and y : 4 is determined by the software MATLAB. The result of the surface fit is shown at the top right in Figure 6-1. The coefficients for the polynomial fit function and the residuals for each point, with a deviation of less than 1 %, are derived from the MATLAB code and implemented into the ATHLET code. The CFD simulation results of the compressor efficiency η_C as a function of the outlet mass flow rate $\dot{m}_{out,C}$ are summarized at the bottom left in Figure 6-1. For the rotational speeds of 50000 rpm, 40000 rpm and 30000 rpm five data points and for 20000 rpm only two data points are available. Because of that, the 20000 rpm results are neglected for the development of the PM. The performance map for the compressor efficiency η_C is determined in consideration of the 15 data points and a linear interpolation technique, which is also used for the implementation into ATHLET. The MATLAB surface plot of η_C as a function of $\dot{m}_{out,C}$ and n_C is shown at the bottom right.

6.2.2 Turbine

The performance maps of the turbine pressure ratio π_T and the turbine efficiency η_T are developed similar to the compressor PM's. Figure 6-2 depicts the results from UDE [61] on the left and the developed PM's on the right.

Simulation results of the turbine pressure ratio π_T are shown at the top left in Figure 6-2 as a function of the sCO_2 inlet mass flow rate $\dot{m}_{in,T}$ and the rotational speed n_T. For the simulations, a constant inlet pressure of 117.45 bar and an inlet temperature of 200 °C are assumed. For all rotational speed, the data points show a non-linear tendency of the pressure ratio π_T with increasing pressure ratios for increasing mass flow rates. Moreover, a constant sCO_2 mass flow rate and increasing rotational speed leads to increasing pressure ratios. For the development of the PM one additional interpolation point is determined at 0 kg/s and 0 rpm, which leads to a pressure ratio of 1. The CFD results and the interpolation point are used for the development of the 3D performance map of the turbine by using MATLAB and a linear interpolation-technique. The result of the surface plot is shown at the top right in Figure 6-2 and the linear interpolation-technique is also applied for the implementation into ATHLET. The data points of the turbine efficiency η_T are summarized at the bottom left in Figure 6-2 as a function of the sCO_2 inlet mass flow rate and the rotational speed. A rotational speed of 40000 rpm leads to a typical tendency of increasing turbine efficiencies with increasing mass flow rates and vice versa. The two marked data points at a mass flow rate $\dot{m}_{in,T}$ of 0.235 kg/s (50000 rpm) and 0.335 kg/s (30000 rpm) are neglected for the development of the PM because they do not match the typical turbine efficiency tendency. Therefore, one new interpolation point is added via linear extrapolating (0.235/13.69) for the 50000 rpm case, and one (0.335/32.93) via linear interpolating for a rotational speed of 30000 rpm. The results of the 3D linear-interpolation surface plot of the turbine efficiency η_T with MATLAB are depicted at the bottom right as a function of the sCO_2 mass flow rate and the rotational speed. The data points and the additional interpolation points are marked as red dots. For the implementation of the PM into ATHLET again the linear interpolation-technique is chosen.

Simulation results - Turbine

Pressure ratio of turbine π_T [-] as function of sCO_2 inlet mass flow rate $\dot{m}_{in,T}$ [kg/s]

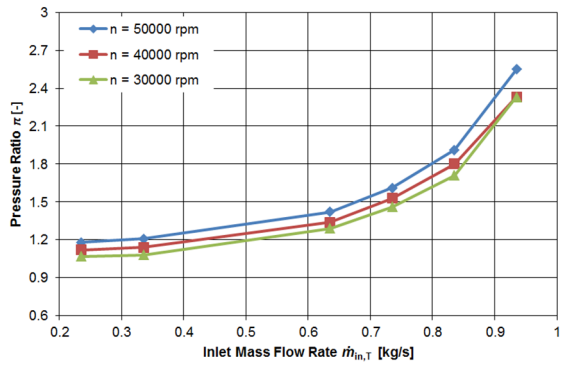

Turbine efficiency η_T [%] as function of sCO_2 inlet mass flow rate $\dot{m}_{in,T}$ [kg/s]

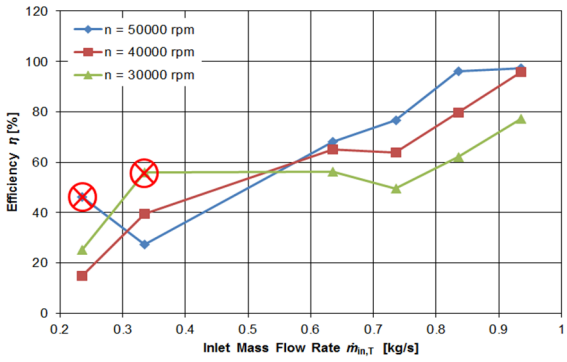

Developed performance maps - Turbine

Performance map of pressure ratio of turbine π_T [-] as function of sCO_2 inlet mass flow rate $\dot{m}_{in,T}$ [kg/s] and rotational speed n_T [1/min]

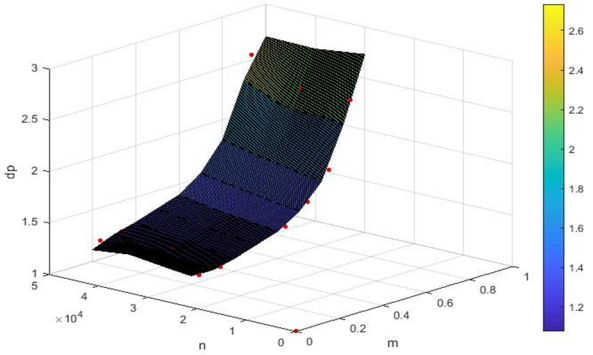

Performance map of turbine efficiency η_T [%] as function of sCO_2 inlet mass flow rate $\dot{m}_{in,T}$ [kg/s] and rotational speed n_T [1/min]

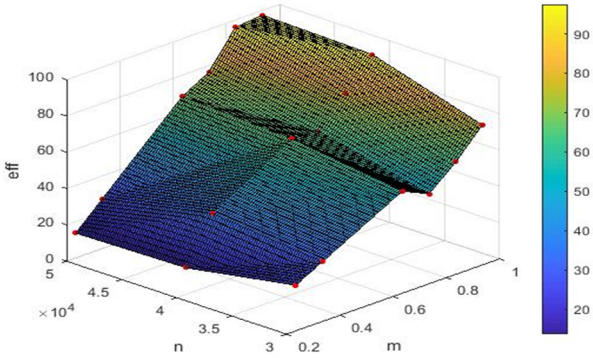

Figure 6-2: Simulation results and developed performance maps for the turbine

6.2.3 Ultimate heat sink

In the air-cooled gas coolers, the waste heat of the sCO2-HeRo cycle is transferred to the ultimate heat sink, the ambient air. The gas coolers are purchased from the German manufacturer Günter GmbH and the experimental investigations take place at the Research Centre Rez, Prague. The experimental setup, boundary conditions and the received results are summarized in Milestone No. 2.6 "Delivery of sink HX performance maps" [62]. For instance, the calculated heat input into the air Q_{air} is shown in the Milestone No. 2.6 as a function of the extracted heat Q_{sCO2} from the sCO_2. The heat transfer ratio $R = Q_{air}/Q_{sCO2}$ has a deviation of less than + 15 % for all measurement points. The results show further that the gas coolers are able to transfer the waste heat for DP and ODP conditions reliably. Taking into account the experimental results and the analyzed data, the heat transfer in the air-cooled gas coolers is simulated in ATHLET according to the developed heat transfer model, as shown in Figure 6-3.

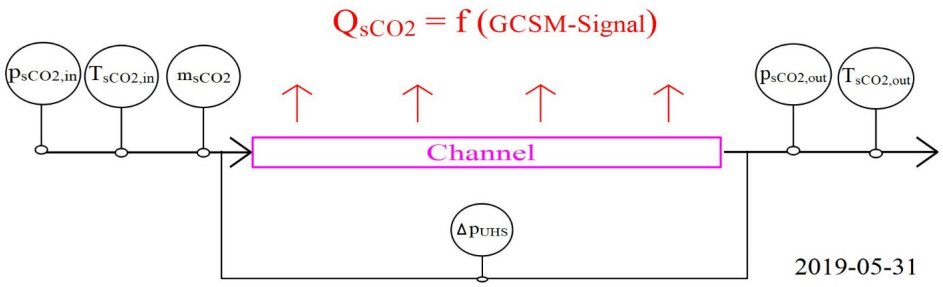

Figure 6-3: Schematic drawing of the heat transfer model for the UHS

In the sCO2-HeRo system the electrically driven fans of the air-cooled gas coolers are used for regulating the transferred heat power of the UHS and thus the sCO_2 inlet temperature of the compressor. This temperature is the most important one. Therefore it is the process controlled parameter in the system, because slight temperature deviations would lead to high density changes of the working fluid at the inlet of the compressor. The transferred heat power is adjusted in the sCO2-HeRo system by using a controller for the rotational speed of the fans. Higher rotational speed leads to higher heat transfer and vice versa. For this reason, the model also includes a controller used for adjusting the transferred heat power. The model starts on the left with the sCO_2 inlet pressure $p_{sCO2,in}$, inlet temperature $T_{sCO2,in}$ and mass flow rate $\dot{m}_{sCO2}$. The pressure drop Δp_{UHS} in the UHS is calculated according to Eq. (6-1) by using the friction loss coefficient ξ according to the Colebrook equation (Eq. (6-2)). The pressure at the outlet of

the UHS $p_{sCO2,out}$ is determined according to Eq. (6-3) and the necessary sCO_2 cooling power according to Eq. (6-4). The enthalpies at the inlet $h_{sCO2,in}$ and outlet $h_{sCO2,out}$ of the UHS are calculated as a function of the inlet and outlet temperatures and pressures. Afterwards, the calculated sCO_2 cooling power Q_{sCO2} is used in ATHLET as a GCSM signal and the implemented PI-controller ensures a constant temperature $T_{sCO2,out}$ at the outlet of the UHS. If $T_{sCO2,out}$ exceeded the target value during the simulation, the PI-controller would automatically increase the cooling power Q_{sCO2} and vice versa.

$$\Delta p_{UHS} = \xi \cdot \frac{l}{d} \cdot \frac{\rho}{2} \cdot v^2 \tag{6-1}$$

$$\frac{1}{\sqrt{\xi}} = -2log_{10}\left(\frac{2.51}{Re\sqrt{\xi}} + \frac{K}{3.71d}\right) \tag{6-2}$$

$$p_{sCO2,out} = p_{sCO2,in} - \Delta p_{UHS} \tag{6-3}$$

$$Q_{sCO2} = \dot{m}_{sCO2} \cdot \left(h_{sCO2,in} - h_{sCO2,out}\right) \tag{6-4}$$

6.2.4 Compact heat exchanger

In the CHX the decay heat is transferred from the steam side of a nuclear power plant to the sCO2-HeRo system. The investigation on the heat transfer between condensing steam and sCO_2 is carried out with heat exchangers according to Table 3-7 at the Institute of Nuclear Technology and Energy System, Stuttgart. The HX's, the test facilities, the measurement points, the results and the data analysis of the low-pressure steam cycle experiments (70 °C / 0.3 bar - glass model) and high-pressure steam cycle experiments (286 °C / 70 bar - nuclear power plant) are described in previous chapters. In the following, the data analysis, the chosen correlations, the comparison between calculated and experimental results and the implementation strategy of the pressure drop and heat transfer model for the CHX into the ATHLET code are described.

The pressure drop $\Delta p_{calc,CHX}$ in the CHX can be determined in general according to Eq. (6-5) with the calculated pressure drop in the channel $\Delta p_{calc,channel}$ and calculated pressure drops due to flow deflections as well as contractions and expansions $\Delta p_{calc,loss}$. The pressure drop in the channel $\Delta p_{calc,channel}$ is determined according to Eq. (6-6) by means of the friction loss coefficient ξ, the channel length l, the channel diameter d, the density of the fluid ρ, and the velocity of the fluid v. Using a HX with a constant channel length l and a constant channel diameter d, Eq. (6-6) can be simplified according to Eq. (6-7). The sCO_2 flow velocity v in Eq. (6-7) can be rewritten with the sCO_2 mass flow rate $\dot{m}_{sCO2}$ and the sCO_2 flow cross section area A according to Eq. (6-8) by using the mass flow rate $\dot{m}_{sCO2}$, the density of the fluid ρ, the volume of the fluid V , the flow velocity of the fluid v, the cross section area A, and the friction loss coefficient ξ. Pressure drops due to flow deflections as well as contractions and expansion are determined according to Eq. (4-11) - Eq. (4-13).

$$\Delta p_{calc,CHX} = \Delta p_{calc,channel} + \Delta p_{calc,loss} \tag{6-5}$$

$$\Delta p_{calc,channel} = \xi \cdot \frac{l}{d} \cdot \frac{\rho}{2} \cdot v^2 \tag{6-6}$$

$$\Delta p_{calc,channel} = \xi \cdot \frac{\rho}{2} \cdot v^2 \tag{6-7}$$

$$\dot{m}_{sCO2} = \rho \cdot V \quad \rightarrow \quad \dot{m}_{sCO2} = \rho \cdot v \cdot A \quad \rightarrow \quad \Delta p_{calc,channel} = \frac{\xi}{2\rho}\left(\frac{\dot{m}_{sCO2}}{A}\right)^2 \tag{6-8}$$

A comparison of calculated sCO_2 pressure drop results $\Delta p_{calc,CHX}$ with experimental result $\Delta p05$ shows that the experimental ones are 2 to 5 times higher, even though that for the calculation of $\Delta p_{calc,CHX}$ also cross section enhancements, cross section reductions, heat inputs and bend losses are considered. The deviation between $\Delta p05$ and $\Delta p_{calc,CHX}$ leads to the development of a pressure drop model (Figure 6-4), which determines the friction loss coefficients ξ_{in} of the inlet plenum I and ξ_{out} of the outlet plenum II. These coefficients are implemented afterwards into the CHX model of the ATHLET code.

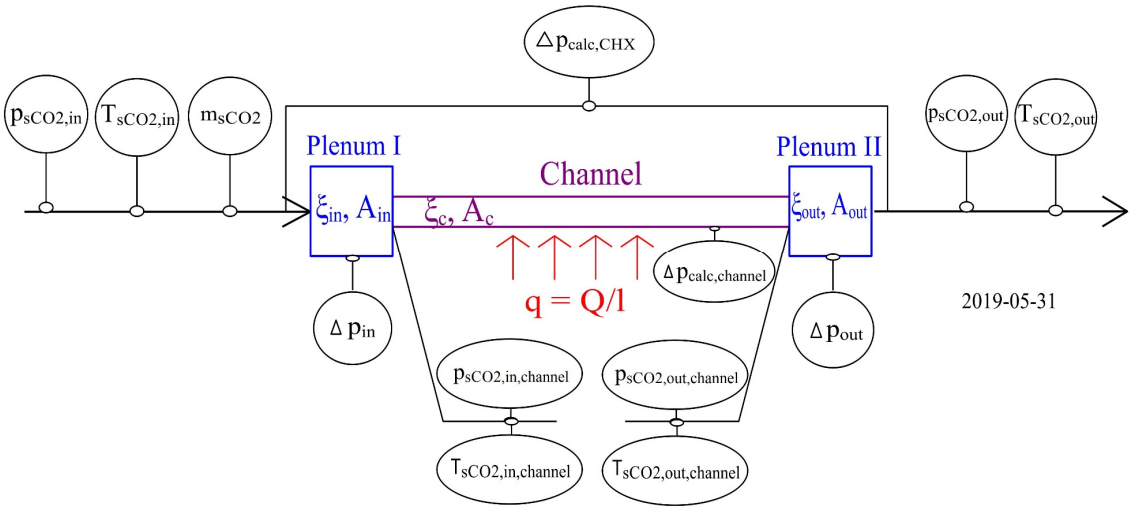

Figure 6-4: Schematic drawing of the pressure drop model for the CHX

Figure 6-4 shows a schematic drawing of the pressure drop model for the CHX, which can be divided into three parts: The inlet plenum "Plenum I", the channel "Channel" and the outlet plenum "Plenum II". The calculation starts on the left with a sCO_2 inlet pressure $p_{sCO2,in}$, an inlet temperature $T_{sCO2,in}$ and a mass flow rate $\dot{m}_{sCO2}$. The pressure drop Δp_{in} at the inlet of the CHX due to flow deflections and cross-section area changes is calculated inside "Plenum I" according to Eq. (6-9) by means of a determined friction loss coefficient ξ_{in}. Pressure changes due to cross-section area enhancements and cross-section area reductions are also taken into account by using the Bernoulli-Equation. The sCO_2 pressure at the inlet of the channel $p_{sCO2,in,channel}$ is calculated according to Eq. (6-10) and the temperature $T_{sCO2,in,channel}$ is assumed to be equal to $T_{sCO2,in}$. The pressure drop in the channel $\Delta p_{calc,channel}$ is calculated according to Eq. (6-7) with the channel length l and diameter d, the fluid density ρ, the flow velocity v, and the friction loss coefficient ξ. ξ is determined by using the Colebrook equation according to Eq. (6-2). The heat input density q is considered as uniformly distributed over the channel length l and the mass, momentum and energy conservation equation must be fulfilled. The pressure at the outlet of the channel $p_{sCO2,out,channel}$ is determined according to Eq. (6-11) and the temperature $T_{sCO2,out,channel}$ is calculated iteratively. The pressure drop Δp_{out} at the outlet is calculated similar to Δp_{in} within "Plenum II" by using Eq. (6-9) with $p_{sCO2,out,channel}$, $T_{sCO2,out,channel}$ and a determined ξ_{out}. The pressure at the outlet of the CHX $p_{sCO2,out}$ is calculated according to Eq. (6-12) and the temperature $T_{sCO2,out}$ is assumed to be equal to $T_{sCO2,out,channel}$. The overall pressure drop of the model $\Delta p_{m,CHX}$ is determined according to Eq. (6-13).

$$\Delta p_{in} = \xi_{in} \cdot \frac{\rho}{2} \cdot v^2 \tag{6-9}$$

$$p_{sCO2,in,channel} = p_{sCO2,in} - \Delta p_{in} + 0.5 * \rho * \left({v_{sCO2,in}}^2 - {v_{sCO2,in,channel}}^2\right) \tag{6-10}$$

$$p_{sCO2,out,channel} = p_{sCO2,in,channel} - \Delta p_{calc,channel} \tag{6-11}$$

$$p_{sCO2,out} = p_{sCO2,out,channel} - \Delta p_{out} + 0.5 * \rho * \left({v_{sCO2,out,channel}}^2 - {v_{sCO2,out}}^2\right) \tag{6-12}$$

$$\Delta p_{m,CHX} = \Delta p_{in} + \Delta p_{calc,channel} + \Delta p_{out} \tag{6-13}$$

After implementing the model into the MATLAB code, an iterative solver is chosen for the determination of the optimum friction loss coefficients ξ_{in} and ξ_{out}, which leads to similar pressure drop results for both the experimental and calculated one. The determined friction loss coefficients ξ_{in} of 204.332 and ξ_{out} of 2.371 are included into ATHLET for recalculating the pressure drops in the investigated CHX. The friction loss coefficient ξ_{in} refers to the inlet diameter of the pipe into the CHX and ξ_{out} to the diameter of the pipe at the outlet of the CHX. Results of the pressure drop model and experimental results are shown in Figure 6-5.

The upper picture in Figure 6-5 shows the experimental sCO_2 pressure drop results (red circles) and the calculated sCO_2 pressure drop results (black X) as a function of the sCO_2 mass flow rate. Both graphs show similar parabolic tendencies of the pressure drop with increasing pressure drop for increasing mass flow rates. The results of the relative prediction errors of the experimental results compared to the calculated results are depicted in the second picture as a function of the sCO_2 mass flow rate. Except for three measurement points, the relative prediction error can be limited to less than 10 % for the determined friction loss coefficients ξ_{in} and ξ_{out} and for more than half of the measurement points to less than 4 %. The picture at the bottom shows the calculated sCO_2 pressure drop results as a function of the measured sCO_2 pressure drop results. The upper black dashed line limits the pressure drop ratio to 110 % and the lower one to 90 %. The depicted results in Figure 6-5 show that the developed pressure drop model of the CHX is able to recalculate the experimental results with quite well accordance.

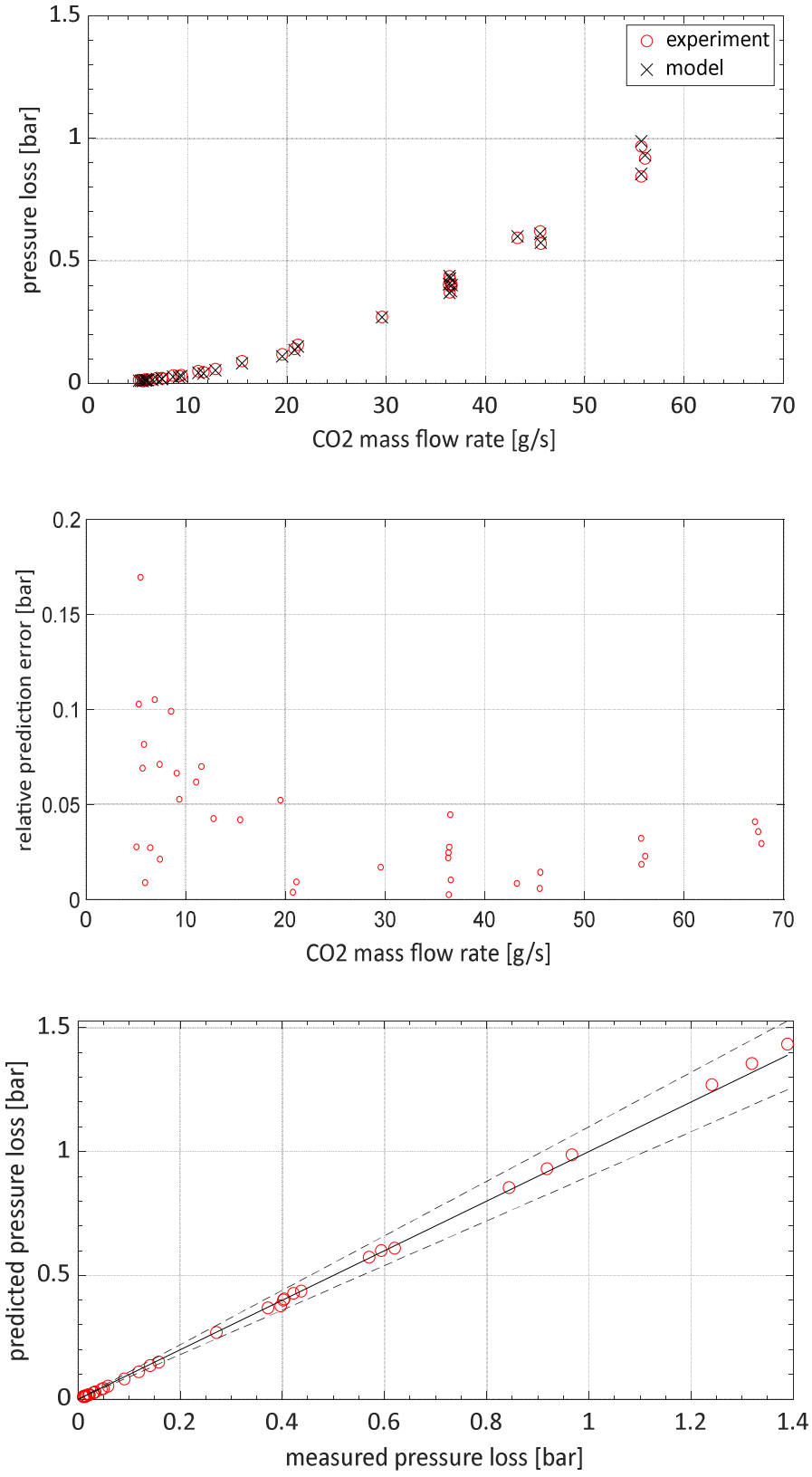

Figure 6-5: CHX pressure drop results of the implemented model

Besides the pressure drop model described above, also a heat transfer model is developed for the calculation of the heat transfer in the investigated compact heat exchanger. A schematic drawing of the model is shown in Figure 6-6.

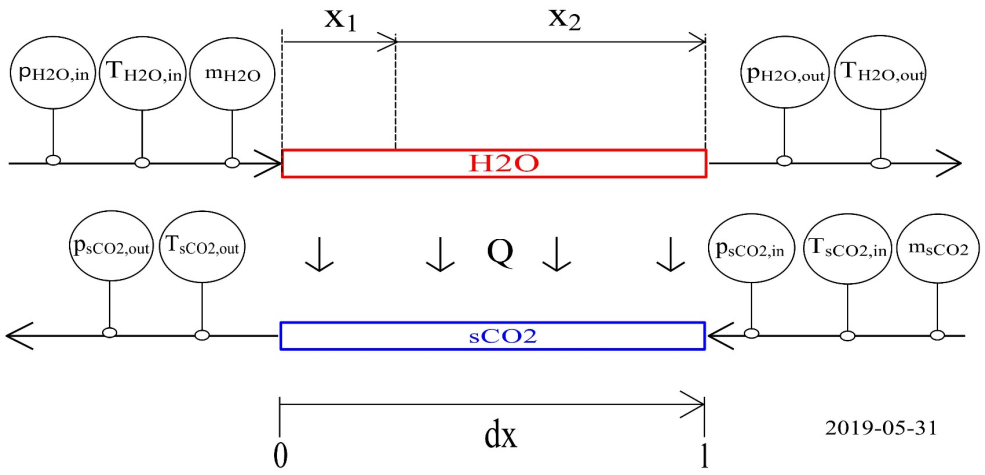

Figure 6-6: Schematic drawing of the heat transfer model for the CHX

At the left hand side of Figure 6-6, the steam enters the heat transfer model for the CHX at the top with the steam inlet pressure $p_{H2O,in}$, inlet temperature $T_{H2O,in}$ and steam inlet mass flow rate $\dot{m}_{H2O}$. Considering the experimental results, with subcooled conditions at the outlet of the CHX on the steam side, the MATLAB model can also calculate subcooled water conditions. It is assumed that saturated steam enters the CHX and flows into the channel in which the heat Q is transferred from the steam side to the sCO_2 side. Due to the heat transfer, the steam is condensed over the channel length l and the sCO_2 is heated. Depending on the steam and sCO_2 inlet conditions, the steam is completely condensed in the model at a channel length x_1 and in the following (channel length x_2) the heat transfer occurs between water and sCO_2. The water temperature at the outlet of the CHX $T_{H2O,out}$ is iteratively calculated and the pressure $p_{H2O,out}$ is assumed to be equal to $p_{H2O,in}$. Because of counter-current flow conditions the sCO_2 enters at the bottom right (Figure 6-6) with an inlet pressure $p_{sCO2,in}$, inlet temperature $T_{sCO2,in}$ and inlet mass flow rate $\dot{m}_{sCO2}$. The heat transfer leads to an increase of the sCO_2 temperature along the channel length l, and the outlet temperature $T_{sCO2,out}$ at the CHX is iteratively determined. The sCO_2 pressure at the outlet is calculated according to model, as shown in Figure 6-4.

The implemented correlations in ATHLET are used to calculate the transferred heat power in the CHX. According to the ATHLET user guide [63] for the steam side the Nusselt correlation for laminar film condensation and the Carpenter-and-Colburn correlation for turbulent film condensation are chosen. One of the two, depending on the flow regime, is used in the channel length x_1 where condensation occurs. The correlation for the calculation of the heat transfer coefficient in the channel length x_2 is determined in ATHLET according to a heat transfer correlation-logic-map, which needs temperature and flow regime inputs. On the sCO_2 side, the Gnielinski correlation is used to determine the heat transfer coefficient. If the calculated Nusselt number is lower than 25, it is automatically set to 25 to avoid numerical instabilities in the code. In consideration of the heat transfer coefficients on both sides, the transferred heat power is calculated by means of the plate thickness and heat conductivity. An iterative calculation process along the channel length l determines e.g. the temperature profiles, the pressure drop profiles, the flow velocity profiles and the transferred heat power on both sides of the CHX.

As an example, results of the temperature profiles in the CHX for the DP investigation with an sCO_2 mass flow rate of 67.7 g/s and an steam condensing power of 585 W as well as for the ODP II investigation with a mass flow rate of 5.5 g/s and a condensing power of the steam of 1097 W are shown in Figure 6-7. The upper picture shows temperature profiles of sCO_2 and H_2O for the bulk and wall as a function of the channel length l for the DP measurement point with a sCO_2 mass flow rate of 67.7 g/s and a steam condensing power of 585 W. Saturated steam enters the CHX on the left, which leads to a bulk temperature of about 286 °C (black x). Due to the heat transfer the steam is condensed at a length of about 15 mm and afterwards it is subcooled to a bulk temperature of about 60 °C. The H_2O temperature profile at the wall (blue +) is lower than the bulk temperature because the heat is transferred from the H_2O bulk via the H_2O wall (blue +) and the sCO_2 wall (green +) into the sCO_2 bulk (red o). The sCO_2 enters the HX at the right with a bulk temperature (red o) of about 40 °C and is heated to a temperature of about 42 °C. The picture at the bottom shows calculated temperature profiles for the ODP II investigation with a sCO_2 mass flow rate of 5.5 g/s and a steam condensing power of 1097 W. The H_2O bulk temperature shows that the steam is condensed at a length of about 45 mm and the sCO_2 bulk temperature is heated from about 40 °C to 100 °C at the outlet of the CHX. A comparison of the two pictures shows that firstly the condensation length of the steam (blue +) and secondly the outlet temperature of the sCO_2 (red o) are increased for the 1097 W scenario. This can be explained by the steam and sCO_2 inlet conditions into the HX.

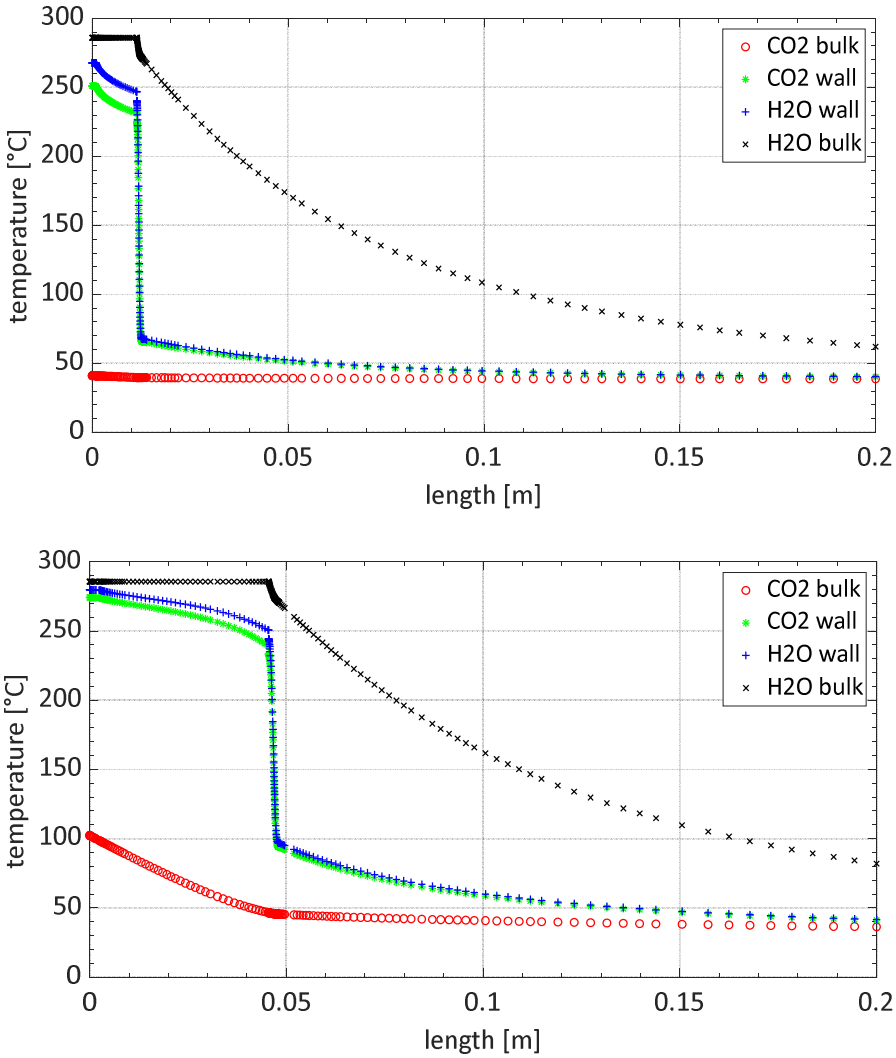

Figure 6-7: CHX temperature profiles of the implemented model for 585 W and 1097 W

Finally, calculated results of the developed heat transfer model and the experimental results are depicted in Figure 6-8. The first picture shows the calculated steam condensation length x_1 as a function of the sCO_2 mass flow rate. On the left it could be seen that for the ODP II investigations, a steam condensing power of about 1100 W leads to an increasing condensation length from about 23 mm to 48 mm for decreasing sCO_2 mass flow rates from 36.6 g/s to 5.5 g/s. Moreover, the calculated condensation length of 8 mm (Q_{sCO2} of 380 W) and 23 mm (Q_{sCO2} of 1100 W) for a sCO_2 mass flow rate of about 36 g/s can be explained by different steam condensing power. The picture at the bottom depicts the calculated sCO_2 heat input as a function of the received experimental results. For all results, there is a linear tendency between the calculated and experimental results. The upper black dashed line limits the ratio to 110 %

and the lower black dashed line to 90 %, which means that the heat transfer model is able to re-calculate the experimental results with a deviation of less than 10 % for all investigated measurement points. The results (Figure 6-8) verify that the developed heat transfer model is able to re-calculate the experimental heat transfer capabilities. Because of that, the implemented heat transfer correlations in the ATHLET code are used for the determination of the heat transfer power in the CHX simulations.

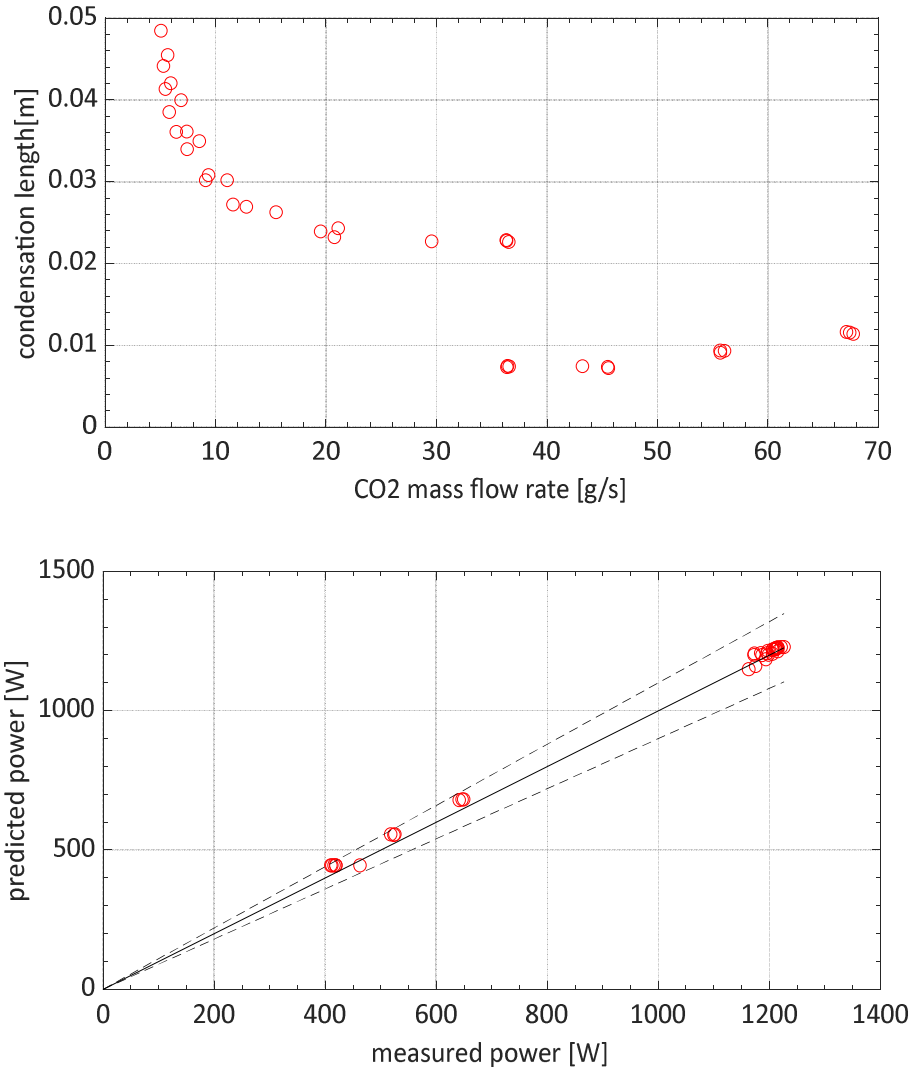

Figure 6-8: CHX heat transfer results of the implemented model

6.3 ATHLET simulations and results

6.3.1 Boundary conditions

After the implementation of the performance maps and the component models into ATHLET 3.1, the boundary conditions for the simulations summarized. The design point values of the sCO2-HeRo system, attached to a LWR, of Venker [10] and the defined design point values are shown in Table 6-1.

Table 6-1: Design point values of the sCO2-HeRo system

Side	Parameter	Unit	Value (J. Venker)	Value
Compressor Inlet (sCO_2)	Pressure	bar	90	90
	Temperature	°C	42.0	42.0
	Enthalpy	kJ/kg	367.00	367.00
	Entropy	kJ/kg·K	1.54	1.54
CHX Inlet (sCO_2)	Pressure	bar	180	129
	Temperature	°C	81.0	62.5
	Enthalpy	kJ/kg	391.00	379.50
	Entropy	kJ/kg·K	1.55	1.55
Turbine Inlet (sCO_2)	Pressure	bar	180	126
	Temperature	°C	281.0	281.0
	Enthalpy	kJ/kg	708.00	720.10
	Entropy	kJ/kg·K	2.28	2.37
UHS Inlet (sCO_2)	Pressure	bar	90	91
	Temperature	°C	219.0	255.4
	Enthalpy	kJ/kg	658.00	699.50
	Entropy	kJ/kg·K	2.31	2.39
CHX Inlet (H_2O)	Temperature	°C	286.0	286.0
UHS Inlet (Air)	Temperature	°C	37.0	37.0
ΔT	Temperature	°C	5.0	5.0

Venker determines a compressor inlet pressure of 90 bar and an inlet temperature of 42 °C (Table 6-1). The sCO_2 is compressed to a pressure of 180 bar and simultaneously compression-heated to a temperature of 81 °C before it enters the CHX. In the CHX it is heated isobaric to a temperature of 281 °C. After the expansion in the turbine the sCO_2 flows with a

pressure of 90 bar and a temperature of 219 °C into the UHS where it is cooled isobaric to a temperature of 42 °C before it re-enters the compressor. The simulations of Venker assume a constant turbine efficiency of 85 %, a constant compressor efficiency of 80 % and no pressure losses. For the current simulations equal compressor inlet conditions are chosen. In consideration of pressure losses and the CFD data from UDE, the pressure at the inlet of the CHX is determined at 129 bar. The temperature at the inlet is calculated by means of the compressor efficiency to 62.5 °C. In the CHX the sCO_2 is heated to a temperature of 281 °C and pressure losses in the CHX and in the pipe lead to a pressure of 126 bar at the inlet of the turbine. According to the implemented performance map, the sCO_2 is expanded in the turbine to a pressure of 91 bar and a temperature of 255.4 °C before it enters the UHS. There the sCO_2 is cooled to a temperature of 42 °C and the pressure drop leads to a pressure of 90 bar at the inlet of the compressor. For all simulations it is assumed that the steam enters the CHX with a temperature of 286 °C, the air temperature on the secondary side of the UHS is 37 °C and the minimum temperature difference for heat transfer (pinch point) is 5 °C.

For the ATHLET simulations, a transferred decay heat of 75 MW is defined, leading in the design point of the sCO2-HeRo system to a sCO_2 mass flow rate of 220 kg/s. Furthermore, five systems in parallel are chosen to be installed. This is beneficial because the systems can be switch-off consecutively according to the decay-heat-curve, leading to increased operational time. Furthermore, using five systems means that each system is designed for a decay heat of 15 MW and a sCO_2 mass flow rate of 44 kg/s. The design of the CHX, for 15 MW, is determined by means of ATHLET and has 14460 rectangular channels with a channel dimension of 2x1 mm and a channel length of 1.1 m. In the simulation it is defined that the steam is completely condensed along the channel length and no sub-cooling occurs. The condensing steam side is simulated by specifying the wall temperature on the H_2O side of the CHX and the implemented Gnielinski correlation is chosen on the sCO_2 side. Pressure losses are calculated according to the developed pressure drop model. The design of the UHS is taken from Venker with 255 parallel channels, a channel length of 15 m and a channel diameter of 25 mm. The sCO_2 temperature at the outlet of the UHS is controlled in ATHLET by using a PI-controller, which controls the cooling power on the air side of the UHS. In reality, the sCO_2 outlet temperature is controlled by the rotational speed of the air fans. The performance maps for the turbine and the compressor efficiency as well as pressure ratio are scaled-up from the glass model conditions to nuclear power plant scale according to the affinity laws for

scaling [64]. For the up-scaling, constant pressure ratios, densities, velocities and efficiencies are assumed. That approach seems to be conservative because the efficiency ratios are assumed to be constant, but a bigger machine will have a higher efficiency. Comparing the design point parameters of the glass model and the up-scaled sCO2-HeRo system (Table 6-1) it must be mentioned that constant density ratios, pressure ratios and velocity profiles could not be applied for the simulations because the design point of the turbine and the compressor of power plant size differs from the glass model design point. First results show that in the design point of the up-scaled sCO2-HeRo system the compressor consumes about 0.53 MW power and the turbine provides 0.91 MW power which leads to an excess power of about 0.38 MW.

6.3.2 Results

The profile of the steam temperature at the inlet of the CHX is derived from investigations of Venker [10] for a retrofitted sCO2-HeRo system into a BWR with adapted depressurization system. It is chosen for specifying the H_2O wall temperature of the CHX. For the simulations in ATHLET 3.1, the channel length of the CHX is divided into 15 control volumes (CV's) according to the nodalisation scheme in Figure 6-9. The sCO_2 enters the CHX at CV1 and leaves the CHX heated at CV15. As there is no specific heat exchanger model in ATHLET, the basic modelling approach is chosen. In this case, only one representative pair of channels (H_2O and sCO_2) is modelled and then scaled by the number of channels. The determined friction loss coefficients at the inlet ξ_{in} and outlet ξ_{out} of the CHX (chapter 6.2.4) are used for the recalculation of the experimental sCO_2 pressure drop results. The connection between the sCO_2 and H_2O side is achieved by using a plate object, which is one heat conduction object. The heat transfer area of each CV is the product of length and width. The length is determined by the chosen number of CV's and the width as well as the thickness can be defined by the user.

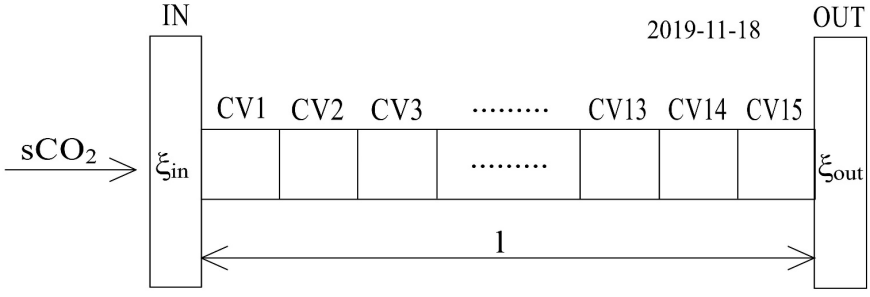

Figure 6-9: Nodalisation scheme of the sCO_2 channel of the CHX

Figure 6-10 depicts simulation results of the sCO_2 temperatures in the CHX for three control volumes of the CHX, namely CV1, CV7 and CV15. CV1 corresponds to the sCO_2 inlet, CV7 to the middle of the CHX and CV15 to the sCO_2 outlet. Due to the decreasing steam temperature, the sCO_2 temperatures in the CHX are also decreasing over the simulation time.

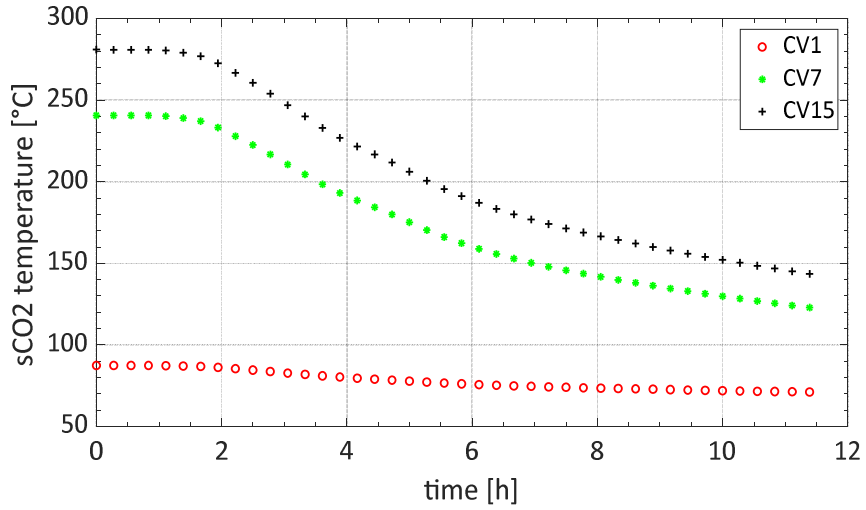

Figure 6-10: Results of the sCO_2 temperature profiles in the CHX for different CV

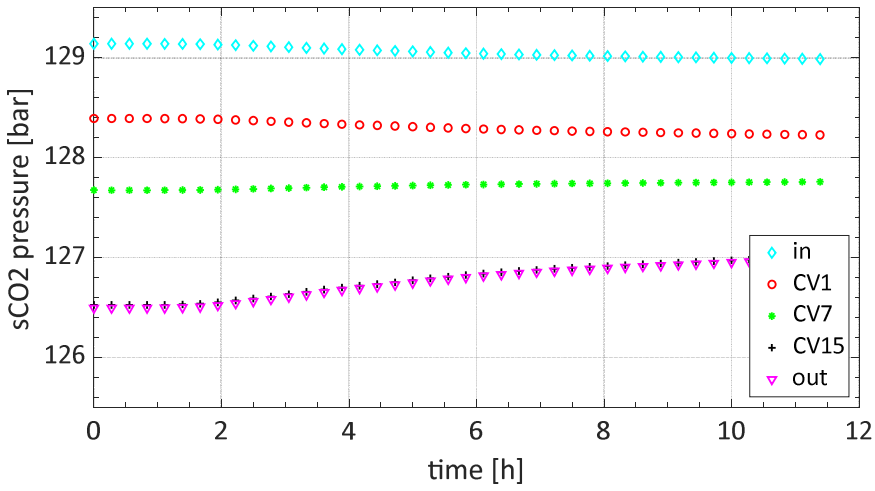

Figure 6-11: Results of sCO_2 pressure for different control volumes

Figure 6-11 shows simulation results of the sCO_2 pressures from the inlet, outlet, CV1, CV7 and CV15 of the CHX as a function of the simulation time. The major part of the pressure loss is due to wall friction, which increases along the length of the CHX as the fluid temperature increases. Consequently, the pressure loss decreases over the simulation time because the outlet temperature of the CHX also decreases. Inflow and outflow effects, flow distribution and changes of the cross section flow area cause the second part of the pressure loss at the inlet and outlet. This pressure loss is modelled as described in the pressure loss model of the CHX (chapter 6.2.4). Concerning this part of the pressure loss, the major part occurs at the inlet of the CHX because of the higher form loss coefficient and the additional pressure loss caused by the reduction of the cross sectional flow area. At the outlet, the expansion of the flow almost decreases the pressure loss to zero.

Figure 6-12 shows the calculated power output of the turbine and the power consumption of the compressor as a function of the simulation time. As a result of decreasing steam temperatures, the power output of the turbine also decreases over time. In contrast, the power consumption of the compressor is nearly constant, which is achieved by keeping the inlet condition constant. Additionally, the efficiencies of the turbine and the compressor are nearly constant due to the only slightly rising mass flow rates and the assumption of a constant rotational speed of the shaft. At the end of the simulation at about 11.5 h, the net power output of 76 kW is not enough to power the fans of the ultimate heat sink with a power consumption of 165 kW, according to Venker [10]. The break-even point is reached after 6.9 h and a steam temperature of 182 °C. The results of Venker show for the “Retrofitted BWR with Adapted Depressurization System” scenario that the break-even point is reached after 11.4 h and a steam temperature of 147 °C. However, the early break-even point here is a consequence of the lower net power output at the start of the simulation and the lower efficiency compared to the model of Venker.

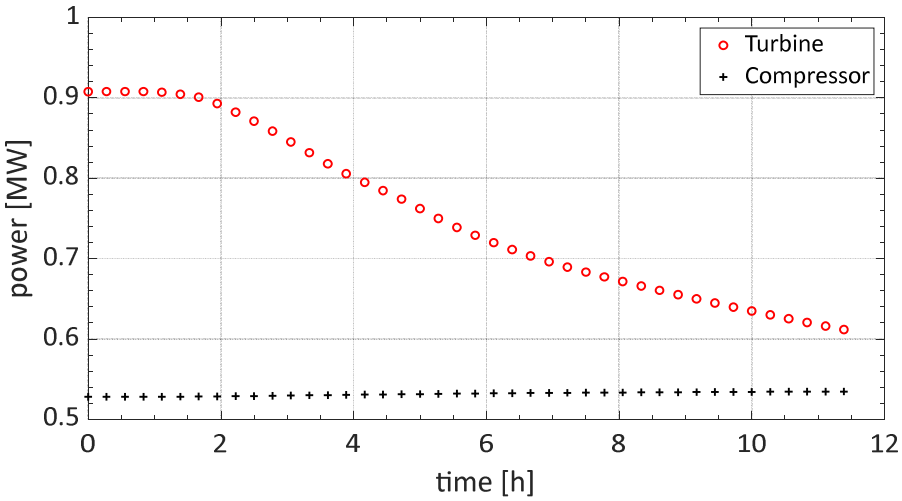

Figure 6-12: Calculated power output of compressor and turbine

Finally, it can be concluded that in further studies extended performance maps should be developed, implemented and used in the ATHLET code. For example, the performance maps of the compressor should be extended for a two-stage compressor, which is able to compress the sCO_2 to a pressure of up to 180 bar. Moreover, the scaling and design of the components for nuclear power plant application needs to be analyzed in more detail to perform more realistic reactor simulations. Additionally, the control strategies of the sCO2-HeRo system should be investigated in more detail and the cycle behavior at DP, ODP and closer the critical point should be experimentally tested at the demonstrator unit at the PWR glass model at GfS, Essen. In the future also a more realistic model of the UHS should be implemented and the interaction between nuclear power plant and attached sCO2-HeRo system should be investigated.

7 Discussion and Perspectives

The design point parameters of the sCO2-HeRo demonstrator unit and for a NPP are determined by means of cycle calculations in consideration of boundary conditions and assumptions, which are discussed as follows. The boundary conditions on the steam side of the sCO2-HeRo demonstrator unit are derived from experiments at the glass model. The water is electrically heated, and because it is made of glass, the operating pressure is limited to pressures lower 1 bar, leading to steam temperatures below 100 °C. Experiments show that decay heat powers between 0 - 12 kW can be provided, a higher power extraction decreases the steam temperature and a decreasing extraction leads to very small transferred heat power to the sCO_2 side. As a compromise, the design point for the decay heat is set to 6 kW, which leads to a saturated steam temperature of about 70 °C and a steam pressure of about 0.3 bar. Comparing the steam conditions, the amount of decay heat and the steam temperatures they are significantly lower in the GM than in a NPP. A nuclear power plant has steam with a pressure of 70 bar and a saturated steam temperature of 286 °C. Venker [10] suggests that 60 MW of decay heat have to be removed by the sCO2-HeRo system in order to achieve a long-term coolability of the nuclear core. Furthermore, the amount of removed decay heat should be adjusted according to the existing decay heat, to ensure a high temperature difference between the ambient air and the steam, which results in increasing operational time of the sCO2-HeRo system. This is realized by using four equal 15 MW sCO2-HeRo units in parallel, instead of one 60 MW unit.

To reduce the complexity and to increase the robustness of the sCO2-HeRo demonstrator unit, a single stage compressor with a pressure ratio of about 1.5 is chosen. To prevent any kind of manufacturing problems of the TCS due to very small components, the minimum sCO_2 mass flow rate is set to 0.65 kg/s. Because of the low steam temperature, an additional slave electrical heater is installed for heating up the sCO_2 to a turbine inlet temperature of 200 °C, which is similar to NPP conditions. The turbine efficiency of 75 % and the compressor efficiency of 65 % are conservative assumptions for such small machines. Both efficiencies are assumed to be constant for the entire range of cycle calculations. In comparison, a multi-stage compressor with a compression ratio of about 3 is selected for a nuclear power plant. The turbine efficiency of 85 %, the compressor efficiency of 75 % and a compression ratio of 3 are also conservative assumptions for such big machines. Both efficiencies are assumed to be constant for the entire range of cycle calculations.

The cycle calculations are performed for both systems in consideration of boundary conditions and assumptions like constant turbine and compressor efficiencies, no heat losses and no pressure losses. With respect to maximum generator excess electricity, the design point parameters of the sCO2-HeRo demonstrator unit are determined as follows: the compressor inlet pressure and temperature are set to 78.3 bar and 33 °C, the turbine inlet pressure and temperature to 117.45 bar and 200 °C and the sCO_2 mass flow rate to 0.65 kg/s. A steam condensing power of 6 kW is determined in the CHX. In the design point, the generator provides an excess electricity of about 9 kW. These data will have to be confirmed once the demonstrator unit at GfS starts operation. Four 15 MW sCO2-HeRo systems in parallel are used for the NPP application. The maximum generator excess electricity of one unit of about 1.38 MW is reached with a compressor inlet pressure and temperature of 90 bar and 42 °C, a turbine inlet pressure and temperature of 180 bar and 280 °C, and a sCO_2 mass flow rate of 47.7 kg/s. For heating the sCO_2 mass flow rate in the CHX a condensing power of the steam of 15 MW is defined.

The experimental investigation on the heat transfer between condensing steam and sCO_2 in diffusion bonded compact heat exchangers takes place in the laboratory of the Institute of Nuclear Technology and Energy Systems (IKE) by using two test facilities.

The SCARLETT test loop provides sCO_2 mass flow rates from 30 g/s to 110 g/s, depending on the compressor performance. The sCO_2 temperature at the inlet of the test section can be varied from 0 °C to 40 °C and the pressure can be adjusted from 75 bar to 110 bar.

The low-pressure steam cycle generates steam similar to the steam conditions at the PWR glass model. The pressure can be adjusted from 0.1 bar to 1 bar and the steam temperature corresponds to the pressure and varies between 50 °C and 100 °C. The water volume flow rate can be varied by the membrane pump from 0.05 l/h to 2.5 l/h and the installed electrical heating power of the evaporator with 1.6 kW is high enough to evaporate the adjusted water volume flow rates. For the heat transfer investigations with steam, such as in an NPP, the high-pressure steam cycle is constructed. The pressure can be adjusted from 1 bar to 105 bar and the corresponding steam temperature varies between 100 °C and 315 °C. The water volume flow rate can be varied, similar to the low-pressure steam cycle, by the HPLC pump from 0.05 l/h to

2.5 l/h and the electrical heating power of the evaporator with 1.6 kW is high enough for evaporation the water volume flow rates. The electrically heated evaporator is the most challenging component of both steam cycles. For further investigations, it would be beneficial to purchase and install an evaporator with increased heating powers, leading to increased steam volume flow rates in the test section.

Within this work, 7 heat exchangers are constructed and manufactured for the experimental heat transfer investigations. To investigate the influence of the channel dimension on phenomena like the heat transfer and the pressure drop, rectangular 2x1 mm and 3x1 mm channels are chosen with respect to recommended channel dimensions for CHX from the literature. The influence of the channel shape is investigated by means of heat exchangers with straight H_2O and Z-shaped sCO_2 channels (IZ) as well as with heat exchangers with straight H_2O and straight sCO_2 channels (II). The IZ channel shape is chosen because it is used for heat exchangers with more than one plate on each side and stacked plates. The II channel shape is selected because it is easy to manufacture and experimental results can be used e.g. for validation. The influence of the plenum geometry is investigated with heat exchangers with 15 channels at 1 plate and 1 plate on each side (15/1) as well as heat exchangers with 5 channels at 1 plate and 3 plates on each side (5/3) because previous investigations show that a more cubic plenum geometry is beneficial for decreasing pressure drop. The experimental heat transfer results of the 15/1 and 5/3 plates show that a steam provision of about 1.2 kW is not sufficient to investigate the heat transfer limits. Therefore, a heat exchanger with 5 channels at 1 plate and 1 plate on each side (5/1) is manufactured and investigated.

The measurement campaigns are classified according to the “Design Point” (DP), the “Out of Design Point” (ODP) and the “Out of Design Point II” (ODPII) campaigns. In the DP experiments, the sCO_2 mass flow rates and water volume flow rates are scaled down in the same ratio as the entire amount of sCO_2 mass flow rate and water volume flow rate, used in the design point of the sCO2-HeRo demonstrator unit at the glass model. The DP investigations are limited by a maximum achievable sCO_2 mass flow rate of 68 g/s and a sCO_2 pressure of 110 bar. The ODP measurement campaigns are performed with a sCO_2 mass flow rate of 37 g/s and gradually

increasing water volume flow rates. The electrical heating power of the evaporator is limited to 1230 W due to internal temperature restrictions. In the ODP II measurements, investigations with a water volume flow rate of 1.74 l/h and a maximum electrical heating power of the evaporator of 1230 W are performed. The sCO_2 mass flow rate is gradually decreased from 37 g/s to about 6 g/s by adjusting a needle valve and bypassing a part of the sCO_2. The minimum adjustable sCO_2 mass flow rate is limited by the valves opening degree of the needle valve, by temperature restriction of the Pt-100 and by increasing sCO_2 mass flow rate fluctuations for decreasing sCO_2 mass flows.

The data analysis starts with experimental pressure drop results of unheated sCO_2 flows. The results show, for instance, that an increasing sCO_2 mass flow rate leads to an increasing sCO_2 pressure drop and that a constant sCO_2 mass flow rate and an increasing sCO_2 inlet pressure leads to decreasing sCO_2 pressure drop, which is in accordance with analytic methods. The results also confirm that the sCO_2 pressure drop is lower for straight sCO_2 channels, compared to Z-shaped channels. In straight channels no sharped-edge deflections exist, which causes this additional pressure drop. For future channel designs, it is recommended to use smooth bends instead of sharp-edged deflections. Besides that, also the plenum geometry has an influence on the pressure drop. In more cubic plenum geometries, a more homogenous mass flow distribution with less turbulences can be developed, leading to decreasing pressure drops.

For heated sCO_2 flows, pressure drop results are shown for instance as a function of the heating load. The heating load is chosen because it represents the ratio of sCO_2 heat input to sCO_2 mass flux and both parameters influence the pressure drop. The results show a strong influence of the sCO_2 mass flux on the sCO_2 pressure drop and a slight influence of the heat input on the pressure drop. The kind of sCO_2 heat input (LP steam cycle or HP steam cycle) and the influence on the pressure drop is further investigated. The results show that the pressure drop is unaffected by the kind of heat input. Only the amount of heat input and the sCO_2 inlet conditions into the heat exchanger, like inlet pressure, inlet temperature and mass flow rate, have an impact. This can be advantageous for future investigations, because expensive and complex test facilities like the high-pressure steam cycle can be replaced by less complex test facilities. Subsequently, the sCO_2 pressure drop is shown as a function of the averaged Nusselt number. It could be seen that decreasing sCO_2 inlet pressures led to increasing Nusselt numbers and increasing pressure drops. On the one hand, increasing Nusselt numbers are beneficial for the heat transfer, but on

the other hand, increasing pressure drops are disadvantageous. This must be considered in the design of the heat exchangers.

The data analysis of heat transfer investigations show, for instance, that the heat is reliably transferred from the steam side to the sCO_2 side for all measurement campaigns and all heat exchangers. As described, it is recommended for future investigations to install an evaporator with higher heating power to provide higher steam volume flow rates at the inlet of the test section. The difference between the calculated steam condensing power and the calculated sCO_2 heat input is described by means of an averaged offset, which can be explained by thermal losses. Thereby it could be seen that the thermal losses are higher for the high-pressure steam cycle experiments, compared to the low-pressure experiments because of higher steam temperatures during operation. The obtained heat transfer results of the 5/1 configuration show that a sCO_2 mass flow rate of about 2 g/s is sufficient to transfer a heat power of about 1250 W from the steam side to the sCO_2 side, which is impressive. Besides that, results of the calculated sCO_2 temperature increase are shown and they are corresponding to analytic methods. The surface temperature results show that there is a symmetrical temperature profile with lower surface temperatures in the center line of the heat exchanger and higher surface temperatures at the outer area.

The design of the CHX for the sCO2-HeRo demonstrator is determined in consideration of measurement results and boundary conditions. The rectangular 2x1 mm channel dimension is chosen with respect to received experimental results. Summarizing the design of the CHX, the choice of an entire number of 14 plate pairs is a consideration of the compactness and the acceptable pressure drop. The number of channels per plate is determined at 15, the effective channel length at 150 mm and the entire number of channels on each side at 210. The integrated plenum geometry at the plates is one innovative aspect of the CHX, because no further welding processes of the plenums is required. The plates are manufactured, diffusion bonded, and after successfully passing a pressures and leakage test, the CHX is installed at the GM. For future designs of HX's, it might be possible to reduce the wall thicknesses, leading to reduced material effort and less space. A conservative and robust design is chosen for the CHX of the sCO2-HeRo demonstrator unit, including for instance a safety factor, a reduction factor of the diffusion bonding process and a conservative allowed material stress of 1.4301.

The development of performance maps and the validation of correlations for heat transfer and pressure drop of the ATHLET code are done before new sCO2-HeRo cycle calculations are carried out for the NPP application. The PM's for the turbine and compressor are derived from CFD calculation results. With polynomial and linear surface interpolation techniques in MATLAB, the PM's for the determination of the efficiencies and pressure ratios are developed for all measurement points with a deviation of less than 1 % compared to the received data points. The results are scaled up in ATHLET to nuclear power plant size according to the affinity laws. For the UHS, a simple heat transfer model is developed in which the sCO_2 outlet temperature is adjusted via heating or cooling. The transferred heat power is controlled in ATHLET by using a PI-controller and in the sCO2-HeRo system by adjusting the rotational speed of the fans. The chosen design of the UHS for the NPP is equal to those of Venker [10]. In consideration of the experimental results of the CHX, a pressure drop model is developed, in which the experimental results can be recalculated for all measurement campaigns with an accuracy of more than 90 % (except three values). Besides that, a heat transfer model is developed as well. The used correlations are already implemented in the ATHLET 3.1 code, and by using them, the model can recalculate the experimental results with a deviation of less than 10 %. Afterwards, the CHX for a NPP is designed with the help of ATHLET. In the simulations it is assumed that the steam is completely condensed at the outlet of the CHX and there is a minimum temperature difference between H_2O and sCO_2 of 5 °C. This leads to a CHX with 14460 rectangular channels with a channel dimension of 2x1 mm and a channel length of 1.1 m. After specifying the components, thermodynamic cycle calculations of the sCO2-HeRo system attached to a LWR are performed. The results show that the steam temperature decreases over the time, which leads to decreasing sCO_2 temperatures in the CHX and thus to lower inlet temperatures at the turbine. Lower turbine inlet temperatures cause lower turbine power and less net power at the generator. The results of the turbine power and compressor power as a function of the simulation time show that excess electricity is provided for more than 12 h. Considering the power consumption of the electrical driven fans with about 186 kW, the operational time of the sCO2-HeRo system is limited to about 7 h. The simulations confirm that the sCO2-HeRo approach is feasible; however, more performance data, especially from the sCO2-HeRo demonstrator unit at the PWR glass model, are needed to improve the current performance maps and to validate correlations for a wider parameter range.

8 Summary

To improve the safety of nuclear power plants, a self-launching, self-propelling and self-sustaining decay heat removal system for retrofitting into NPPs is investigated in the European sCO2-HeRo project. To prevent core damage in case of a station-blackout and loss-of-ultimate-heat-sink accident scenario, the system should be able to transfer the decay heat reliably from the reactor core to an ultimate heat sink, e.g. the ambient air. The system consists of a compressor, a compact heat exchanger, a turbine, a sink heat exchanger and a generator. Within the project a two-scale approach is applied. To demonstrate the feasibility, a small-scale demonstrator unit is first designed, manufactured and retrofitted into the PWR glass model. Single-effect experiments are performed to determine the design of each component of the demonstrator unit. Then the obtained results of the single-effect experiments are used to develop heat transfer and pressure drop models, to develop performance maps and to validate correlations. Afterwards, they are implemented into the German thermal-hydraulic code ATHLET, transferred to component models on nuclear power plant size and new cycle calculations are performed.

This work starts with a description of the pressurized water reactor glass model in which the sCO2-HeRo demonstrator unit is installed. The demonstrator unit is used on the one hand to receive experimental data for code validation and on the other hand to showing the feasibility of such a system. Next, the setup of the sCO2-HeRo demonstrator unit is described. To support the construction of the demonstrator at the glass model, a piping and instrumentation diagram is developed. It includes the components, the measurement devices and a unique nomenclature. For reasons of clarity, it is divided into 8 sections. The setup of the sCO2-HeRo system, attached to the steam generator of a nuclear power plant, is described by means of a schematic drawing. Further, sCO2-HeRo cycle calculations are carried out for both systems and the design point parameters are determined with respect to maximum generator excess electricity, boundary conditions and assumptions. For the demonstrator unit, one sCO2-HeRo system is defined. It transfers in the design point a simulated decay heat power of 6 kW from the reactor core to the ultimate heat sink. Four sCO2-HeRo systems in parallel are chosen for the nuclear power plant application. Each system can transfer a decay heat power of 15 MW from the nuclear core to the ambient air.

In the second part of this work, the test facility and the heat exchanger test plates are described. The experimental investigations take place in the sCO_2 SCARLETT loop providing sCO_2 under defined conditions, and in a steam cycle. The low-pressure steam cycle is designed and build to provide steam with a pressure of 0.3 bar and a saturated steam temperature of about 70 °C, which is similar to the steam conditions of the PWR glass model. The high-pressure steam cycle is constructed to generate steam similar to the steam conditions of a nuclear power plant (70 bar / 286 °C). For the experimental investigations, seven heat exchanger configurations are designed and manufactured. These could be classified according to the channel dimension (3x1 mm / 2x1 mm), the number of channels per plate and number of plates (15/1 / 5/1 / 5/2 / 5/3) as well as the channel shape (II / IZ). The mechanical design of the heat exchangers is determined by transforming rectangular channel geometries into circular pipe geometries. These pipe geometries are used in the following to determine the minimum wall thickness by means of ordinary calculation methods. After manufacturing the plates, they are diffusion bonded. Stainless steel 1.4301 is chosen as plate material.

The third part of this work includes the determination of the measurement parameters and the experimental investigations. In the “Design point” (DP) experiments the sCO_2 mass flow rates and water volume flow rates are scaled down in the same ratio as the entire amount of sCO_2 mass flow rate and water volume flow rate, used in the design point of the sCO2-HeRo demonstrator unit at the glass model. To investigate the heat transfer e.g. also “Out of design point” (ODP) a constant sCO_2 mass flow rate and gradually increasing water volume flow rates are applied. In the “Out of design point II” (ODP II) measurements, a constant water volume flow rate and a gradually decreasing sCO_2 mass flow rate are chosen. The pressure drop results of unheated sCO_2 flows show for instance a parabolic increase of the pressure drop for increasing sCO_2 mass flow rates and decreasing pressure drops for increasing sCO_2 inlet pressures. Furthermore, an increasing flow area leads to decreasing sCO_2 pressure drops, for constant sCO_2 mass flow rates and sCO_2 inlet pressures. A comparison of calculated pressure drop results and experimental results shows that the experimental ones are always 2 to 3 times higher. This could be attributable primarily to the inappropriate plenum geometry and the unsuitable sCO_2 inflow conditions into the plenum. The results show further that a straight channel shape reduces the sCO_2 pressure drop significantly, compared to the results of the Z-shaped channels. The plenum geometry also influences the pressure drop with decreasing sCO_2 pressure drops for more cubic plenum geometries and vice versa. For heated sCO_2 flows,

the pressure drop results confirm a strong influence of the sCO_2 mass flow rate on the pressure drop and an influence of the heat input on the pressure drop, which can be explained by changes of the flow velocity and the fluid density. The kind of heat input from the steam (LP / HP) and the influence of the sCO_2 pressure drop is also investigated. The results show, for instance, that the pressure drop is not influenced by the kind of steam heat input. Only the amount of heat input and the sCO_2 inlet conditions into the heat exchanger influence the sCO_2 pressure drop. The results of the heat transfer investigations also show linear profiles of the calculated sCO_2 heat input as a function of the calculated condensing power of the steam, only with varying offsets for the high-pressure and low-pressure steam cycle. This could be explained by higher thermal losses at the high-pressure steam cycle due to higher operation temperatures compared with the low-pressure steam cycle. The heat transfer results show further that a heat exchanger with 5 channels at each side and an effective straight channel length of 150 mm is sufficient to transfer a heat power of about 1250 W from the steam side to the sCO_2 side. Finally, the temperatures on the surface of the heat exchanger are measured. The results show symmetrical temperature profiles with lower surface temperatures in the center line of the HX and higher surface temperatures at the outer area. Furthermore, a higher sCO_2 heat input leads to increasing surface temperatures, especially at the top of the heat exchanger.

The compact heat exchanger for the sCO2-HeRo demonstrator unit is designed in consideration of boundary conditions and received experimental data. After constructing and manufacturing the plates the CHX is diffusion bonded before a pressure and leakage test is carried out. Finally, it is installed at the PWR glass model at GfS, Essen.

The thermal-hydraulic simulation of the sCO2-HeRo system for a nuclear power plant by using the ATHLET 3.1 code with advanced models is the last part of that work. For this, correlations are validated with experimental data and performance maps as well as models for heat transfer and pressure drop are developed. For instance, performance maps for the compressor and turbine are developed by means of CFD data and experimental results. Afterwards, these performance maps are transferred according to the affinity laws to component models on power plant size and implemented into the ATHLET code. For the simulation of the transferred heat power in the ultimate heat sink, a heat transfer model is developed in consideration of experimental data. To simulate the CHX in ATHLET, a pressure drop and heat transfer model

is developed. Both are validated with experimental results and the necessary friction loss coefficients for calculating the pressure drop are implemented into the ATHLET code. The design of the CHX for the nuclear power plant application is determined with ATHLET before advanced sCO_2-HeRo cycle simulations are carried out. The simulation results show that the break-even point of the system is reached after about 6.9 h due to decreasing steam temperatures, leading to decreased turbine excess power. This value is mainly determined by the low efficiency of the turbine and compressor, which are obtained after up-scaling the components of the sCO2-HeRo demonstrator unit. The rotor design of the demonstrator unit could not be optimized for the small size of a few centimeter. For instance, the height of the turbine blade is about 1 mm, leaving no space for improvement. It is expected that larger turbomachines (MW size) will be operated with higher efficiency, thus prolonging the grace time to the expected 72 hrs.

9 Bibliographie

[1] International Energy Agency (IEA): Statistics Data Browser - Energy Consumption. 2019. (https://www.iea.org/statistics)

[2] Bundesministerium für Wirtschaft und Energie (BMWi): Energiedaten: Gesamtausgabe. Stand: August 2018.

[3] Deutsches Atomforum e. V. (DAtF): Kernkraftwerke in Europa. Berlin, 2017.

[4] Deutsches Atomforum e. V. (DAtF): Kernenergie Basiswissen. Berlin, 2013.

[5] Foratom: Nuclear Energy Is Essential To EU Low Carbon Future. Brussels, 2019.

[6] Deutsches Atomforum e. V. (DAtF): Sicherheit ist das oberste Gebot. Berlin, 2013.

[7] YILMAZ, Ö.; POHLNER, G.; BUCK, M.; STARFLINGER, J.: Design Consideration For A Core-Catcher Concept Based On Bottom Flooding Through Porous Concrete. Proceedings of the 11th International Topical Meeting on Nuclear Reactor Thermal Hydraulics, Operation and Safety (NUTHOS-11). Gyeongju, Korea, 2016.

[8] FISCHER, M.: The Severe Accident Mitigation Concept And The Design Measures For Core Melt Retention Of The European Pressurized Reactor (EPR). Nuclear Engineering and Design 230, p. 169 - 180, 2004.

[9] GRASS, G.; KULENOVIC, R.; STARFLINGER, J.: Experimental Investigtion On Long Closed Two Phase Thermosyphons To Be Applied In Spent Fuel Pools For Passive Heat Removal. Proceedings of the 26th International Conference - Nuclear Energy for New Europe (NENE2017). Bled, Slovenia, 2017.

[10] VENKER, J.: Development And Validation Of Models For Simulation Of Supercritical Carbon Dioxide Brayton Cycle And Application To Self-Propelling Heat Removal Systems In Boiling Water Reactors. University of Stuttgart, IKE2-156, ISSN-0173-6892. Stuttgart, Germany, 2015.

[11] VENKER, J.: A Passive Heat Removal System Retrofit For BWRs. Nuclear Engineering International 711, p. 14 - 17, 2013.

[12] VENKER, J.; STARFLINGER, J.; SCHAFFRATH, A.: Code Development And Simulation Of The Supercritical CO2 Heat Removal System. Proceedings of the European Nuclear Conference. Warsaw, Poland, 2016.

[13] VENKER, J.; VON LAVANTE, D.; BUCK, M.; GITZEL, D.; STARFLINGER, J.: Interaction Between Retrofittable And Existing Emergency Cooling Systems In BWRs. Proceedings of the 10th International Topical Meeting on Nuclear Thermal-Hydraulics, Operation and Safety (NUTHOS-10). Okinawa, Japan, 2014.

[14] VENKER, J.; VON LAVANTE, D.; BUCK, M.; GITZEL, D.; STARFLINGER, J.: Transient Analysis Of An Autarkic Heat Removal System. Proceedings of the 2014 International Congress on Advances in Nuclear Power Plants (ICAPP 2014). Charlotte, USA, 2014.

[15] VENKER, J.; VON LAVANTE, D.; BUCK, M.; GITZEL, D.; STARFLINGER, J.: Concept Of A Passive Cooling System To Retrofit Existing Boiling Water Reactors. Proceedings of the 2013 International Congress on Advances in Nuclear Power Plants (ICAPP 2013). Jeju, South Korea, 2013.

[16] STRAETZ, M.; STARFLINGER, J.; MERTZ, R.; SEEWALD, M.; SCHUSTER, S.; BRILLERT, D.: Cycle Calculations Of A Small Scale Heat Removal System With Supercritical CO2 As Working Fluid. Proceedings of the 14th International Conference on Nuclear Engineering (ICONE25). Shanghai, China, 2017.

[17] Tokyo Electric Power Company: Fukushima Nuclear Accident Analysis Report. 2012.

[18] AHN, Y.; BAE, S. J.; KIM, M.; CHO, S. K.; BAIK, S.; LEE, J. I.; CHA, J. E.: Review Of Supercritical CO2 Power Cycle Technology And Current Status Of Research And Development. Nuclear Engineering and Technology 47, p. 647 - 661, 2015.

[19] VOJACEK, A.; HACKS, A.; MELICHAR, T.; FRYBORT, O.; HAJEK, P.: Challenges In Supercritical CO2 Power Cycle Technology And First Operational Experience At CVR. Proceedings of the 2nd European supercritical CO2 Conference. Essen, Germany, 2018.

[20] GAMPE, U.; HENOCH, J.; RATH, S.; GERBETH, G.; HAMPEL, U.; HANNEMANN, F.; GLOS, S.: Concept And Preliminary Design Of A 600 °C+ sCO2 Test Facility. Proceedings of the 2nd European supercritical CO2 Conference. Essen, Germany, 2018.

[21] FLAIG, W.; MERTZ, R.; STARFLINGER, J.: Setup Of The Supercritical CO2 Test-Facility „SCARLETT“ For Basic Experimental Investigations Of A Compact Heat Exchanger For An Innovative Decay Heat Removal System. Proceedings of the 14th International Conference on Nuclear Engineering (ICONE25). Shanghai, China, 2017.

[22] KIMBALL, K. J.: Supercritical Carbon Dioxide Power Cycle Development Overview. Proceedings of the 4th International Symposium - Supercritical CO2 Power Cycles Technologies for Transformational Energy Conversion. Pittsburgh, USA, 2014.

[23] VOJACEK, A.: Workshop „The Supercritical CO2 Heat Removal System” - sCO2 Experimental Loop and CVR R&D Activities. Rez, Prague, 2017.

[24] WRIGHT, S. A.; RADEL, R. F.; VEMON, M. E.; ROCHAU, G. E.; PICKARD, P. S.: Operation And Analysis Of a Supercritical CO2 Brayton Cycle. Sandia Report - SAND2010-0171. Albuquerque, New Mexico, 2010.

[25] AHN, Y.; LEE, J.; KIM, S. G.; LEE, J. I.; CHA, J. E.; LEE, S.: Design Consideration Of Supercritical CO2 Power Cycle Integral Experimental Loop. Energy 86, p. 115 - 127, 2015.

[26] CARLSON, M. D.; KRUIZENGA, A. K.; SCHALANSKY, C.; FLEMING, D. F.: Sandia Progress On Advanced Heat Exchangers For sCO2 Brayton Cycles. Proceedings of the 4th International Symposium - Supercritical CO2 Power Cycles Technologies for Transformational Energy Conversion. Pittsburgh, USA, 2014.

[27] NIKITIN, K.; KATO, Y.; NGO, L.: Printed Circuit Heat Exchanger Thermal Hydraulic Performance In Supercritical CO2 Experimental Loop. International Journal of Refrigeration 29, p. 807 - 814, 2006.

[28] NGO, T. L.; KATO, Y.; NIKITIN, K.; TSUZUKI, N.: New Printed Circuit Heat Exchanger With S-shaped Fins For Hot Water Supplier. Experimental Thermal and Fluid Science 30, p. 811 - 819, 2006.

[29] MA, T.; XU, X. Y.; CHEN, Y. T.; WANG, Q. W.: Study On Local Thermal-hydraulic Performance and Optimization Of Zigzag-Type Printed Circuit Heat Exchanger At High Temperature. Energy Conversion Management 105, p. 55 - 56, 2015.

[30] MA, T.; XIN, F.; XU, X. Y.; CHEN, Y. T.; WANG, Q. W.: Effect Of Fin-Endwall Fillet On Thermal Hydraulic Performance Of Airfoil Printed Circuit Heat Exchanger. Applied Thermal Engineering 89, p. 1087 - 1095, 2015.

[31] LEE, S. M.; KIM, K. Y.: Multi-Objective Optimization Of Arc-Shaped Ribs In The Channels Of A Printed Circuit Heat Exchanger. International Journal of Thermal Science 94, p. 1 - 8, 2015.

[32] LEE, S. M.; KIM, K. Y.; KIM, S. W.: Multi-Objective Optimization Of a Double-Faced Type Printed Circuit Heat Exchanger. Applied Thermal Engineering 60, p. 44 - 50, 2013.

[33] SONG, H.; METER, J. V.; LOMPERSKI, S.; CHO, D.; KIM, H. Y.; TOKUHIRO, A.: Experimental Investigations Of A Printed Circuit Heat Exchanger For Supercritical CO2 And Water Heat Exchange. Proceedings of the 5th Korea-Japan Symposium on Nuclear Thermal Hydraulics and Safety (NTHAS5). Jeju Island, South Korea, 2006.

[34] TSUZUKI, N.; KATO, Y.; ISHIDUKA, T.: High Performance Printed Circuit Heat Exchanger. Applied Thermal Engineering 27, p. 1702 - 1707, 2007.

[35] CHU, W.; LI, X.; MA, T.; CHEN, Y.; WANG, Q.: Experimental Investigation On SCO2-Water Heat Transfer Characteristics In A Printed Circuit Heat Exchanger With Straight Channels. International Journal of Heat and Mass Transfer 113, p. 184 - 194, 2017.

[36] SEEWALD, M.; STRAETZ, M.; FREUTEL, T.: Deliverable D1.1 „Release thermodynamic cycle parameters“. sCO2 HeRo Project (2015 - 2018). Germany, 2015.

[37] HACKS, A.; SCHUSTER, S.; DOHM, H. J.; BENRA, F.; BRILLERT, D.: Turbomachine Design for Supercritical Carbon Dioxide Within the sCO2-HeRo.eu Project. Proceedings of the ASME Turbo Expo. Oslo, Norway, 2018.

[38] DOSTAL, V.; DRISCOLL, M. J.; HEJZLAR, P.: A Supercritical Carbone Dioxice Cycle for the Next Generation. Nuclear Reactors, Tech. Rep. MIT-ANP-TR-100, Massachusetts Institute of Technology, USA, 2004.

[39] WRIGHT, A.; CONBOY, T. M.; ROCHAU, G. E.: Overview of Supercritical CO2 Power Cycle Development at Sandia National Laboratories. Proc. University Turbine Systems Research Workshop Columbus. Ohio, USA, 2011.

[40] HACKS, A.; FREUTEL, T.; STRAETZ, M.; VOJACEK, A.; HECKER, F.; STARFLINGER, J.; BRILLERT, D.: Operational Experiences and Design of the sCO2-HeRo loop. Proceedings of the 3rd European supercritical CO2 Conference. Paris, France, 2019.

[41] ELMESS Thermosystemtechnik GmbH & Co. KG, Nordallee 1, 29525 Uelzen, Germany. www.elmess.de.

[42] Schick - Gase + Technik + Kälte: Datenblatt: R744 / CO2: Kohlendioxid - ein unbegrenzt verfügbarer und natürlicher Stoff. Vaihingen/Enz, Germany, 2018.

[43] LEMMON, E. W.; HUBER, M. C.; MCLINDEN M. O.: Refprop - Reference Fluid Thermodynamic and Transport Properties, Standard Reference Database 23, Version 9.0. National Institute of Standards and Technology (NIST). Boulder, CO, USA, 2010.

[44] SHAH, R. K.; SEKULIC, D. P.: Fundamentals Of Heat Exchanger Design. Wiley: 2003.

[45] BAEHR, H. D.; STEPHAN, K.: Wärme- und Stoffübertragung (8. Auflage). Springer-Verlag: Berlin, Heidelberg, 2013.

[46] HEIDEMANN, W.: Unterlagen zur Vorlesung - Berechnung von Wärmeübertragern. Stuttgart, Germany, 2016.

[47] Ätztechnik Herz GmbH & Co. KG: Broschüre: Ätzen - schnell - sauber - gratfrei. Epfendorf am Neckar, Germany, 2019. (https://www.aetztechnik-herz.de/wp-content/uploads/2016/07/Layout-Prosp-18-S-herz-Image-D_47_Download.pdf)

[48] HESSELGREAVES, J. E.: Compact heat exchangers. Pergamon: Amsterdam, New York, 2001.

[49] RUSNALDY: Diffusion Bonding: An Advanced Of Material Process. Journal of ROTASI - Volume 3, Nomor 1, Januari 2001.

[50] SARANAM, V. R.; PAUL, B. K.: Feasibility Of Using Diffusion Bonding For Producing Hybrid Printed Circuit Heat Exchangers For Nuclear Energy Applications. Procedia Manufacturing 26, p. 560 - 569, 2018.

[51] KE-Technologie GmbH: Gespräch 2017. Stuttgart, Germany, 2017.

[52] Deutsche Edelstahlwerke: Datenblatt: 1.4301 - X5CrNi18-10. Witten, Deutschland, 2007.

[53] Aalco Metals Ltd: Stainless Steel: 1.4301 Sheet and Plate. Wednesbury, UK, 2018.

[54] PIERRES, R. L.; SOUTHALL, D.; OSBORNE, S.: Impact Of Mechanical Design Issues On Printed Circuit Heat Exchangers. In Proceedings of sCO2 Power Cycle Symposium 2011. Boulder, USA, 2011.

[55] JENTZ, I.; ANDERSON, M.; SUN, X.: Modelling Of The Mechanical Integrity Of Arifoil PCHE. In Proceedings of the 16th International Topical Meeting on Nuclear Reactor Thermal Hydraulics (NURETH-16). Chicago, USA, 2015.

[56] DUBBEL, H.; GROTE, K.: Taschenbuch für den Maschinenbau, 2005.

[57] ALTENBACH, H.; DREYER. H. J.: Holzmann/Meyer/Schumpich - Technische Mechanik - Festigkeitslehre (12. Auflage). Springer-Verlag: Wiesbaden, 2016.

[58] Verein Deutscher Ingenieure (VDI): VDI-Wärmeatlas. VDI-Verlag: Düsseldorf, Germany, 2013.

[59] BOHL, W.; ELMENDORF, W.: Technische Strömungslehre (15. Auflage). Vogel-Buchverlag: Würzburg, 2014.

[60] FLAIG, W.: Thermohydraulische Untersuchung Eines Diffusionsgeschweißten Kompaktwärmeübertragers Zur Ertüchtigung Eines Wärmeabfuhrsystems Mit Kohlenstoffdioxid Als Arbeitsmittel. Stuttgart, Germany, 2019.

[61] GOVINDAN, S.; SCHUSTER, S.: Deliverable D 3.2 „Calculated Performance Map of the Turbo-Machine Set for ATHLET“. sCO2 HeRo Project (2015 - 2018). Germany, 2017.

[62] VOJACEK, A.: Milestone M2.6 „Delivery of sink HX performance maps“. sCO2 HeRo Project (2015 - 2018). Germany, 2017.

[63] AUSTREGESILO, H.; BALS, C.; HORA, A.; LERCHL, G.; ROMSTEDT, P.; SCHÖFFEL, P.; CRON, D. VON DER; WEYERMANN, F.: ATHLET Mod 3.0 Cycle A - Models and Methods. Gesellschaft für Anlagen- und Reaktorsicherheit (GRS): 2012.

[64] BOHL, W.; ELMENDORF, W.: Strömungsmaschinen 1 - Aufbau und Wirkungsweise (11. Auflage). Vogel-Buchverlag: Würzburg, 2014.

[65] KSG Kraftwerks-Simulator-Gesellschaft mbH, GfS Gesellschaft für Simulatorschulung mbH: Schulung am Reaktor-Glasmodell. Essen, Germany, 2019. (https://simulatorzentrum.de/wp-content/uploads/2018/07/Schulung-am-Reaktor-Glasmodell-05-2019.pdf)

[66] ANGELINO, G.: Perspectives for the Liquid Phase Compression Gas Turbine, Trans. ASME, J. Eng. Power, pp. 229–236, 1967.

[67] ANGELINO, G.: Carbon Dioxide Condensation Cycles for Power Production, Trans. ASME, J. Eng. Power, pp. 287–295, 1968.

[68] ANGELINO, G.: Real Gas Effects in Carbon Dioxide Cycles, ASME Paper 69-GT-102, 1969.

[69] FEHER, E. G.: The Supercritical Thermodynamic Power Cycle, Energy Conversion, vol. 8, pp. 85–90, 1968.

[70] HACKS, A.; VOJACEK, A.; DOHMEN, H. J.; BRILLERT, D.: Experimental investigation of the sCO2-HeRo Compressor. Proceedings of the 2nd European supercritical CO2 Conference 2018. Essen, Germany, August 2018.

[71] GLOS, S.; WECHSUNG, M.; WAGNER, R.; HEIDENHOF, A.; SCHLEHUBER, D.: Evaluation of sCO2 Power Cycles for Direct and Waste Heat Applications. Proceedings of the 2nd European supercritical CO2 Conference. Essen, Germany, 2018.

[72] PERSICHILLI, M.; KACLUDIS, A.; ZDANKIEWICZ, E.; HELD, T.: Supercritical CO2 Power Cycle Developments and Commercialization: Why sCO2 can Displace Steam. Proceedings of the Power-Gen India & Central Asia Conference 2012. Pragati Maidan, New Delhi, India, 19-21 April 2012.

[73] MILLER, J. D.; BUCKMASTER, D. J.; HART, K.; HELD, T. J.; THIMSEN, D.; MAXSON, A.; PHILLIPS, J. N.; HUME, S.: Comparison of Supercritical CO2 Power Cycles to Steam Rankine Cycles in Coal-Fired Applications. Proceedings of the ASME Turbo Expo 2017. Charlotte, North Carolina, USA, 26-30 July 2017.

[74] LEWIS, T. G.; ROCHAU, G. E.: Developments with Sandia's Supercritical Carbon Dioxide Brayton Cycle and Advance Energy Technologies. Sandia National Laboratories Report SAN2012-3293C. USA, 2012.

[75] STRAETZ, M.: Milestone No. 1.2 „Review measurement points“. sCO2 HeRo Project (2015 - 2018). Germany, 2016.

[76] HACKS, A.: Deliverable D1.5 „Start-up system hardware“. sCO2 HeRo Project (2015 - 2018). Germany, 2016.

Appendix A

Fluid properties of sCO_2

CO_2 is a colorless, non-flammable, non-toxic and abundantly available natural fluid. It is chemically inactive, heavier than air and it has a narcotic effect in higher concentrations. It has no ozone depletion potential and a negligible direct effect on global warming if used as a working fluid in closed systems [42].

A phase diagram of CO_2 is shown below. It can be divided in general into 4 parts: the solid, the liquid, the gaseous and the supercritical part. The sublimation curve (marked in red) is the boundary line between the solid and gaseous phase of CO_2. It starts at 0 bar and - 273.15 °C and ends at the triple-point T_{tr} at 5.2 bar and - 56.6 °C. The triple-point is unique because it is the only point where the solid, liquid and gaseous phase can occur at the same time. The melting curve (marked in green) is the boundary line between the solid and liquid phase and starts at the triple-point. The blue marked boundary line between the liquid and gaseous phase is shown by the vapor pressure curve, which starts at the triple-point and ends at the critical point p_c at a pressure of 73.8 bar and a temperature of 31 °C. The supercritical region is located above the critical point. In addition, the solid and gaseous phase can occur simultaneously at the sublimation curve, the solid and liquid phase at the melting curve and the liquid and gaseous phase at the vapor pressure curve.

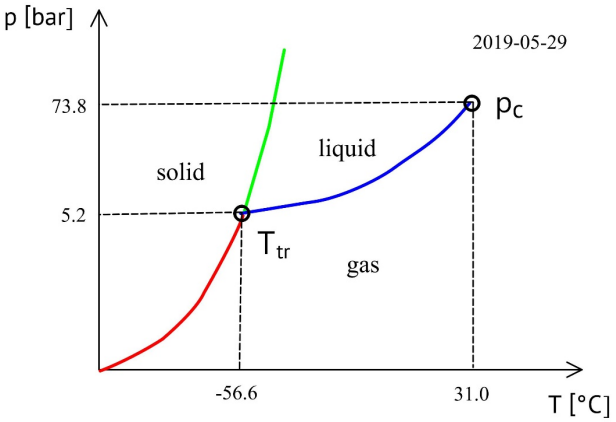

Phase diagram of CO_2

For a more detailed visualization of the CO_2 fluid properties, the isobaric specific heat capacity c_p, the fluid density ρ and the dynamic viscosity μ are shown below as a function of the CO_2 temperature T and the CO_2 pressure p. Additionally, the calculated heat transfer coefficient α is shown as a function of the CO_2 temperature T and the CO_2 pressure p.

The graphs of the isobaric specific heat capacity c_p are shown in the upper picture. They have similar tendencies with steep gradients of c_p near the critical and pseudocritical points. The maximum value of c_p and maximum gradients exist at the critical point (31 °C / 74 bar) and decrease for parameters that are further away from the critical point. For instance, the value of c_p increases at a pressure of 70 bar from 2 kJ/(kg·K) at 0 °C to 14 kJ/(kg·K) at 29 °C before it decreases again to 2 kJ/(kg·K) at 100 °C. Furthermore, the values show a symmetrical profile with a steep increase of c_p at temperatures just before the pseudocritical point (70 bar / 29 °C) and a steep decrease right after the pseudocritical point. Similar trends can be seen for other CO_2 pressures, with a shift of the maximum of c_p towards higher temperatures for increased pressures and vice versa.

The fluid density ρ of CO_2 is shown in the second picture. For example, a pressure of 70 bar leads to a fluid density of about 1000 kg/m³ at 0 °C and decreases to 700 kg/m³ at 28 °C. A slight temperature increase near the pseudocritical point (70 bar / 29 °C) leads to a strong decrease of the fluid density from 700 kg/m³ at 28 °C to 300 kg/m³ at 30 °C, which can be explained as a shift from the liquid to the gaseous phase. A further temperature increase to 100 °C leads to a density of about 120 kg/m³. It can be seen that the gradient of the fluid density change increases for pressures lower than 74 bar and decreases for pressures higher than the critical pressure (74 bar). This can be seen for instance at the 120 bar graph, in which the density starts at about 1000 kg/m³ at 0 °C and decreases nearly linearly to 600 kg/m³ at 50 °C. Near the pseudocritical point (120 bar / 54 °C) the gradient is significantly lower than for 70 bar, namely to 450 kg/m³ at 60 °C and 250 kg/m³ at 100 °C. Similar trends, just with different gradients, can be observed for varying CO_2 pressures.

The graphs of the dynamic viscosity μ are shown in the third picture. It can be seen that a variation of the CO_2 pressure between 60 bar and 120 bar leads to similar tendencies of the dynamic viscosity of about 1.1E-04 Pa·s at 0 °C and 2.0E-05 Pa·s at 100 °C. Just the gradient of the dynamic viscosity change decreases with higher pressures and the location is shifted towards higher temperatures. This can be seen for instance at the 60 bar and 120 bar graphs. A CO_2 pressure of 60 bar and a temperature increase of 1 °C near the pseudocritical point (60 bar / 22 °C) leads to significant dynamic viscosity changes from 6.5E-05 Pa·s at 21.5 °C to 1.9E-05 Pa·s at 22.5 °C. Comparing this with the 120 bar graph, the pseudocritical point is shifted towards a temperature of 54 °C and the gradient of the dynamic viscosity change near that pseudocritical point is lower, which leads to dynamic viscosity changes from 3.9E-05 Pa·s at 53.5 °C to 3.8E-05 Pa·s at 54.5 °C.

The graphs of the calculated heat transfer coefficients α are shown in the bottom. A rectangular flow area of 2x1 mm and a sCO_2 mass flow rate of 3.1 g/s are chosen for the calculation. The Nusselt number Nu is calculated according to the correlation of Gnielinski [58] by using the Reynold number Re and Prandtl number Pr. The depicted graphs show firstly similar tendencies with higher α values near the critical point and secondly that the maximum of α is shifted towards higher temperatures for higher pressures. For instance, a pressure of 60 bar leads to a heat transfer coefficient of 8000 W/(m²·K) at 0 °C, which increases rapidly near the pseudocritical point (60 bar / 22 °C) to 11700 W/(m²·K) at 22 °C before it decreases again to 4300 W/(m²·K) at 100 °C. At a pressure of 80 bar the heat transfer coefficient starts at 8000 W/(m²·K) at 0 °C, increases rapidly near the critical point to about 34000 W/(m²·K) at 35 °C and decreases to 4700 W/(m²·K) at 100 °C.

1) Specific heat capacity c_p

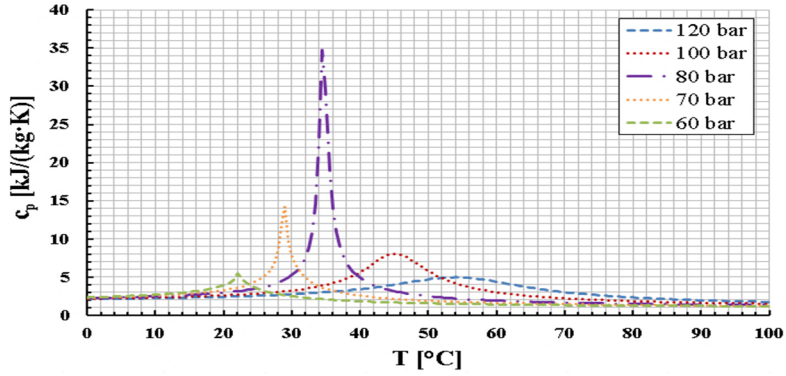

2) Density ρ

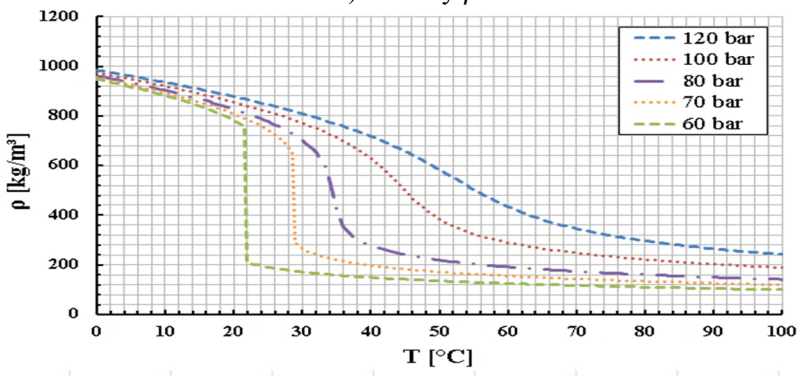

3) Dynamic viscosity μ

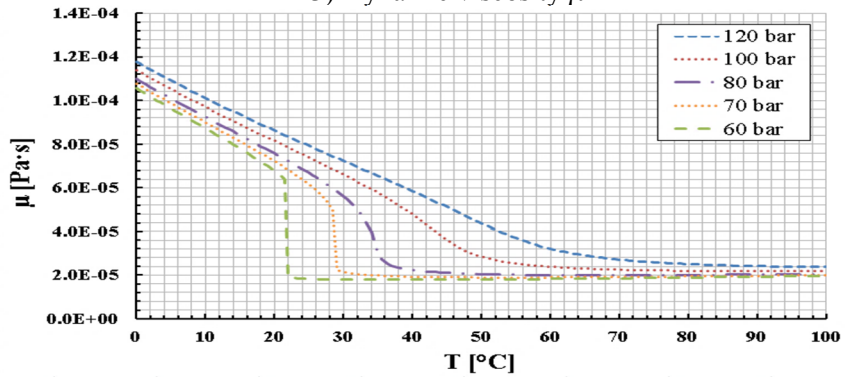

4) Heat transfer coefficient α

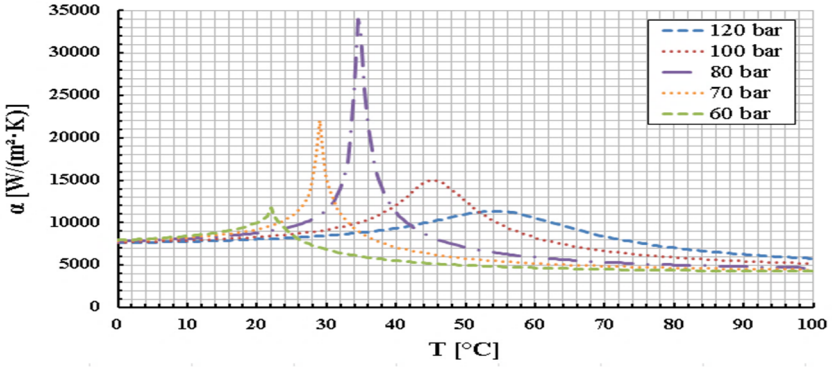

Fluid properties of CO_2 and heat transfer coefficient

Appendix B

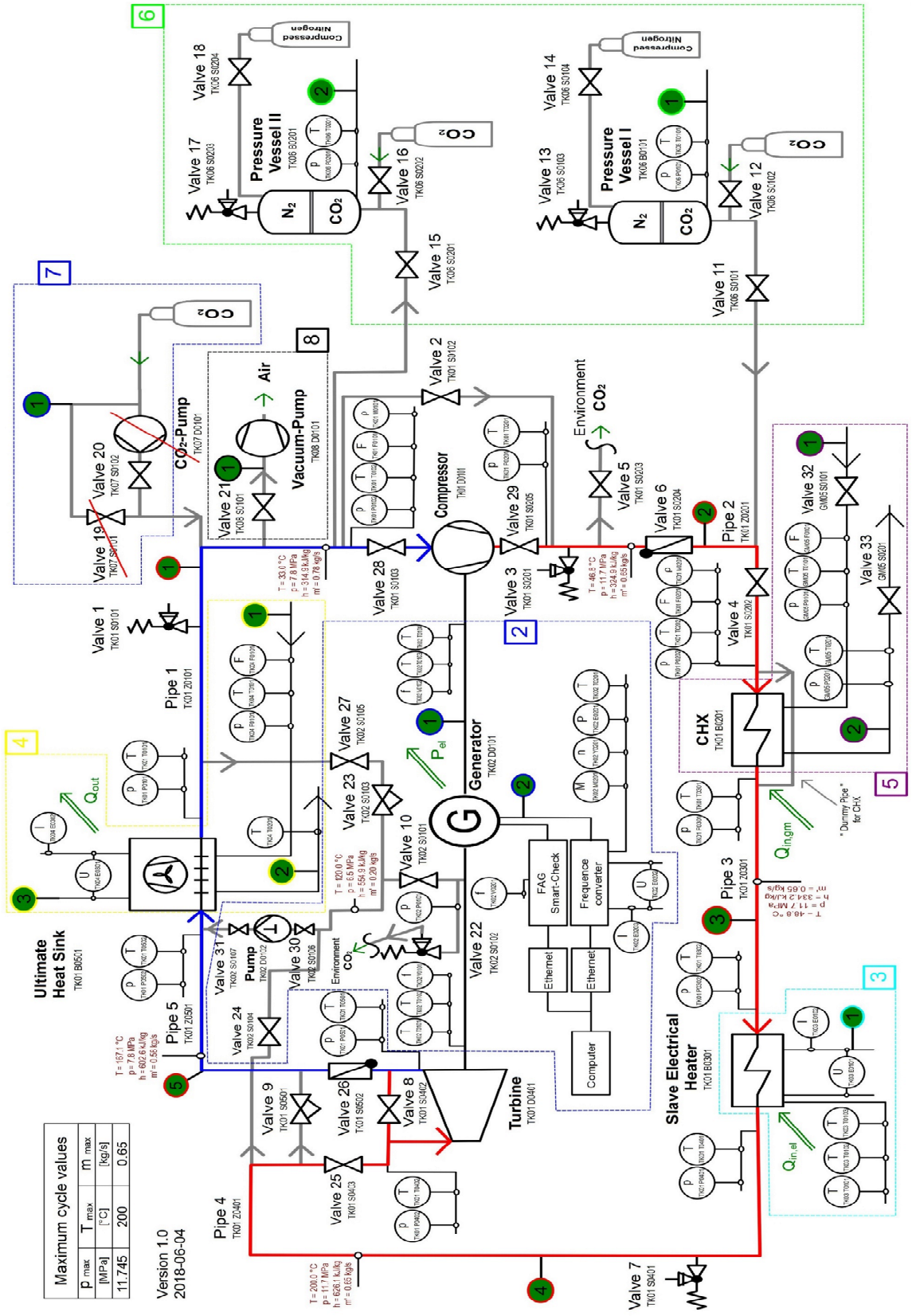
Pressure Vessel II
Pressure Vessel I
Compressed Nitrogen
CO2-Pump
Vacuum-Pump
Air
Environment CO2
Compressor
Generator
Turbine
CHX
Slave Electrical Heater
Ultimate Heat Sink
Pump
FAG Smart-Check
Frequence converter
Ethernet
Computer
Valve 1
Valve 2
Valve 3
Valve 4
Valve 5
Valve 6
Valve 7
Valve 8
Valve 9
Valve 10
Valve 11
Valve 12
Valve 13
Valve 14
Valve 15
Valve 16
Valve 17
Valve 18
Valve 19
Valve 20
Valve 21
Valve 22
Valve 23
Valve 24
Valve 25
Valve 26
Valve 27
Valve 28
Valve 29
Valve 30
Valve 31
Valve 32
Valve 33
Pipe 1
Pipe 2
Pipe 3
Pipe 4
Pipe 5
Maximum cycle values
p max [MPa] 11.745
T max [°C] 200
m max [kg/s] 0.65
Version 1.0
2018-06-04

Appendix C

Heat exchanger configuration AAA

1) Cover plate

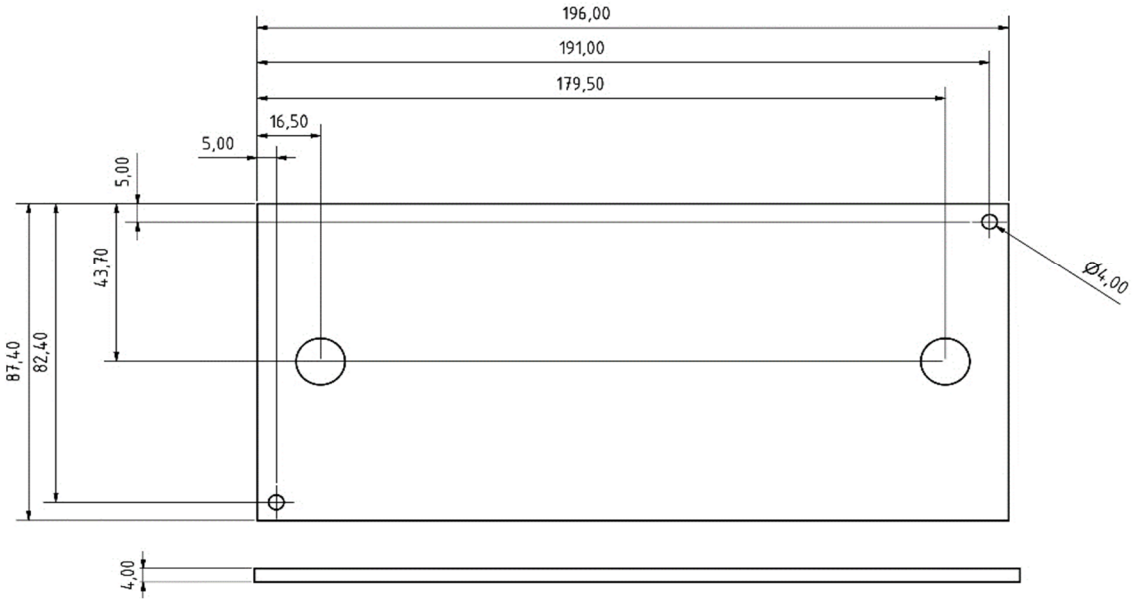

2) H_2O plate

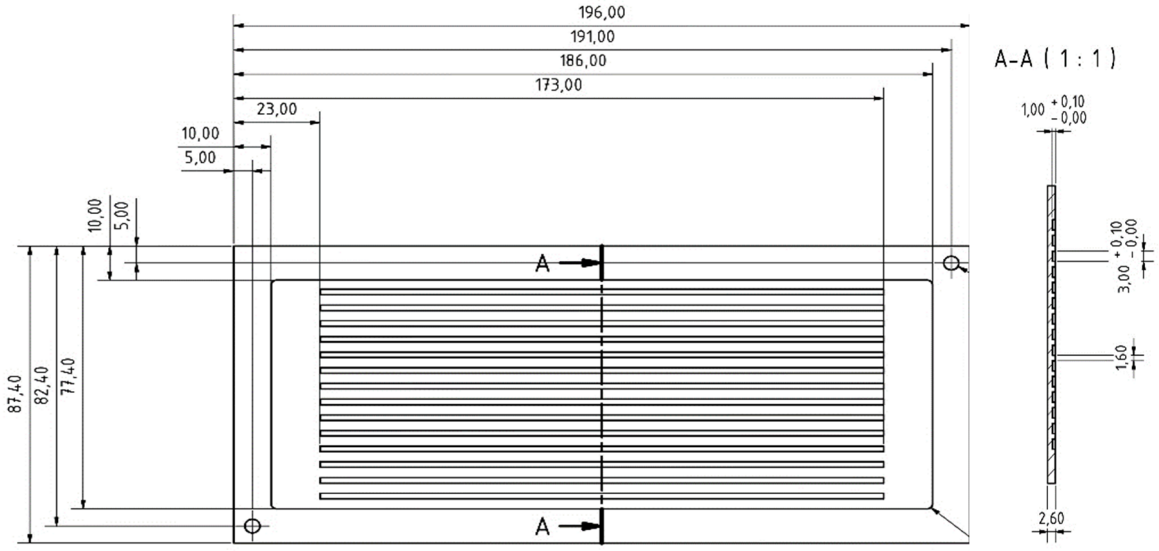

3) sCO_2 plate

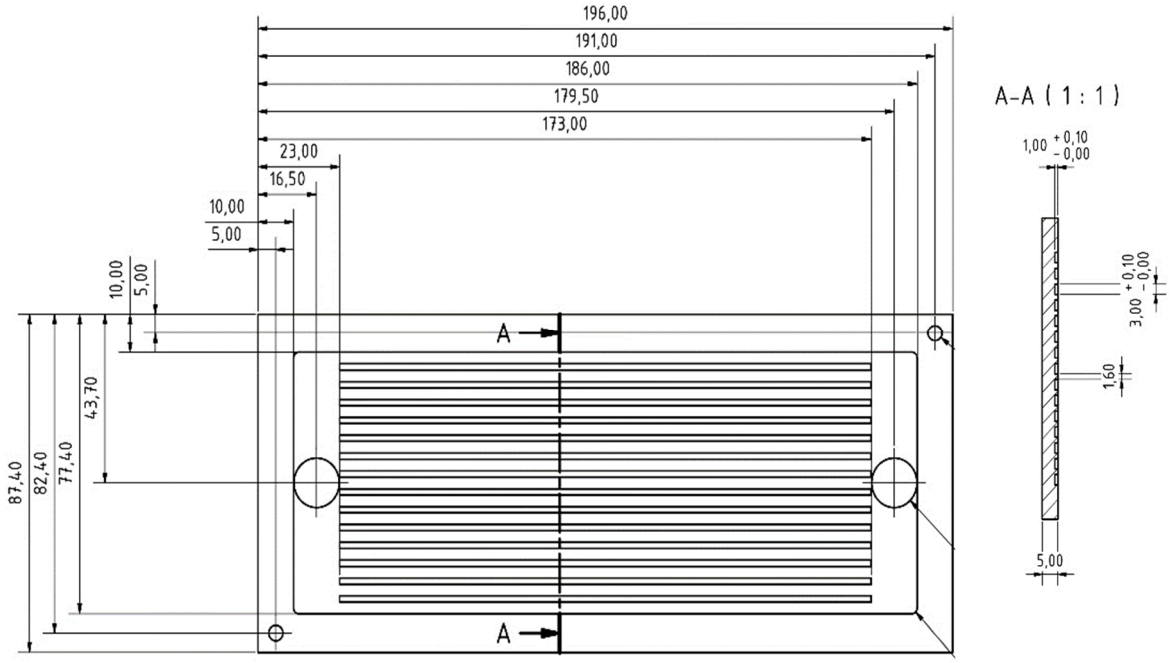
196,00
191,00
186,00
179,50
173,00
23,00
16,50
10,00
5,00
10,00
5,00
43,70
87,40
82,40
77,40
A
A
A-A (1 : 1)
1,00 +0,10 -0,00
3,00 +0,10 -0,00
1,60
5,00

Heat exchanger configuration AAB

1) Cover plate

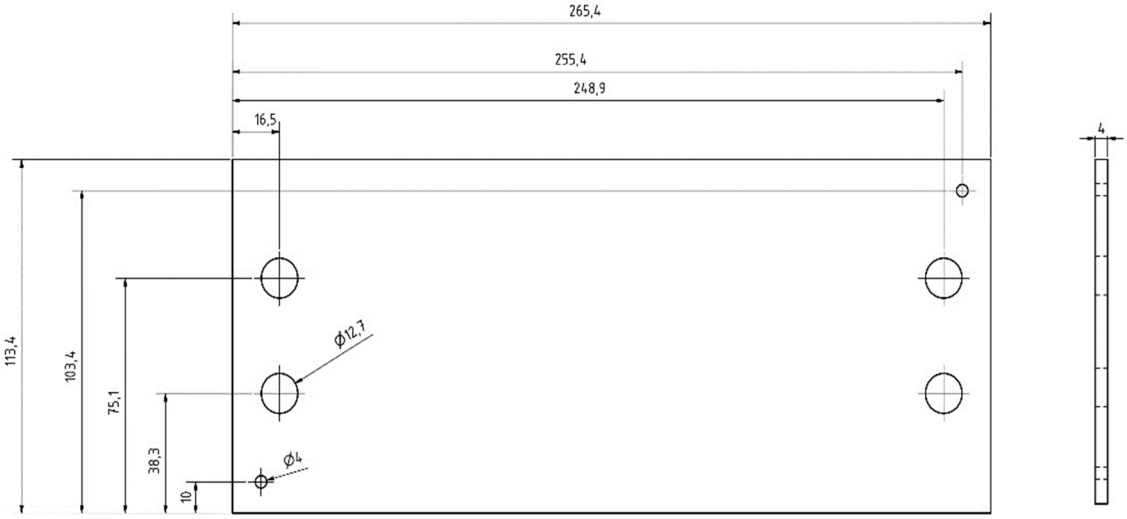

2) H_2O plate

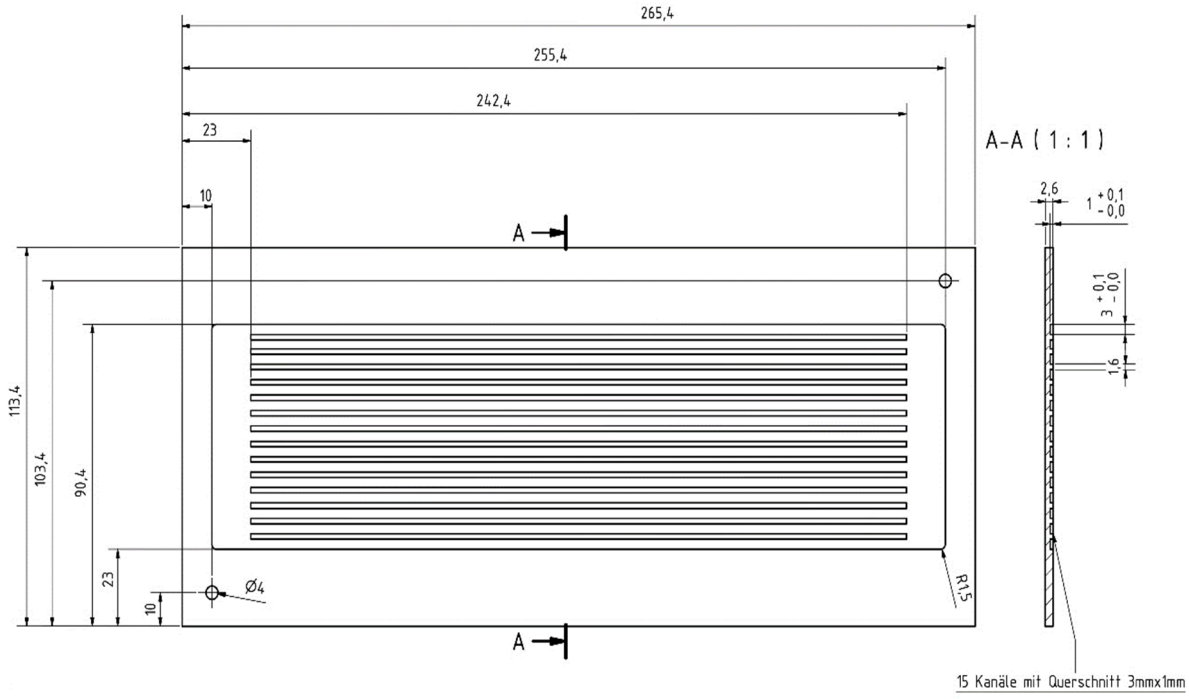

3) sCO_2 plate

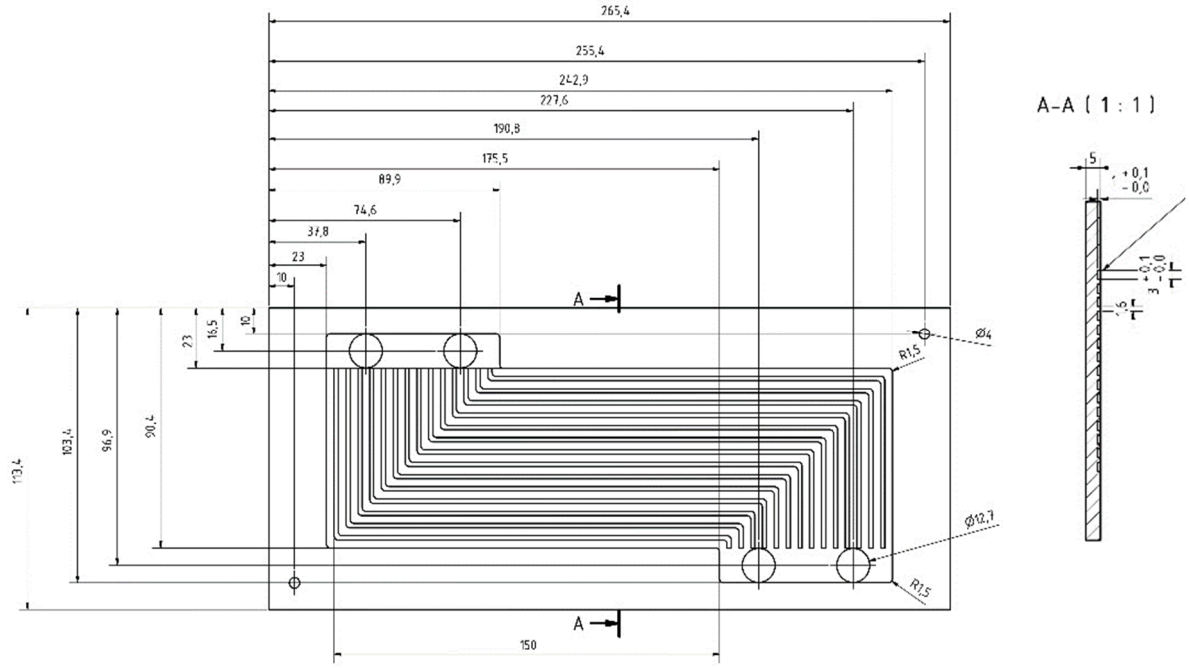
265,4
255,4
242,9
227,6
190,8
175,5
89,9
74,6
37,8
23
10
A
A
150
113,4
103,4
96,9
90,4
23
16,5
10
Ø4
R1,5
Ø12,7
R1,5
A-A (1 : 1)
5
+0,1
-0,0
3
+0,1
-0,0
1,5

Heat exchanger configuration BAA

1) Cover plate

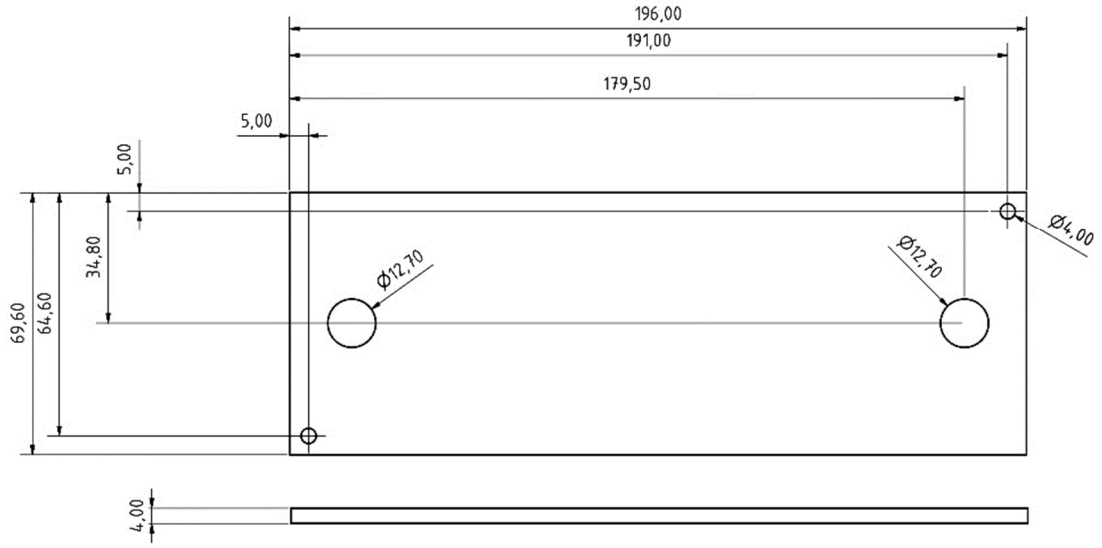

3) H_2O plate

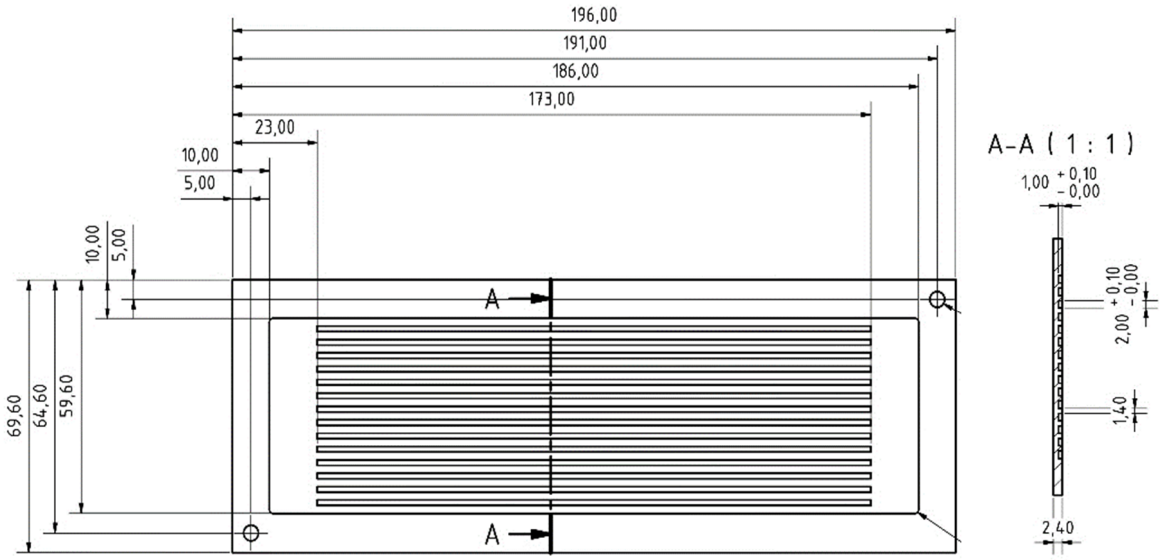

3) sCO_2 plate

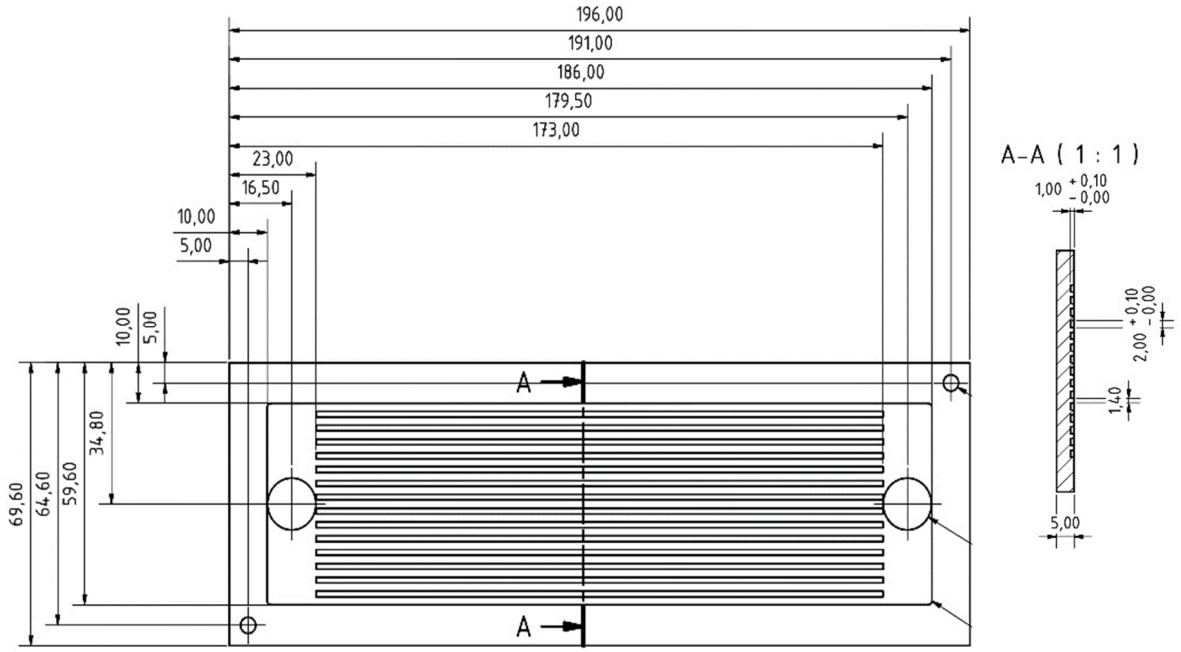
196,00
191,00
186,00
179,50
173,00
23,00
16,50
10,00
5,00
10,00
5,00
34,80
59,60
64,60
69,60
A
A
A–A (1 : 1)
1,00 + 0,10 – 0,00
2,00 + 0,10 – 0,00
1,40
5,00

Heat exchanger configuration BAB

1) Cover plate

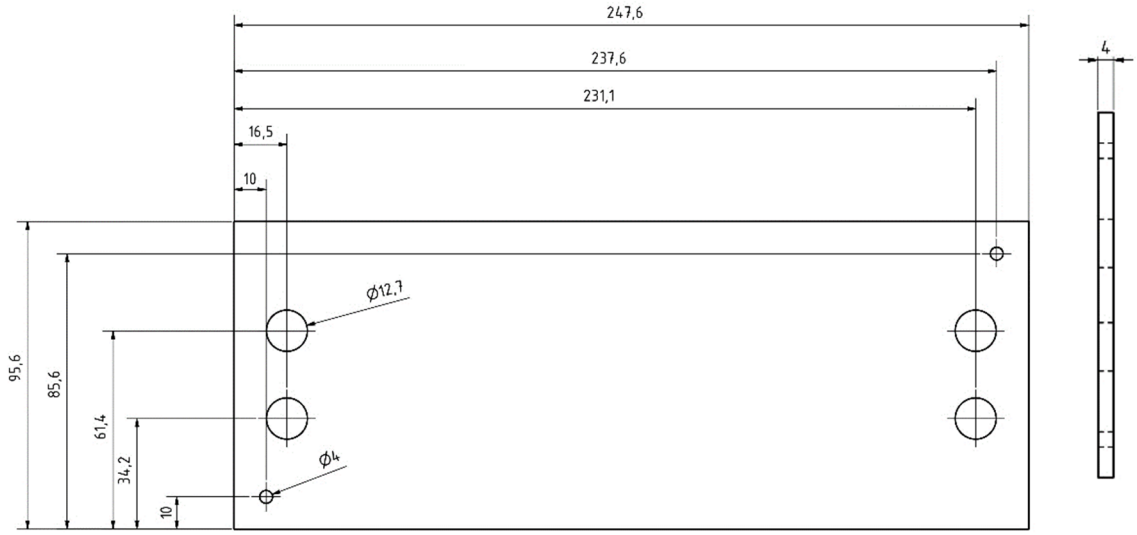

2) H_2O plate

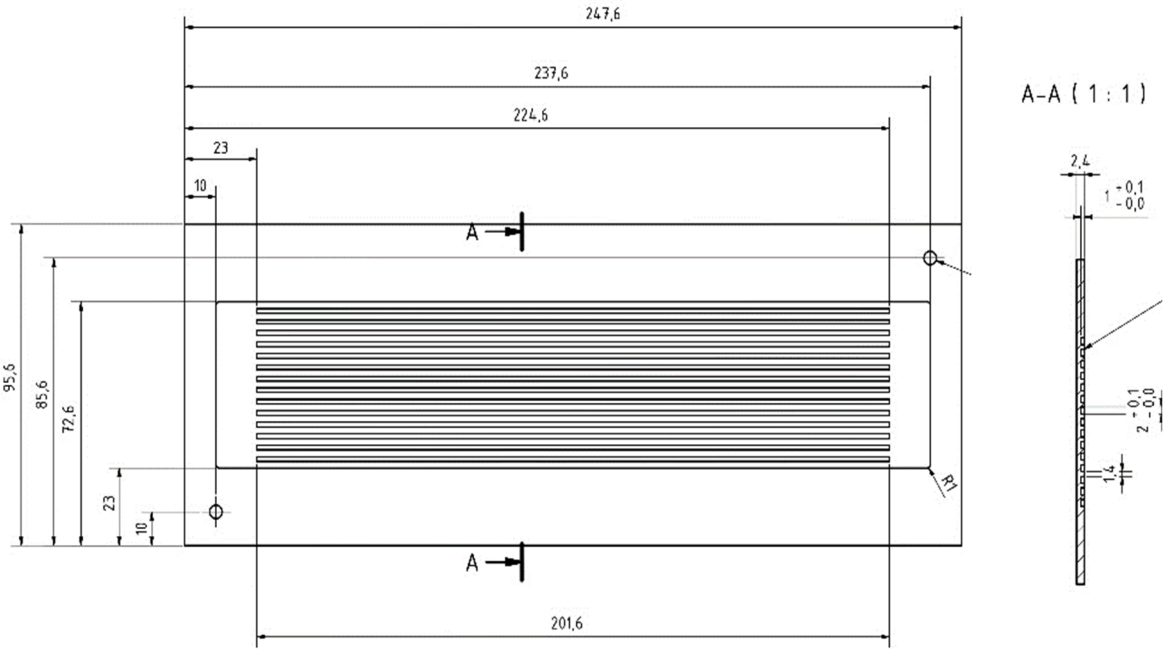

3) sCO_2 plate

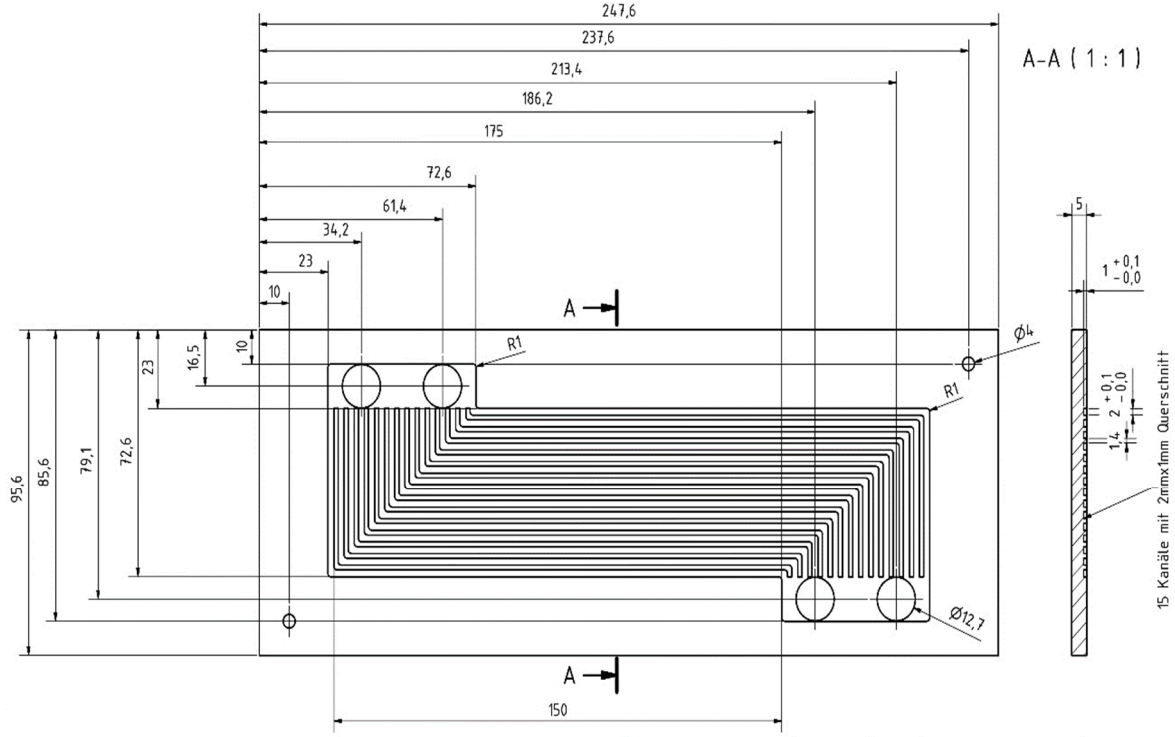
247,6
237,6
213,4
186,2
175
72,6
61,4
34,2
23
10
A
A
A-A (1 : 1)
R1
R1
ϕ4
Ø12,7
150
95,6
85,6
79,1
72,6
23
16,5
10
5
1 +0,1 −0,0
2 +0,1 −0,0
1,4
15 Kanäle mit 2mmx1mm Querschnitt

Heat exchanger configuration BBB
Heat exchanger configuration BCB
Heat exchanger configuration BDB

1) Cover plate

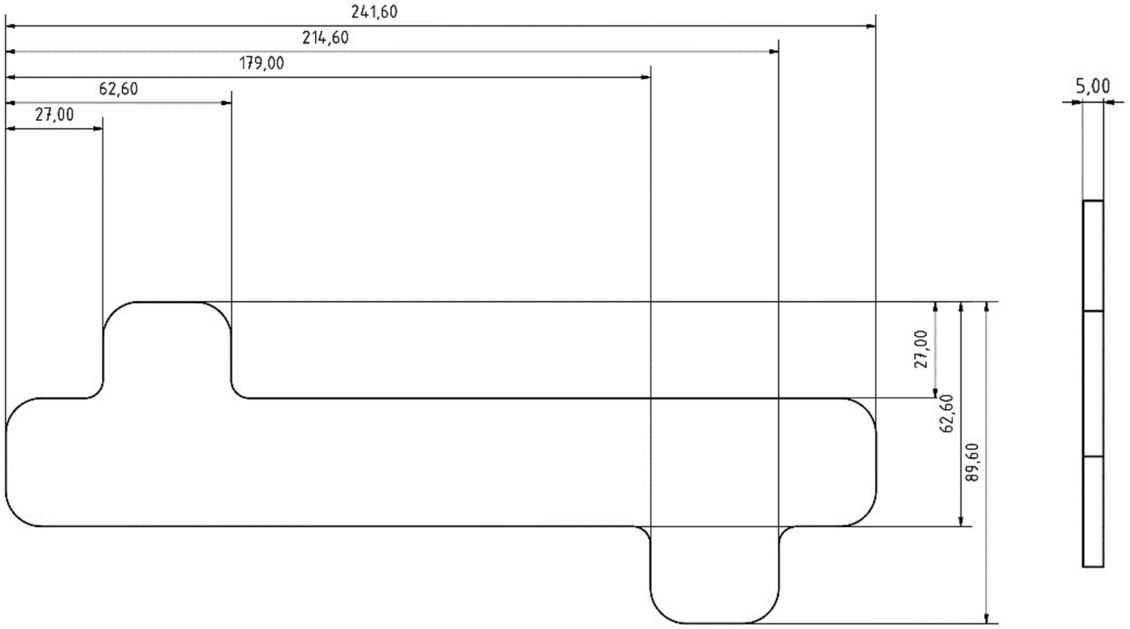

2) sCO_2 plate

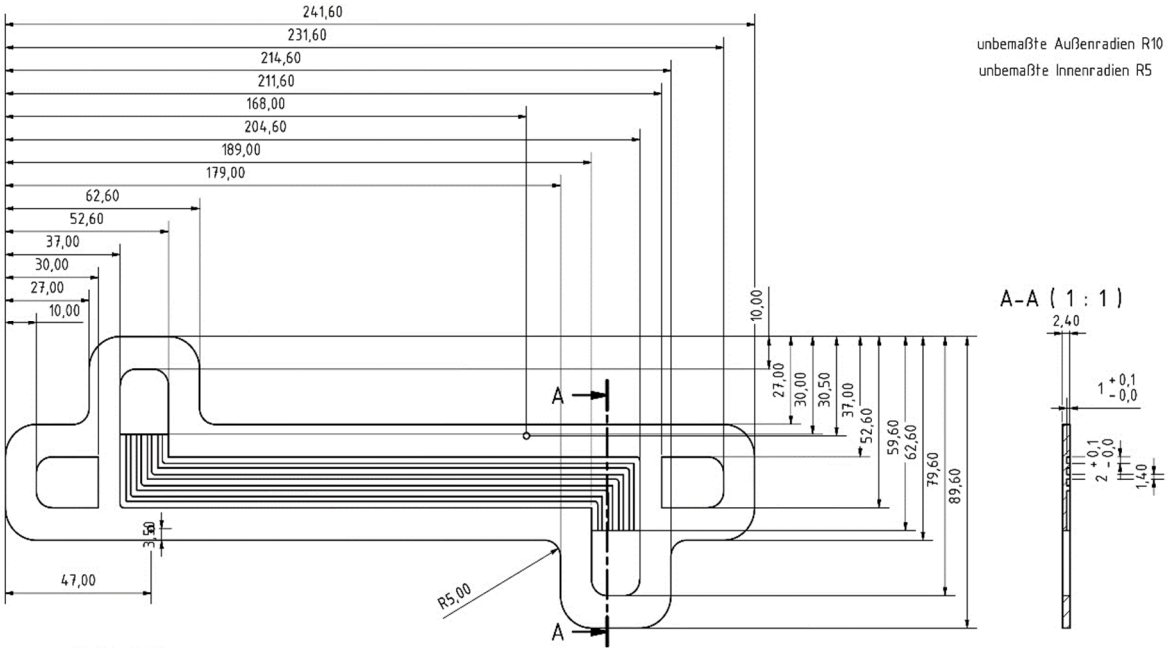

3) H_2O plate

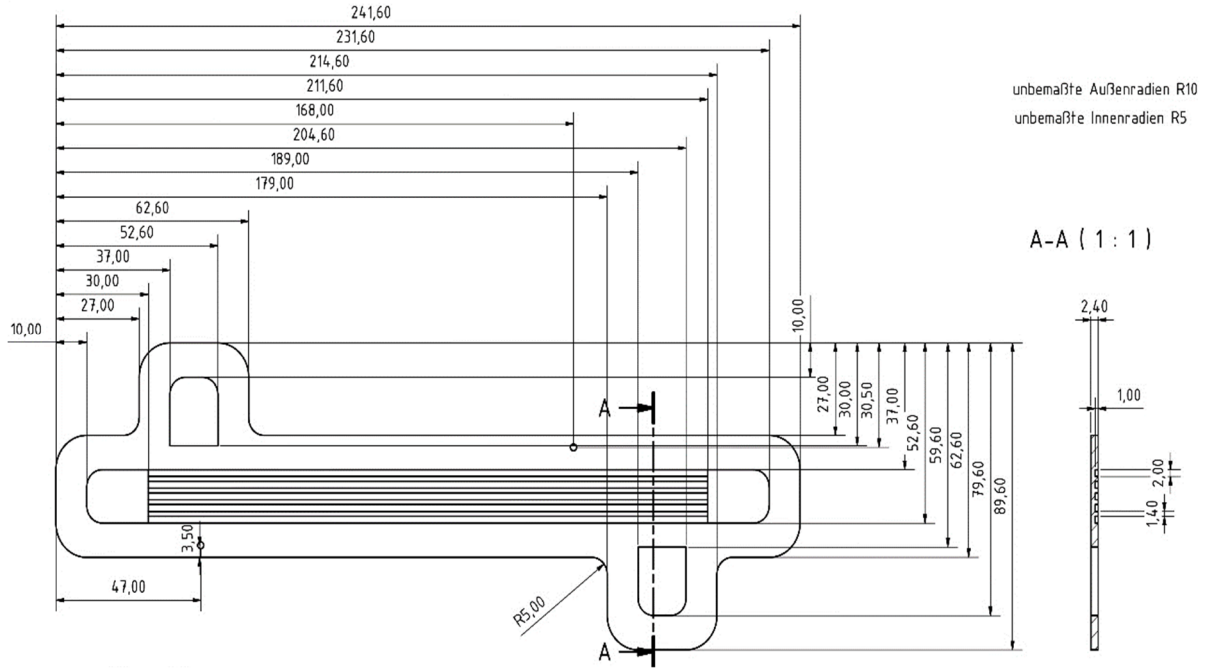

4) sCO_2 cover plate

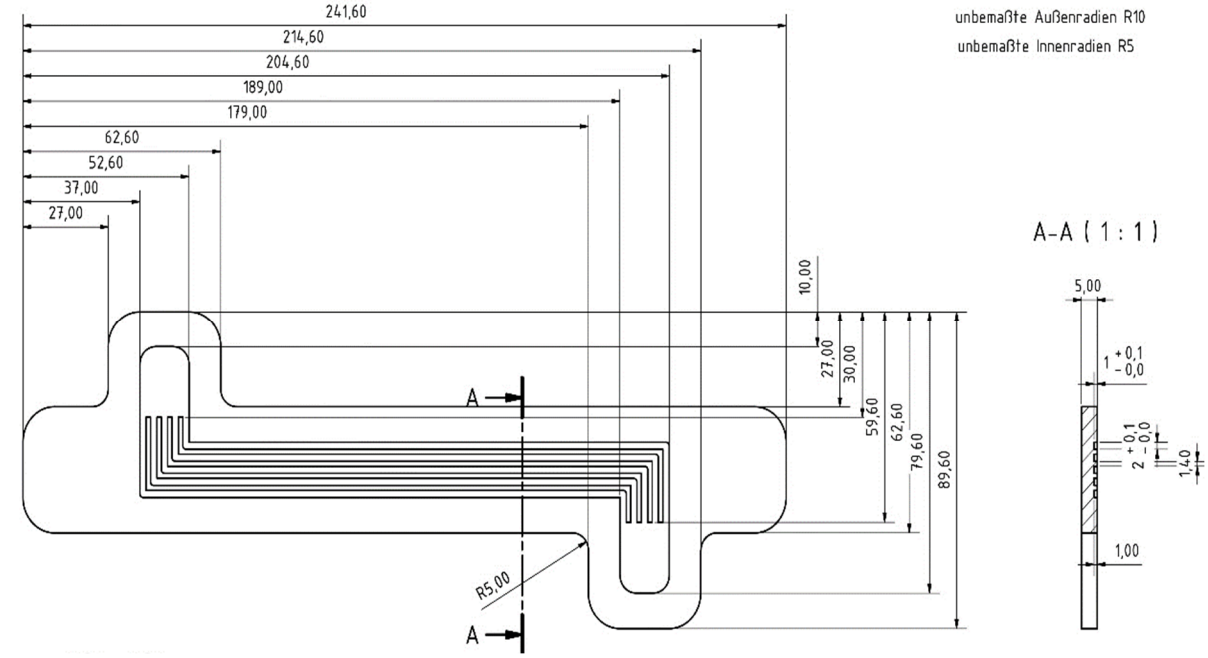

Appendix D

Low-pressure steam cycle / sCO_2 SCARLETT loop											
3x1 mm / 15/1 / IZ											
	$\dot{m}_{H2O}$	$p02$	$p04$	$T03$	$T04$	$Q_{in,Eva}$	$\dot{m}_{sCO2}$	$\Delta p05$	$p06$	$T07$	$T08$
	[l/h]	[bar]	[bar]	[°C]	[°C]	[W]	[g/s]	[bar]	[bar]	[°C]	[°C]
DP (1)	0.54	0.317	0.300	69.99	37.72	385	36.94	0.675	109.282	39.21	41.23
	0.61	0.321	0.299	70.23	37.83	455	45.98	0.975	108.824	39.38	41.11
	0.74	0.329	0.300	70.75	37.48	550	55.92	1.425	108.343	39.13	40.78
	0.97	0.354	0.311	72.34	38.28	678	67.35	2.053	107.516	39.12	40.63
DP (2)	0.55	0.323	0.305	70.42	36.68	389	36.45	0.672	99.255	39.34	40.59
	0.64	0.332	0.309	71.02	37.21	462	45.28	1.023	98.803	39.24	40.34
	0.79	0.360	0.330	72.87	37.51	549	56.15	1.548	98.148	39.02	39.93
	0.95	0.359	0.317	72.68	36.82	685	67.40	2.226	97.177	38.63	39.35
DP (3)	0.53	0.336	0.320	71.33	37.58	374	36.90	0.728	94.214	38.99	39.80
	0.67	0.346	0.325	71.99	37.77	452	45.66	1.106	93.746	39.10	39.69
	0.79	0.358	0.329	72.72	37.40	544	52.30	1.493	93.021	39.15	39.66
	0.98	0.352	0.307	72.21	37.55	685	67.81	2.459	92.134	38.83	38.74

Low-pressure steam cycle / sCO_2 SCARLETT loop											
2x1 mm / 15/1 / IZ											
	$\dot{m}_{H2O}$	$p02$	$p04$	$T03$	$T04$	$Q_{in,Eva}$	$\dot{m}_{sCO2}$	$\Delta p05$	$p06$	$T07$	$T08$
	[l/h]	[bar]	[bar]	[°C]	[°C]	[W]	[g/s]	[bar]	[bar]	[°C]	[°C]
DP (1)	0.51	0.331	0.325	78.24	38.53	383	36.75	0.372	109.312	39.22	41.42
	0.63	0.323	0.315	70.99	38.07	462	45.69	0.547	108.876	39.12	41.20
	0.77	0.342	0.330	72.65	37.57	556	54.83	0.794	108.385	38.44	40.55
	0.94	0.328	0.312	71.52	38.30	684	67.79	1.190	107.546	39.25	41.10
ODP (4)	0.62	0.329	0.321	72.96	38.03	462	36.85	0.377	109.283	39.18	41.89
	0.76	0.325	0.313	72.52	38.02	556	36.95	0.367	109.274	39.11	42.28
	0.94	0.332	0.314	75.93	38.23	684	36.84	0.371	109.346	39.16	43.12
	1.19	0.322	0.296	70.61	38.83	822	36.60	0.385	109.521	39.18	43.99
	1.47	0.343	0.304	81.20	39.09	1014	36.61	0.390	109.437	39.16	44.92
	1.81	0.371	0.315	94.19	43.21	1221	36.67	0.394	109.593	39.18	45.94
DP (2)	0.53	0.314	0.306	70.43	38.12	389	36.79	0.388	99.251	39.23	40.74
	0.67	0.323	0.316	71.10	38.00	462	45.72	0.592	98.842	39.00	40.39
	0.78	0.318	0.307	70.78	38.02	556	55.73	0.874	98.143	38.94	40.20
	0.95	0.326	0.311	71.37	37.91	684	68.02	1.311	97.172	38.91	39.98
ODP (5)	0.66	0.332	0.324	71.71	38.04	475	37.03	0.395	99.252	39.15	40.96
	0.77	0.333	0.322	71.72	38.21	556	36.86	0.394	99.382	39.18	41.36
	0.94	0.329	0.312	71.82	38.10	684	36.98	0.401	99.473	39.14	41.80
	1.17	0.346	0.321	90.48	38.45	819	36.69	0.400	99.247	39.22	42.43

	1.48	0.363	0.328	81.87	38.55	1006		36.54	0.404	99.618	39.25	43.11
	1.84	0.370	0.317	82.44	40.20	1214		36.73	0.416	99.533	39.23	43.76
DP (3)	0.51	0.321	0.314	83.48	37.66	384		36.53	0.405	94.873	39.20	40.29
	0.65	0.334	0.325	72.16	37.77	465		45.64	0.623	94.626	39.06	40.03
	0.78	0.330	0.317	71.95	37.65	566		55.69	0.906	94.794	38.91	39.85
	0.96	0.354	0.339	73.89	37.90	685		67.67	1.367	94.879	38.97	39.71
ODP (6)	0.68	0.319	0.310	70.88	37.97	462		36.65	0.408	94.743	39.17	40.50
	0.79	0.333	0.320	77.01	37.99	563		36.78	0.413	94.854	39.10	40.73
	0.98	0.348	0.332	92.00	38.05	685		36.54	0.413	94.633	39.17	41.10
	1.19	0.341	0.317	83.02	38.23	828		36.89	0.428	94.901	39.16	41.47
	1.51	0.350	0.312	94.04	38.44	1006		36.52	0.431	94.878	39.27	42.02
	1.78	0.378	0.320	93.74	39.67	1228		36.76	0.445	94.613	39.19	42.57

High-pressure steam cycle / sCO_2 SCARLETT loop

3x1 mm / 15/1 / II

	$\dot{m}_{H2O}$	$p02$	$p04$	$T03$	$T04$	$Q_{in,Evap}$		$\dot{m}_{sCO2}$	$\Delta p05$	$p06$	$T07$	$T08$
	[l/h]	[bar]	[bar]	[°C]	[°C]	[W]		[g/s]	[bar]	[bar]	[°C]	[°C]
DP (1)	-	-	-	-	-	-		37.00	-	110.000	-	-
	0.64	70.154	70.107	279.18	37.49	477		45.66	0.087	109.043	39.20	41.19
	0.79	70.149	70.099	284.67	38.03	580		55.93	0.131	108.460	39.15	41.14
	0.98	69.940	69.902	284.56	38.07	693		68.10	0.194	107.681	38.96	40.94
ODP (4)	0.63	69.988	69.951	283.96	38.20	475		37.09	0.063	109.394	39.26	41.85
	0.79	70.181	70.139	284.73	38.35	585		36.91	0.063	109.416	39.17	42.41
	0.98	69.953	69.910	284.62	38.40	700		36.84	0.062	109.424	39.17	43.06
	1.18	70.325	70.275	285.04	38.49	855		36.92	0.062	109.430	39.16	43.93
	1.39	70.190	70.149	284.94	38.61	1039		36.91	0.063	109.417	39.19	44.92
	1.72	70.356	70.296	285.08	38.69	1252		37.11	0.063	109.418	39.17	45.90
ODP II (7)	1.80	70.372	70.314	285.09	39.06	1252		23.34	0.025	109.926	39.19	49.05
	1.80	70.377	70.326	285.09	39.36	1251		18.15	0.016	109.895	39.27	51.96
	1.80	70.382	70.338	285.08	39.66	1251		15.07	0.008	110.129	39.34	54.22
	1.63	70.380	70.298	285.03	39.86	1252		13.48	0.005	110.138	39.30	55.04
	1.80	70.405	70.302	285.06	40.91	1252		11.93	0.005	110.160	39.35	57.32
	1.62	70.405	70.306	285.07	42.68	1252		10.24	0.005	110.161	39.33	60.91
	1.76	70.402	70.311	285.08	45.11	1252		8.89	0.005	110.173	39.36	65.66
DP (2)	-	-	-	-	-	-		37.00	-	100.000	-	-
	0.63	70.182	70.125	282.39	38.33	481		45.62	0.093	98.897	39.21	40.61
	0.79	70.239	70.165	284.71	38.40	585		55.76	0.140	98.167	39.25	40.60
	0.98	70.086	70.020	284.66	38.31	700		67.74	0.208	97.295	39.19	40.47
ODP (5)	0.63	70.119	70.060	284.54	38.54	481		36.81	0.060	99.279	39.38	41.10
	0.79	70.160	70.104	284.69	38.71	578		36.94	0.061	99.320	39.38	41.50
	0.98	69.912	69.870	284.54	38.67	693		37.08	0.061	99.262	39.31	41.88
	1.18	70.244	70.193	284.94	38.73	847		36.79	0.061	99.267	39.32	42.47
	1.39	69.863	69.809	284.58	38.87	1029		36.80	0.062	99.356	39.32	43.13

	1.80	70.387	70.314	285.07	39.07	1252		37.09	0.064	99.322	39.34	43.86
ODP II (8)	1.80	70.371	70.259	285.00	37.94	1253		35.73	0.062	99.398	39.14	43.86
	1.78	70.314	70.221	284.96	38.84	1251		20.74	0.020	99.929	39.37	46.93
	1.77	70.305	70.229	284.97	39.12	1252		16.30	0.012	100.024	39.37	49.08
	1.80	70.303	70.232	285.00	40.52	1252		11.96	0.005	100.101	39.36	53.98
	1.80	70.301	70.229	284.98	43.05	1251		9.98	0.005	100.121	39.36	59.26
	1.80	70.276	70.207	284.97	44.90	1251		9.09	0.005	100.133	39.33	62.87
DP (3)	-	-	-	-	-	-		37.00	-	95.00	-	-
	0.63	70.214	70.146	284.57	38.46	482		45.61	0.099	93.743	39.08	40.07
	0.80	70.206	70.141	284.72	38.51	579		55.59	0.148	93.099	39.06	39.99
	0.98	69.925	69.856	284.56	38.48	694		67.58	0.220	92.207	38.82	39.69
ODP (6)	0.63	70.107	70.039	284.58	38.21	481		36.70	0.064	94.244	39.23	40.49
	0.80	70.206	70.125	284.77	38.34	578		36.80	0.065	94.236	39.22	40.76
	0.98	69.944	69.873	284.68	38.30	692		36.82	0.065	94.246	39.23	41.09
	1.18	70.114	70.045	284.90	38.54	847		36.78	0.065	94.244	39.29	41.55
	1.39	69.845	69.787	284.65	38.60	1029		36.70	0.066	94.248	39.26	42.02
	1.80	70.227	70.161	284.94	38.48	1252		36.92	0.068	94.197	39.10	42.47
ODP II (9)	1.80	70.337	70.242	285.07	39.19	1252		18.34	0.016	94.946	39.52	46.50
	1.80	70.346	70.265	285.07	39.53	1252		14.18	0.009	95.033	39.45	49.58
	1.80	70.315	70.236	285.07	40.49	1252		11.73	0.005	95.076	39.47	53.35
	1.80	70.299	70.228	285.04	42.33	1252		10.59	0.005	95.059	39.41	56.49
	1.80	70.310	70.241	285.06	44.28	1252		9.57	0.005	95.123	39.43	60.25
	1.80	70.300	70.227	285.05	46.38	1252		8.77	0.005	95.095	39.45	64.30
High-pressure steam cycle / sCO_2 SCARLETT loop												
3x1 mm / 15/1 / IZ												
	$\dot{m}_{H2O}$	$p02$	$p04$	$T03$	$T04$	$Q_{in,Eva}$		$\dot{m}_{sCO2}$	$\Delta p05$	$p06$	$T07$	$T08$
	[l/h]	[bar]	[bar]	[°C]	[°C]	[W]		[g/s]	[bar]	[bar]	[°C]	[°C]
DP (1)	-	-	-	-	-	-		37.00	-	110.000	-	-
	0.62	70.008	70.002	283.91	39.86	479		45.74	0.911	109.974	39.00	40.87
	0.80	70.350	70.337	284.23	38.53	580		55.74	1.328	110.372	39.10	40.93
	0.98	70.302	70.291	284.16	38.43	692		67.79	1.945	109.598	39.01	40.70
ODP (4)	0.63	70.535	70.536	284.18	39.67	482		36.51	0.594	110.392	39.31	41.67
	0.79	70.512	70.500	284.21	38.58	577		36.51	0.597	110.425	39.22	42.21
	0.98	70.346	70.330	284.08	38.41	691		36.67	0.600	110.391	39.26	42.87
	1.18	70.543	70.524	284.39	38.47	845		36.47	0.598	110.390	39.18	43.71
	1.39	70.511	70.490	284.37	38.44	1026		36.65	0.605	110.441	39.11	44.60
	1.80	70.325	70.296	284.22	38.72	1237		36.78	0.616	110.438	39.25	45.74
ODP II (7)	1.80	70.630	70.581	284.55	38.69	1239		36.45	0.612	110.399	39.22	45.68
	1.80	70.556	70.536	284.46	38.57	1238		16.48	0.143	111.069	39.38	52.44
	1.80	70.514	70.500	284.43	38.47	1237		9.19	0.051	110.128	38.81	63.82
	1.80	70.483	70.480	284.40	40.89	1237		5.74	0.024	110.154	38.98	95.39

	1.79	70.525	70.521	284.45	44.06	1237		4.47	0.017	110.177	38.82	128.07
	1.80	70.466	70.450	284.36	47.97	1237		3.92	0.014	110.157	38.73	151.05
DP (2)	-	-	-	-	-	-		37.00	-	100.000	-	-
	0.63	70.780	70.703	285.98	36.84	476		45.31	1.003	98.848	38.93	40.06
	0.79	70.675	70.631	285.94	37.75	586		55.41	1.463	99.254	39.20	40.25
	0.98	70.640	70.598	285.96	38.29	701		68.03	2.172	99.450	39.22	40.09
ODP (5)	0.63	70.672	70.619	286.02	38.30	473		36.70	0.662	99.299	39.25	40.79
	0.80	70.650	70.605	285.99	38.27	577		36.72	0.663	99.335	39.18	41.16
	0.98	70.557	70.514	285.89	38.29	700		36.76	0.664	99.348	39.19	41.63
	1.18	70.465	70.422	285.73	38.52	846		36.73	0.668	99.284	39.27	42.23
	1.39	70.458	70.413	285.67	38.60	1018		36.72	0.670	99.323	39.26	42.82
	1.64	70.583	70.545	285.78	38.75	1239		36.48	0.674	99.339	39.25	43.59
ODP II (8)	1.74	70.680	70.635	285.91	38.94	1239		18.67	0.197	99.931	39.46	47.80
	1.80	70.643	70.588	285.84	38.94	1239		12.99	0.106	100.052	39.42	52.43
	1.80	70.637	70.586	285.84	39.35	1239		7.89	0.048	100.081	39.50	70.40
	1.80	70.671	70.613	285.84	41.05	1239		5.62	0.029	100.143	39.33	101.36
	1.78	70.605	70.545	285.78	45.00	1239		4.20	0.019	100.148	39.33	146.61
DP (3)	-	-	-	-	-	-		37.00	-	95.000	-	-
	0.63	70.859	70.774	285.97	37.76	480		45.54	1.056	94.722	38.95	39.67
	0.80	70.693	70.635	285.82	37.73	587		55.72	1.536	95.118	38.94	39.61
	0.98	70.672	70.619	285.83	37.90	693		67.93	2.310	94.348	38.75	39.11
ODP (6)	0.63	70.396	70.361	285.58	38.35	480		36.44	0.676	95.248	39.32	40.44
	0.80	70.329	70.294	285.51	38.39	577		36.54	0.685	95.241	39.28	40.73
	0.98	70.516	70.477	285.69	38.13	693		36.87	0.697	95.202	39.08	40.90
	1.18	70.343	70.306	285.55	38.54	857		36.72	0.698	95.214	39.29	41.53
	1.39	70.687	70.641	285.92	38.72	1030		36.66	0.701	95.199	39.31	42.02
	1.74	70.670	70.626	285.86	38.78	1252		36.80	0.715	95.171	39.30	42.58
ODP II (9)	1.79	70.793	70.731	286.01	38.88	1252		18.95	0.214	95.866	39.44	46.57
	1.80	70.800	70.740	286.04	39.09	1252		12.45	0.105	95.990	39.52	52.69
	1.80	70.639	70.592	285.93	39.33	1252		8.01	0.053	96.047	39.49	71.04
	1.80	70.583	70.542	285.86	40.48	1252		5.58	0.031	96.120	39.18	105.03

High-pressure steam cycle / sCO_2 SCARLETT loop

2x1 mm / 15/1 / II

	$\dot{m}_{H2O}$	$p02$	$p04$	$T03$	$T04$	$Q_{in,Eva}$		$\dot{m}_{sCO2}$	$\Delta p05$	$p06$	$T07$	$T08$
	[l/h]	[bar]	[bar]	[°C]	[°C]	[W]		[g/s]	[bar]	[bar]	[°C]	[°C]
DP (1)	-	-	-	-	-	-		37.00	-	110.00	-	-
	0.63	70.188	70.114	284.64	37.24	471		45.62	0.163	108.987	39.04	40.96
	0.79	69.980	69.925	284.63	37.94	580		55.47	0.239	108.523	39.45	41.40
	0.98	70.232	70.174	284.94	38.43	693		67.36	0.350	107.666	39.39	41.30
ODP (4)	0.63	70.187	70.126	284.74	38.21	475		36.70	0.105	109.458	39.40	41.80
	0.79	69.955	69.904	284.68	38.48	577		36.49	0.104	109.443	39.47	42.45

	0.98	70.090	70.054	284.83	38.66	701		36.68	0.106	109.460	39.40	43.10
	1.18	70.514	70.456	285.22	38.67	857		36.73	0.107	109.449	39.38	43.93
	1.39	70.141	70.087	284.87	38.85	1040		36.45	0.106	109.470	39.38	44.91
	1.75	70.160	70.109	284.90	39.20	1252		36.41	0.107	109.453	39.47	46.00
ODP II (7)	1.80	70.452	70.381	285.15	39.46	1252		19.97	0.032	110.010	39.48	50.47
	1.80	70.650	70.587	285.35	39.89	1252		14.90	0.016	110.075	39.43	53.72
	1.80	70.780	70.688	285.48	40.48	1252		12.34	0.010	110.130	39.40	56.85
	1.80	70.491	70.432	285.23	41.40	1252		10.79	0.006	110.135	39.44	59.96
	1.80	70.710	70.637	285.40	42.77	1252		9.91	0.005	110.183	39.36	62.39
	1.80	70.664	70.572	285.36	46.07	1252		9.16	0.005	110.185	39.37	64.70
DP (2)	-	-	-	-	-	-	-	37.00	-	100.000	-	-
	0.63	70.274	70.171	284.73	36.84	479		45.46	0.173	98.896	39.21	40.55
	0.80	70.037	69.958	284.68	37.64	581		55.49	0.255	98.252	39.02	40.37
	0.98	70.552	70.480	285.22	37.99	703		67.48	0.373	98.496	38.86	40.25
ODP (5)	0.63	70.000	69.925	284.54	37.91	483		36.66	0.115	99.36	39.23	41.00
	0.80	69.975	69.913	284.66	38.30	579		36.65	0.117	99.331	39.22	41.39
	0.98	70.153	70.090	284.83	38.46	693		36.61	0.117	99.321	39.20	41.84
	1.18	70.479	70.399	285.13	38.50	858		36.57	0.117	99.345	39.18	42.47
	1.39	70.098	70.026	284.80	38.64	1030		36.65	0.118	99.337	39.17	43.08
	1.75	70.047	69.986	284.76	38.99	1265		36.50	0.119	99.348	39.25	43.93
ODP II (8)	1.80	70.211	70.140	284.91	39.29	1265		19.62	0.036	99.921	39.39	47.58
	1.78	70.364	70.293	285.06	39.63	1265		15.23	0.021	100.029	39.39	50.15
	1.77	70.489	70.414	285.16	40.03	1264		13.08	0.015	100.073	39.41	52.42
	1.80	70.463	70.407	285.15	40.62	1265		11.29	0.011	100.104	39.40	55.61
	1.80	70.263	70.186	284.94	41.25	1264		10.30	0.009	100.129	39.33	58.15
DP (3)	-	-	-	-	-	-		37.00	-	95.000	-	-
	0.63	70.237	70.143	284.70	37.33	479		46.00	0.189	93.735	39.25	40.15
	0.80	69.998	69.915	284.63	37.76	581		55.80	0.273	94.149	38.95	39.95
	0.98	70.115	70.042	284.78	37.92	694		67.84	0.395	94.252	38.71	39.73
ODP (6)	0.63	70.056	69.983	284.58	38.11	476		36.94	0.122	95.237	39.21	40.53
	0.80	70.248	70.178	284.92	38.42	578		36.82	0.123	95.153	39.20	40.87
	0.98	70.197	70.128	284.88	38.53	701		36.96	0.124	95.226	39.25	41.27
	1.18	70.551	70.475	285.23	38.59	848		36.98	0.122	95.227	39.27	41.71
	1.39	70.694	70.599	285.35	38.64	1030		36.98	0.126	95.225	39.20	42.18
	1.75	70.210	70.149	284.89	39.02	1252		37.00	0.126	95.230	39.23	42.81
ODP II (9)	1.80	70.355	70.281	285.07	39.40	1252		18.69	0.034	95.884	39.38	46.61
	1.80	70.549	70.485	285.28	39.80	1252		14.95	0.021	95.972	39.41	49.09
	1.80	70.626	70.583	285.36	40.17	1252		12.77	0.015	96.007	39.41	51.69
	1.80	70.673	70.593	285.39	40.92	1252		10.70	0.010	96.042	39.41	55.96
	1.80	70.630	70.559	285.39	41.82	1252		9.61	0.008	96.049	39.36	59.71
	1.80	70.640	70.582	285.39	43.30	1252		8.68	0.006	95.296	39.37	64.75
	1.80	70.601	70.527	285.33	46.52	1252		7.69	0.005	95.341	39.42	71.28

High-pressure steam cycle / sCO_2 SCARLETT loop												
2x1 mm / 15/1 / IZ												
	$\dot{m}_{H2O}$	$p02$	$p04$	$T03$	$T04$	$Q_{in,Eva}$		$\dot{m}_{sCO2}$	$\Delta p05$	$p06$	$T07$	$T08$
	[l/h]	[bar]	[bar]	[°C]	[°C]	[W]		[g/s]	[bar]	[bar]	[°C]	[°C]
DP (1)	-	-	-	-	-	-		37.00	-	110.000	-	-
	0.63	70.202	70.171	284.95	37.82	473		45.57	0.570	110.056	39.20	41.07
	0.79	70.126	70.103	284.90	38.08	577		55.70	0.845	110.561	39.24	41.15
	0.98	70.210	70.196	285.00	38.24	692		67.74	1.242	109.634	39.28	41.08
ODP (4)	0.63	69.974	69.949	285.12	38.37	474		36.38	0.372	109.497	39.42	41.79
	0.80	69.981	69.975	285.18	38.42	578		36.58	0.373	109.462	39.25	42.24
	0.98	70.006	69.995	285.23	38.45	693		36.62	0.376	109.470	39.27	42.92
	1.18	70.062	70.057	285.26	38.62	847		36.59	0.383	109.452	39.34	43.86
	1.39	70.164	70.141	285.32	38.68	1028		36.52	0.386	109.455	39.28	44.77
	1.80	70.233	70.204	285.45	38.66	1251		36.71	0.389	109.452	39.32	45.86
ODP II (7)	1.78	70.202	70.140	285.40	38.95	1250		19.51	0.119	110.064	39.43	50.69
	1.80	70.190	70.130	285.44	39.22	1250		11.58	0.046	110.229	39.39	58.22
	1.80	70.155	70.102	285.43	39.59	1253		9.10	0.030	110.247	39.35	65.49
	1.80	70.174	70.114	285.44	40.47	1253		7.42	0.020	110.259	39.35	76.07
	1.71	70.151	70.108	285.43	41.84	1253		6.44	0.015	110.271	39.28	86.85
	1.70	70.116	70.076	285.41	44.94	1253		5.81	0.012	110.269	39.27	96.62
	1.79	70.145	70.094	285.44	48.78	1253		5.46	0.010	110.276	39.26	102.86
DP (2)	-	-	-	-	-	-		37.00	-	100.000	-	-
	0.63	70.427	70.384	285.18	35.74	472		45.51	0.620	99.881	38.91	40.17
	0.79	70.458	70.415	285.20	37.19	580		56.08	0.918	99.260	38.84	40.07
	0.98	70.261	70.234	285.03	37.84	693		67.42	1.320	99.445	39.18	40.27
ODP (5)	0.63	70.265	70.230	285.53	36.77	478		36.59	0.402	99.332	39.20	40.77
	0.79	70.180	70.161	285.46	37.68	579		36.34	0.396	99.357	39.36	41.36
	0.98	70.161	70.150	285.45	38.17	692		36.49	0.400	99.321	39.36	41.80
	1.18	70.134	70.129	285.40	38.25	857		36.57	0.401	99.301	39.27	42.34
	1.39	70.275	70.271	285.54	38.59	1029		36.70	0.407	99.311	39.36	42.99
	1.80	70.197	70.175	285.47	38.80	1251		36.32	0.404	99.321	39.38	43.78
ODP II (8)	1.76	70.200	70.120	285.44	38.98	1239		29.56	0.271	99.605	39.36	44.74
	1.74	70.107	70.080	285.40	39.16	1239		20.76	0.140	99.904	39.39	46.93
	1.79	70.078	70.022	285.36	39.42	1238		12.79	0.059	100.077	39.48	52.72
	1.77	69.993	69.984	285.30	39.80	1239		9.36	0.034	100.130	39.43	61.54
	1.80	69.946	69.907	285.22	40.91	1239		7.39	0.023	100.152	39.33	74.48
	1.80	69.917	69.892	285.14	44.29	1239		5.94	0.015	100.169	39.39	94.42
	1.79	70.087	70.053	285.32	49.50	1240		5.28	0.011	100.188	39.21	105.58
DP (3)	-	-	-	-	-	-		37.00	-	95.000	-	-
	0.63	70.092	70.062	284.83	37.76	475		46.81	0.594	96.672	39.03	40.20
	0.79	70.357	70.329	285.15	37.58	569		55.69	0.967	94.159	38.97	39.67
	0.98	70.157	70.124	284.89	37.88	700		67.11	1.389	94.320	38.99	39.61
	0.63	70.092	70.066	285.29	37.98	474		36.43	0.422	94.266	39.20	40.31

ODP (6)	0.80	69.858	69.829	285.12	38.38	577		36.56	0.429	94.223	39.29	40.67
	0.98	70.154	70.109	285.35	38.50	700		36.53	0.425	94.269	39.28	41.01
	1.18	70.420	70.340	285.49	37.34	856		36.48	0.429	94.247	39.17	41.29
	1.39	70.389	70.301	285.47	38.22	1028		36.60	0.434	94.272	39.33	41.87
	1.80	70.244	70.198	285.41	38.64	1240		36.36	0.437	94.272	39.38	42.49
ODP II (9)	1.80	70.312	70.282	285.46	38.89	1240		21.10	0.158	94.775	39.53	45.35
	1.80	70.272	70.238	285.46	39.15	1240		15.47	0.091	94.956	39.57	48.42
	1.80	70.288	70.256	285.48	39.34	1240		11.05	0.050	95.055	39.49	55.31
	1.80	70.248	70.218	285.48	39.71	1240		8.53	0.033	95.047	39.50	66.23
	1.79	70.319	70.291	285.56	40.52	1240		6.88	0.023	95.083	39.49	81.80
	1.78	69.819	69.783	285.05	43.29	1240		5.67	0.016	95.123	39.46	102.34
	1.78	70.103	70.078	285.34	49.43	1240		5.06	0.012	95.125	39.46	116.32

High-pressure steam cycle / sCO_2 SCARLETT loop

2x1 mm / 5/1 / IZ

	$\dot{m}_{H2O}$	$p02$	$p04$	$T03$	$T04$	$Q_{in,Evap}$		$\dot{m}_{sCO2}$	$\Delta p05$	$p06$	$T07$	$T08$
	[l/h]	[bar]	[bar]	[°C]	[°C]	[W]		[g/s]	[bar]	[bar]	[°C]	[°C]
DP (1)	-	-	-	-	-	-		-	-	-	-	-
ODP (4)	0.63	70.322	70.277	284.51	37.54	474		36.54	4.263	109.413	39.37	40.83
	0.80	70.487	70.440	284.38	37.75	574		36.65	4.451	109.269	39.36	41.49
	0.98	70.921	70.869	285.08	38.46	692		36.57	4.312	109.408	39.29	41.94
	1.18	70.899	70.857	285.07	40.23	847		36.64	4.360	109.414	39.40	42.77
	1.39	70.717	70.674	284.89	42.91	1028		36.59	4.364	109.423	39.36	43.59
	1.80	70.866	70.823	285.00	49.65	1251		36.68	4.314	109.405	39.33	44.44
ODP II (7)	1.80	70.702	70.651	284.84	52.03	1251		22.43	1.905	109.901	39.32	48.51
	1.80	70.579	70.534	284.77	57.42	1251		11.38	0.601	110.145	39.29	57.30
	1.80	70.355	70.301	284.52	68.67	1251		5.94	0.238	110.208	38.79	82.85
	1.80	69.952	69.915	284.09	98.95	1251		3.13	0.112	110.259	38.70	149.72
	1.76	70.345	70.282	284.44	148.64	1251		1.93	0.061	110.281	38.48	203.11
DP (2)	-	-	-	-	-	-		-	-	-	-	-
ODP (5)	0.63	69.448	69.403	283.69	36.95	479		36.62	4.183	100.302	39.12	39.66
	0.79	69.480	69.431	283.65	37.29	584		36.65	4.381	100.312	39.08	40.00
	0.98	69.455	69.407	283.65	38.15	691		36.65	4.417	100.307	39.10	40.39
	1.18	69.532	69.461	283.63	39.58	856		36.38	4.409	100.333	39.03	40.92
	1.39	69.522	69.444	283.66	42.05	1029		36.54	4.502	100.307	38.92	41.31
	1.80	70.596	70.557	284.83	46.78	1251		36.41	4.613	99.272	39.25	41.79
ODP II (8)	1.80	70.573	70.518	284.76	49.45	1251		20.65	1.668	99.855	39.31	46.05
	1.80	70.516	70.461	284.65	54.23	1251		10.49	0.538	100.053	39.36	56.72
	1.78	70.348	70.299	284.49	67.04	1251		5.64	0.216	100.138	39.17	94.21
	1.78	70.119	70.072	284.33	89.38	1251		3.67	0.124	100.172	39.05	149.67
	1.76	69.562	69.523	283.70	149.05	1251		2.45	0.071	100.177	38.88	206.73

	1.79	69.203	69.160	283.39	188.23	1251		1.95	0.050	100.199	38.95	229.32
DP (3)	-	-	-	-	-	-		-	-	-	-	-
ODP (6)	0.63	70.323	70.285	284.51	40.41	475		36.50	2.318	95.167	39.12	38.71
	0.79	70.389	70.348	284.56	37.80	578		36.93	2.000	95.086	39.20	38.95
	0.98	70.349	70.313	284.52	37.96	700		37.02	1.873	95.177	39.16	39.22
	1.18	70.521	70.479	284.69	38.70	846		37.09	1.932	95.103	39.19	39.50
	1.39	70.678	70.636	284.80	40.68	1027		36.67	2.111	95.188	39.16	39.96
	1.80	70.672	70.616	284.79	45.98	1249		36.95	1.959	95.132	39.17	40.30
ODP II (9)	1.80	70.605	70.554	284.79	49.62	1249		17.39	1.312	95.067	39.41	46.05
	1.80	70.571	70.529	284.74	52.67	1250		11.66	0.676	94.991	39.49	52.70
	1.80	70.541	70.494	284.68	58.33	1251		7.66	0.357	95.042	39.43	70.51
	1.80	70.615	70.533	284.78	78.51	1253		4.01	0.152	95.092	38.97	135.23
	1.80	70.687	70.615	284.84	147.42	1251		2.43	0.077	95.120	38.91	210.90
No heat input / sCO_2 SCARLETT loop												
3x1 mm / 15/1 / II												
	$\dot{m}_{H2O}$	$p02$	$p04$	$T03$	$T04$	$Q_{in,Evap}$		$\dot{m}_{sCO2}$	$\Delta p05$	$p06$	$T07$	$T08$
	[l/h]	[bar]	[bar]	[°C]	[°C]	[W]		[g/s]	[bar]	[bar]	[°C]	[°C]
DP (1)	-	-	-	-	-	-		36.63	0.059	109.372	39.13	-
	-	-	-	-	-	-		45.55	0.083	110.010	39.29	-
	-	-	-	-	-	-		55.45	0.124	109.432	39.32	-
	-	-	-	-	-	-		68.06	0.192	109.461	38.96	-
ODP II (7)	-	-	-	-	-	-		19.24	0.015	110.002	39.36	-
	-	-	-	-	-	-		11.14	0.005	110.176	39.09	-
	-	-	-	-	-	-		7.37	0.005	110.225	39.00	-
DP (2)	-	-	-	-	-	-		36.68	0.058	100.294	39.17	-
	-	-	-	-	-	-		45.49	0.089	99.780	39.00	-
	-	-	-	-	-	-		55.62	0.133	100.290	38.93	-
	-	-	-	-	-	-		67.69	0.195	99.378	38.68	-
ODP II (8)	-	-	-	-	-	-		18.00	0.012	99.928	39.31	-
	-	-	-	-	-	-		11.51	0.005	100.068	39.17	-
	-	-	-	-	-	-		8.01	0.005	100.101	39.09	-
DP (3)	-	-	-	-	-	-		36.61	0.062	94.177	39.33	-
	-	-	-	-	-	-		45.84	0.097	94.667	39.19	-
	-	-	-	-	-	-		56.18	0.144	95.077	38.96	-
	-	-	-	-	-	-		67.65	0.205	95.153	38.83	-
ODP II (9)	-	-	-	-	-	-		19.04	0.014	94.801	39.40	-
	-	-	-	-	-	-		12.72	0.007	94.941	39.19	-
	-	-	-	-	-	-		8.14	0.005	95.010	38.95	-

No heat input / sCO_2 SCARLETT loop

3x1 mm / 15/1 / IZ

	$\dot{m}_{H2O}$	$p02$	$p04$	$T03$	$T04$	$Q_{in,Evap}$		$\dot{m}_{sCO2}$	$\Delta p05$	$p06$	$T07$	$T08$
	[l/h]	[bar]	[bar]	[°C]	[°C]	[W]		[g/s]	[bar]	[bar]	[°C]	[°C]
DP (1)	-	-	-	-	-	-		36.71	0.607	110.366	39.03	-
	-	-	-	-	-	-		45.07	0.898	109.962	39.04	-
	-	-	-	-	-	-		55.90	1.349	110.347	38.87	-
	-	-	-	-	-	-		67.75	1.963	109.551	38.93	-
ODP II (7)	-	-	-	-	-	-		20.41	0.195	110.531	39.34	-
	-	-	-	-	-	-		15.18	0.109	110.037	39.29	-
	-	-	-	-	-	-		11.24	0.059	110.096	39.16	-
	-	-	-	-	-	-		8.02	0.028	110.130	39.02	-
DP (2)	-	-	-	-	-	-		36.13	0.658	99.337	39.05	-
	-	-	-	-	-	-		45.23	1.022	98.893	39.28	-
	-	-	-	-	-	-		55.50	1.506	99.263	39.23	-
	-	-	-	-	-	-		68.12	2.210	99.391	39.07	-
ODP II (8)	-	-	-	-	-	-		20.56	0.216	99.891	39.35	-
	-	-	-	-	-	-		14.26	0.106	99.981	39.47	-
	-	-	-	-	-	-		11.14	0.065	100.061	39.38	-
	-	-	-	-	-	-		7.93	0.032	100.110	39.18	-
DP (3)	-	-	-	-	-	-		36.31	0.708	94.278	38.69	-
	-	-	-	-	-	-		45.68	1.074	94.791	39.07	-
	-	-	-	-	-	-		55.26	1.577	94.246	38.95	-
	-	-	-	-	-	-		66.52	2.261	94.295	38.88	-
ODP II (9)	-	-	-	-	-	-		20.34	0.226	94.816	39.28	-
	-	-	-	-	-	-		15.34	0.131	94.935	39.51	-
	-	-	-	-	-	-		11.01	0.068	95.002	39.53	-
	-	-	-	-	-	-		8.01	0.035	95.020	39.41	-

No heat input / sCO_2 SCARLETT loop

2x1 mm / 15/1 / II

	$\dot{m}_{H2O}$	$p02$	$p04$	$T03$	$T04$	$Q_{in,Evap}$		$\dot{m}_{sCO2}$	$\Delta p05$	$p06$	$T07$	$T08$
	[l/h]	[bar]	[bar]	[°C]	[°C]	[W]		[g/s]	[bar]	[bar]	[°C]	[°C]
DP (1)	-	-	-	-	-	-		36.29	0.112	109.350	39.14	-
	-	-	-	-	-	-		45.33	0.157	109.963	39.26	-
	-	-	-	-	-	-		55.55	0.232	110.474	39.09	-
	-	-	-	-	-	-		68.11	0.346	109.510	39.26	-
	-	-	-	-	-	-		19.10	0.029	109.979	39.21	-

ODP II (7)	-	-	-	-	-	-		11.46	0.009	110.122	39.05	-
	-	-	-	-	-	-		7.30	0.005	110.184	38.83	-
DP (2)	-	-	-	-	-	-		36.62	0.112	99.245	39.19	-
	-	-	-	-	-	-		45.94	0.171	99.786	38.93	-
	-	-	-	-	-	-		55.99	0.252	100.204	39.20	-
	-	-	-	-	-	-		68.15	0.372	99.403	39.10	-
ODP II (8)	-	-	-	-	-	-		20.21	0.033	99.835	39.33	-
	-	-	-	-	-	-		11.28	0.008	100.024	39.24	-
	-	-	-	-	-	-		7.24	0.005	100.079	39.16	-
DP (3)	-	-	-	-	-	-		36.73	0.119	94.158	39.23	-
	-	-	-	-	-	-		44.62	0.172	94.695	39.10	-
	-	-	-	-	-	-		55.40	0.261	95.034	38.98	-
	-	-	-	-	-	-		67.03	0.373	95.210	38.81	-
ODP II (9)	-	-	-	-	-	-		19.51	0.032	94.735	39.10	-
	-	-	-	-	-	-		11.08	0.008	94.965	39.45	-
	-	-	-	-	-	-		7.20	0.005	95.018	39.23	-
No heat input / sCO_2 SCARLETT loop												
2x1 mm / 15/1 / IZ												
	$\dot{m}_{H2O}$	$p02$	$p04$	$T03$	$T04$	$Q_{in,Evap}$		$\dot{m}_{sCO2}$	$\Delta p05$	$p06$	$T07$	$T08$
	[l/h]	[bar]	[bar]	[°C]	[°C]	[W]		[g/s]	[bar]	[bar]	[°C]	[°C]
DP (1)	-	-	-	-	-	-		36.54	0.426	109.667	39.13	-
	-	-	-	-	-	-		45.44	0.581	110.091	39.42	-
	-	-	-	-	-	-		55.70	0.854	109.483	38.93	-
	-	-	-	-	-	-		67.73	1.248	109.622	39.10	-
ODP II (7)	-	-	-	-	-	-		14.47	0.060	110.080	38.96	-
	-	-	-	-	-	-		10.85	0.033	110.167	39.06	-
	-	-	-	-	-	-		6.62	0.011	110.221	38.82	-
DP (2)	-	-	-	-	-	-		36.47	0.415	99.799	39.03	-
	-	-	-	-	-	-		45.59	0.623	99.919	38.93	-
	-	-	-	-	-	-		55.81	0.919	100.247	39.21	-
	-	-	-	-	-	-		67.97	1.354	99.415	38.99	-
ODP II (8)	-	-	-	-	-	-		24.14	0.167	99.760	39.31	-
	-	-	-	-	-	-		16.41	0.078	99.956	39.22	-
	-	-	-	-	-	-		10.05	0.028	100.055	39.15	-
	-	-	-	-	-	-		6.58	0.010	100.098	38.82	-
DP (3)	-	-	-	-	-	-		36.78	0.433	95.221	39.22	-
	-	-	-	-	-	-		45.81	0.667	94.760	39.09	-
	-	-	-	-	-	-		55.33	0.952	95.139	38.85	-
	-	-	-	-	-	-		67.42	1.381	95.397	38.81	-

ODP II (9)	-	-	-	-	-	-		23.47	0.168	94.789	38.58	-
	-	-	-	-	-	-		11.95	0.043	94.937	39.27	-
	-	-	-	-	-	-		7.18	0.013	95.014	38.93	-

No heat input / sCO₂ SCARLETT loop

2x1 mm / 5/1 / IZ

	$\dot{m}_{H2O}$	$p02$	$p04$	$T03$	$T04$	$Q_{in,Eva}$		$\dot{m}_{sCO2}$	$\Delta p05$	$p06$	$T07$	$T08$
	[l/h]	[bar]	[bar]	[°C]	[°C]	[W]		[g/s]	[bar]	[bar]	[°C]	[°C]
DP (1)	-	-	-	-	-	-		36.56	4.112	110.322	39.01	-
ODP II (7)	-	-	-	-	-	-		15.91	0.838	110.021	39.08	-
	-	-	-	-	-	-		10.43	0.375	110.130	39.03	-
	-	-	-	-	-	-		6.18	0.140	110.170	38.72	-
	-	-	-	-	-	-		4.78	0.082	110.194	38.71	-
DP (2)	-	-	-	-	-	-		37.01	4.297	99.232	39.21	-
ODP II (8)	-	-	-	-	-	-		24.44	1.918	99.698	39.30	-
	-	-	-	-	-	-		14.23	0.682	99.955	39.24	-
	-	-	-	-	-	-		7.41	0.195	100.050	39.15	-
	-	-	-	-	-	-		4.85	0.084	100.065	38.59	-
DP (3)	-	-	-	-	-	-		36.74	3.679	95.089	39.15	-
ODP II (9)	-	-	-	-	-	-		18.98	1.248	94.778	39.39	-
	-	-	-	-	-	-		12.44	0.556	94.946	39.25	-
	-	-	-	-	-	-		8.25	0.250	94.979	39.45	-
	-	-	-	-	-	-		5.32	0.106	95.014	39.32	-

No heat input / sCO₂ SCARLETT loop

2x1 mm / 5/2 / IZ

	$\dot{m}_{H2O}$	$p02$	$p04$	$T03$	$T04$	$Q_{in,Eva}$		$\dot{m}_{sCO2}$	$\Delta p05$	$p06$	$T07$	$T08$
	[l/h]	[bar]	[bar]	[°C]	[°C]	[W]		[g/s]	[bar]	[bar]	[°C]	[°C]
DP (1)	-	-	-	-	-	-		36.67	0.989	109.391	38.77	-
	-	-	-	-	-	-		45.70	1.396	110.054	39.21	-
	-	-	-	-	-	-		55.69	2.044	110.415	39.02	-
	-	-	-	-	-	-		67.58	2.995	109.624	38.96	-
ODP II (7)	-	-	-	-	-	-		15.33	0.181	110.119	39.28	-
	-	-	-	-	-	-		8.67	0.058	110.242	39.10	-
	-	-	-	-	-	-		5.69	0.025	110.265	38.89	-
	-	-	-	-	-	-		36.51	0.974	99.306	39.22	-

DP (2)	-	-	-	-	-	-		45.57	1.490	99.821	38.93	-
	-	-	-	-	-	-		55.14	2.139	100.263	38.83	-
	-	-	-	-	-	-		67.42	3.185	99.431	38.66	-
ODP II (8)	-	-	-	-	-	-		15.41	0.183	99.993	39.44	-
	-	-	-	-	-	-		9.16	0.064	100.076	39.17	-
	-	-	-	-	-	-		5.60	0.023	100.122	39.11	-
DP (3)	-	-	-	-	-	-		36.74	1.035	95.165	39.13	-
	-	-	-	-	-	-		45.64	1.592	94.685	38.95	-
	-	-	-	-	-	-		55.79	2.331	94.998	38.99	-
	-	-	-	-	-	-		67.58	3.372	95.079	38.73	-
ODP II (9)	-	-	-	-	-	-		16.45	0.218	94.911	39.42	-
	-	-	-	-	-	-		9.17	0.069	95.008	39.29	-
	-	-	-	-	-	-		5.70	0.025	95.077	39.11	-

No heat input / sCO_2 SCARLETT loop

2x1 mm / 5/3 / IZ

	$\dot{m}_{H2O}$	$p02$	$p04$	$T03$	$T04$	$Q_{in,Evap}$		$\dot{m}_{sCO2}$	$\Delta p05$	$p06$	$T07$	$T08$
	[l/h]	[bar]	[bar]	[°C]	[°C]	[W]		[g/s]	[bar]	[bar]	[°C]	[°C]
DP (1)	-	-	-	-	-	-		36.62	0.307	109.417	39.12	-
	-	-	-	-	-	-		45.46	0.438	109.942	39.18	-
	-	-	-	-	-	-		55.86	0.652	110.397	39.16	-
	-	-	-	-	-	-		67.54	0.948	109.604	38.95	-
ODP II (7)	-	-	-	-	-	-		14.69	0.049	110.103	39.18	-
	-	-	-	-	-	-		10.25	0.022	110.178	39.08	-
	-	-	-	-	-	-		6.72	0.008	110.214	38.93	-
DP (2)	-	-	-	-	-	-		36.91	0.315	100.245	39.16	-
	-	-	-	-	-	-		45.61	0.474	99.862	38.94	-
	-	-	-	-	-	-		55.56	0.691	100.277	39.05	-
	-	-	-	-	-	-		67.98	1.025	99.319	38.74	-
ODP II (8)	-	-	-	-	-	-		16.36	0.062	99.942	39.31	-
	-	-	-	-	-	-		10.16	0.022	100.051	39.28	-
	-	-	-	-	-	-		6.80	0.008	100.096	39.08	-
DP (3)	-	-	-	-	-	-		36.44	0.324	95.172	39.28	-
	-	-	-	-	-	-		46.05	0.512	94.676	38.95	-
	-	-	-	-	-	-		55.40	0.730	95.031	39.05	-
	-	-	-	-	-	-		67.86	1.073	95.168	38.85	-
ODP II (9)	-	-	-	-	-	-		15.56	0.060	94.890	39.54	-
	-	-	-	-	-	-		10.82	0.027	95.021	39.46	-
	-	-	-	-	-	-		6.74	0.008	95.031	39.14	-